SBUF

PROJEKTNR. 14029

SmartCem Monitoring – självövervakande betong
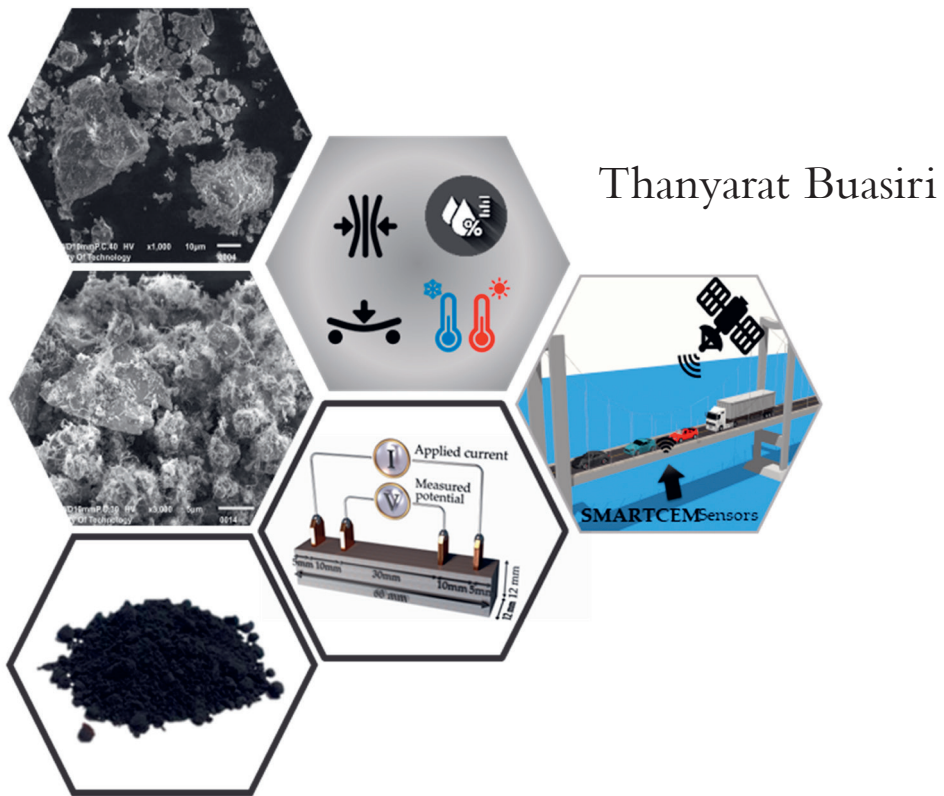
Slutrapport

Thanyarat Buasiri
LTU

2023-11-09
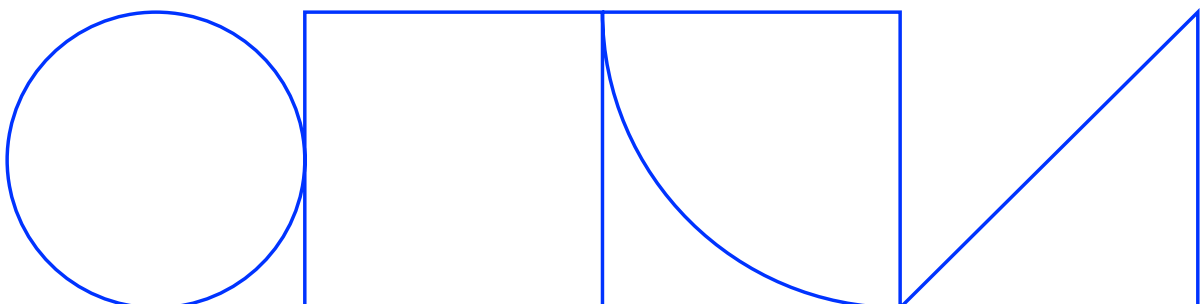
LULEÅ TEKNISKA UNIVERSITET

SKANSKA

Sensing capability of nanomodified Portland cement composites

Thanyarat Buasiri

Building Materials

LULEÅ
UNIVERSITY
OF TECHNOLOGY

DOCTORAL THESIS

Sensing capability of nanomodified Portland cement composites

Thanyarat Buasiri

Building Materials
Department of Civil, Environmental and Natural Resources Engineering
Luleå University of Technology
SE-97187 Luleå, Sweden
October 2023

Front Page: The cover image shows a schematic overview of the research.

Academic Thesis

For the Degree of Doctor of Philosophy (Ph.D.) in Building Materials, which by due permission of the Technical Faculty Board at Luleå University of Technology will be publicly defended on:

Wednesday, October 11ᵗʰ, 2023, 10:00 am
Room A109, Luleå University of Technology

Opponent Examiner:

Prof. Jan Olek
Lyles School of Civil Engineering, Purdue University, USA

Examining committee:

Prof. Jeanette Orlowsky
Building Materials, TU Dortmund University, Germany

Prof. Lawrence Sutter
Material Science & Engineering, Michigan Technological University, USA

Associate Prof. Fernando José Forte Garrido Branco
Civil Engineering, University of Coimbra, Portugal

Principal Supervisor:

Prof. Andrzej Cwirzen
Building Materials, Luleå University of Technology, Sweden

Assistant Supervisors:

Associate Prof. Karin Habermehl-Cwirzen
Building Materials, Luleå University of Technology, Sweden

Acknowledgements

Acknowledgements

A special thanks to my second mom in Luleå, Aomjai K., for her unwavering love, support, and encouragement. Her presence in my life has been a source of inspiration and comfort, and her belief in my abilities has propelled me forward during this doctoral journey. Her guidance and wisdom have been invaluable, and I am truly grateful for her role in shaping both my academic pursuits and personal growth.

I want to extend my heartfelt gratitude to Waleerat N., Sulawan S., and Thitima P., those remarkable individuals who, though not family by blood, have embraced me with a sense of kinship throughout this journey. Your unwavering support, camaraderie, and encouragement have been an invaluable presence. Thank you for being a significant part of this accomplishment.

To my beloved boyfriend and future husband, Tawatnon N., your unwavering love and support have been my anchor throughout this doctoral journey. Every step of the way, you have been my rock, my confidant, and my greatest cheerleader. Your patience and kindness have provided the solace I needed during moments of stress. With you by my side, the difficulties transformed into opportunities, and the victories became all the more joyful. Thank you for being my constant source of strength, for believing in my dreams, and for sharing this incredible journey with me. I love you to the moon and back.

Last but not least, I want to express my deepest gratitude to my family. This achievement is not mine alone but a reflection of your love, guidance, and dedication. To my parents, you have instilled in me the values of diligence and perseverance from the very beginning. Your sacrifices, both the ones I have witnessed and those that remain unseen, have laid the sturdy foundation upon which this accomplishment stands. Your unconditional love has fortified my determination. To my grandfather and grandmother, your wisdom and life experiences have been a source of inspiration. Your stories and teachings have resonated deeply, reminding me of the importance of embracing challenges and pursuing knowledge with unyielding dedication. To my uncle and aunt, your belief in my potential and your words of wisdom have propelled me forward during moments of doubt. To my brothers and sisters, your camaraderie and belief in my abilities have emboldened me to overcome obstacles with resilience. To my lovely niece and nephew, you are the embodiment of the future I aspire to build. Your innocent smiles have been a constant reminder of the purpose behind my pursuit of knowledge. I hope to inspire you to chase your dreams.

<div align="center">

"ทุกคนคะ พลอยได้เป็นซุปเปอร์ด็อกแล้วนะคะ"

</div>

<div align="right">

Thanyarat Buasiri

Luleå, October 2023

</div>

Summary

As the demand for smart infrastructure grows, researchers and engineers are seeking innovative solutions to enhance the safety, reliability, and durability of concrete structures. Traditional cement-based materials have been fundamental to construction due to their strength and versatility. However, their inability to provide real-time health and performance data has limited their potential. In response, self-sensing cement-based composites have emerged as revolutionary technologies, combining the strengths of traditional materials with the ability to sense and respond to environmental changes. Sensing cement-based composites are advanced materials that possess the ability to measure various physical and chemical parameters. Achieved through the incorporation of conductive fibers i.e., carbon nanofibers (CNFs), carbon nanotubes (CNTs), and graphene nanoplatelets (GNPs) into standard cementitious matrixes, these composites enable the phenomenon of self-sensing. This self-sensing is grounded in the conductive material's capacity to undergo changes in its electrical properties.

The primary aim of this research is to pioneer the development of an innovative self-sensing cement-based composite, designed to function as a sophisticated sensory system within the framework of a structural health monitoring (SHM) system for concrete structures. The research focuses on nanomodified Portland cement (SmartCem) as a key component in these self-sensing composites. The SmartCem material is composed of particles with attached CNFs that are synthesized in situ through the chemical vapor deposition (CVD) technique. SmartCem improves the dispersion of conductive materials within the cement matrix, enabling its use as a sensing material. The investigation reveals that SmartCem composites exhibit robust piezoresistive behavior, reacting to mechanical stresses and indicating structural stress or strain. These composites not only respond to mechanical stress but also variations in humidity and temperature, making them versatile for various monitoring applications. The concentration of SmartCem within the composite material emerges as a crucial factor determining sensitivity. Optimal concentrations result in a well-established conductive network, enhancing the composite's ability to detect changes in parameters like stress, strain, temperature, and humidity. Additionally, SmartCem mortar proves effective in monitoring the hydration process and tracking stress-strain changes in concrete structures, contributing to their integrity and safety. The study substantiates these findings through modeling and substantiates the sensing properties linked to several possible mechanisms within the SmartCem composite. The research further extends to preliminary field testing, showcasing the possibility of using SmartCem composites as a sensor in real-world scenarios. These validations underscore the potential of SmartCem composites to be

utilized in the development of integrated monitoring systems for concrete structures and mark a significant step forward in structural health monitoring technology.

Keywords: Sensing cementitious composites, Nanomodified Portland cement, SmartCem, Carbon nanofibers, CNF, Piezoresistive materials, sensor, Cement-based sensor, Self-monitoring, Sensing capability

Sammanfattning

I takt med att efterfrågan på smart infrastruktur växer, söker forskare och ingenjörer innovativa lösningar för att förbättra betongkonstruktioners säkerhet, tillförlitlighet och hållbarhet. Traditionella cementbaserade material har länge utgjort basen för byggande på grund av deras hållfasthet och mångsidighet. Deras oförmåga att tillhandahålla realtidsdata om konstruktionens tillstånd och prestanda har däremot begränsat deras potential. För att lösa problematiken har självkännande cementbaserade kompositer utvecklats till en revolutionerande teknologi som kombinerar de traditionella materialens fördelar med förmågan att känna av och reagera på förändringar i omgivningen. Självkännande cementbaserade kompositer är avancerade material som har förmågan att mäta olika fysiska och kemiska parametrar. Detta uppnås genom att införliva konduktiva fibrer, såsom kolnanofibrer (CNFs), kolnanorör (CNTs) och grafennanoskivor (GNPs), i cementmatrisen, vilket möjliggör kompositens självkännande. Självkännande bygger på det ledande materialets förmåga att genomgå förändringar i sina elektriska egenskaper.

Den främsta målsättningen med denna forskning är att vara en pionjär inom utvecklingen av en innovativ självkännande cementbaserad komposit, utformad för att fungera som ett sofistikerat sensorsystem inom ramen för ett strukturellt tillståndsövervakningssystem (SHM) för betongkonstruktioner. Forskningen fokuserar på nanomodifierad Portlandcement (SmartCem) som en nyckelkomponent i de självkännande kompositerna. SmartCem-materialet består av partiklar med bundna CNFs som syntetiseras på plats genom tekniken för kemisk avlagring i gasfas (CVD). SmartCem förbättrar spridningen av ledande material inom betongmatrisen, vilket möjliggör dess användning som ett sensormaterial. Undersökningen visar att SmartCem-kompositer uppvisar ett robust piezoresistivt beteende, reagerar på mekaniska påfrestningar och indikerar strukturella spänningar eller töjningar. Dessa kompositer reagerar inte bara på mekanisk belastning utan också på variationer i luftfuktighet och temperatur, vilket gör dem mångsidiga för olika övervakningsapplikationer. Koncentrationen av SmartCem inom kompositmaterialet framträder som en avgörande faktor som styr känsligheten. Optimala koncentrationer resulterar i ett väletablerat ledande nätverk, vilket förstärker kompositens förmåga att upptäcka förändringar i parametrar som spänning, töjning, temperatur och luftfuktighet. Dessutom visar sig SmartCem-bruk vara effektivt för övervakning av hydratationsprocessen och uppföljning av spännings-töjningsförändringar i betongkonstruktioner, vilket bidrar till ökad integritet och säkerhet. Studien bekräftar resultaten genom modellering och bevisar de sensoriska egenskaperna som är kopplade till flera möjliga mekanismer inom SmartCem-kompositen. Forskningen sträcker sig även till preliminära fälttester som demonstrerar möjligheten att använda SmartCem-kompositer som sensorer i verkliga

scenarier. Dessa valideringar understryker potentialen att använda SmartCem-kompositer vid utvecklingen av integrerade övervakningssystem för betongkonstruktioner och markerar ett betydande steg framåt för teknologierna inom tillståndsbedömning.

Nyckelord: Självkännande cementbaserade kompositer, Nanomodifierad portlandcement, SmartCem, Kolnanofibrer, CNF, Piezoresistiva material, Sensorer, Cementbaserade sensorer, Självövervakning, Avkänningsförmåga

สรุปงานวิจัย (Summary in Thai)

เนื่องจากความต้องการโครงสร้างพื้นฐานอัจฉริยะมีมากขึ้น นักวิจัยและวิศวกรจึงมองหานวัตกรรมเพื่อเพิ่ม
ความปลอดภัย ความน่าเชื่อถือ และความทนทานของโครงสร้างคอนกรีต แม้ว่าวัสดุซีเมนต์ทั่วไปที่ใช้ในการก่อสร้าง
มีความแข็งแรงและใช้งานได้หลากหลาย แต่มีข้อจำกัดในการตรวจสอบสถานะและประสิทธิภาพแบบเรียลไทม์ วัสดุ
ซีเมนต์คอมโพสิตรับรู้และตรวจสอบตนเองเป็นเทคโนโลยีปฏิวัติวงการที่ผสมผสานความแข็งแกร่งของวัสดุซีเมนต์
แบบดั้งเดิมเข้ากับความสามารถในการรับรู้และตอบสนองต่อการเปลี่ยนแปลงทางสิ่งแวดล้อม วัสดุซีเมนต์คอมโพสิต
รับรู้และตรวจสอบตนเองมีความสามารถในการติดตามตัวแปรต่างๆ ทั้งทางกายภาพและทางเคมี โดยเกิดจากการ
รวมกันของเส้นนำไฟฟ้า เช่น เส้นใยนาโนคาร์บอน, ท่อนาโนคาร์บอน และแผ่นนาโนกราฟีน ฯลฯ เข้ากับซีเมนต์
เมทริกซ์มาตรฐาน ทำให้เกิดความสามารถในการรับรู้และตรวจสอบตนเองขึ้น ซึ่งหลักการพื้นฐานของการรับรู้และ
ตรวจสอบตนเองดังกล่าว สามารถอธิบายได้จากการเปลี่ยนแปลงคุณสมบัติทางไฟฟ้าของวัสดุซีเมนต์คอมโพสิต

วัตถุประสงค์หลักของงานวิจัยนี้คือการพัฒนานวัตกรรมวัสดุซีเมนต์คอมโพสิตรับรู้และตรวจสอบตนเอง เพื่อ
ทำหน้าที่เป็นเซ็นเซอร์ที่ใช้ในระบบการตรวจสอบสุขภาพของโครงสร้างคอนกรีต งานวิจัยนี้มุ่งเน้นไปที่การนำ
ปูนซีเมนต์ปอร์ตแลนด์ที่ผ่านการดัดแปลงระดับนาโน หรือที่เรียกว่า สมาร์ทซีเมนต์ มาใช้เป็นส่วนประกอบสำคัญใน
การสร้างวัสดุซีเมนต์คอมโพสิตรับรู้และตรวจสอบตนเอง อนุภาคสมาร์ทซีเมนต์ประกอบด้วยเส้นใยนาโนคาร์บอนที่มี
การสังเคราะห์ในแหล่งกำเนิด โดยใช้กระบวนการทางเคมีในการสร้างชั้นเคลือบผิวที่มีความบริสุทธิ์สูง หรือเทคนิค
การเคลือบซีวีดี (Chemical Vapor Deposition) ซึ่งสามารถช่วยปรับปรุงการกระจายตัวของวัสดุนำไฟฟ้า
ภายในซีเมนต์เมทริกซ์ และยังช่วยเพิ่มระดับการรับรู้และการตอบสนองของคอมโพสิตที่พัฒนาขึ้น

จากผลงานวิจัยแสดงให้เห็นว่าการใช้สมาร์ทซีเมนต์ในการสร้างวัสดุซีเมนต์คอมโพสิตรับรู้และตรวจสอบ
ตนเอง หรือตลอดงานวิจัยนี้เรียกว่า สมาร์ทซีเมนต์คอมโพสิต มีพฤติกรรมต้านทานเพียโซที่แข็งแกร่ง
(piezoresistive) ตอบสนองต่อความเค้นเชิงกล อีกทั้งยังแสดงพฤติกรรมการตอบสนองต่อการเปลี่ยนแปลงของ
ความชื้นและอุณหภูมิอีกด้วย ทำให้สมาร์ทซีเมนต์คอมโพสิตมีความหลากหลายสำหรับการใช้งานในการตรวจสอบตัว
แปรต่างๆ ปริมาณของสมาร์ทซีเมนต์เป็นปัจจัยสำคัญปัจจัยหนึ่งในการกำหนดความไวในการรับรู้ต่อการเปลี่ยนแปลง
โดยปริมาณของสมาร์ทซีเมนต์ที่เหมาะสมที่สุด (percolation threshold) ส่งผลให้เกิดโครงข่ายนำไฟฟ้าที่
มั่นคง ทั้งยังเพิ่มความสามารถของสมาร์ทซีเมนต์คอมโพสิตในการตรวจจับการเปลี่ยนแปลงของตัวแปรต่างๆ เช่น
ความเค้น, การเสียรูป, อุณหภูมิ และความชื้น นอกจากนี้สมาร์ทซีเมนต์คอมโพสิตยังสามารถทำหน้าที่เป็นเซนเซอร์ที่มี
ประสิทธิภาพในการติดตามกระบวนการไฮเดรชั่นและติดตามการเปลี่ยนแปลงของความเค้น-ความเครียด ซึ่ง
ความสามารถดังกล่าวดังกล่าวมีส่วนช่วยเพิ่มความสมบูรณ์และความปลอดภัยในโครงสร้างคอนกรีต ผลการศึกษายัง
สนับสนุนผลลัพธ์เหล่านี้ผ่านการสร้างแบบจำลองและพิสูจน์คุณสมบัติในการตรวจสอบ โดยเชื่อมโยงกับกลไกที่
เป็นไปได้หลากหลายประการที่เกิดขึ้นภายในสมาร์ทซีเมนต์คอมโพสิต งานวิจัยยังขยายไปถึงการทดสอบภาคสนาม
เบื้องต้น โดยผลงานวิจัยแสดงให้เห็นถึงความเป็นไปได้ของการใช้สมาร์ทซีเมนต์คอมโพสิตเพื่อทำหน้าที่
เปรียบเสมือนเซ็นเซอร์ตรวจสอบในสถานการณ์จริง ทั้งนี้การตรวจสอบดังกล่าวยังเน้นย้ำถึงศักยภาพของสมาร์ท

ซีเมนต์คอมโพสิตในการพัฒนาระบบการตรวจสอบแบบบูรณาการสำหรับโครงสร้างคอนกรีต และถือเป็นก้าวสำคัญในการก้าวไปข้างหน้าของเทคโนโลยีการตรวจสอบสุขภาพของโครงสร้างคอนกรีตอีกด้วย

คำสำคัญ: การตรวจจับวัสดุผสมซีเมนต์, วัสดุซีเมนต์ตรวจสอบตนเอง, ปูนซีเมนต์ปอร์ตแลนด์ดัดแปลงนาโน, สมาร์ทซีเมนต์, สมาร์ทซีเมนต์คอมโพสิต, เส้นใยนาโนคาร์บอน, วัสดุเพียโซรีซิสทีฟ, การตรวจสอบตนเอง, ความสามารถในการตรวจสอบตนเอง

Table of Contents

List of Figures

List of Tables

Notations

Term	Description
Percolation threshold	A critical point at which a conductive network within the matrix becomes interconnected enough to facilitate the efficient transmission of electrical signals.
Nanomodified Portland cement or SmartCem	In situ synthesized CNFs directly on ordinary Portland cement particles using the CVD method.
Self-monitoring cement-based composite	An advanced construction material designed to incorporate self-sensing capabilities.
Sensitivity	The degree of responsiveness or change in electrical properties of the sensing composites due to changes in an influent factor.
SmartCem composite	A self-sensing composite consists of a cement-based matrix and SmartCem.
Structural health monitoring	A process for monitoring changes in structures and providing real-time information on structural conditions.
Tunneling	A phenomenon where electrons have the ability to pass through energy barriers between two conducting materials when the gap between them is sufficiently small

Chemical symbol	Description	Chemical symbol	Description
Al	Aluminium	K_2O	Potassium oxide
Al_2O_3	Aluminium (III) oxide	K_2SO_4	Potassium sulphate
Ar	Argon	LiCl	Lithium chloride
C	Carbon	Mg	Magnesium
Ca	Calcium	MgO	Magnesium oxide
$CaCO_3$	Calcium carbonate	Na_2O	Sodium oxide
CaO	Calcium oxide	NaCl	Sodium chloride
Fe	Iron	O	Oxygen
Fe_2O_3	Iron (III) oxide	S	Sulfur
H_2	Hydrogen	Si	Silicon
K	Potassium	SiO_2	Silicon dioxide
K_2CO_3	Potassium carbonate	SO_3	Sulfur trioxide

Notations

Abbreviation	Description	Abbreviation	Description
AC	Alternating current	MWCNT	Multi-walled carbon nanotube
B15	Quartz sand (150 μm)	NC	Normal concrete
CB	Carbon black	pH	Potential of hydrogen
CBCC	Carbon black cement-based sensors	R^2	The coefficients of determination
CEM I 42.5N	Ordinary Portland cement type I 42.5N	RC	Reinforced concrete
CF	Carbon fiber	RH	Relative humidity
CFRC	Carbon fiber-reinforced concrete	s/b	Sand-to-binder ratio
CNF	Carbon nanofiber	SCC	Self-compacting concrete
CNT	Carbon nanotube	SED	Secondary electron detector
CV	Coefficient of variation	SEM	Scanning electron microscope
CVD	Chemical vapor deposition	SEM -EDS	Scanning electron microscopy
DC	Direct current	SF	Steel fiber
EDX/EDS	Energy dispersive X-ray spectrometer	SHM	Structural health monitoring
FCR	Fractional change in electrical resistivity	SmartCem	Nanomodified Portland cement
GF	Gauge factor	SMAs	Shape memory alloys
GNP	Graphene nanoplatelet	SP	Polycarboxylate-based superplasticizer
GP	Graphite powder	SWCNT	Single-walled carbon nanotube
LOI	Loss on ignition	TG	Thermogravimetric
LVDT	Linear Variable Differential Transformer	TGA	Thermogravimetric analysis
MLG	Multilayer graphene	w/b	Water-to-binder ratio

Chapter 1

Introduction

T he majority of civil infrastructure is made of concrete structures. While engineering accidents occurring during the service period of concrete structures can be avoided by good structural design, some unexpected extreme situations are still threatening their safety and durability. Deterioration of concrete structures can be caused by a number of factors, including corrosion of reinforcing bars (Cabrera, 1996), cracking (Basheer et al., 1996), freeze-thaw attack (Hobbs, 2001), carbonation (Chi et al., 2002), alkali-silica reaction, etc. (Boyd & Skalny, 2007; Darwin et al., 2008). In some cases, the absence of condition assessment tools and timely maintenance caused concrete structures to fall into an ultimate state of disrepair. That requires a significant effort to restore them to a safe or functional condition. Therefore, it is desirable that the condition of concrete structures be assessed or monitored throughout their service life. Early evaluation of the health of concrete structures to mitigate deterioration or prevent abrupt catastrophes is crucial for extending the service life and ensuring the safety of lives and property.

Structural health monitoring (SHM) is a process for monitoring changes in structures and providing real-time information on structural conditions for safety evaluation and subsequent maintenance planning. The components of a typical SHM system include a sensory system and an evaluation system. The fundamental part is to establish a stable and reliable sensing system. The SHM system uses various types of sensors to determine a number of crucial parameters, for instance, stress, strain, crack formation, humidity, and temperature (S. Ding et al., 2019). Most of the sensors used in SHM for concrete structures are metallic. Therefore, there is no material compatibility between these sensors and the concrete, as well as poor durability, a high cost, and a short lifespan (Monteiro et al., 2017), The growing global demand for smart infrastructure has prompted researchers, engineers, and policymakers to explore novel solutions that can enhance the safety, reliability, and durability of

buildings, bridges, highways, and other civil engineering structures. Traditional cement-based materials have long been the backbone of construction due to their strength, versatility, and cost-effectiveness. However, the inability of these conventional materials to provide real-time health and performance data has limited their potential. Therefore, self-sensing cement-based composites have been developed as the latest option for SHM sensing technology.

Self-sensing cement-based composites have emerged as groundbreaking technologies with the potential to revolutionize the construction industry. Combining the essential properties of traditional cementitious materials with the capability to sense and respond to environmental stimuli, these intelligent composites open a new frontier in the creation of resilient, sustainable, and efficient infrastructure.

At the macroscopic level, self-sensing cement-based composites generally consist of non-conductive cementitious matrix and conductive fibers, **Figure 1-1.**
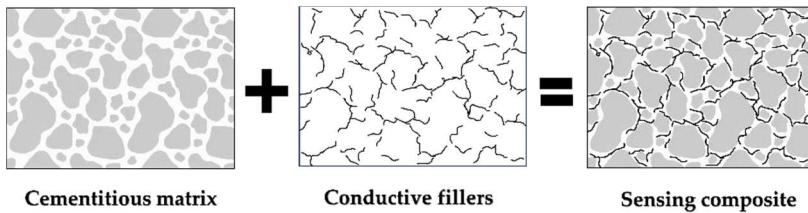
Figure 1-1 Structure of a self-sensing composite

Carbon-based materials have been predominantly used due to their excellent mechanical and electrical properties. However, achieving a sufficiently even distribution of these phases within the hydrated binder matrix has been one of the main obstacles to achieving strong self-sensing capability. The dispersibility depends on several factors, such as the concentration of conductive phases, their geometrical shape, applied processing methods, or surface functionalization. The hydrophobic nature of carbon-based materials results in a strong tendency for agglomeration, especially at higher pH values of the pore solution, typical for Portland cement-based concretes. A common procedure to spread conductive fillers in cementitious matrixes is to use a water dispersion with surfactants wrapped around nanomaterials to make a homogeneous water dispersion (Hilding et al., 2003). The produced dispersion is then added to the mix as part of the mixing water.

An alternative to water dispersion is the synthesis of nanomaterials (carbon nanofibers and carbon nanotubes) directly on Portland cement particles using a chemical vapor deposition (CVD) reactor (Nasibulin et al., 2009; Nasibulina et al., 2010). The nanomodified Portland cement can partly replace regular Portland cement during the production of mortars or concretes. The solution enabled an even

distribution of nanomaterials. The research presented in this thesis is a continuation of scientific work that was initiated in 2009 at the Helsinki University of Technology in Finland, where the synthesis technology was invented. However, the focus was on the electrical properties and self-sensing capabilities of mortars containing various amounts of nanomodified Portland cement.

1.1 Aim and objectives.

Aim:

To develop a novel self-sensing cement-based composite that can be used as a sensory system in the structural health monitoring system of concrete structures that will be reliable, have high sensitivity, easy to install, robust, and durable.

Objectives:

- Evaluate the effects of nanomodified Portland cement (SmartCem) on the sensing capabilities of cementitious composites.

- Understand what the sensing mechanism in different exposures is.

- Verify the self-sensing capability of full-scale concrete elements and structures.

1.2 Scientific approach

This study focused on the sensing capability of SmartCem composites. Initially, this work started with a review of the relevant literature to acquire fundamental knowledge related to the sensing properties of cement-based composites containing different types of conductive materials. This part was followed by the evaluation of the sensing capabilities of SmartCem composites exposed to various types of external loading, variable ambient temperature, and humidity. The sensing mechanisms and prediction models were studied in the last part of this research using a combination of theoretical, experimental, and mathematical approaches.

1.3 Research questions

I.   Is it possible to create a self-sensing composite based on Portland cement? What material combinations give the best results, and what are the most common problems? **(Paper I)**

II.   Can nanomodified Portland cement (SmartCem) be used to induce a self-sensing capability in Portland cement-based composites? **(Paper II, III, IV, V)**

III.   What are the mechanisms controlling the self-sensing capabilities of the SmartCem composites? **(Paper VI)**

IV.   What is the threshold amount of SmartCem for a self-sensing composite? **(Paper II, III, IV, V)**

V.   Can the SmartCem composites be used as sensors in a structural health monitoring system for concrete structures? **(Paper V)**

VI.   What is the most influential parameter for the sensitivity of the SmartCem composite? **(Paper II, III, IV, V, VI)**

1.4   Limitations

The research conducted exhibited certain limitations:

- Only two types of SmartCem were used in this study. The optimized synthesis parameters that were set in a pre-study (unpublished test results).

- Experiments were performed on small test specimens due to the limited amount of synthesized SmartCem.

- The focus of this doctoral thesis was on experimental research. The full-scale onsite monitoring tests have been ongoing while preparing this thesis; therefore, only some results are presented.

1.5   Chapter overview

This is a compilation thesis based on six scientific articles. The thesis is presented in six chapters, which are briefly described below.

Chapter 1 provides an overview of the context information of this work, including the formulated research question, aims, objectives, and limitations.

Chapter 2 describes the background of this work and contains a literature review focusing on the sensing capability of cement-based composites.

Chapter 3 provides a description of the materials and methods used in this work.

Chapter 4 describes the test outcomes, analyses, and discussions regarding the test outcomes. Highlighted the most important aspects of the research.

Chapter 5 proposes equations for predicting the electrical properties of SmartCem composites based on a combination of theoretical, experimental, and mathematical approaches.

Chapter 6 summarizes the research findings, formulates conclusions, and briefly discusses the possibility of future work.

1.6   List of appended papers

Paper I

"State of the art on sensing capability of poorly or nonconductive matrixes with a special focus on Portland cement–based materials", Buasiri, T., Habermehl-Cwirzen, K., Krzeminski, L., & Cwirzen, A., Published in Journal of Materials in Civil Engineering, 31(11) on 22 August 2019.

Paper II

"Piezoresistive load sensing and percolation phenomena in Portland cement composite modified with in-situ synthesized carbon nanofibers" Buasiri, T., Habermehl-Cwirzen, K., Krzeminski, L., & Cwirzen, A., Published in Nanomaterials, 9(4) on 10 April 2019.

Paper III

"Role of carbon nanofiber on the electrical resistivity of mortar under compressive load", Buasiri, T., Habermehl-Cwirzen, K., Krzeminski, L., & Cwirzen, A., Published in Transportation Research Record: Journal of the Transportation Research Board, 1–6 on 10 September 2020.

Paper IV

"Novel humidity sensors based on nanomodified Portland cement" Buasiri, T., Habermehl-Cwirzen, K., Krzeminski, L., & Cwirzen, A., Published in Scientific Reports, 1–10 on 14 April 2021.

Paper V

"Monitoring temperature and hydration by mortar sensors made of nanomodified Portland cement", Buasiri, T., Kothari, A., Habermehl-Cwirzen, K., Krzeminski, L., & Cwirzen, A., Submitted.

Paper VI

"Sensing mechanisms of nanomodified Portland cement composite" Buasiri, T., Habermehl-Cwirzen, K., Krzeminski, L., & Cwirzen, A., Submitted.

1.7   Additional publications/conferences

Other publications/conferences (not included in the thesis)

Paper VII

"Eco-uhpc as repair material—bond strength, interfacial transition zone and effects of formwork type", Kothari, A., Rajczakowska, M., Buasiri, T., Habermehl-Cwirzen, K., Cwirzen, A., Published in Materials 2020, 13, 5778 on 17 December 2020.

Paper VIII

"Piezoresistive behavior of electric arc furnace slag and graphene nanoplatelets asphalt mixtures for self-sensing pavements", Gulisano, F., Buasiri, T., Apaza, F.R.A., Cwirzen, A., Gallego, J., Published in Automation in Construction, Volume 142 in October 2022.

Paper IX

"Early age performance of OPC-GGBFS-concretes containing belite-CSA cement cured at sub-zero temperatures", Kothari, A., Buasiri, T., Cwirzen, A., Submitted.

Conferences participation:

The 1st International Conference on Smart Materials for Sustainable Construction (SMASCO), Luleå, Sweden, on December 10-12, 2019.

4th RILEM Annual Week And 40th Cement and Concrete Science Conference on August 31- September 4, 2020 (Online).

ACI Concrete Convention (The World's Gathering Place for Advancing Concrete) in San Francisco, CA, USA, on April 2-6, 2023.

Chapter 2

Literature review

2.1   Sensing cement-based composites

The term "self-sensing cement-based composite" refers to a type of smart or functional composite that has the capability to sense its condition and environment. These composites are also known as self-monitoring, or self-diagnosing cement-based composites (Han et al., 2017). The categorization of sensing cement-based composites can be divided into two main types: nonintrinsic and intrinsic self-sensing cement-based composites. In the case of nonintrinsic, external sensors or actuators, such as strain gauges, which have been commonly used since the 1930s (Benmokrane et al., 2007), optical fiber sensors (H. Wang et al., 2019), piezoelectric ceramics (H. Zhang et al., 2016), electrochemical sensors (Muralidharan et al., 2008), shape memory alloys (SMAs) (Song et al., 2006), and conductive polymer composites (Ou & Han, 2009) are either embedded, attached, or interfaced to develop self-sensing cement-based composites for structural health monitoring. The concept of intrinsic self-sensing concrete and structures was proposed in 1993 (P.-W. Chen & Chung, 1993). The intrinsic self-sensing cement-based composite is fabricated by mixing conductive fillers into conventional cement-based composites to increase their ability to sense while maintaining or even improving their mechanical properties. This composite can sense itself, eliminating the need for additional external sensors. Note that the concept of sensing cement-based composites mentioned in this work refers to the intrinsic self-sensing.

Generally, the sensing cement-based composite consists of two main phases: matrix materials and conductive fillers. The matrix materials, including cement paste, cement mortar, and concrete serve as a binder as well as provide structural functions. Apart from Portland cement-based composites, the use of sulfoaluminate cement (Cheng et al., 2011), geopolymer cement (Saafi et al., 2013), and asphalt concrete (X.

Liu & Wu, 2011) as matrix materials for sensing cement-based composites has been reported. Since a saturated and dried cementitious composite always behaves like a poor semiconductor or insulator due to its high resistivity, the conductive fillers play an essential role in providing sensing capability as well as improved structural performance. The conductive fillers, which can range in size from macroscale to nanoscale, fibrous to particle, single to hybrid, and carbonaceous to metallic should be electrically conductive and chemically stable. Carbon-based materials such as carbon nanotubes (CNTs), carbon nanofibers (CNFs), carbon blacks (CBs), and multilayer graphene (MLG) are considered highly favorable conductive fillers. This is primarily due to their exceptional mechanical, thermal, and electrical properties (Georgakilas et al., 2015; Mendoza Reales & Dias Toledo Filho, 2017).

Sensing could be defined as monitoring changes in electrical properties occurring in the matrix as a response to the application of external force, the development of stress, deformation, or strain due to loading, or ongoing deterioration processes. The self-sensing cement-based composite is a composite material having complex electrical properties, i.e., electrical resistance, electrical capacitance, and dielectric characteristics in varying degrees. The types of sensing signals are different for the measurement of the electrical properties of the composite depend on the selected methods and equipment.

2.2   Electrical signal

2.2.1   Electrical resistivity

Electrical resistivity is a fundamental material property that characterizes the intrinsic resistance of a material to the passage of electrical current. The sensing capability of self-sensing cement-based composites arises from alterations in the conductive network present within the composite's matrix. Consequently, the volumetric electrical resistivity can be used as a comprehensive indicator of their sensing behavior. In accordance with Ohm's law, the electrical resistivity ρ can be expressed as:

$$\rho = \frac{RA}{L} \tag{1}$$

where: R is the electrical resistance of the sensing composite, A is the cross-section area, and L is the distance between two electrodes.

2.2.2   Impedance or Electrical Reactance

Impedance (Z) is the total opposition that an electrical circuit shows to the flow of alternating current (AC). It combines both resistance (R) and reactance (X) in a complex form, while the electrical reactance specifically refers to the opposition caused by reactive elements (capacitors or inductors) in the circuit (Han et al., 2014c). Impedance is a complex quantity that has both magnitude and phase angle. It can be calculated using the following formula:

$$Z = R + iX \tag{2}$$

2.2.3   Electric Capacitance or Relative Dielectric Constant

Electric capacitance is defined as the ability of a capacitor to store an electric charge when a voltage is applied across its terminals. It is denoted C and measured in farads (F). One farad represents the capacitance of a capacitor that can store one coulomb of charge when a one-volt potential difference is applied across its terminals. Electric capacitance (C) can be expressed as:

$$C = \frac{\kappa \varepsilon_0 S}{l} \tag{3}$$

where: κ and ε_0 are the relative dielectric constant and the vacuum dielectric constant, respectively, S is area of the conducting samples and l is the distance between the electrodes.

2.2.4   Percolation theory

The relationship between the concentration of functional filler and the electrical property of a composite is determined by the percolation process (L. Wang & Aslani, 2019), as shown in **Figure 2-1**. This process shifts materials properties from insulating to semiconductive and conductive (H. Li et al., 2006; X. Wang et al., 2002; Xie et al., 1996). Three zones are usually formed while increasing the amount of conductive filler: insulation, percolation, and conduction.

In the insulation zone, the electrical resistivity of the composite is very high and shows little or no change with increasing concentrations of the filler. Its amount is too low to create conductive paths. The average distance between the conductive particles is too large for an effective movement of electrons.

In the percolation threshold zone, the adjacent conductive particles start to touch each other. This leads to the formation of conductive networks, which lower the resistivity by many orders of magnitude (Chung, 2002a). The resistivity will decrease with increasing filler content until the shortest conductive pathway is formed. The significant decrease in resistivity has been described as a percolation threshold.

In a conductive zone, the conductive filler concentration is higher than the percolation threshold, and fillers can be regarded as fully contacting each other. A further increase in the amount of filler does not alter the resistivity of the composite.
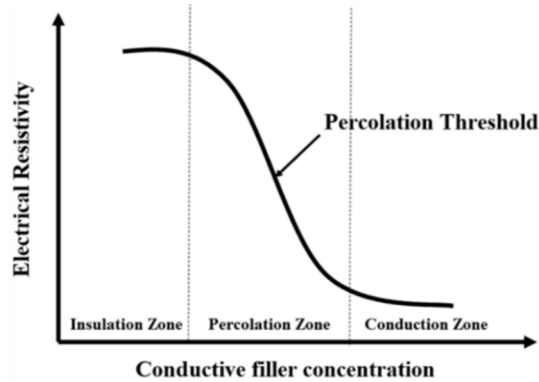
Figure 2-1 Electrically conductive mechanisms for sensing cement-based composites during the percolation process. (Buasiri et al., 2020)

2.3   Measurements of electrical properties

The electrical properties could be explained by resistance, resistivity, or conductivity. At present, there is no specific standard for the electrical resistance testing method. The measured resistance should be converted to resistivity by using an appropriate correction factor. Different specimen geometries, configurations, electrode types, and methods all affect the electrical resistivity of cementitious composites (Tian & Hu, 2012), which causes the electrical resistivity to vary (Dehghanpour et al., 2020). Therefore, the selected method is crucial to ensuring the reliability and repeatability of the test measurement. This chapter presents an overview of the various methods for measuring electrical resistance in the literature as well as a selection of methods specifically for evaluating SmartCem composites.

The electrical resistance measurement methods can be classified based on the electrode arrangement, which is the two-probe method and the four-probe method. In the four-probe method, the outer two electrodes are used to apply the current, and the inner two electrodes measure the potential difference, while in the two-probe method, the two electrodes are used to both supply the current and measure the voltage difference. Direct current (DC) and alternating current (AC) are typically the current sources for electrical resistance measurement. However, the polarization effect occurs when using DC. The polarization effect is caused by a chemical reaction at electrodes that liberates hydrogen and oxygen, which are deposited around the electrodes in the form of a thin film and make the electrical resistance go up

exponentially (Banthia et al., 1992). The electrical resistance measurement of cement-based composites should not be determined by a single measurement in order to use DC. Drying the specimens can be used to limit polarization (Payakaniti et al., 2017). Another way is to record the change in resistance measurement for the unloaded specimen and/or apply the DC until reaching the stabilized resistance measurement (pre-charge) ahead of conducting the actual test. In addition, AC is recommended to lessen the polarization effect to an acceptable range by increasing the applied AC frequency (Hou & Lynch, 2005).

According to **Figure 2-2**, the electrode can be attached to or embedded in the tested composites. For attached electrodes such as endplates, tape, or wire electrodes, it is necessary to apply a conductive adhesive in order to minimize the contact resistance between the specimen and the electrodes. According to (Han et al., 2007), the embedded electrode is considered more appropriate for conducting resistivity measurements in cementitious materials when compared to the electrode that is attached externally. This preference is primarily attributed to the embedded electrode's superior durability and lower polarization. An appropriate choice for electrodes necessitates possessing excellent electrical conductivity, exerting minimal influence on the mechanical and electrical characteristics of the composite, exhibiting high resistance to corrosion, and demonstrating commendable durability. Copper is an ideal material for an embedded electrode that meets all the requirements mentioned above (Azhari & Banthia, 2017).
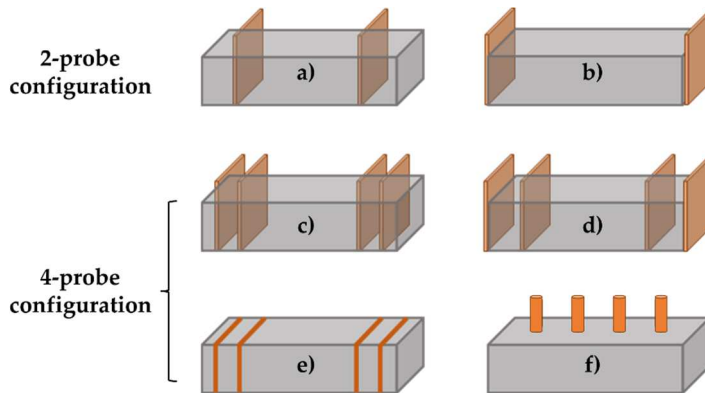
Figure 2-2 Electrode configurations for electrical resistance measurement of cementitious composites a) two-probe embedded b) two-probe attached, c) four-probe embedded, d) two-probe embedded and two-probe attached, e) four-rod attached, and f) four-rod embedded.

The methods used in the electrical measurement of cement-based are available in the literature, as summarized in **Table 2-1.**

Table 2-1 The electrical measurement methods.
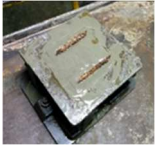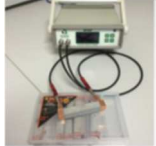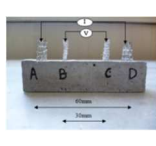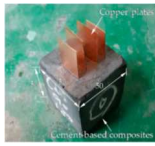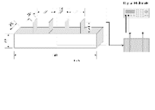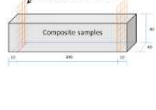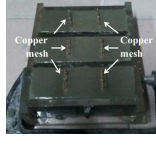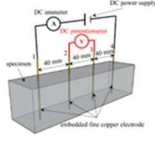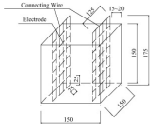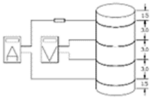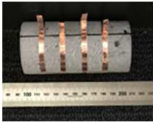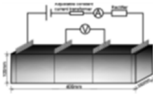
Matrix	Paste			
Test method	2-probe method		4-probe method	
Reference	(Sasmal et al., 2017)	(X. Li et al., 2018)	(Konsta-Gdoutos & Aza, 2014)	(Yoo et al., 2017)
Electrode configuration & Specimen size	1 50x50x50 mm	2 15x15x110 mm	3 20x20x80 mm	4 50x50x50 mm
Test power	DC (5-15 V)	AC (1000 Hz)	DC	-
Test instrument	Digital Multimeter	Resistivity meter	Digital Multimeter	LCR meter
Matrix	Mortar			
Test method	2-probe method			4-probe method
Reference	(Kim et al., 2014)	(Y. Liu et al., 2018)	(Q. Liu et al., 2016)	(Liang et al., 2022)
Electrode configuration & Specimen size	5 25x26x150 mm	6 40x40x160 mm	7 50x50x150 mm	8 40x40x160 mm
Test power	-	AC	-	DC
Test instrument	Digital Multimeter	Digital Multimeter	Electrical resistance collection device	Digital Multimeter

Table 2-1 Continue.

Matrix	Concrete			
Test method	2-probe method	4-probe method		
Reference	(J. Wu et al., 2015)	(Gao et al., 2011)	(Dong et al., 2021)	(J. Sun et al., 2021)
Electrode configuration & Specimen size	 9 150x150x150 mm	 10 ø 6"x12"	 11 ø 50 x 100 mm	 12 100x100x400 mm
Test power	DC (3 V)	DC (1.5 V)	DC	-
Test instrument	Digital Multimeter	Ammeter and Voltmeter	Digital Multimeter	Digital Multimeter

1. Reprinted from Composites Part A: Applied Science and Manufacturing, Vol. 100, Sasmal et al., "Electrical conductivity and piezo-resistive characteristics of CNT and CNF incorporated cementitious nanocomposites under static and dynamic loading", pp. 227-243, © 2017, with permission from Elsevier.
2. Reprinted from Cement and Concrete Composites, Vol. 92, Li et al., "Dispersion of graphene oxide agglomerates in cement paste and its effects on electrical resistivity and flexural strength", pp. 145-157, © 2018, with permission from Elsevier.
3. Reprinted from Cement and Concrete Composites, Vol. 53, Konsta-Gdoutos & Aza, "Self sensing carbon nanotube (CNT) and nanofiber (CNF) cementitious composites for real time damage assessment in smart structures", pp. 162-169, © 2014, with permission from Elsevier.
4. Reprinted from Yoo et al., 2017 ©MDPI under CC-BY 4.0, https://creativecommons.org/licenses/by/4.0/.
5. Reprinted from Composite Structures, Vol. 107, Kim et al., "Enhanced effect of carbon nanotube on mechanical and electrical properties of cement composites by incorporation of silica fume", pp. 60-169, © 2014, with permission from Elsevier.
6. Reprinted from Composites Part A: Applied Science and Manufacturing, Vol. 115, Y. Liu et al., "Ohmic heating curing of electrically conductive carbonnanofiber/cement-based composites to avoid frost damage under severely low temperature", pp. 236-246, © 2018, with permission from Elsevier.
7. Reprinted from Construction and Building Materials, Vol. 127, Q. Liu et al., "Experimental investigation on mechanical and piezoresistive properties of cementitious materials containing graphene and graphene oxide nanoplatelets", pp. 565-576, © 2016, with permission from Elsevier.
8. Reprinted from Construction and Building Materials, Vol. 357, Liang et al., "Measurement and simulation of electrical resistivity of cement-based materials by using embedded four-probe method", © 2022, with permission from Elsevier.
9. Reprinted from Construction and Building Materials, Vol. 75, Wu et al., "Three-phase composite conductive concrete for pavement deicing", pp. 129-135, © 2015, with permission from Elsevier.
10. Reprinted from Gao et al., © 2011, with permission from IOP Publishing Ltd., http://iopscience.iop.org/0964-1726.
11. Reprinted from Construction and Building Materials, Vol. 270, Y. (Dong et al., "Mechanical and electrical properties of concrete incorporating an iron-particle contained nano-graphite by-product", © 2021, with permission from Elsevier.
12. Reprinted from Construction and Building Materials, Vol. 281, J. Sun et al., "The effect of graphite and slag on electrical and mechanical properties of electrically conductive cementitious composites", © 2021, with permission from Elsevier.

2.4 Sensing mechanisms

The sensing mechanism is based on changes in the electrical properties of materials due to the action of external or internal factors or forces. The following factors can be considered (S. Ding et al., 2019; Han, Ding, et al., 2015):

(I)   Change in the intrinsic resistivity of conductive fillers. This change can be attributed to the deformation of local bonding caused by stress.

(II)   Change in bonding between conductive fillers and matrix. This change in resistivity is primarily attributed to the phenomena of filler push-in and pull-out, which occur during compression and tension.

(III)   Change of contact between conductive fillers. The application of an external force results in the reorganization and alignment of conductive fillers, which subsequently causes the formation and/or destruction of conductive pathways.

(IV)   Change in tunneling resistance between functional fillers. This change is attributed to the change in interparticle properties.

(V)   Change in capacitance. The presence of conductive fillers can be considered a capacitance plate. The application of an external force induces changes in both the distance between the capacitance plates and the relative dielectric constant, thereby causing fluctuations in the capacitance.

The aforementioned factors may work together to contribute to sensing properties. However, it is important to note that only one or a few of these factors dominate in specific regions of the conductivity curve. In the insulation zone, even when an external force is applied to the composite, a conductive path is difficult to form. Changes in capacitance are the primary factor. As a consequence, the composite has no or minimal sensing capabilities. At the initial stage of the percolation zone, the change in capacitance, the change in intrinsic resistance of fillers, and the change in bonding between filler and matrix are the dominant factors. Near the percolation threshold, the primary factors are the variation in tunneling distance between fillers, the variation in contact between fillers, the variation in bonding between filler and matrix, and the variation in the intrinsic resistance of conductive fillers. At the end of the percolation zone, the change in contact between fillers, the change in tunneling distance between fillers, and the change in intrinsic resistance of fillers play leading roles. Multiple variables influence the sensing properties of the composite in each section of the percolation zone. Therefore, the sensing composites in the percolation zone have good sensing properties. In the conductive zone, the change in contact between fillers and the change in intrinsic resistance of fillers become the dominant factors. The conductive network inside the composite stabilizes and becomes hard to change under loading. As a result, the composite will have more stable sensing properties and low sensing sensitivity (S. Ding et al., 2019; Han, Ding, et al., 2015).

2.5 Factors affecting sensing properties.

2.5.1 Concentration and dispersion of conductive fillers

The concentration of conductive filler plays a crucial role in the formation and density of the conductive network. As such, it is an important parameter that significantly affects sensing properties. Based on the percolation theory, it is generally observed that the electrical resistivity tends to decrease as the concentration of conductive filler increases. The formation of conductive networks inside the composite is improved by increasing the concentration of conductive materials (L. Zhang, Han, et al., 2017). The resistivity of sensing composites will be the lowest when the formation of the shortest conductive pathway occurs. However, higher concentrations of conductive fillers do not always result in lower electrical resistance. Due to the large specific surface area of functional fillers, especially nanofillers, the high-water absorption of conductive fillers will result in poor workability, which will lead to higher resistance. Besides that, functional fillers tend to agglomerate, which affects the formation of conductive networks. Therefore, it is crucial to determine the optimal concentration of conductive materials used in the sensing cement-based composites. The dispersion uniformity of conductive fillers greatly affects the sensing behavior of self-sensing cement-based composites. Ideally, it is important for conductive fillers to be evenly distributed within the composites to establish an efficient conductive network. The use of ultrasonication combined with surface treatment using surfactant enabled the production of matrixes with well-dispersed nanomaterials (Cwirzen et al., 2008; Yazdanbakhsh et al., 2010). Increasing the amount of surfactants can improve the dispersion; however, excessive amounts can result in the formation of air bubbles. This can interrupt the formation of a conductive path and ultimately lead to the bleeding and segregation of the composites (W. Zhang et al., 2018). The ultrasonic treatment is necessary to disperse nanomaterials. In addition, process parameters must be optimized, including the used frequency, energy as well as the duration of sonication. Too high ultrasonic energy can damage or shorten the conductive filler, such as CNFs or CNTs (W. Zhang et al., 2018).

2.5.2 Curing process

The sensing capability of cement-based composites is influenced by the applied curing process due to its effects on hydration and thus on the formed microstructure of the binder matrix. This process leads to the filling of internal pores with additional hydration products (Z. Liu et al., 2013). At an early age, the amount of chemically unbound-free water is higher, which enables the development of ionic conduction (M. Sun et al., 2002). Over time, the porosity and moisture content decrease, leading

to an increase in resistivity (Al-Dahawi, Öztürk, et al., 2016; Yildirim et al., 2015). In addition, it is probable that the hydration products will wrap the conductive phases and disrupt the conductive network, leading to a substantial increase in electrical resistivity (Al-Dahawi, Sarwary, et al., 2016a).

2.5.3   Temperature

A rise or decrease in temperature can result in expansion or contraction of the sensing cement-based composites, which would change the distance between the adjacent conductive fillers. Moreover, a change in temperature will also cause an increase or decrease in the transition energy of the electrons in conductive fillers. As the temperature increases, some electrons will gain additional energy and will act as charge carriers. They will transfer this energy between conductive fibers due to the tunneling phenomenon. It will result in decreased electrical resistivity (Bing et al., 2006). Therefore, temperature has a significant impact on the electrical conductivity and sensing properties of composites.

2.5.4   Ambient humidity

The water content of the sensing composite depends on many factors, including the environmental humidity. Exposing sensing composites to low ambient relative humidity causes the moisture to evaporate. While exposure to high humidity causes condensation and a gradual filling up of the capillary pores (Rajabipour & Weiss, 2007a). This results in the formation of additional connections between the already existing electrically conductive paths. Consequently, the ultimate electrical resistivity varies and depends on the exposure and its history (S. Ding et al., 2019).

2.6   Conductive fillers

2.6.1   Steel fibers

Steel fibers (SFs) are widely used as reinforcement (Berrocal et al., 2018). They have high tensile strength and modulus of elasticity, which can improve the flexural strength and ductility of composites and limit drying shrinkage and cracking (Buasiri, Habermehl-Cwirzen, & Cwirzen, 2019). SFs are good electrical conductors, thereby enabling their use as conductive fillers in cement-based sensing composites.

(Banthia et al., 1992) showed that inclusion of 5 wt.% SF in the cement paste resulted in a significant 40% increase in flexural strength and a nearly 90% reduction in electrical resistivity. (Wen & Chung, 2003) developed a cement paste containing steel fibers at a volume fraction of 0.36 vol%. It was observed that the resistivity of the SFs-reinforced matrixes increased in tension and decreased in compression. (Teomete &

Kocyigit, 2013) added 0.20-1.50 vol.% of 6-mm-long fibers to test mixes and observed an increase in the electrical resistivity in tension, which was associated with the formation of microcracks. (You et al., 2017) argue that the incorporation of 3 vol.% of SF into concrete has a negligible effect on the electrical resistivity as the fiber content exceeds the percolation threshold. However, as the curing time increases, the formation of rust on steel fibers will block the conductive networks, resulting in a significant increase in the resistivity. Consequently, it is impractical to use SF as the primary conductive material as it requires the application of a rust inhibitor (J. Wu et al., 2015). Furthermore, the variation in resistivity of SF-reinforced conductive concrete at different electrode positions can be attributed to the sedimentation of SF due to its high density (Fiala et al., 2016). Large aspect ratios facilitate the agglomeration of long fibers, which can result in higher resistivity (Berrocal et al., 2018). Therefore, it is recommended to combine a small amount of SF with a variety of other functional additives (L. Wang & Aslani, 2019).

2.6.2   Graphite powder

Graphite (GP) is a carbon polymorph that exhibits a layered and planar structure. The carbon atoms are arranged in a hexagonal lattice, forming a honeycomb pattern (Ribeiro et al., 2005). The softness of graphite can be attributed to the relatively loose arrangement of covalent bonds between its constituent atoms. The classification of this phenomenon is based on its mode of occurrence and origin, resulting in three distinct forms: flake, crystalline (lumpy), and cryptocrystalline (amorphous) (Han et al., 2014b). Graphite has excellent thermal and electrical conductivity properties, a high level of refractoriness, and consistent chemical stability.

For example, (El-Dieb et al., 2018) incorporated 7 vol.% of graphite powder into concrete. The obtained results indicated that the conductivity was increased threefold. In order to attain a high level of conductivity, a large number of graphene particles (GP) are required. However, an excessive amount of GP will lead to increased porosity, thereby negatively impacting strength.

2.6.3   Graphene nanoplatelet

Graphene nanoplatelets (GNPs) belong to the family of graphene-based materials. Graphene, the parent material, is a single layer of carbon atoms arranged in a two-dimensional honeycomb lattice. GNPs are essentially small platelet-like structures composed of multiple layers of graphene stacked on top of each other, forming a nanoplatelet structure (S. Sun et al., 2017). The unique properties of graphene include exceptional mechanical strength, high thermal and electrical conductivity, a large surface area, and low cost (Q. Liu et al., 2016).

For example, (S. Sun et al., 2017) investigated the piezoresistive properties of cementitious composites filled with graphene nanoplatelets (GNPs). The purpose of that study was to examine changes in the electrical properties of GNP-cementitious composites subjected to cyclic compressive stress under different quasi-static and dynamic loading conditions. The findings indicate that the electrical resistivity decreased as the GNP content increased until it reached the percolation threshold, which was approximately 2 vol.%. The piezoresistive effect was stable and repeatable within the elastic regime. However, at high loading rates, the amplitudes of change in the electrical resistivity decreased with time, demonstrating a slight dynamic loading rate dependence.

2.6.4   Carbon black

Carbon black (CB) is an amorphous form of carbon with a high ratio of surface area to volume. Several commercially available CBs are typically nanosized. The benefits of carbon black are its lightweight, high chemical and thermal stability, good electrical conductivity, and low cost (Wen & Chung, 2007). CB is one of the electrically conductive particulates that can reduce electrical resistance, improve aggregate interface durability, and increase the density of cementitious composites (Y. Ding et al., 2013). Carbon black is currently one of the most widely used functional fillers to incorporate sensing capabilities into cementitious matrixes.
For example, (H. Li et al., 2006, 2008) developed a cement paste containing CB for strain sensing. During loading, the resistivity showed a linear decrease with an increase in the compressive strain until the point of failure was reached. The occurrence of crack formation marked a bump in the otherwise nearly linear correlation. The percolation threshold of CB was between 12 and 20 wt.% of cement.

2.6.5   Carbon fiber

Carbon fiber (CF) is primarily composed of carbon atoms and has a diameter typically between 7 µm and 15 µm (Chung, 2001). The carbon content usually exceeds 92 wt.% (Huang, 2009). The utilization of CF as reinforcement in cementitious matrixes is attributed to its remarkable tensile strength and elastic modulus. This property allows CF to effectively impede the formation and propagation of microcracks, thereby improving both the flexural strength and flexural toughness of the cementitious matrix. Additionally, CF reinforcement contributes to the reduction of drying shrinkage and enhances the overall durability of the material (Chuang et al., 2017). Another area of application is the production of self-sensing cementitious composites.
For example, (Al-Dahawi, Sarwary, et al., 2016b), produced 50-mm cubic sensing mortars that contained 12-mm long CFs to assess their self-sensing capabilities when subjected to compressive loading. The results indicate that it was possible to detect

even small levels of deformation, starting from the initiation of the loading. Upon evaluating the percolation thresholds, mechanical properties, and piezoresistive properties, the findings showed that the percolation threshold was approximately 1 wt.%. Other studies demonstrated that carbon fiber-reinforced concrete (CFRC) has piezoresistive properties when subjected to cyclic loading (Chung, 2002b; Wen & Chung, 1999, 2003). In the elastic regime, the fractional change in electrical resistance decreased during loading and increased upon unloading. The study also showed irreversible piezo resistivity when the applied strain exceeded 0.2%. Therefore, it can be concluded that the CFRC was not appropriate for the purpose of stress-strain sensing when subjected to heavy loads.

2.6.6   Carbon nanofibers

Carbon nanofibers (CNFs) consist of cylindrical layers of graphene arranged in cones, plates, or cup shapes (Guadagno et al., 2013; Mo & Roberts, 2013; Rana et al., 2016). These layers form a cylindrical nanostructure. The stacking of these layers results in CNFs having a larger surface area, and the fiber's edges can enhance its bonding with the matrix material (Mo & Roberts, 2013). CNFs have diameters of up to 200 nm and lengths ranging from 50 to 200 μm (Yazdani & Mohanam, 2014). The incorporation of CNFs into cement-based composites not only enhances electrical properties but also improves other properties, i.e., tensile and flexural strengths, tensile ductility, flexural toughness, and reduced drying shrinkage (Cwirzen, 2021; Han, Sun, et al., 2015). A large number of studies showed that CNFs induced strong sensing capabilities.

For example, (Gao et al., 2009) observed that an increase in the concentration of CNFs decreased the electrical resistance, which can be attributed to the tunnel CNF conductivity effect. Excessive CNF amounts appeared to have limited impact on the sensing capabilities when exposed to the increasing strain. (Konsta-Gdoutos & Aza, 2014) examined the piezoresistive behavior of a cementitious matrix containing CNF subjected to cyclic compression loading within the elastic range. The resistivity tended to decrease during loading and increase during unloading. The resistivity of the sensing composite containing 0.1% by weight of CNF showed an average change in the electrical resistivity of 5.0%. This response is sufficient for application in strain sensors.

2.6.7   Carbon nanotubes

Carbon nanotubes (CNTs) have a cylindrical structure consisting of rolled hexagonal graphite sheets. (Iijima, 1991) was one of the first to observe CNTs. CNTs can be synthesized as single-walled carbon nanotubes (SWCNTs) or multi-walled carbon nanotubes (MWCNTs). That exhibit extraordinary physical, mechanical, and electrical properties (Cwirzen, 2021). They are nanosized, have high strength and

Young's modulus, a strong deformation response, high ductility, a high aspect ratio, excellent electrical (Bhatia et al., 2010; Guadagno et al., 2011; Thostenson et al., 2009) thermal (Guthy et al., 2007; Thostenson et al., 2009; Yang et al., 2008), and conductivity (Thostenson et al., 2001). Many researchers have conducted studies on the potential use of CNT/cement composites as sensors. A self-sensing MWCNT/cement composite used to monitor traffic showed remarkable responsiveness to loads generated by passing (Han et al., 2009). As shown by (Nam et al., 2016), the percolation threshold of the cement-based matrix containing MWCNT was 0.25% by weight. With this amount, the largest change in electrical resistance was recorded. The efficacy of a sensor using 0.2 wt.% MWCNT was validated via a vehicle-loading experiment, demonstrating its capability to accurately detect variations in load.

2.6.8   Cement with synthesized in-situ CNFs

One of the largest obstacles to creating strong, electrically, or thermally conductive CNT/CNF composites is the difficulty of obtaining a good dispersion of the carbon nanomaterials in the hardened binder matrix. Typically, time-consuming steps of carbon nanomaterial purification, functionalization and mixing with matrix are required. An alternative solution, which is also the core of this PhD thesis, is to synthesize CNTs/CNFs directly on Portland cement particles using chemical vapor deposition (CVD) (Nasibulin et al., 2009; Nasibulina et al., 2010). The composites based on such modified Portland cement showed a uniform dispersion, resulting in increased compressive strength and a decrease in the electrical resistivity of the hardened paste by one order of magnitude. (Cwirzen et al., 2009). The present PhD thesis aims to use these materials for sensing applications using piezoresistive properties.

2.6.9   Hybrid

Promising outcomes were observed in hybrid fiber systems that contained two or more types of fiber. A combination of micro- and nano-sized fibers leads to enhanced mechanical properties, an increased interfacial area between adhering fillers, and improved electrical conductivity. Research findings have indicated that hybrid conductive fillers improve sensing capabilities, i.e., greater accuracy and sensitivity (Luo et al., 2011). Moreover, it has been observed that hybrid functional fillers exhibit better sensing properties compared to single fillers. (Han, Ding, et al., 2015). In addition, hybrid fillers can form conducting networks at lower concentrations (S. Wu et al., 2005).

Numerous studies have focused on hybrid fillers to enhance their self-sensing capability, sensing reliability, and sensitivity. For example, (Ou & Han, 2009) demonstrated that cement-based strain sensors have strong piezoresistive properties.

This was achieved by adding 0.18 vol.% of CF and 15 vol.% of CB into the cementitious matrix. The strain sensors were subjected to compressive strain, and their performance was shown to be consistent and replicable. The detection of compressive strain in concrete beams and columns under field conditions was possible. (Rovnaník et al., 2017) showed that the use of CNTs and GP enabled them to achieve high electrical conductivity and mechanical strength. The electrical resistivity decreased by up to 80% by using 0.1 wt.% CNT with 2 wt.% GP. Similarly, the incorporation of 15 wt.% CF and 1 wt.% MWCNTs significantly enhanced the electrical conductivity and sensing capability (Azhari & Banthia, 2012). Compared to composites containing only CF, the hybrid composite showed enhanced signal quality, improved dependability, and greater sensitivity when subjected to both monotonically and cyclically applied strain. The insertion of 0.1 vol.% CF and 0.5 vol.% MWCNTs resulted in composites exhibiting the highest strain-sensing property. The gauge factor (GF) achieved a value of 160.3. The sensing capabilities shown by the GF were comparable to those seen in cement composites containing 1 vol.% MWCNTs (Lee et al., 2017).

2.7 Example applications of sensing cement-based composites

2.7.1 SHM

The real-time monitoring and structural health assessment of concrete structures are of crucial importance due to the extensive utilization of concrete as a construction material and the still-growing use of concrete structures in various applications. Severe structural failure can occur because of the cumulative damage caused by exposure to aggressive environments. The concept of SHM offers a means by which the safety and durability of a structure can be assessed throughout its operational lifespan, with the aim of ensuring its functional performance and long-term viability. Sensing cement-based composites used for SHM possess the capability to readily monitor alterations in stress or strain occurring within the compromised sections of structures, ensuring the normal operation of structures. Typically, it can be used in various configurations, such as bulk, coating, sandwich, bonded, and embedded forms, **Figure 2-3**.

The term bulk form refers to the configuration in which all structural elements, such as beams and columns, are constructed entirely from sensing cement-based composites. (W. Wang et al., 2006) evaluated the relationship between the fractional change in electrical resistance and fatigue life for carbon fiber reinforced concrete (CFRC) four-point bending columns subjected to cyclic flexural loading. Monitoring the damage condition in CFRC can be achieved through the measurement of the

electric resistance. Residual resistance is observed during the progression of load cycling. It is noted that as the stress ratio increases, the strain develops at a faster rate, leading to greater fatigue damage. Consequently, the irreversible increase in residual resistance is also greater. The test results indicated that carbon fiber concrete can be used to monitor fatigue damage and anticipate its fatigue life.
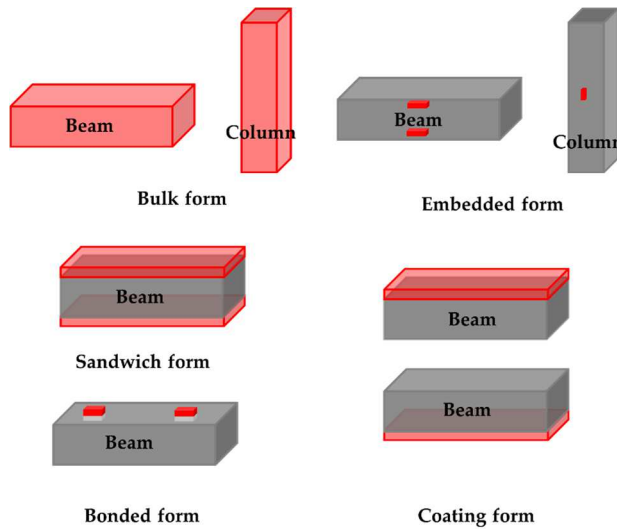
Figure 2-3 Typical application arrangements of self-sensing cement-based composites for SHM (the red, gray, and white parts represent the sensing composites, cementitious matrix, and adhesive, respectively)

The term coating form refers to the condition where a single surface of a component is covered by a layer of sensing composites. (Wen & Chung, 2001) were the first to apply a carbon fiber cement paste coating to either the tensile or compressive side of cement paste beams subjected to three-point bending. The electrical resistance of the strain-sensing coating showed a reversible increase on the tension side and a reversible decrease on the compression side.

In the sandwich arrangement, both the top and bottom surfaces of a component are covered with layers of sensing composites. This arrangement was used, for example, by (S. Wu et al., 2007) who applied carbon fiber reinforced concrete (CFRC) layers on both the top and bottom of reinforced concrete (RC) beams. The location and thickness of the CFRC layer impacted the initial electrical resistance and other electrical properties of the beam. The identified relationships between electrical resistance, loading, deflection, and crack formation enabled monitoring of the extent of damage to the designed beams.

Another application is to fabricate sensing composites as sensors with dimensions of coarse aggregate (Han & Ou, 2007). These sensors can be attached to a concrete component using adhesive, a technique commonly referred to as bonded form. (Baeza et al., 2013) studied the strain-sensing and damage-sensing functional properties of such a solution. They bonded either self-sensing carbon fiber or carbon nanofiber composites on the top, bottom, and sides of the RC beam. The results indicated that both CF and CNF cement-based sensors were capable of measuring strains on the surface of a conventionally reinforced concrete beam. The cement paste containing 2% CNF (by mass of cement) was the most sensitive dosage. Moreover, thinner sensors showed higher sensing capability when attached to an RC element.

The concept of the embedded form uses premanufactured, sensing cement-based sensors for monitoring concrete structures. For example, (Xiao et al., 2011) embedded carbon black cement-based sensors (CBCC) into three different stress zones (i.e., uniaxial compression, combined compression and shear, and uniaxial tension zones) of RC beams and investigated the strain sensing properties under four-point bending. The results showed good sensing properties under uniaxial tension and compressive strain and nearly no sensitivity to shear stress. The reduced shear stress sensitivity was related to the decreased maximum compressive strain.

2.7.2   Traffic detection

Traffic detection is a crucial aspect of managing traffic flow. Factors such as traffic flow rate, vehicle speeds, vehicle categorization, and traffic density have become increasingly vital for effective traffic management and road pavement design. Nowadays, traffic sensors are typically installed beneath the road surface or positioned alongside the road. However, these embedded sensors suffer from a limited lifespan and can even contribute to pavement deterioration due to their material incompatibility. Moreover, traditional sensors are prone to producing unreliable data due to their susceptibility to the effects of external environmental factors (Han et al., 2014a). Additionally, conventional sensors have a restricted detection range, rendering them impractical for broad implementation (Shi & Chung, 1999).

The implementation of sensing cement-based composites for traffic detection could address some of the listed problems. Sensing cement-based composites can accurately gauge traffic flow and vehicle speeds and even conduct weigh-in-motion measurements (Han et al., 2009). (Shi & Chung, 1999) studied concrete containing carbon fiber, 5 mm long, 0.5 or 1.0 wt.% of cement, for traffic monitoring and weighing in motion, which was done in the laboratory. The resistance decreased reversibly with increasing stress up to 1 MPa and was independent of the vehicle's speed up to 55 mph. A novel self-sensing CNTs containing concrete pavement system for traffic detection was proposed by (Han et al., 2013). The CNT concrete

sensors can identify the front wheel and the rear wheel of the vehicles passing by the changes that occur in the voltage signal. The integrated system has the advantages of high detection precision, high anti-jamming ability, easy installation and maintenance, a long service life, and good structural properties. The road test results showed that the new system performs very well and can be applied to real-time online detection.

Chapter 3

Materials and methods

3.1 Materials

3.1.1 Portland cement

Ordinary Portland cement (CEM I 42.5N) supplied by Cementa Sweden was used as a substrate for synthesizing carbon nanofibers (CNFs) on the nanomodified Portland cement, the so-called "SmartCem", and for all studied mortar samples. The chemical compositions of CEM I 42.5 N are shown in **Table 3-1.**

Table 3-1 The chemical composition of CEM I 42.5N.

Oxides (%)	CaO	SiO$_2$	Al$_2$O$_3$	Fe$_2$O$_3$	MgO	Na$_2$O	K$_2$O	SO$_3$	LOI
	63.30	21.20	3.40	4.12	2.20	0.18	0.56	2.70	2.50

3.1.2 Nanomodified Portland cement (SmartCem)

The SmartCem material is composed of particles with attached CNFs that are synthesized in situ through the chemical vapor deposition (CVD) technique, **Figure 3-1**. The CVD method is one of the commonly used techniques to grow carbon nanomaterials (Bajwa et al., 2008; MacKenzie et al., 2010). The process uses a high-temperature furnace where a catalyst is present and exposed to a continuous flow of gaseous carbon feedstock. The CVD method is simple and can be used in large-scale manufacturing (Qi et al., 2010).

Figure 3-1 SmartCem as produced.

The used CVD reactor was manufactured by the CVD Equipment Corporation. The SmartCem was produced on ordinary Portland cement (CEM I 42.5N) from Cementa-Sweden. The cement particles naturally contain efficient catalysts, including iron (III) oxide (Fe_2O_3).

The synthesis of SmartCem in the present work used high-purity ethylene as the main carbon source, and the synthesis temperature was 750 °C with a synthesis time of 120 min. Hydrogen gas (H_2, 99.99999%) was used as the reducing agent and argon (Ar) as the transportation medium. All of the gases used were industrial-grade.

The synthesis process started with placing 10 grams of cement powder (CEM I 42.5N) on four quartz boats made of tube halves, **Figure 3-2**.

Figure 3-2 Placement of Portland cement in quartz tube halves in the CVD reactor.

The quartz tube of the CVD reactor had 70 mm in diameter and 50 cm in length. In the first step, samples were subjected to a degassing process at a low pressure of 0.001 mbar and a temperature of 90 °C for 60 minutes. Next, the temperature was increased to 110 °C and maintained for 20 minutes in order to eliminate gaseous pollutants and moisture. After that, the cement samples were subjected to a heating

process, reaching a maximum temperature of 740 °C. This heating was carried out in an argon atmosphere, maintaining a pressure of 1,010 mbar. The rate of heating was 5 °C per minute. Once the temperature was stabilized, the cement samples underwent a reduction reaction for 15 minutes. This reaction took place in an atmosphere consisting of a mixture of hydrogen and argon, with flow rates of 500 standard cubic centimeters per minute (sccm) and 200 sccm, respectively. Following the reduction of the catalyst surface, the reactor temperature was maintained at 750 °C with a flow rate of 1 standard liter per minute (SLM) of argon. Then, a combination of reactive gases was introduced for synthesis, consisting of 100 sccm of ethylene, 400 sccm or 500 sccm of hydrogen for SmartCem I and SmartCem II, respectively, and 600 sccm of argon for 120 minutes. After that, the cement samples required purification to remove the amorphous carbon phases, which are by-products of the synthesis. This purification process was carried out in an atmosphere consisting of a mixture of hydrogen and argon, with flow rates of 100 sccm and 1,000 sccm, respectively. The last stage included cooling down to 200 °C at a rate of 12 °C per minute under an inert atmosphere, followed by degassing under vacuum and further cooling to 20°C in argon. **Figure 3-3** shows a schematic diagram of the CVD process of SmartCem synthesis, and **Figure 3-4** presents a flow chart that outlines the various steps involved in the synthesis processes.
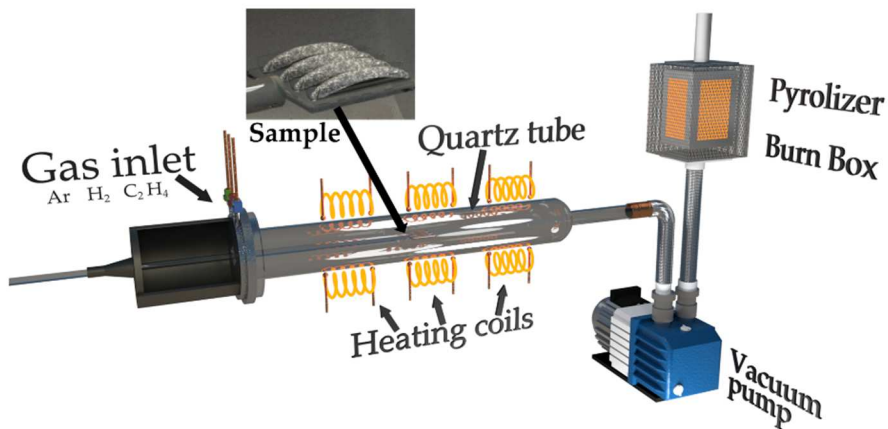
Figure 3-3 Schematic diagram of the SmartCem synthesis using the CVD reactor (Buasiri et al., 2019).
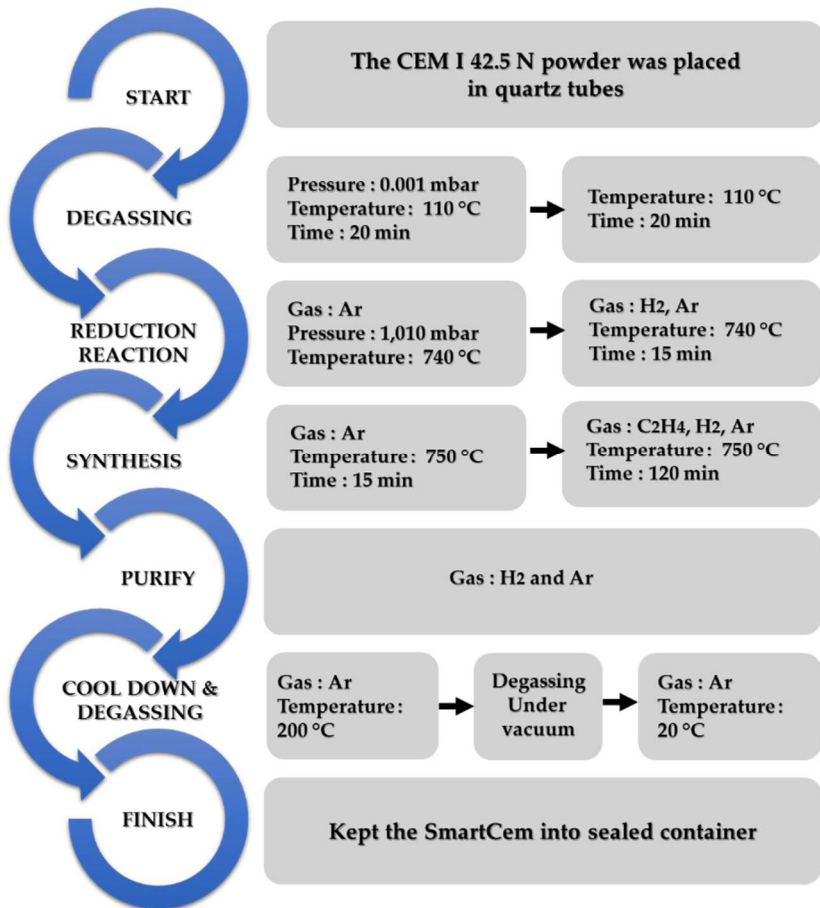
Figure 3-4 The synthesis procedure of the SmartCem.

3.1.3   Aggregates

Quartz sand (B15), having a maximum particle size of 150 μm was used to produce mortar and concrete samples. Natural granite aggregates with particle sizes of 0–4 mm and 4–8 mm provided by Jehander HeidelbergCement were used as fine and coarse aggregates, respectively. The particle size distribution of used aggregates is shown in **Figure 3-5**.
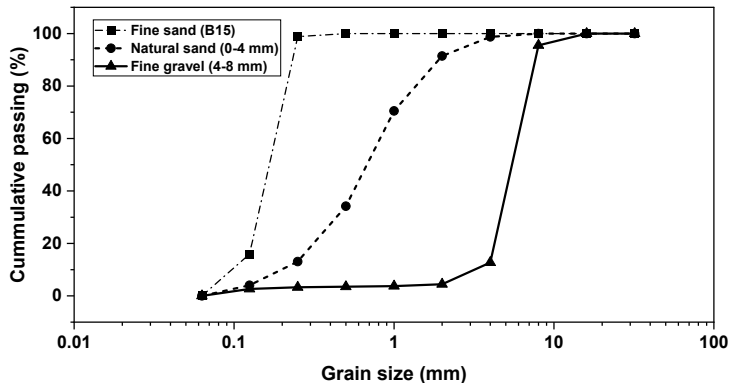
Figure 3-5 Grading curve of aggregates.

3.1.4   Admixture

Polycarboxylate-based superplasticizer (SP) type MasterGlenium produced by Grace Chemical was used to control the workability of fresh mixes.

3.1.5   Mixing machines

Two types of mixers were used to prepare test samples, **Figure 3-6**. A Bredent vacuum mixer was used to prepare mortar samples, while a Hobart mixer was used to produce concrete samples.

a)   **b)**
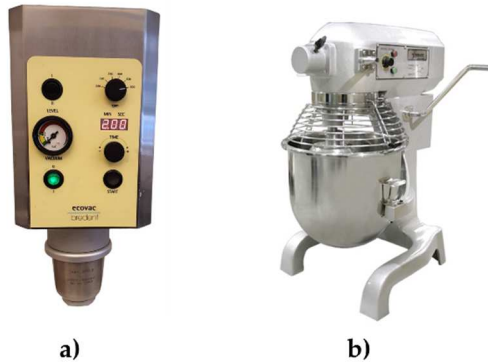
Figure 3-6 Mixers a) Bredent vacuum mixer and b) Hobart mixer-10L

3.1.6 Mix designs

The water-to-binder ratio (w/b) for all mortar samples was 0.35, while the sand-to-binder ratio (s/b) was 1. Additionally, each sample contained 0.8 wt.% of the superplasticizer. SmartCem was used to replace the cement in different proportions, namely: 0 wt.% (Ref), 2 wt.% (S2), 4 wt.% (S4), 6 wt.% (S6), 8 wt.% (S8), and 10 wt.% (S10) by the total weight of the binder. Mortars were used to produce sensors.

Two types of concrete were used for the laboratory study. Normal concrete (NC) was produced in the laboratory, while self-compacting concrete (SCC) was produced and delivered by the local ready-mix concrete distributor, Snells Betong och Ballast, Luleå, Sweden. NC and SCC were used for semi-large-scale tests.

The mix compositions of mortar and concrete samples are shown in **Table 3-2** and **Table 3-3**, respectively.

Table 3-2 Mix proportions for mortars.

Mix	w/b	s/b	Superplasticizer	Cement	SmartCem I	Calculated quantities of CNFs
			(**wt.% of binder**)			
Ref	0.35	1	0.8	100	0	0.000
S2	0.35	1	0.8	98	2	0.054
S4	0.35	1	0.8	96	4	0.108
S6	0.35	1	0.8	94	6	0.163
S8	0.35	1	0.8	92	8	0.217
S10	0.35	1	0.8	90	10	0.271

Table 3-3 The concrete mix composition.

Materials	Self-compacting concrete (SCC)	Normal concrete (NC)
	(kg/m³)	(kg/m³)
Portland Cement (CEM I 42.5N)	-	400
Portland Cement (CEM II/A-V 52.5N)	340	-
Limestone filler—KM200	160	-
Fine aggregate (B15)	-	179
Fine aggregate (0–4)	1,021	1,075
Coarse aggregate (4–8)	-	537
Coarse aggregate (8–16)	802	-
Superplasticizer	-	3.0
MasterGlenium SKY 823	3.4	-
Water	187	180

3.2   Methods

3.2.1   Sample preparation

The nanomodified Portland cement composites were prepared as mortar beams. The mortars were mixed using a Bredent vacuum mixer and subsequently cast into Teflon molds made in-house. The dimensions of the mortar specimens used in this study were 12 mm × 12 mm × 60 mm. Each mortar sample contained copper electrodes, which had a thickness of 0.25 mm, a width of 5 mm, and a length of 15 mm. The number of electrodes depended on the studied method. After casting for 24 hours, mortar samples were demolded and connected with soldered copper wires to the measuring devices. With the objective of mitigating the oxidation of electrodes, heat shrink tubes were used to isolate the ends connected to wires. All specimens were cured in different conditions until further testing. A schematic diagram of sample preparation and mix proportions used for the test mortars is shown in **Figure 3-7** and **Table 3-2,** respectively.
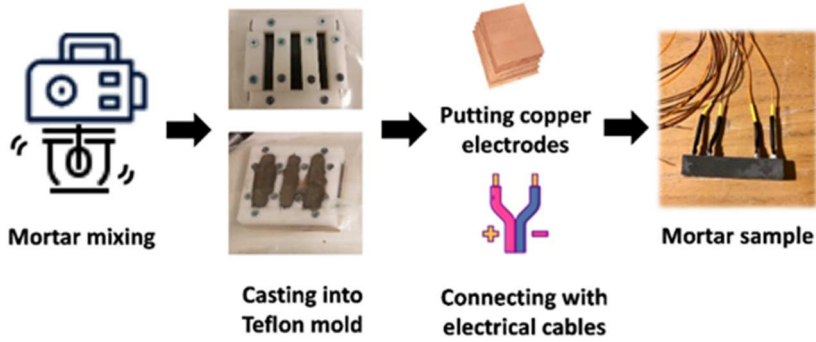
Figure 3-7 Preparation of mortar samples.

The laboratory-manufactured normal-strength concrete (NC) was prepared using a 10-liter Hobart mixer. The specimens of NC were cubic in shape, measuring 100 mm on each side, **Figure 3-8.** SCC beams had dimensions of 300 mm x 300 mm x 2500 mm**.** All specimens were cured under laboratory conditions. The mix compositions for concrete are shown in **Table 3-3.**
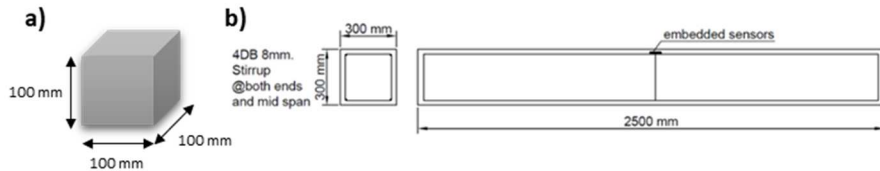
Figure 3-8 Concrete specimen a) 100 mm cube and b) semi-large-scale beam.

3.2.2   Mechanical properties

The mechanical properties of mortar samples were limited to compressive and flexural strengths. A Wykeham Farrance 50 kN UCS loading machine (**Figure 3-9**) with the Catman Easy version 5.2 software was used to record the applied force to the mortar specimens.

The SCC beam was tested for three-point bending with the setup following the SS-EN 12390-5:2009 standard (EN, 2019). The used displacement rate was 0.03 mm/s. The distance between supports was 1500 mm.

Figure 3-9 Compression machine.

3.2.3 Temperature gradient

The temperature development recorded was measured by embedding a thermocouple in the test specimens and connecting it to a TC-08 device type using Pico technology with the PicoLog6 software, **Figure 3-10**.

Figure 3-10 Thermocouple and TC-08 device.

3.2.4 Humidity development

The humidity measurements were taken using a commercial humidity sensor of type SHT85 from Sensirion.

3.2.5 Morphology and microstructure

3.2.5.1 SEM -EDS

The morphology of the SmartCem particles and the elemental composition of SmartCem I were determined using a Jeol JSM-IT100 scanning electron microscope (SEM) combined with a QUANTAX energy dispersive X-ray spectrometer (EDX) from Bruker Corporation, Billerica, MA, USA, **Figure 3-11.** The images were acquired utilizing the secondary electron detector (SED) at magnifications of 3,000x and 12,000x. The accelerating voltage was 7 kilovolts (kV), while the accelerating current was 30 microamperes (μA).
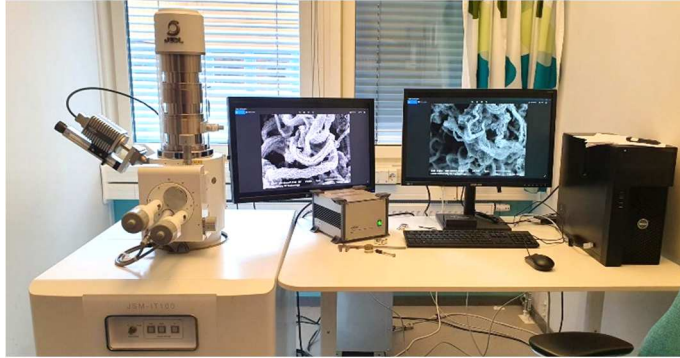
Figure 3-11 Scanning electron microscopy (SEM-EDS)

3.2.5.2 TGA test

Thermogravimetric (TG) analysis was performed using a thermal analyzer type NETZSCH STA 449F3 Jupiter® with a temperature increase rate of 10 °C/min and an operating temperature range between 20 and 1,000 °C in an atmosphere of air flowing at 50 mL/min.

3.2.6 Electrical resistivity measurements

The measurements were carried out using a digital multimeter of type Keysight 34465A, **Figure 3-12.** In order to determine the best method to measure changes in the electrical resistivity of the studied mortars, three different configurations (EM I, EM II, and EM III) were studied, **Figure 3-13**.

Figure 3-12 Digital multimeter.

All samples were made from mortar mix S10. Copper plate electrodes (5mm x 15mm x 0.25 mm) were used, and their number depended on the tested configuration.
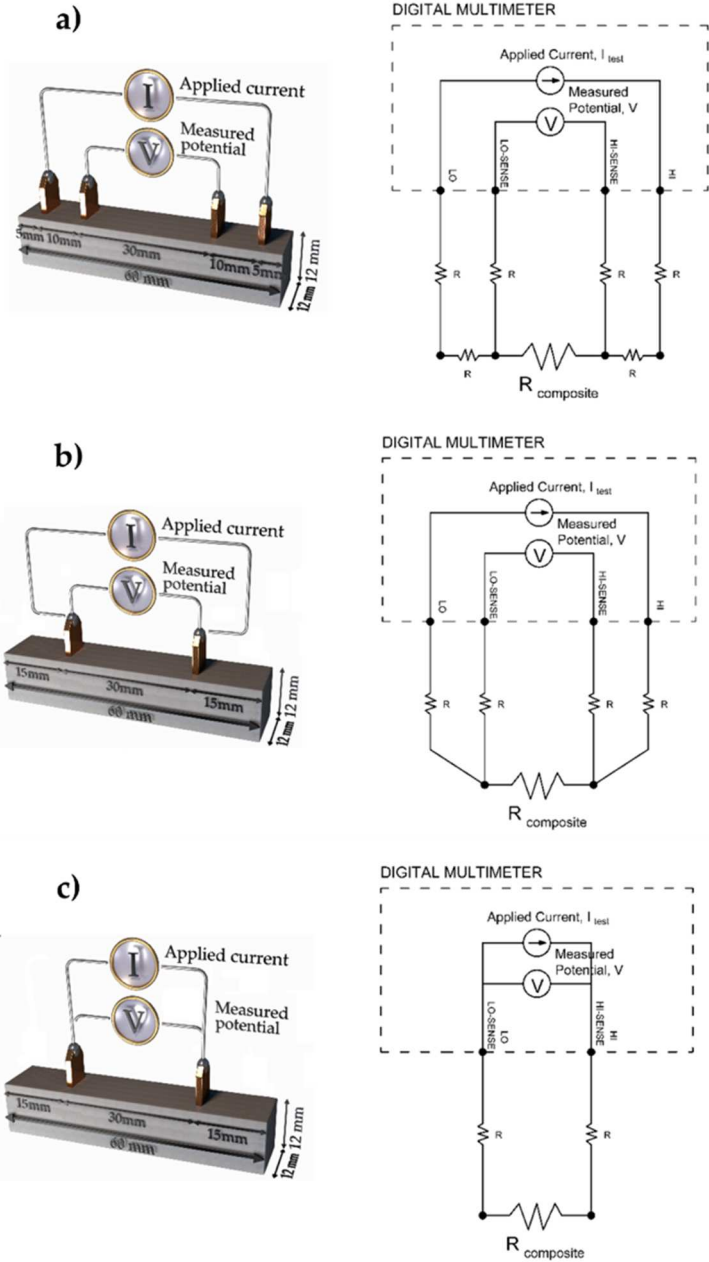
Figure 3-13 The studied configurations and the electrical diagrams of a) the four-probe method (EMI), b) the two-probe with four wires (Kelvin) method (EMII), and c) the two-probe method (EMIII).

For the EM I configuration, the electrical resistance was measured using the four-probe method. The direct current was applied between the two outer electrodes, and the potential was measured between the two inner electrodes. The distance between the inner electrodes was 30 mm, and the distance between the outer electrodes was 50 mm. The EM II configuration was a 4-wire Kelvin resistance measurement. The electrical measurement was done by connecting two wires on each HI and LO side. The test current flows between the two outside wires and the two wires inside to measure the potential difference. The two electrodes are at a distance of 30 mm. In the EM III configuration, which is set up similarly to EM II, the electrical measurements were done using a two-probe method. Two wires were connected to the electrodes. The current and potential difference measurements were made on the same wire.

Table 3-4 shows the comparison of average electrical resistance measurements, standard deviation, and percentage of coefficient of variation (CV) for all three configurations. The results show that the EM I configuration (the four-probe method) has the lowest variation coefficient and a small scatter of the data. The EMI configuration was used to measure the electrical resistance of SmartCem composites for all studies. To limit the polarization effect of SmartCem composite, the measurements were done after a stable electrical resistance reading was observed.

Table 3-4 Comparison between the results obtained using the proposed configurations.

Configuration	Average resistance (Ω)	Standard deviation, sd (Ω)	CV (%)
EM I	229856.229	6971.216	3.033
EM II	732502.550	76008.888	10.377
EM III	778297.891	81266.813	10.441

The electrical conductivity (σ_e) can be calculated using an **equation (4)**:

$$\sigma_e = \frac{1}{\rho} = \frac{L}{RA} \tag{4}$$

The fractional change in electrical resistivity (FCR) can explain the sensitive behavior of the composites by using the following **equation (5)**:

$$FCR\ (\%) = \frac{\Delta\rho}{\rho_0} \times 100 = \frac{\rho - \rho_0}{\rho_0} \times 100 \tag{5}$$

where: ρ is the electrical resistivity ($\Omega\cdot$m), ρ_0 is the initial electrical resistivity ($\Omega\cdot$m), L is internal electrode distance (m), A is electrode area (m²), and R is the measured resistance (Ω).

3.2.7   Sensing properties in small-scale testing

3.2.7.1   Load sensitivity

The piezoresistive properties of SmartCem composites were examined under varying loading conditions. The electrical resistance was measured at the same time as the load was applied. The mortar specimen was tested 28 days after casting. The stress was applied using a Wykeham Farrance 50 kN UCS loading machine, and the electrical measurement was conducted following the procedures outlined in **Section 3.2.6**.

For compressive stress sensing, the compression load was applied to the SmartCem mortar specimens placed vertically with a loading rate of 0.05 cm/min. During the bending test, a flexural load was applied to the SmartCem mortar specimens until they reached the point of failure. The specimens under investigation were positioned in a horizontal orientation. The load rate used in the experiment was 0.0001 cm/min. The test setups are shown in **Figure 3-14.**
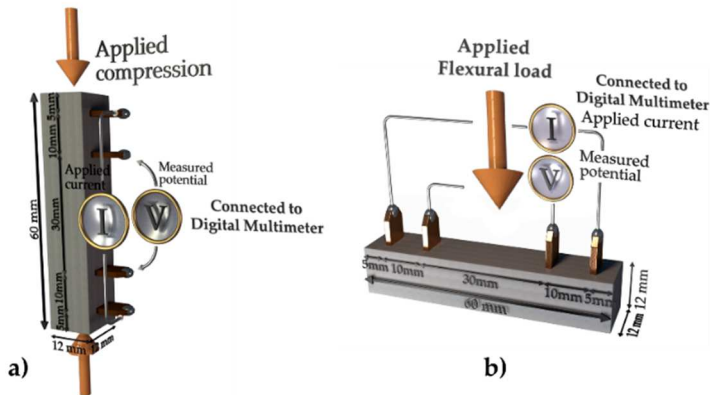
Figure 3-14 The electrical measurement setup under a) compression load and b) flexural load.

The stress sensitivity (S_σ) was calculated as follows:

$$S_\sigma \ (\% / MPa) = \frac{\Delta FCR_\sigma (\%)}{\Delta \sigma} \tag{6}$$

where: $\Delta\sigma = \sigma - \sigma_0$ is the change of stress between the stress σ and the initial stress σ_0.

3.2.7.2 Humidity sensitivity

The humidity chambers were prepared to study the humidity-sensitive properties of SmartCem composites. The custom-made chambers consisted of sealed glass containers containing various types of saturated salt solutions. These included lithium chloride (LiCl), potassium carbonate (K_2CO_3), sodium chloride (NaCl), and potassium sulphate (K_2SO_4), which can maintain relative humidities of 11%, 43%, 75%, and 97%, respectively (Young, 1967). A commercial humidity sensor of type SHT85 produced by Sensirion was installed in each container as a reference. The 28-day SmartCem mortars were kept in the controlled humidity chambers, and the electrical resistance was measured after 24 hours. **Figure 3-15** shows the test setup for humidity-sensitive properties. The humidity sensitivity ($S_{Humidity}$) was calculated as follows (Tang et al., 2011):

$$S_{Humidity}\ \left(\%/\%RH\right)=\frac{\left(\Delta\sigma/\sigma_0\right)\times100}{\Delta\%RH} \tag{7}$$

where: $\Delta\sigma$ is the change of electrical resistance, σ_0 is initial resistance and $\Delta\%RH$ is the change in relative humidity.
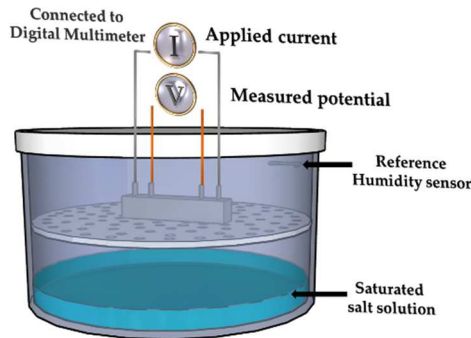
Figure 3-15 The test setup for humidity-sensitive studies of SmartCem mortar.

3.2.7.3 Temperature sensitivity

The temperature-sensitive property of SmartCem composites was studied across four distinct temperature conditions: -20°C, 0°C, 20°C, and 40°C. Prior to the start of the experiment, a protective layer of thin plastic sheeting was applied to the 28-day specimens in order to mitigate the potential influence of extraneous variables, such as humidity. All specimens were placed within a chamber that maintained a controlled temperature for a duration of 24 hours, and then the electrical resistance

measurements were started, **Figure 3-16.** The temperature sensitivity ($S_{Temperature}$) was calculated as follows:

$$S_{Temperature} \ \left(\% / °C\right) = \frac{\left(\Delta\sigma / \sigma_0\right) \times 100}{\Delta T} \tag{8}$$

where: $\Delta\sigma$ is the change of electrical conductivity, σ_0 is initial resistivity and ΔT is the change in temperature.
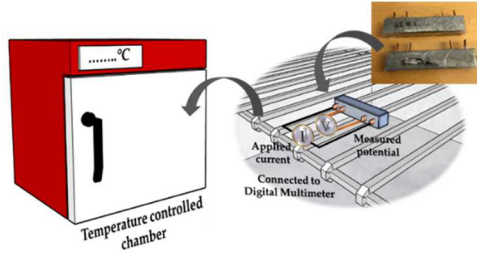
Figure 3-16 The test setup for temperature-sensitive studies of SmartCem mortar.

3.2.8 Semi-large-scale testing

Two types of concrete were produced for this study: NC 100 mm cube samples and a SCC beam, **Figure 3-17**. The SmartCem mortar containing 4 wt.% of SmartCem (S4) was embedded in the concrete immediately after casting to monitor the hydration processes (both temperature and humidity). The commercial humidity sensor type SHT85 produced by Sensirion and a thermocouple were also embedded near the SmartCem sensor as a reference. Following the casting process, a plastic sheet was applied to the upper surface of the specimens. The electrical measurements were continuously conducted over a period of 7 days, as shown in **Figure 3-17**.

After approximately four months, the SCC beam was tested with 3-point bending. Within this section, the SmartCem sensor functions as a stress or strain sensor. The stain gauge and Linear Variable Differential Transformer (LVDT) sensors were positioned in a close position to the SmartCem sensor as a reference. The test setup and the location of the embedded sensor are shown in **Figure 3-18.**
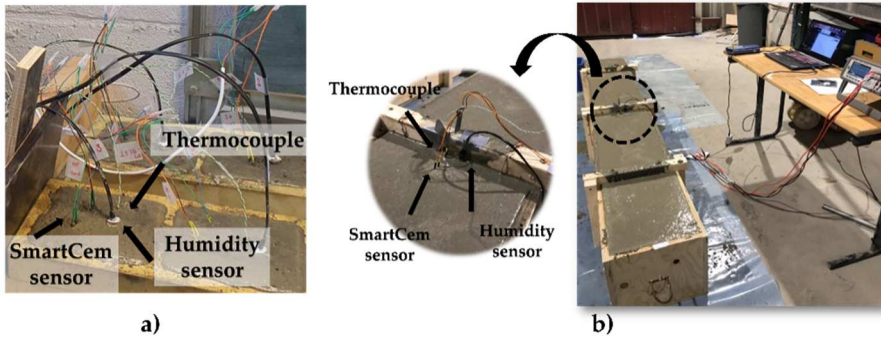
Figure 3-17 Arrangement of embedded sensors for hydration monitoring of a) the NC and b) the SCC beam.
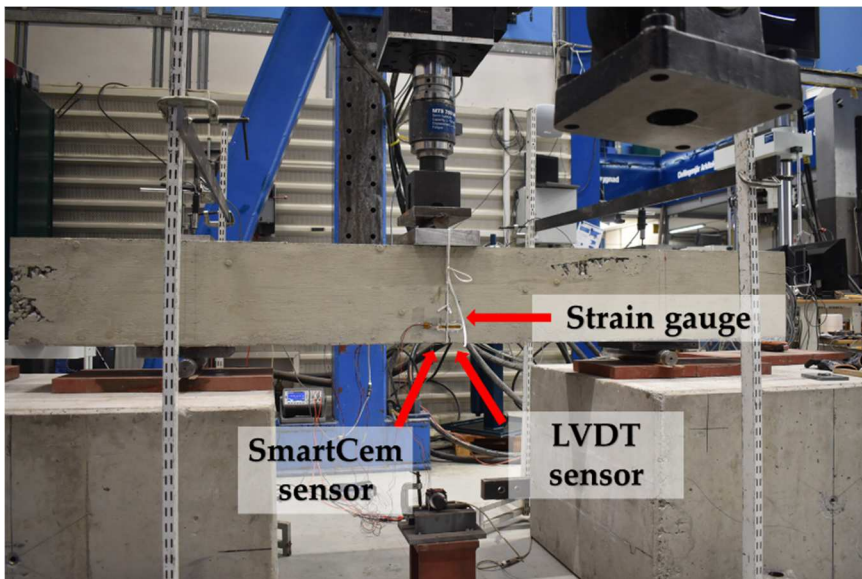
Figure 3-18 The test setup for SCC beam stress and strain monitoring.

3.2.9   Full-scale on-site monitoring

The SmartCem monitoring system was developed with the purpose of monitoring the condition of concrete structures through the implementation of SmartCem sensors. In the present work, the monitoring of a newly built bridge in Saittarova, Sweden, was selected to implement the SmartCem monitoring system to monitor the hydration process of the bridge deck and later to monitor the stress or strain and freeze-thaw cycles. The full-scale onsite monitoring tests have been ongoing while preparing this thesis; therefore, only some results are presented.

Chapter 4

Experimental study - results and discussion

4.1   Characterization of SmartCem

4.1.1   Morphology

The morphology of the SmartCem particles was examined using the Jeol JSM-IT100 scanning electron microscope (SEM). The images were acquired utilizing the secondary electron detector (SED) at magnifications of 12,000x. The accelerating voltage was 7 kilovolts (kV), while the accelerating current was 30 microamperes (µA). **Figure 4-1** shows carbon-based nanomaterials deposited on the cement particles for SmartCem I and SmartCem II. Based on the SEM images, it can be observed that the predominant type of carbon nanomaterial present is carbon nanofibers (CNFs). The formed CNFs were very curly. The diameter was 10-50 nm, whereas the length, as estimated from the obtained images, varied between 3 µm and 20 µm for both types of SmartCem.
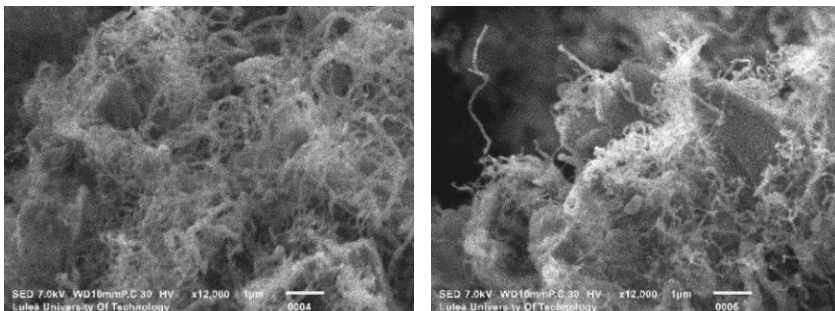
Figure 4-1 SEM images of SmartCem I (left) and SmartCem II (right) (Buasiri et al., 2019)

4.1.2   Energy Dispersive Spectrometry (EDS) analysis

The elemental composition of SmartCem I was determined using EDS spectroscopy from Bruker (Bruker Corporation, Billerica, MA, USA). The carbon content of SmarCem I was determined at three different locations where CNFs were observed. The results, presented in **Table 4-1**, indicated that the normalized carbon content ranged from 9 wt.% to 27 wt.%. This variation was related to the number of CNFs being penetrated by the electron beam. The SEM-EDS image showed that CNFs do not form a complete coverage of the cement surface, **Figure 4-2**. CNFs were formed only in certain locations where the catalyst was available. The catalytic sites contained ferrite and aluminate phases (Warakulwit et al., 2015).
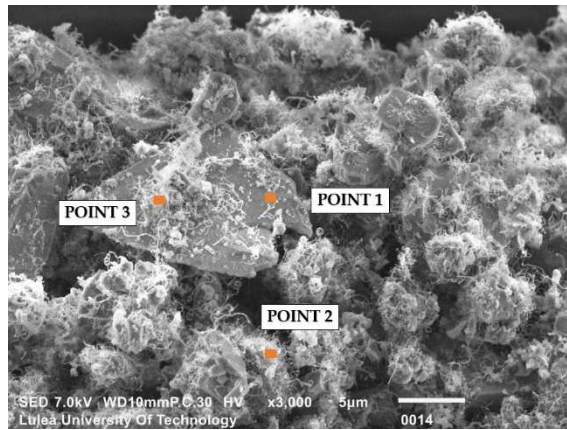
Figure 4-2 SEM-EDS image of SmartCem I

Table 4-1 Quantitative results obtained by EDS analysis for SmartCem I

Element in SmartCem I (wt. %)	C	O	Mg	Al	Si	S	K	Ca	Fe
POINT 1	8.98	20.16	2.71	1.34	9.77	3.98	1.32	50.91	0.83
POINT 2	17.51	20.26	2.54	1.57	9.42	3.72	1.26	42.66	1.06
POINT 3	26.96	23.19	2.32	1.87	8.28	2.91	1.22	31.96	1.29

4.1.3   Thermogravimetric (TG) analysis

Thermogravimetric (TG) analysis was performed using a thermal analyzer type NETZSCH STA 449F3 Jupiter® with a temperature increase rate of 10 °C/min and an

operating temperature range between 20 and 1,000 °C in the air atmosphere flowing at 50 mL/min. **Figure 4-3** shows the recorded weight loss profiles. The weight losses between 20-450°C, 450-650°C, and 650-800°C were attributed to the loss of adsorbed water molecules, the decomposition of carbon deposits (Dunens et al., 2009), and the de-carbonation of calcium carbonate ($CaCO_3$) (De la Torre et al., 2001), respectively. The mass loss was used to estimate the quantities of carbon phases (mostly CNFs) in SmartCem. The estimated quantities equaled approximately 2.71 wt.% and 2.51 wt.% for SmartCem I and SmartCem II, respectively. With a higher amount of carbon-based materials, SmartCem I was selected and used to produce the nanomodified Portland cement composite for further studies. Note that the SmartCem mentioned in the following work refers to the SmartCem I.
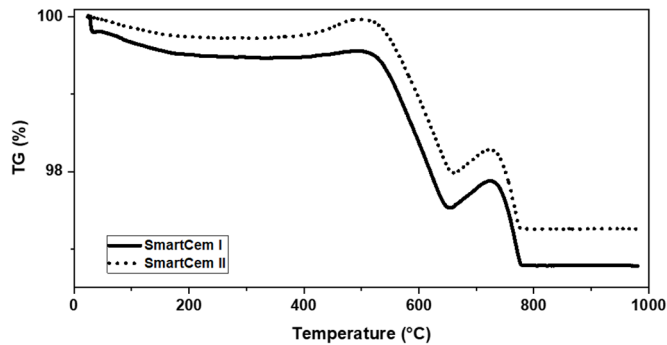
Figure 4-3 TG analysis of SmartCem I and SmartCem II (Buasiri et al., 2019).

4.2 Sensing capability of SmartCem composites in small-scale laboratory testing

4.2.1 Sensing response under compression

The load-sensing capability of SmartCem composites is directly related to their piezoresistive response. Piezoresistive response refers to the phenomenon where the electrical properties of a composite change when it is subjected to mechanical strain or stress. The partial substitution of Portland cement by the SmartCem material has affected the piezoresistive response of the mortar samples. **Figure 4-4** and **Figure 4-5** show the response of SmartCem mortars under compressive stress. The findings of this study indicate that, across all samples containing varying quantities of SmartCem, there was a decrease in the fractional change in electrical resistivity as the compressive stress increased, until its failure.
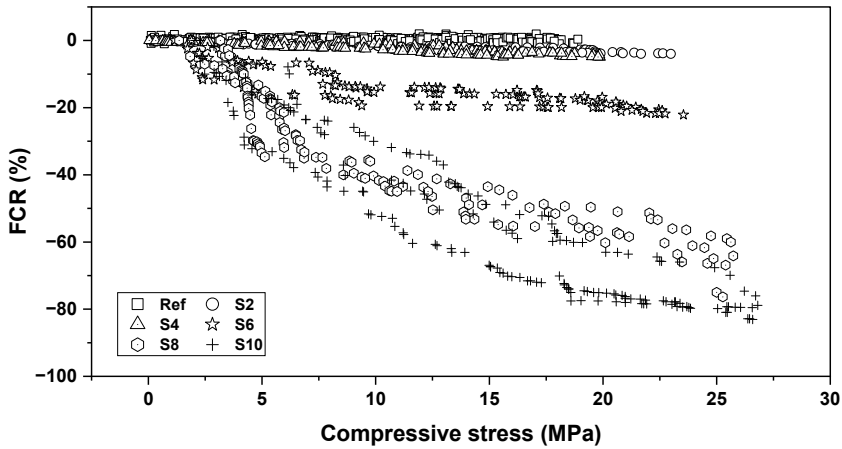
Figure 4-4 Fractional change in electrical resistivity of the SmartCem mortars under compressive stress (Data from paper II, III and VI).

There are three distinct groups of piezoresistive responses, while the reference sample stays unchanged, **Figure 4-5 a)**. In the first group, S2 and S4 samples exhibited little piezoresistive effects in response to the applied compressive stress, **Figure 4-5 b) and c)**. This phenomenon could be attributed to the limited quantity of conductive materials, which led to the inter-particle distance of the conductive cement particles being too large. Thus, less electrically conductive paths can be formed through the composite. In the subsequent group, S6 samples showed a moderate change in FCR up to approximately 20%, **Figure 4-5 d)**. In the final group, S8 and S10 samples exhibited a strong piezoresistive response, with the FRC reaching approximately 90% at the ultimate compressive stress point, **Figure 4-5 e) and f)**.

SmartCem composites showed a piezoresistive response in two stages of nearly linear relationships. In the first stage, mortar samples, especially S6, S8, and S10, had a very high sensitivity to the applied compressive load up to around 6 MPa. In the second loading stage, from 6 MPa until failure, the change was smaller. The piezoresistive response can be related to the intrinsic piezoresistive property of the CNFs. The applied compressive load leads to the deformation-induced formation of effective conductive paths as well as changes in the tunneling distance and the contact points.
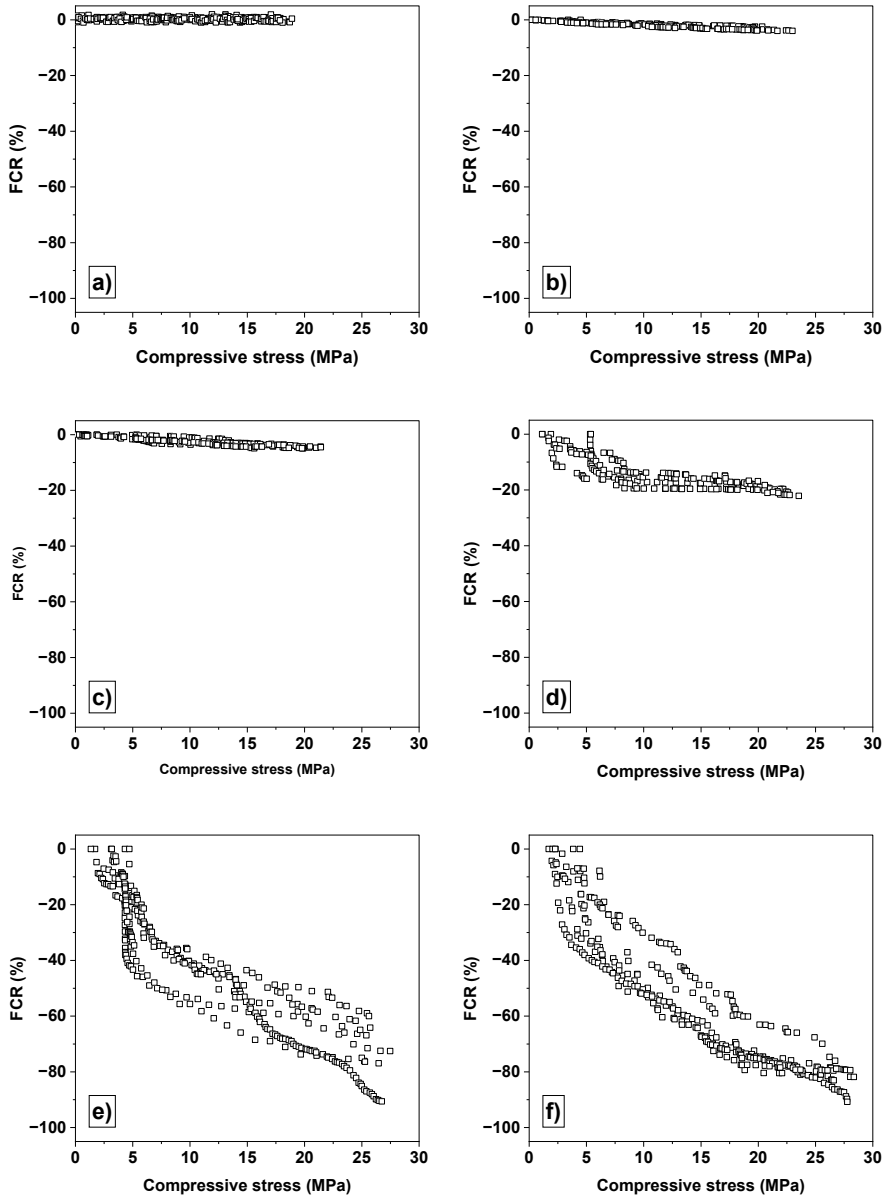
Figure 4-5 Fractional change in electrical resistivity of the SmartCem mortars under compressive stress of a) Reference, b) S2, c) S4, d) S6, e) S8, and f) S10. (Data from paper II, III and VI).

The SmartCem composites showed a negative stress sensitivity coefficient under the applied compressive stress. The calculated stress sensitivities of mortar samples using **equation (6)** are presented in **Table 4-2.** The highest sensitivity was achieved in the samples containing 10 wt.% of the SmartCem. The sensing capability of the studied composites could be related to the amount of CNF present in the matrix and, thus, to the percolation threshold. Based on the results obtained, the percolation threshold values were around 7 wt.% of the SmartCem (~0.1897 wt.% of CNFs), **Figure 4-6**.

The SmartCem composites appear to be potentially suitable for applications for stress sensors and smart concrete structures as it showed significantly higher sensitivities in comparison with earlier results shown in **Table 4-3.** Earlier studies achieved lower stress sensitivity. For example, (Yu & Kwon, 2009) reached an 8.4% change in the electrical resistivity for an applied compressive load of 5.2 MPa, while (Danoglidis et al., 2016) showed a higher sensitivity, reaching 12% for 5.0 MPa of the samples containing the same amount of MWCNT at 0.1 wt.%. (Thomoglou et al., 2023) studied the piezoresistive sensibility of mortar containing 0.1 wt.% SWCNT, which reached approximately a 30% change in impedance.
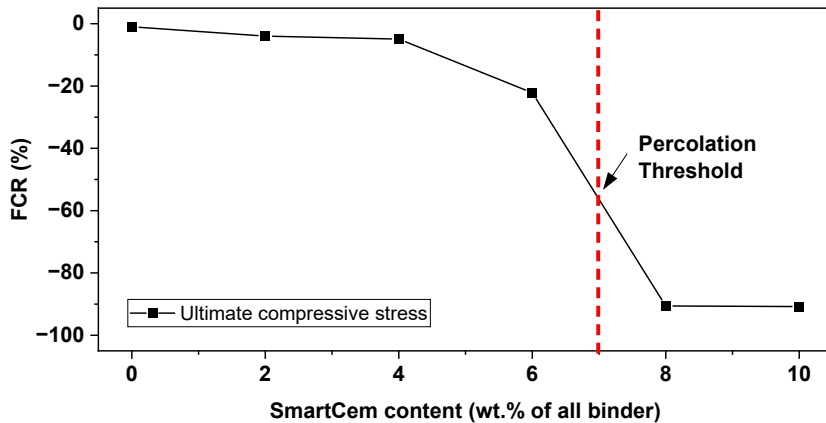
Figure 4-6 Effects of SmartCem content on the fractional change in electrical resistivity under applied the ultimate compressive stress of mortar samples.

Table 4-2 The calculated sensitivity of SmartCem composites under compressive stress.

Mix	Calculated stress sensitivity coefficient, $S_{\sigma,comp}$ (%/MPa)
Ref	~0
S2	-0.176
S4	-0.253
S6	-0.962
S8	-3.220
S10	-3.343

Table 4-3 Change in electrical properties of cementitious composites containing carbon-based materials under applied compressive stress by other researchers compared with results obtained from mix S10.

Reference	Amount of conductive materials	Applied stress (MPa)	
		Change in electrical properties	
(Yu & Kwon, 2009)	0.06 wt.% MWCNT	5.2	8.6
		8.8 %	10.3 %
	0.10 wt.% MWCNT	5.2	8.6
		8.4 %	11.4 %
(Danoglidis et al., 2016)	0.10 wt.% MWCNT	5.0	-
		12 %	
	0.50 wt.% MWCNT	5.0	-
		3 %	
(Zhang et al., 2017)	2.14 vol.% MWCNT	4.0	-
		6.8 %	
(Thomoglou et al., 2023)	0.10 wt.% SWCNT	-	8.0
			30 %
	0.50 wt.% CF	-	8.0
			6 %
Present work mix S10	0.271 wt.% CNF	5.0	26.0
		~40 %	~90 %

4.2.2   Sensing response under three-point bending

Under bending, the tension and compression sides of sensing composites exhibit opposite behaviors, consistent with the sensing behavior under tension and compression alone. The sensitivity of the tension side is greater than that of the compression side when subjected to the same deflection of the sensing composite. The sensing behavior of the composites, considering through-thickness under applied flexural load, becomes complicated due to the compensation of the electrical properties between the tension zone and the compression zone (S. Ding et al., 2019). **Figure 4-7** shows the relationship between the fractional change in electrical resistivity of the SmartCem composites and the flexural stress in a three-point bending test. Based on the trend of the curve, the fractional change in electrical resistivity increased with increasing flexural stress.
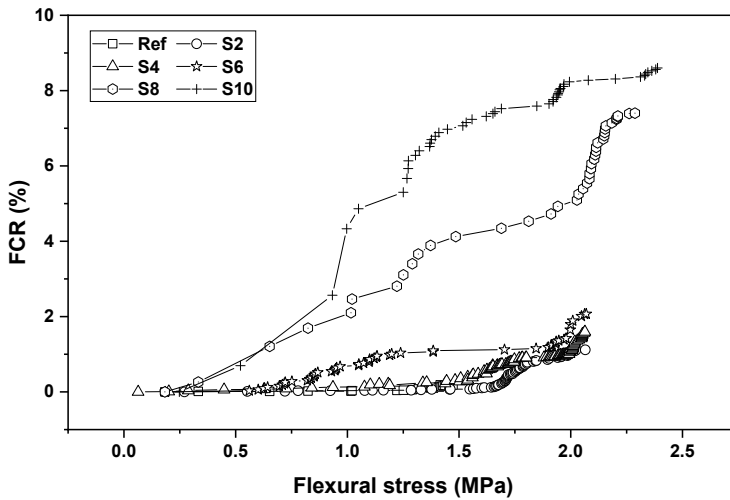
Figure 4-7 Fractional change in electrical resistivity of the SmartCem mortars under flexural stress.

The response can be categorized into two main regimes. The first contains small increases in the FCR of the composite, while the second contains a sudden increase in the FCR, which is typically linked to multiple crack formation and propagation, see the red circle in **Figure 4-8**. The two regimes demonstrate the remarkable damage sensing potential of the composites, wherein a sudden increase in the FCR could provide early warnings of an upcoming catastrophic failure.

There are three distinct groups of piezoresistive responses under flexural load. The first group consists of reference, S2 and S4 samples, the FCR remains unchanged up to the flexural stress of around 1.5 MPa and followed by an abrupt change until failure, **Figure 4-8 a), b) and c)**. The S6 sample was more sensitive, with cracks detected earlier at the flexural stress of 0.5 MPa, **Figure 4-8 d)**. The last group, S8 and

S10, showed a strong piezoresistive response. FCR increased continuously, which was attributed to the merging of multiple crack paths and the complete collapse of the conductive network. That corresponded to an approximately 8% increase in the fractional change of electrical resistivity, **Figure 4-8 e) and f).**
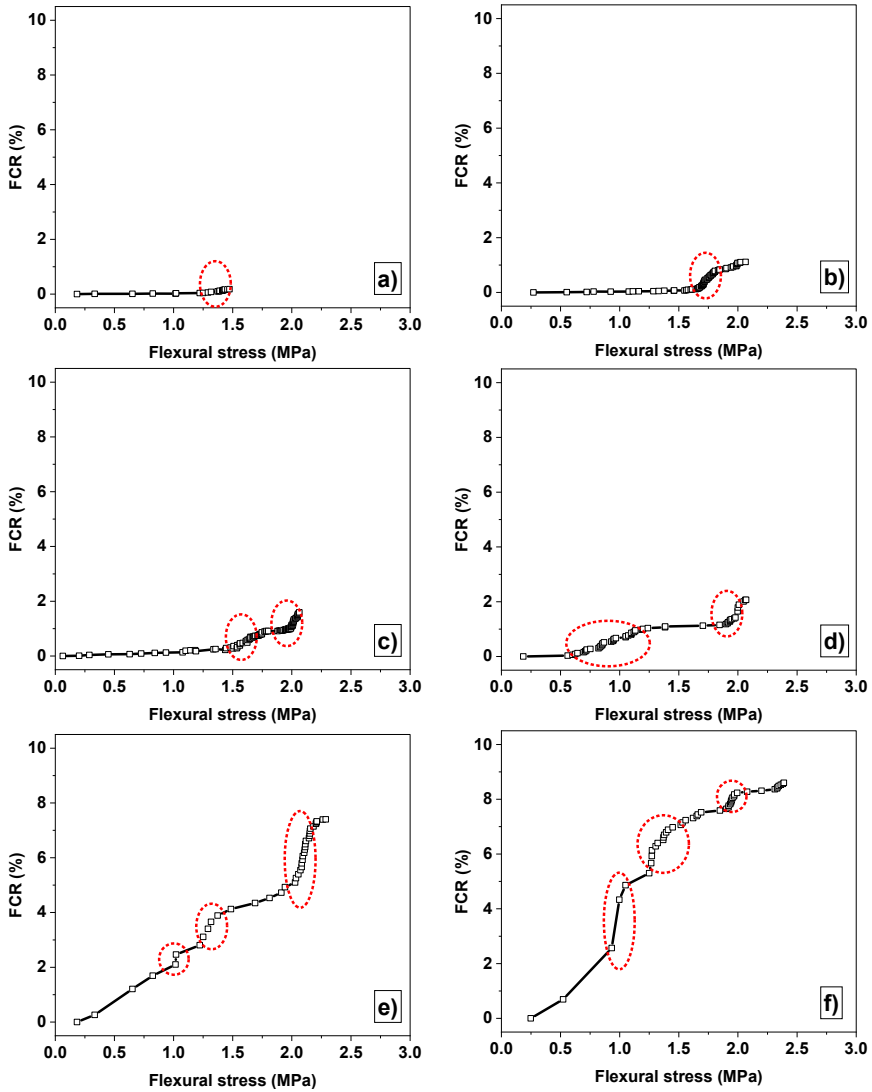
Figure 4-8 Fractional change in electrical resistivity of the SmartCem mortars under flexural stress of a) Reference, b) S2, c) S4, d) S6, e) S8, and f) S10.

The calculated stress sensitivity of mortar samples subjected to flexural stress using **equation (6)** is presented in **Table 4-4.** The highest sensitivity was achieved for samples containing 10 wt.% of the SmartCem with a sensitivity value of 4.018 %/MPa. According to the percolation theory, the percolation threshold values were around 7 wt.% of the SmartCem (~0.1897 wt.% of CNFs), **Figure 4-9.**

Table 4-5 shows examples of the flexural piezoresistive sensing capability of cementitious composites incorporating varying amounts of carbon-based materials. The FCR of S10 reached around 9% at the applied ultimate flexural stress, with the mortar containing a low amount of CNFs. The flexural sensing capability sensing composites contained 0.6 wt.% CNFs and 0.6 wt.% MWCNTs showed the same FCR of 8% as reported by (Dalla et al., 2016) and (Naeem et al., 2017), respectively. The obtained results demonstrated that the SmartCem composites have the potential to be used as damage sensors, with their sensitivity being higher in comparison with other sensing cement-based composites.
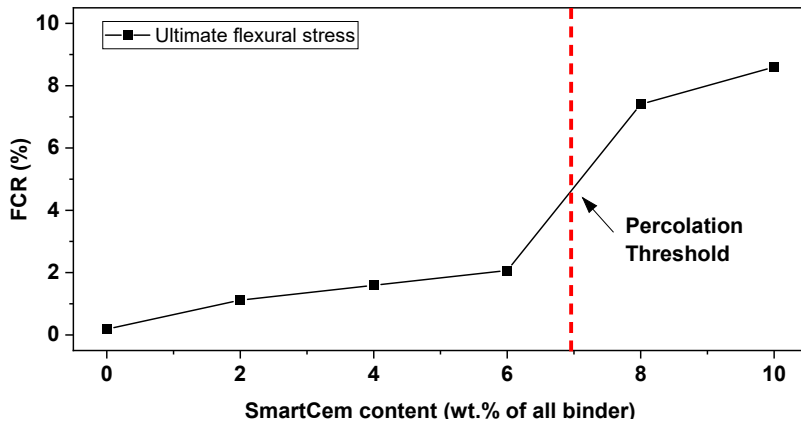
Figure 4-9 Effects of SmartCem content on the fractional change in electrical resistivity under applied ultimate flexural stress of mortar samples.

Table 4-4 The calculated sensitivity of SmartCem composites under flexural stress.

Mix	Calculated stress sensitivity coefficient, $S_{\sigma,bend}$ (%/MPa)
Ref	0.168
S2	0.622
S4	0.797
S6	1.098
S8	3.518
S10	4.018

Table 4-5 Comparison of change in electrical properties of cementitious composites containing carbon-based materials under applied flexural stress.

Reference	Amount of conductive materials	Change in electrical properties
(B. Chen & Liu, 2008)	0.8 wt.% CF	~2 %
(Dalla et al., 2016)	0.6 wt.% CNF	~8 %
(Naeem et al., 2017)	0.3 wt.% MWCNT	~0.4 %
	0.6 wt.% MWCNT	~8 %
Present work mix S10	0.271 wt.% CNF	~9%

4.2.3 Sensing response under variable ambient humidity

The most common phenomenon for humidity-sensitive properties of sensing cement-based composites is a change in the electrical conductivity due to the absorption or desorption of water molecules. The variation of ambient humidity affects the internal humidity level and movement of the free water in the composites, leading to a change in the electrical conductivity.

The recorded electrical conductivities of the SmartCem composites exposed to four different ambient humidity levels are presented in **Figure 4-10**. The obtained results showed that the electrical conductivity increased with higher humidity for all samples. At 11% RH, all mortar samples showed a similar electrical conductivity of approximately 4×10^{-3} S/m. Mortars incorporating 2-6 wt.% of SmartCem showed a similar weak response as the reference mortar samples of around 0.4 **%/ %RH**. The

maximum sensitivity was obtained for the S10 sample, with a sensitivity of 9.653 **%/ %RH, Table 4-6.** The percolation threshold was around 7 wt.% of SmartCem, which corresponded to around 0.19 wt.% of CNFs, **Figure 4-11.**
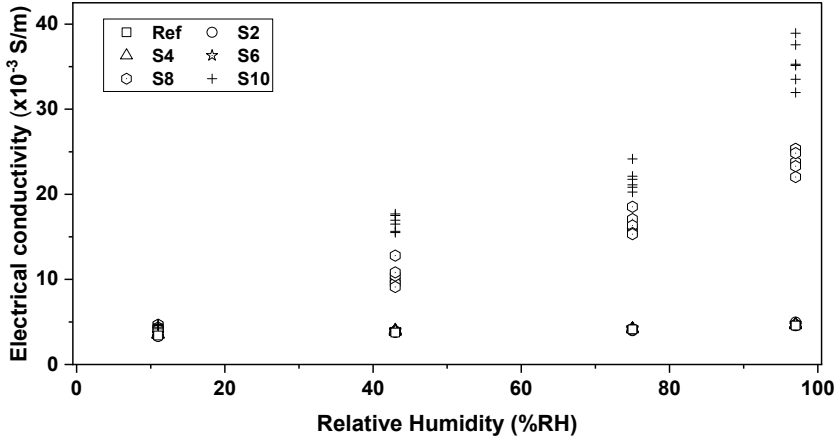
Figure 4-10 Effects of ambient relative humidity on the electrical conductivity of the SmartCem mortars. (Data from paper IV and VI).
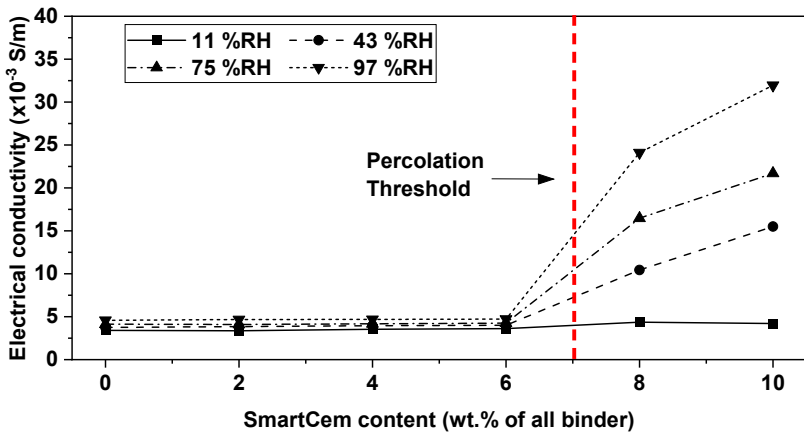
Figure 4-11 Effects of SmartCem content and ambient relative humidity on the average electrical conductivity (Data from paper IV and VI).

Table 4-6 The calculated humidity sensitivity of SmartCem composites over the range 11%RH to 97 %RH. (Data from paper IV and VI).

Mix	Calculated humidity sensitivity coefficient of conductivity, $S_{Humidity}$ (%/ %RH)
Ref	0.356
S2	0.379
S4	0.399
S6	0.454
S8	6.616
S10	9.653

4.2.4   Sensing response under varied ambient temperature

The relation between temperature and electrical conductivity is presented in **Figure 4-12**Error! Reference source not found.**.** The results showed increasing electrical conductivity with increasing temperature for all samples. A very similar trend was observed for Ref, S2, S4, and S6 samples, with a small change in electrical conductivity in the temperature range between -20 ℃ and 40 ℃. However, S8 and S10 samples showed a moderate change in conductivity when exposed to temperatures between 20 ℃ and 40 ℃.
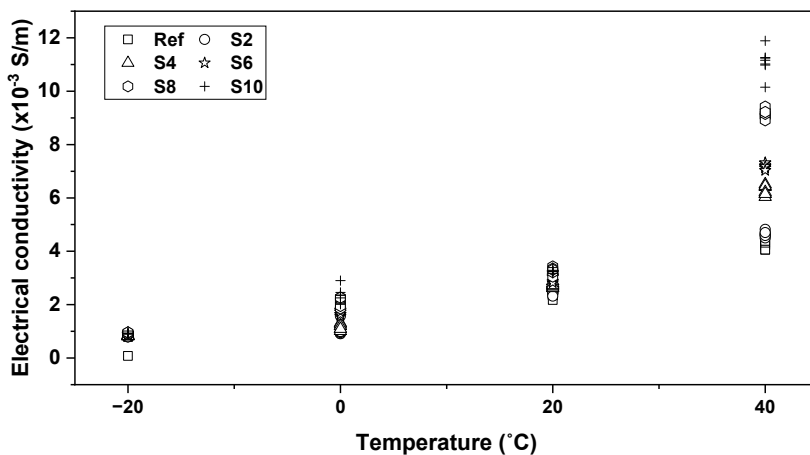
Figure 4-12 Effects of ambient temperature on the electrical conductivity of the SmartCem mortars (Data from paper V and VI).

Table 4-7 shows the calculated temperature sensitivity of all mortar samples. There was a small increase in sensitivity as the quantity of SmartCem increased. This could be related to a higher number of thermally activated charge carriers. A higher amount of CNFs has presumably formed conductive interconnected networks

throughout the solidified binder matrix. The highest temperature sensitivity was measured for the cementitious composites containing 10 wt.% of SmartCem. Its sensitivity was shown to be roughly 11% higher when compared to the reference sample. The percolation threshold value for the studied mortars could be estimated based on **Figure 4-13.** Independently of the temperature, the percolation threshold was estimated to equal ~5 wt.% of the nanomodified Portland cement, which corresponded to ~0.136 wt.% of CNFs.

Table 4-7 The calculated temperature sensitivity of SmartCem composites over the range -20 ˚C to 40 ˚C. (Data from paper V and VI).

Mix	Calculated temperature sensitivity coefficient of conductivity, $S_{temperature}$ (%/ ˚C)
Ref	7.151
S2	7.923
S4	10.976
S6	11.996
S8	14.882
S10	18.315
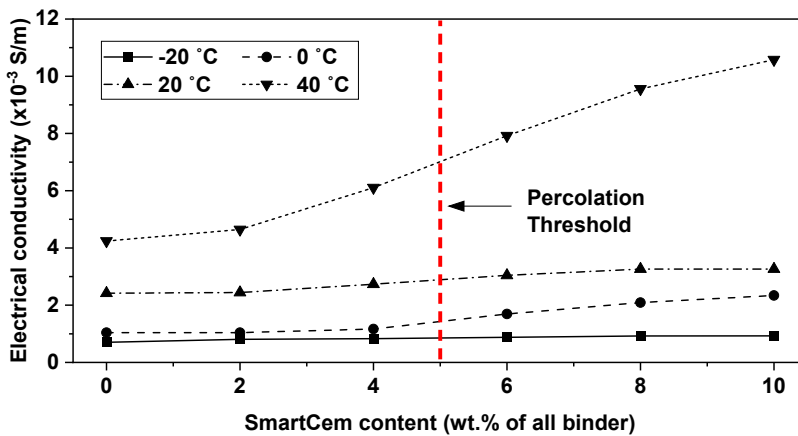
Figure 4-13 Effects of SmartCem content and exposed temperature on the measured electrical conductivity (Data from paper V and VI) .

4.3   SmartCem composites as a monitoring sensor in semi-large-scale laboratory testing

4.3.1   Hydration monitoring

The monitoring of the hydration process is primarily focused on temperature, humidity, and moisture content. The impact of these parameters on the observed electrical resistivity measured by the developed cement-based sensors was assessed. The hydration monitoring of normal strength concrete (NC) was conducted by using the reference sensors (Ref), which did not contain CNFs and SmartCem sensors containing 4 wt.% of SmartCem (S4). The humidity sensor type SHT-85 from Sensirion and a thermocouple were used as references. The moisture content of the NC was measured using the oven-drying method. All sensors were embedded at 50 mm depth into the 100 mm NC cube, **Figure 3-8.** The variations in electrical resistivity were observed throughout the first seven-day period, **Figure 4-14.** The reference mortar sensor showed a nearly linear relationship between resistivity and passing time. The SmartCem mortar sensor showed changes in electrical resistivity that corresponded to the kinetics of Portland cement hydration.

A continuous increase in electrical resistivity was observed for the reference mortar during the entire measuring period. This increase was only related to the decrease in moisture content due to cement hydration, **Figure 4-14 c)**.

In the case of the SmartCem sensors, changes in electrical resistivity can be related to the hydration process. Generally, the electrical resistivity of the cementitious matrixes is affected by the chemical composition of the pore solution, the connectivity of pores, the fraction of capillary porosity, and the volume fractions of the hydration products (Z. Liu et al., 2014). Thus, the first rapid decrease in resistivity could be attributed to the increasing concentration of calcium (Ca^{2+}), sodium (Na^+), potassium (K^+), hydroxyl ions (OH^-), and sulfate (SO_4^{2-}) ions due to the ongoing dissolution of Portland cement particles (Tu et al., 2021). After the initial dissolution, there is a period of relatively slow progress. This could be related to the competitive balance between the ion dissolution and formation of the hydration products, especially ettringite and calcium hydroxide. The electrical resistivity might fluctuate during this stage. Later, with the progressing hydration processes, the formation of hydration products is enhanced, thus leading to increased electrical resistivity. This could also be related to the significantly decreased number of charged ions present in the pore solution (Tu et al., 2021). The maximum measured resistivity reached around 6000 Ω.cm 48 hours after casting. At a later time, the hydration slows down, and hydration products tend to be thicker and larger, while the capillary porosity is significantly reduced, leading to the observed decrease in the electrical resistivity. After that period, a nearly constant and slightly decreasing electrical resistivity was

measured. The reduced number of ions present in the pore solution due to progressing hydration and the densification of the binder matrix microstructure, which facilitated electron jumping between CNFs could be indicated as the main causes. Other factors could also include lower pore connectivity (El-Enein et al., 1995; Tu et al., 2021; Wei & Xiao, 2013).

Cement hydration is a complex process involving various chemical reactions, and the microstructure of the hydrated cement paste greatly influences the properties of the concrete. Several parameters affect changes in electrical properties during the hydration process. Therefore, the consideration of a correlation between only one parameter, either the hydration temperature, humidity, or moisture content, and the electrical resistivity measured by the mortar sensors was weak. **Figure 4-14 a)** shows the temperature of NC cubes varied between 23 °C and 25 °C, and in this range, the temperature sensitivity of both the Ref and S4 sensors was very low, **Figure 4-12**. Thus, these results indicated that the electrical conductivity is independent of the developed temperature during the early stage of hydration for the SmartCem sensors.

The hydration monitoring using SmartCem sensors was also studied on another type of cement and a larger structure. **Figure 4-15** shows the recorded electrical resistivity of SmartCem sensors and the temperature measured by thermocouples of beam made of self-compacting concrete (SCC). Changes in electrical resistivity were well aligned with the ongoing hydration processes.

Overall, the results showed that the SmartCem sensor could be potentially used to monitor the hydration process of concrete.
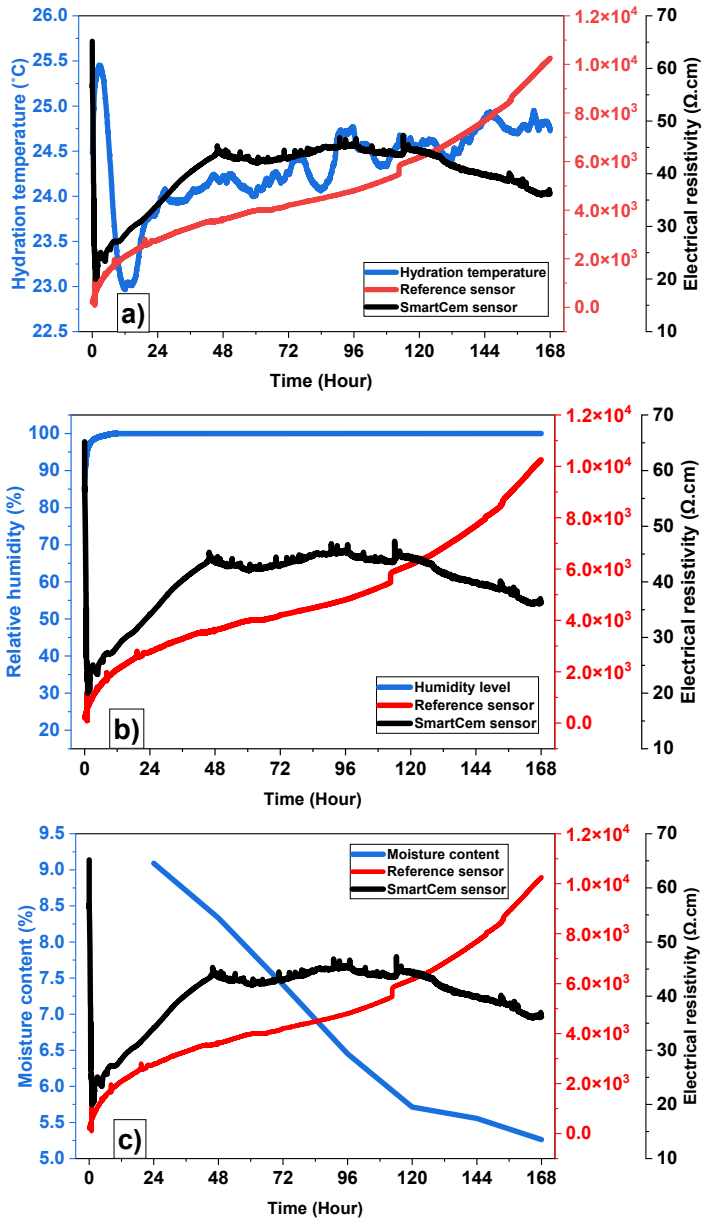
Figure 4-14. The change in electrical resistivity of NC was measured by the Ref sensor and the SmartCem sensor (S4) versus a) the hydration temperature b) humidity development and c) moisture content of NC for 7 days. (Data from paper V)
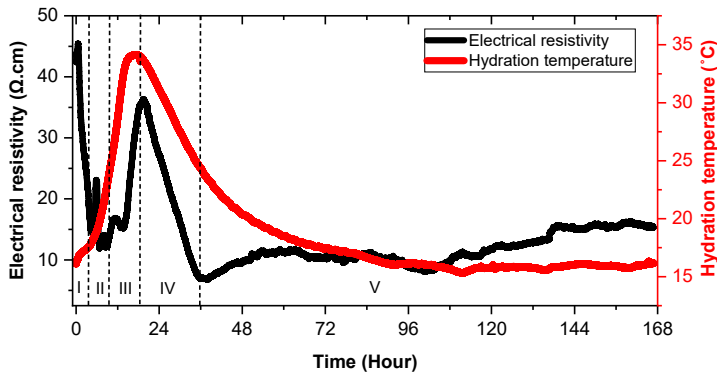
Figure 4-15 The measured electrical resistivity of the SCC beam obtained by the SmartCem sensor and the hydration temperature evolution for 7 days. (Buasiri, et al., 2023a)

4.3.2   Stress-Strain monitoring

The SCC beam was four months old when the stress-strain monitoring using the SmartCem was done. The beam was subjected to flexural stress with three-point bending. The SmartCem sensor (S4) was embedded near the concrete surface (25 mm depth from the surface) at the middle span of the SCC beam immediately after casting. The strain gauge was installed on the concrete surface as a reference at almost the same location as the SmartCem sensor.

The variation pattern of the electrical resistivity of the SmartCem sensor due to the applied flexural stress is shown in Figure 4-16. The change in electrical resistivity of the SCC beam was measured by the SmartCem sensor (S4) versus the applied flexural stress until the failure time. **Figure 4-16**. Based on the trend of the electrical resistivity vs. flexural stress curve, the response can be categorized into two main regimes. The first is the elastic regime, in which the stress increased until the point of fluctuation was approximately 3 MPa. In this stage, the concrete surface at the bottom is subjected to tensile stresses, and the electrical resistivity increases when the flexural stress increases. The second regime occupies a range after the elastic state and until the ultimate failure point. At this point, small cracks may start to form in the tensile zone of the SCC concrete. As the stress increases beyond the yield point, the cracks continue to propagate, and the concrete starts to exhibit plastic deformation. The reinforcement bars embedded within the concrete resist the tension and help control the crack width. At this time, the concrete surface transitions from being tensile to being compressive, resulting in a decrease in the electrical resistivity when increasing the flexural stress. It can be presumed that the flexural stress at the middle bottom of the SCC beam can be monitored by using the embedded SmartCem sensor. The electrical resistivity is directly proportional to the applied flexural stress

until reaching the yield point, then the resistivity is inversely proportional to the applied loading until the rupture point.
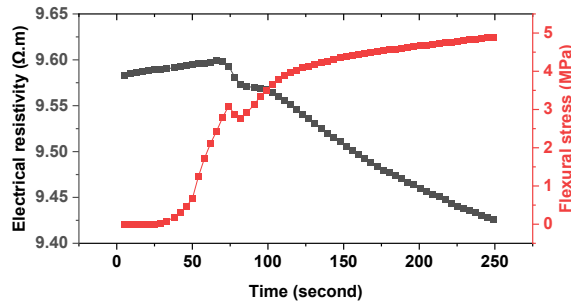
Figure 4-16. The change in electrical resistivity of the SCC beam was measured by the SmartCem sensor (S4) versus the applied flexural stress until the failure time.

To study the strain monitoring of the SCC beam, a commercial strain gauge was installed as a reference for comparison**. Figure 4-17** shows the change in electrical resistivity of the embedded SmartCem sensor and the response from the strain gauge. The variations in electrical resistivity recorded by the SmartCem sensor could reflect changes in length in the axial direction of the SCC beam measured by a strain gauge. The electrical resistivity increased when the strain increased. At the elastic stage, the electrical resistivity increased with strain. It is linked to the stretching of the tested SCC beam under load, which increased the distance between the CNFs and thus resulted in higher electrical resistivity. On the other hand, when the applied flexural load was beyond the yield point, the concrete surface turned from tensile to compression. This resulted in a gradual strain decrease along with the measured electrical resistivity. The obtained results showed that the SmartCem sensor could be used as a monitoring sensor in a structural monitoring system.
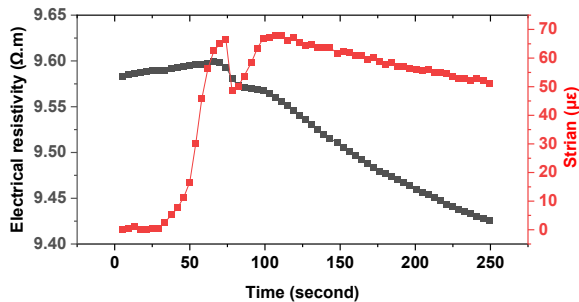
Figure 4-17 The change in electrical resistivity of the SCC beam was measured by the SmartCem sensor (S4) versus the change in strain measured by a commercial strain gauge under the applied flexural load until the failure time.

4.4 Full-scale field testing

To verify the laboratory test results, full-scale onsite monitoring has been conducted. During the preparation of this thesis, the field test was still ongoing. Therefore, only results related to 3 days of monitoring hydration are presented. The used SmartCem monitoring system is shown in **Figure 4 18.** The system consists of four main parts: the data acquisition system, the real-time accessibility system, the electricity supply system, and the data analysis system.

Figure 4-18 The design of the SmartCem monitoring system.

The new-build concrete bridge used in this study was provided by the Swedish Transport Administration (Trafikverket). The bridge is located in Saittalova (the northern part of Sweden). Structural drawings and positions of installed sensors are shown in **Figure 4-19** and **Figure 4-20**, respectively.
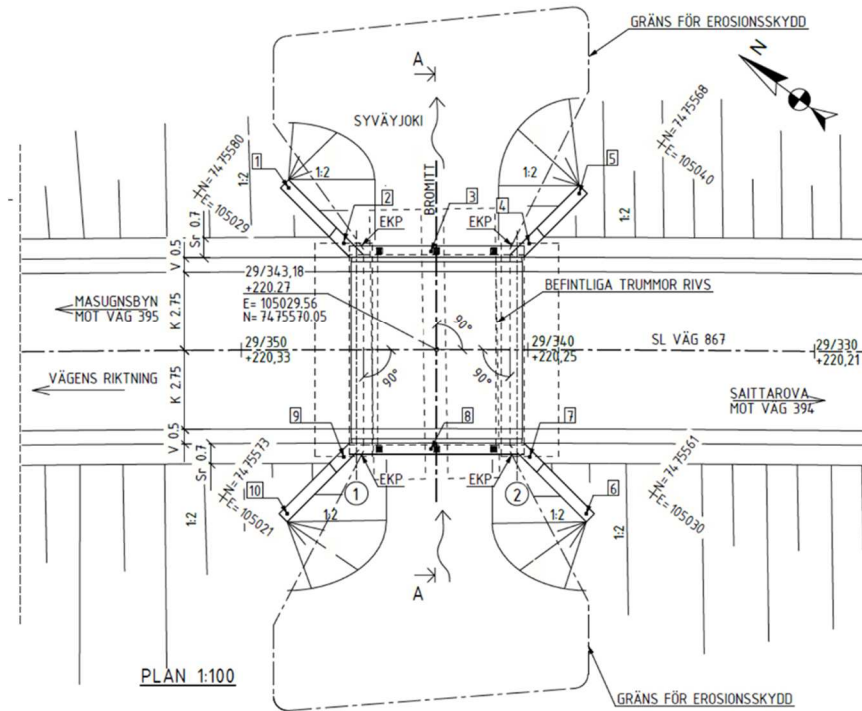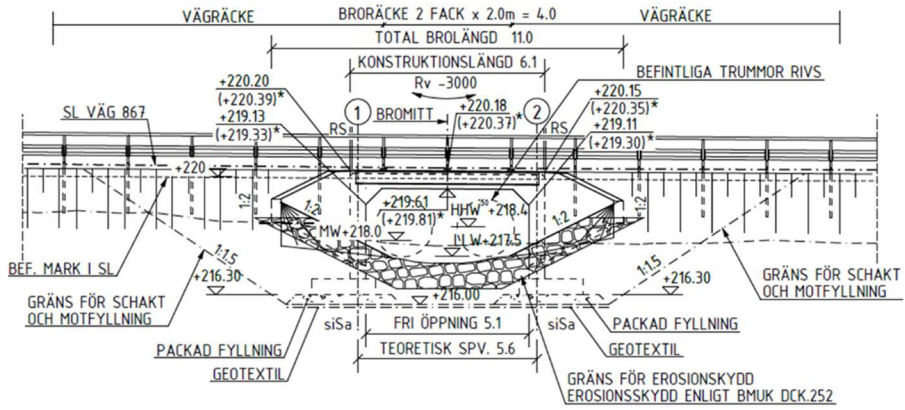
Figure 4-19 Plan and side view of the studied concrete bridge.
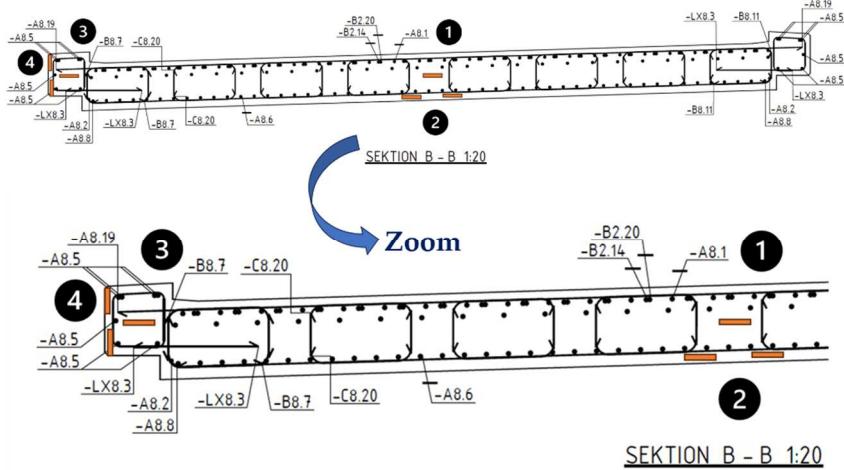
Figure 4-20 Four locations of installed sensors, including SmartCem sensors and commercial reference sensors.

The results reported in this section focus on the hydration monitoring of the concrete bridge deck at location 1, **Figure 4-20**. The SmartCem sensor (S8) was placed at a depth of roughly 200 mm from the surface, beside a commercially available thermocouple. **Figure 4-21** shows the variation of the electrical resistivity of the bridge measured by the SmartCem sensor over a period of three days. The recorded electrical resistivity showed a consistent pattern with the kinetics of hydration, which were well aligned with a change in temperature during ongoing hydration processes. **Figure 4-22 and Figure 4-23** show a few pictures taken at the construction site.
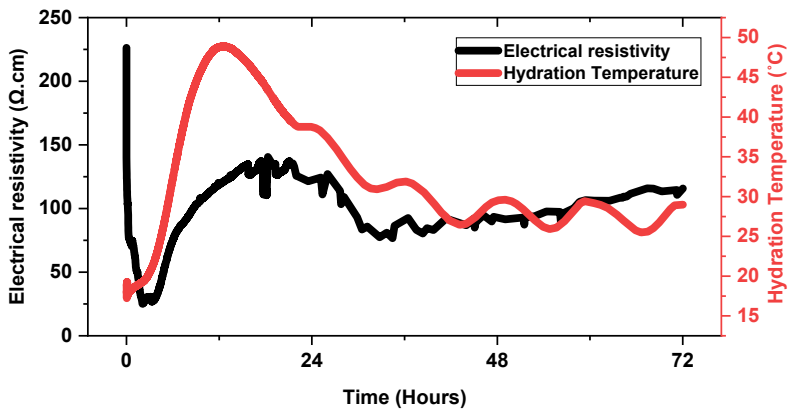
Figure 4-21 The measured electrical resistivity of the concrete bridge desk at location 1 obtained by the SmartCem sensor and the hydration temperature evolution for 3 days.

Figure 4-22 The construction site is in Saittarova, Sweden.

Figure 4-23 SmartCem sensors ready to be installed (left) and after installation of SmartCem sensors at the studied locations (right)

Chapter 5

Mechanisms and Modelling

The sensing mechanisms and models, based on multiple theories, were used to understand how SmartCem composites respond when exposed to various factors, including variations in compressive stress, strain, humidity, or temperature. Chapter 5 was redrafted based on (Buasiri, et al., 2023b)

According to the conductive path and tunneling theories, the distance between the conducting materials changes when stress is applied. As compression increases, the composites deform, resulting in the reconstruction of the conducting paths, **Figure 5-1 a)**. The deformation of the composite reduces the gap between the conductive materials. It is possible for an electron to tunnel (move) between neighboring conducting materials when the gap between them is sufficiently small, which leads to the development of conductive paths, **Figure 5-1 b)**.
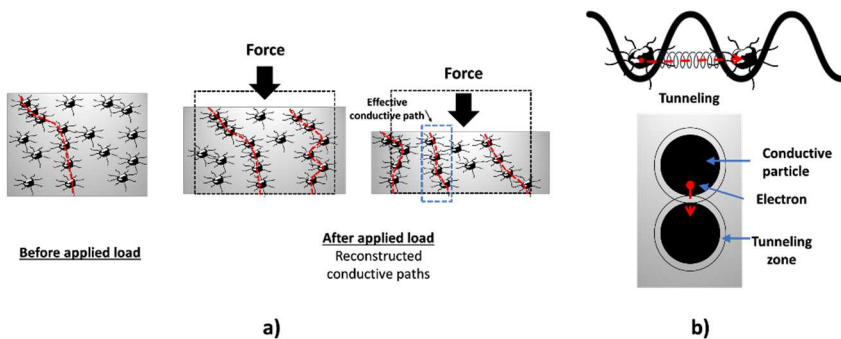
Figure 5-1 a) Change of the composite and the conductive paths when applied compressive force and b) The tunneling effect. (Adapted from (Buasiri, et al., 2023b))

The resistance of each conductive path (R_i) is a combination of the resistance of conductive particle and the resistance of the cementitious matrix between the adjacent conductive particles (L. Zhang, Ding, et al., 2017) , **Figure 5-2**.

$$R_i \approx n_i(R_c + R_m)$$ (9)

where: R_c and R_m are the resistance of the conductive particle and cementitious matrix, respectively, and n_i is the number of conductive particles in each conductive path.
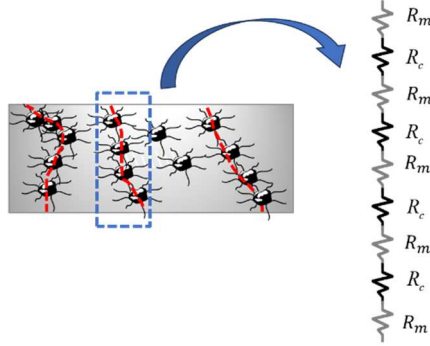
Figure 5-2 Schematic diagram of the electrical resistance of the effective conductive path.

As $R_c \ll R_m$, the resistance across the conductive particle may be neglected, and the resistance of the effective conductive path can be simplified as **equation (10)**:

$$R_i \approx n_i R_m$$ (10)

The electrical resistance of the SmartCem composite (R) can be approximated as the parallel electrical resistance of k effective conductive paths within the composite, which can be expressed using the following **equation (11)**:

$$R = \frac{1}{\dfrac{1}{R_1}+\dfrac{1}{R_2}+\dfrac{1}{R_3}+.....+\dfrac{1}{R_k}......} = \frac{1}{\dfrac{1}{n_1 R_m}+\dfrac{1}{n_2 R_m}+\dfrac{1}{n_3 R_m}+.....+\dfrac{1}{n_k R_m}} = \frac{R_m}{\alpha}$$ (11)

$$\alpha = \frac{1}{n_1}+\frac{1}{n_2}+\frac{1}{n_3}+.....+\frac{1}{n_k}$$ (12)

Based on the tunneling current density model (J) proposed by Simmons (Simmons, 1963; Simmons & Unterkofler, 1963), the electrical resistance of the SmartCem composites can be expressed using **equation (13)**:

$$R = \left(\frac{1}{\alpha}\right)\left(\frac{8\pi s}{3e^2 \gamma a^2}\right)\exp(\gamma s)$$ (13)

$$\gamma = \frac{4\pi \left(2m\varphi\right)^{1/2}}{\hbar} \tag{14}$$

where: $\hbar$ is the Planck's constant, s is the tunneling distance between the adjacent conductive particles, e is the electron charge, m is the electron mass, φ is the height of the potential barrier between the adjacent particles, and a^2 is the effective cross-section area.

Then, the electrical resistivity (ρ) can be calculated as **equation (15)**:

$$\rho = \frac{RA}{L} = \frac{A}{L}\left(\frac{1}{\alpha}\right)\left(\frac{8\pi \hbar s}{3e^2 \gamma a^2}\right)\exp\left(\gamma s\right) \tag{15}$$

where: L is the distance between internal electrodes, A is electrode area, and R is the measured resistance.

Under compressive stress, the fractional change in the electrical resistivity of the SmartCem composites (FCR) can be calculated using **equation (16)**:

$$FCR \ (\%) = \frac{\rho - \rho_0}{\rho_0}\times 100 = \left(\frac{\rho}{\rho_0} - 1\right)\times 10 \tag{16}$$

where: ρ_0 is the initial electrical resistivity.

Substituting **equation (15)** into **equation (16)**, yields

$$FCR \ (\%) = \frac{\rho - \rho_0}{\rho_0}\times 100 = \left(\frac{\rho}{\rho_0} - 1\right)\times 100 = \left(\frac{s}{s_0}\exp\left(\gamma(s - s_0)\right) - 1\right)\times 100 \tag{17}$$

Based on the stress-strain relationship under compression and making Taylor expansion of the exponential function, **equation (17)** can be derived as **equation (18)**. The details of the derived equation can be seen in Paper VI.

$$FCR \ (\%) = \left(A\sigma + B\sigma^2 + C\sigma^3 + ...\right)\times 100 \tag{18}$$

where: A, B, C are the coefficients of the polynomial equation.

The quadratic polynomial was used to fit the data in **Figure 4-5**. The fitting curve for the SmartCem mortar according to the proposed models in **equation (18)** are shown in **Figure 5-3**. **Table 5-1** shows fitting parameters, with the coefficients of determination (R²) of the developed model being relatively high. Therefore, the effective conductive paths and tunneling theory can well describe the piezoresistive behavior of the SmartCem composites.
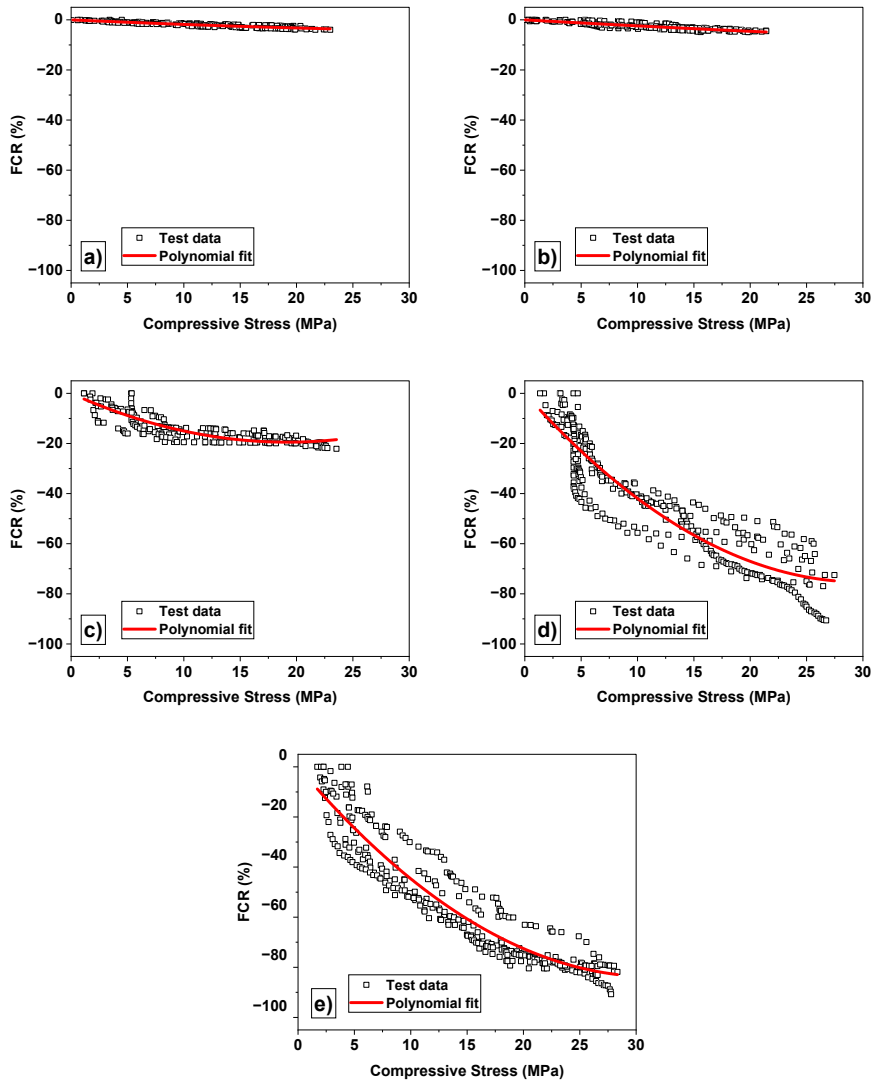
Figure 5-3. Fitted curves according to equation (19) of fractional change in electrical resistivity of SmartCem mortars under compressive stress a) S2, b) S4, c) S6, d) S8, and e) S10.

Table 5-1 The parameters obtained by fitting the fractional change in resistivity-compressive stress curves in Figure 5-3.

Mix	Model equation	R^2
S2	FCR (%) = $-0.2029\sigma + 0.00202\sigma^2$	0.96631
S4	FCR (%) = $-0.25448\sigma + 0.00129\sigma^2$	0.94201
S6	FCR (%) = $-2.03052\sigma + 0.05924\sigma^2$	0.9661
S8	FCR (%) = $-5.03367\sigma + 0.08409\sigma^2$	0.96725
S10	FCR (%) = $-5.30494\sigma + 0.08396\sigma^2$	0.98119

The electrical properties of the SmartCem composites are influenced by fluctuations in ambient relative humidity (RH). Absorption or desorption of water molecules affects the electrical connectivity of the conductive phases due to capillary condensation, **Figure 5-4 a)**. The process of moisture evaporation occurs when composites are subjected to low levels of relative humidity. In contrast, at high levels of relative humidity, the water vapor adsorbs on the external surface and later diffuses and condenses into water, gradually filling up the abundant pores (Rajabipour & Weiss, 2007a). At a certain level of humidity, the water molecules provide transportation paths for ions and create "bridges" between existing electrically conductive paths, **Figure 5-4 b)**. These phenomena change the interconnection between matrix–matrix, fiber–fiber and fiber-matrix resulting in a change in the ultimate electrical conductivity of the composites.
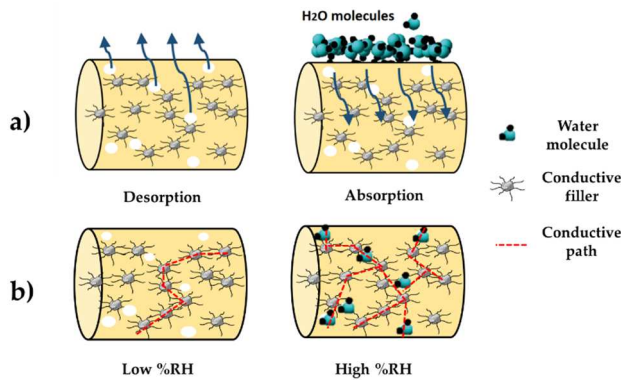
Figure 5-4 Effect of ambient humidity on a) the microstructure of the matrix and b) conductive paths in the matrix (Buasiri et al., 2021)

The electrical conductivity of the cementitious composites (σ_e) can be described based on a modified parallel law in which the system is made of n phases (Rajabipour & Weiss, 2007b).

$$\sigma_e = \sum_{i=1}^{n}\left(\sigma_i \phi_i \beta_i\right) \tag{19}$$

where: σ_i, ϕ_i, β_i are the electrical conductivity, volume fraction, and connectivity factor of each constitutive component i

It was assumed that the electrical conductivity of SmartCem composites for sensing the variation of humidity ($\sigma_{e,h}$) is a combination of the conductivity of the cementitious phase (σ_m), the conductivity of conductive CNFs (σ_c) and the conductivity of the liquid phase (σ_l). As σ_c and $\sigma_l \gg \sigma_m$, the conductivity across the cementitious matrix may be neglected, and the electrical conductivity can be simplified as **equation (20)**:

$$\sigma_{e,h} = \sigma_c \phi_c \beta_c + \sigma_l \phi_l \beta_l \tag{20}$$

where: σ_c, ϕ_c, and β_c are the electrical conductivity, volume fraction, and connectivity of the conductive filler (CNFs), σ_l, ϕ_l, and β_l are the electrical conductivity, total liquid-filled porosity, and pore connectivity of the liquid phase.

According to the volume fraction of the pore fluid (ϕ_l) is approximately the total volume of saturated pores located inside the composite due to capillary condensation (V_{sat}) divided by the total volume of all constituents of the composite (V_t), the maximum radius of saturated pore ($r_{\max}$) that remains saturated depends on the ambient humidity and can be described by Kelvin's equation for porous materials (Dullien, 1979). Assuming all pores inside of the composite have an ellipsoidal shape, the electrical conductivity of the SmartCem composite can be derived as **equation (21)**:

$$\sigma_{e,h} = \sigma_c \phi_c \beta_c + \sum\left(\sigma_l \frac{n_i \frac{4}{3}\pi\left(\frac{-2\gamma V_m}{R_g T\left[\ln\left(\%RH/100\right)\right]}\right)r_2 r_3}{V_t}\beta_l\right)_{r=\max} + \sum\left(\sigma_l \frac{n_j V_{psat}}{V_t}\beta_l\right)_{r<r_{\max}} \tag{21}$$

where: γ and V_m are the surface tension and the molar volume of the pore fluid, R_g is the universal gas constant, T is an absolute temperature in Kelvin, $\%RH$ is the ambient humidity

in percentage, r_2, r_3 are the radius of pores in different directions, n_i and n_j is the total number of saturated pores, and V_{psat} is the volume of a single saturated pore.

Therefore, the electrical conductivity of the SmartCem composite describing the humidity-dependent behavior can be simplified as the **equation (22)**. The details of the derived equation can be found in Paper VI.

$$\sigma_{e,h} = A + \frac{B}{\left[\ln\left(\%RH/100\right)\right]} \tag{22}$$

where: A and B are the coefficients of the nonlinear equation.

The nonlinear equation was used in **equation (22)** to fit the data in **Figure 4-10**. The fitting curve for the SmartCem mortars according to the proposed model are shown in **Figure 5-5**. **Table 5-2** shows the fitting parameters with the coefficients of determination (R²) of the developed model.

Table 5-2 The parameters obtained by fitting the electrical conductivity-relative humidity curves in Figure 5-5.

Mix	Model equation	R²
S2	$\sigma_{e,h} = 3.70585 - 0.03029/\left[\ln\left(\%RH/100\right)\right]$	0.72864
S4	$\sigma_{e,h} = 3.83140 - 0.02675/\left[\ln\left(\%RH/100\right)\right]$	0.74896
S6	$\sigma_{e,h} = 3.8955 - 0.02582/\left[\ln\left(\%RH/100\right)\right]$	0.72793
S8	$\sigma_{e,h} = 9.4637 - 0.46153/\left[\ln\left(\%RH/100\right)\right]$	0.71535
S10	$\sigma_{e,h} = 12.87000 - 0.70635/\left[\ln\left(\%RH/100\right)\right]$	0.73391
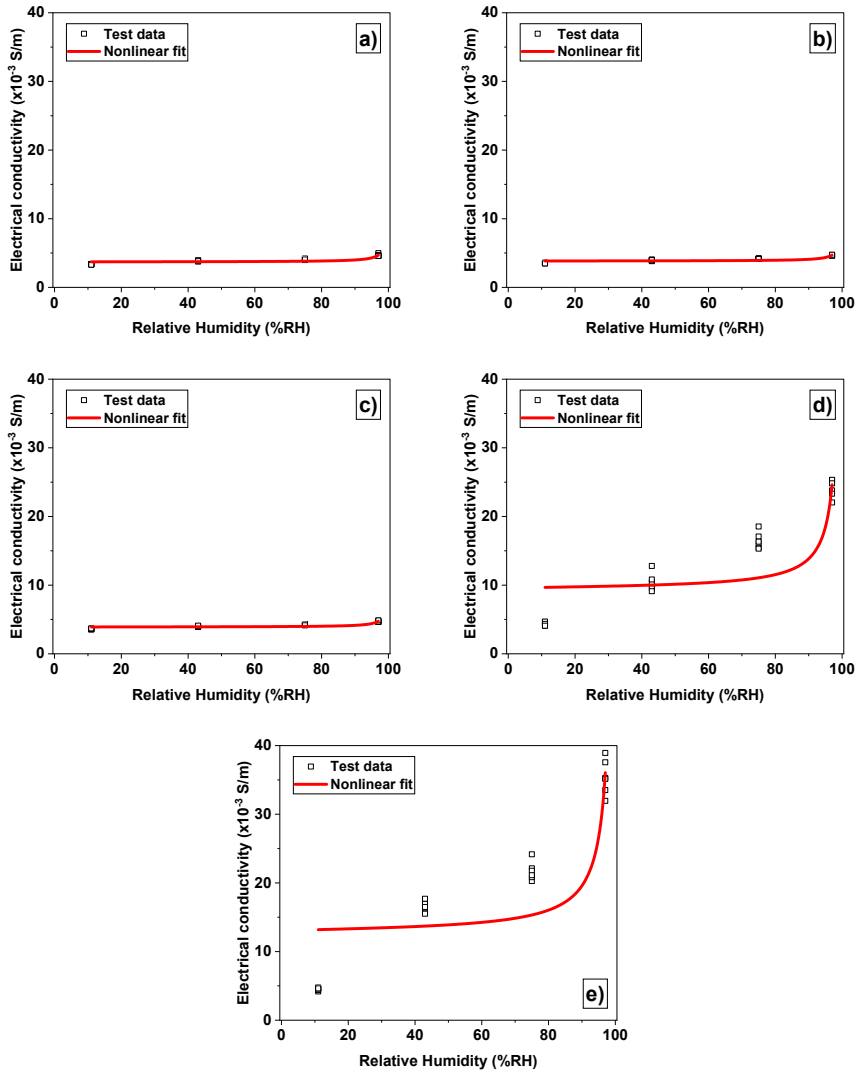
Figure 5-5 Fitted curves according to equation (22) of the electrical conductivity of SmartCem mortars exposed to a variety of ambient humidity levels a) S2, b) S4, c) S6, d) S8, and e) S10.

The electrical conductivity of cement-based composites is influenced by temperature variations, a phenomenon explicable through two primary mechanisms: **1)** the alteration of the composite matrix due to thermal deformations, and **2)** the mobility of thermally stimulated charge carriers, facilitated by the phenomenon of thermal fluctuation-induced tunneling conduction, (S. Ding et al., 2019).

The phenomenon of thermal expansion or contraction in SmartCem occurs as a response to temperature alterations. Composite expands when heated and contracts when cooled, **Figure 5-6** . The thermal expansion led to a separation or loosening of contacts between the conductive fibers due to larger distances between each fiber. This may result in decreased electrical conductivity. In contrast, the thermal contraction that occurs at lower temperatures may result in compression or tighter contact between conductive fibers. This enhanced contact can facilitate the formation of conductive paths and increase electrical conductivity.
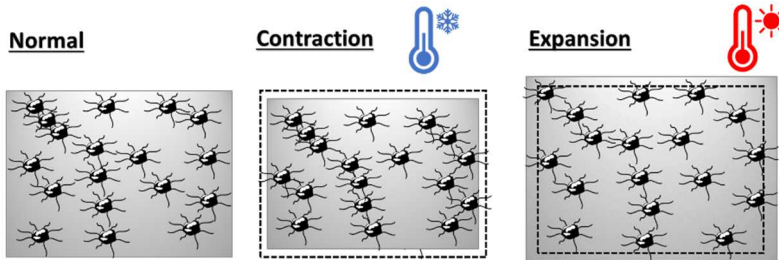
Figure 5-6 Expansion and contraction of the composite due to the change in ambient temperature.

The effect of thermal fluctuation-induced tunnelling corresponds to a higher temperature at which charge carriers acquire additional kinetic energy. This allows them to overcome energy barriers and move more freely through the matrix, resulting in higher electrical conductivity. The thermal activation of charge carriers is correlated with activation energy, which is the energy required for charge carriers to transition from localized to mobile states.

Based on the model of tunneling current density (J) as a function of temperature proposed by Hill (Hill, 1969) and the thermal expansion or contraction of composites could change the tunneling distance. Therefore, the tunneling current is given by **equation (23)**. The details of the derived equation can be seen in Paper VI.

$$J = \frac{\varphi e^2 BV}{\left(s_0\left[1+\alpha_c(T-T_0)\right]\right)^2 \hbar \sin \pi BR_g T} \exp\left(\frac{4\pi(2m\varphi)^{1/2}\left(s_0\left[1+\alpha_c(T-T_0)\right]\right)}{\hbar} - \frac{E_a}{R_g T}\right)$$

(23)

where: $A = 4\pi s (2m)^{1/2}/\hbar$; $B = A/2\varphi^{1/2}$, $\hbar$ is the Planck's constant, s is the tunneling distance between adjacent conductive particles, s_0 is initial tunneling distance, e is the electron charge, m is the electron mass, φ is the height of the potential barrier between adjacent particles, V is the voltage drop cross tunnel, T is an absolute temperature in Kelvin, T_0 is an initial temperature in Kelvin, α_c is the coefficient of linear thermal expansion in composite, R_g is the universal gas constant, and E_a is the activated energy.

Normally $\alpha_c (T - T_0) \ll 1$, the term of $\left(s_0 \left[1 + \alpha_c (T - T_0) \right] \right)^2 \approx s_0^2$. Then,

$$J \approx \frac{k_1 V}{s_0^2} \exp\left(k_2 s_0 \left[1 + \alpha_c (T - T_0) \right] - \frac{E_a}{R_g T} \right) \tag{24}$$

where: $k_1 = \varphi e^2 B/\hbar \sin \pi B R_g T$, $k_2 = 4\pi (2m\varphi)^{1/2}/\hbar$

Based on **equation (24)**, the electrical conductivity of the SmartCem composites due to the tunneling effect and thermal deformation can be calculated as follows:

$$\sigma_{e,t} = \frac{L}{R_t A_e} = \frac{L k_1 a^2}{A_e s_0^2} \exp\left(k_2 s_0 \left[1 + \alpha_c (T - T_0) \right] - \frac{E_a}{R_g T} \right) \tag{25}$$

where: $a^2 = A_e$ is the effective cross-section area. L is internal electrode distance, and R is the measured resistance.

However, in the present work, the effect of thermal fluctuation-induced tunneling conduction is dominant. the thermal deformation of the nanomodified Portland cement composite is neglected due to small effect of thermal expansion at the temperature range used in this study. Then, **equation (25)** can be simplified as follows **equation (26)**:

$$\sigma_{e,t} = \frac{L k_1}{s_0^2} \exp\left(-\frac{E_a}{R_g T} \right) = C \exp\left(-\frac{D}{T_c + 273.15} \right) \tag{26}$$

where: C, D are constant and T_c is the temperature in Celsius.

The nonlinear equation in **equation (26)** was used to fit the data in **Figure 4-12**. The fitting curve for the SmartCem mortars according to the proposed model are shown in **Figure 5-7.** The model closely matches the experimental data with R^2 values greater than 0.95. The findings confirmed that the tunneling effect of thermal induction is

important in the sensing behavior of SmartCem composites within the studied temperature range.
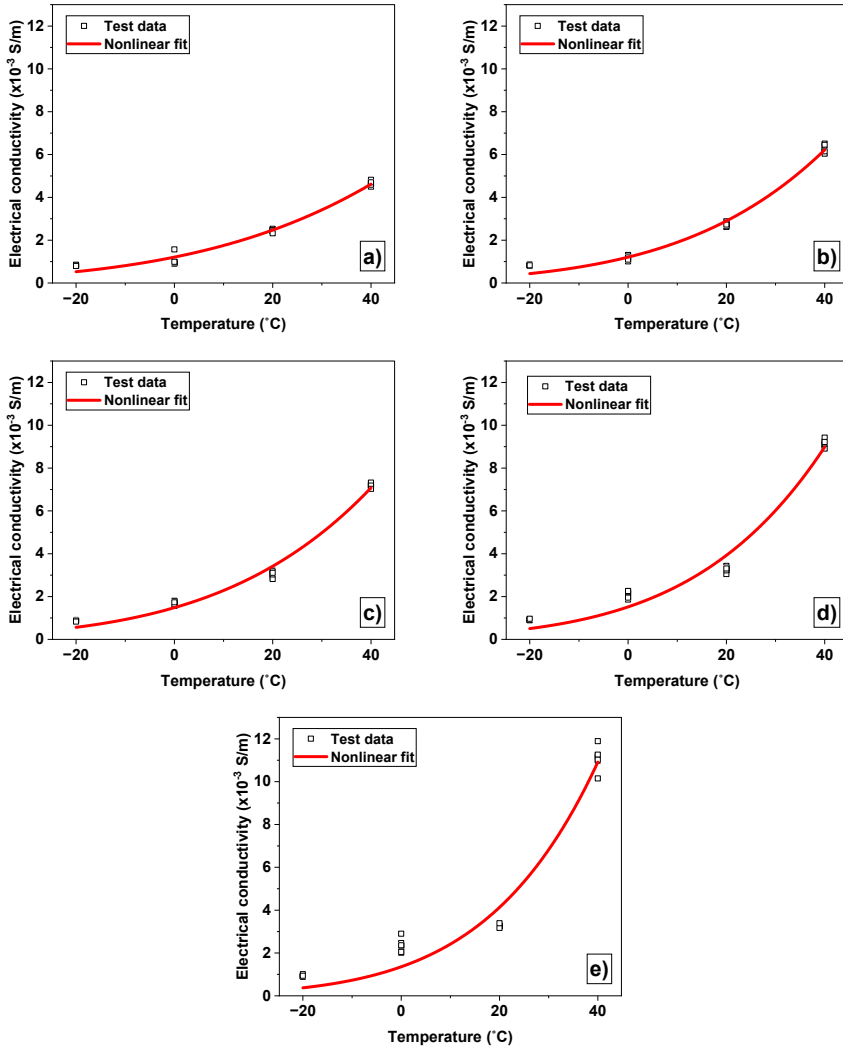
Figure 5-7 Fitted curves according to equation (26) of the electrical conductivity of SmartCem mortars exposed to a variety of temperatures a) S2, b) S4, c) S6, d) S8, and e) S10.

Table 5-3 The parameters obtained by fitting the electrical conductivity-temperature curves in Figure 5-7.

Mix	Model equation	R²
S2	$\sigma_{e,t} = 43.536 \exp\left(-2865.747/T_c + 273.15\right)$	0.97890
S4	$\sigma_{e,t} = 445.447 \exp\left(-3500.952/T_c + 273.15\right)$	0.98770
S6	$\sigma_{e,t} = 304.125 \exp\left(-3340.836/T_c + 273.15\right)$	0.98604
S8	$\sigma_{e,t} = 1678.733 \exp\left(-3800.974/T_c + 273.15\right)$	0.97461
S10	$\sigma_{e,t} = 16732.194 \exp\left(-4460.158/T_c + 273.15\right)$	0.96225

Chapter 6

Conclusions

6.1   Concluding remarks

The research covered by this doctoral thesis yields several key conclusions that can be summarized as follows:

- The nanomodified Portland cement, named in this work as SmartCem, represents an innovative material developed to enhance the dispersion of carbon-based materials within the cementitious matrix.

- The investigation revealed that SmartCem composites exhibit robust piezoresistive behavior, demonstrating a clear change in electrical resistivity in response to applied mechanical stresses. This piezoresistive property enables the composites to sense and indicate structural stress or strain, which has important implications for real-time structural health monitoring. The sensitivity and response characteristics of SmartCem to different stress conditions provide a basis for its application in early damage detection and assessment.

- The sensing capabilities of SmartCem composites extend beyond mechanical stress response and also include variations in humidity and temperature. The sensitivity of SmartCem composite is intricately linked to the concentration of SmartCem. The responsiveness of the composite to different parameters is characterized by distinct thresholds for added amounts of SmartCem. In other words, the concentration of SmartCem within the composite material plays a crucial role in determining how effectively it can sense changes in various factors such as stress, strain, temperature, and humidity. At lower concentrations, the composite's conductive network may not be well-established, leading to a lower or lack of sensitivity. As the concentration increases, the conductive network becomes more interconnected, resulting in a higher sensitivity.

- The SmartCem composite exhibited its highest sensitivity when containing 10 wt.% of SmartCem. The threshold amount of SmartCem, for both compression and flexural stress sensing and humidity sensing is approximately 7 wt.% of the total binder, which corresponds to ~0.1897 wt.% of CNFs. While the percolation threshold is at 5 wt.% of the SmartCem (~0.1355 wt.% of CNFs) for temperature sensitivity. This phenomenon underscores the importance of optimizing the concentration of SmartCem to achieve the desired sensitivity levels for specific sensing applications.

- One of the significant findings is that SmartCem mortar can effectively be used as a sensor to monitor the hydration process. By observing changes in electrical resistivity, the material offers insights into the kinetics of cement hydration, which is a crucial aspect of concrete's setting and hardening. Additionally, the SmartCem mortar has the ability to track stress-strain changes in concrete structures in real-time, thus contributing to overall structural safety and reliability.

- The study investigated the sensing mechanisms of this material. The piezoresistive phenomenon was intricately linked to the critical threshold concentration of CNFs within the SmartCem composite as well as to the tunneling effect. The dynamics of water absorption, desorption, and the presence of chemically bound water have proven crucial in humidity sensing. Moreover, the preeminence of thermal fluctuation-induced tunneling conduction has been established as the principal driver of temperature sensitivity.

- Transitioning from laboratory settings to real-world applications, the study included field testing of the SmartCem sensors on a full-scale concrete bridge deck. The successful implementation of the monitoring system demonstrated the feasibility of integrating SmartCem into practical construction scenarios.

6.2   Answering research questions

I.   Is it possible to create a self-sensing composite based on Portland cement? What material combinations give the best results, and what are the most common problems? (Paper I)

- Yes, it is possible to create a self-sensing composite based on Portland cement. The general approach to creating self-sensing cement composites involves incorporating various types of conductive materials into cementitious systems to enable self-sensing capabilities.

- Several material combinations have shown promising results for creating self-sensing cement-based composites. The choice of materials depends on the specific sensing mechanism being used. Carbon-based materials have been predominantly used due to their remarkable mechanical and electrical properties.

- Obtaining a sufficiently even distribution of conductive phases within the hydrated binder matrix has been one of the main obstacles to achieving strong self-sensing capability.

II.   Can nanomodified Portland cement (SmartCem) be used to induce a self-sensing capability in Portland cement-based composites? (Paper II, III, IV, V)

- Yes, nanomodified Portland cement (SmartCem) has shown great potential for inducing self-sensing capabilities in Portland cement-based composites. Partially replacing pristine cement with SmartCem. The created composite possesses a remarkable sensing property, which means that its electrical resistance changes in response to, for example, mechanical strain or stress and varied environmental conditions.

III.   What are the mechanisms controlling the self-sensing capabilities of the SmartCem composites? (Paper VI)

The mechanisms depend on the application, the desired parameters to be sensed, and the overall goals of the sensing system in cementitious materials.

- The piezoresistive effect is a fundamental mechanism for stress-strain sensing. When mechanical stress or strain is applied to the SmartCem composite, the geometrical arrangement of the CNFs changes and alters its electrical conductivity. The application of stress or strain can also alter the spacing and alignment of the CNFs. As the arrangement changes, the electron tunneling between CNFs can also be affected, leading to alterations in electrical resistance.

  The percolation threshold is the critical concentration of conductive particles required within a composite matrix to establish a continuous conductive pathway. The percolation threshold marks the point at which a conductive network is formed. This enables an efficient transfer of electrical charges through the material. Once this threshold is reached, even minor changes in the arrangement of nanofibers can cause significant changes in the composite's overall electrical conductivity, making it responsive to applied stress or strain.

- The humidity sensing capabilities of SmartCem composites are controlled by a combination of various mechanisms:

Conductivity Changes: Conductive materials can also undergo changes in electrical conductivity as they interact with moisture. In humid conditions, water molecules can provide a conductive pathway between the conductive particles, enabling the flow of ions and electrons. This increased conductivity can be measured and used to deduce the humidity level.

Adsorption and Absorption: Porous cement-based composites can adsorb and absorb moisture from the surrounding environment. As water molecules are adsorbed onto the surface and absorbed into the composite's pores, they interact with the conductive materials. This interaction can lead to swelling or changes in the interparticle distances of the conductive components, affecting their electrical properties.

Capillary Action: Moisture can also be drawn into the pores of the composite through the capillary suction created in the porous cement matrix. The presence of moisture in pores can influence the conductivity or dielectric properties of conductive materials, enabling humidity sensing.

Diffusion and Permeation: Water vapor can diffuse through the porous structure of the composite and interact with the conductive materials. Depending on the type of conductive material used and its interaction with water molecules, changes in electrical properties can occur, facilitating humidity sensing.

- The temperature-sensing capabilities of SmartCem composites involve various mechanisms. These include thermal expansion, temperature variations, and interactions between conductive components.

Thermal Expansion: Cement-based composites experience thermal expansion and contraction as the result of temperature change. Conductive materials within the matrix can also be affected by temperature-induced dimensional changes.

Thermal fluctuation-induced tunnelling: Temperature changes could impact the movement of electrons within the material. Electrons overcome energy barriers that they typically wouldn't have enough energy to surmount. Temperature changes could potentially affect the behavior of these electrons, allowing them to tunnel through barriers more easily as thermal energy increases.

IV.   What is the threshold amount of SmartCem for a self-sensing composite? (Paper II, III, IV, V)

- The threshold amount of SmartCem for both compression and flexural stress sensing and humidity sensing is approximately 7 wt.% of the total binder, which corresponds to ~0.1897 wt.% of CNFs. While the percolation threshold is 5 wt.% of the total binder (~0.1355 wt.% of CNFs) for the temperature sensing.

V.   Can the SmartCem composites be used as sensors in a structural health monitoring system for concrete structures? (Paper V)

- Yes, the SmartCem composites can potentially be used as sensors in a structural health monitoring (SHM) system for concrete structures. The findings of this research showed that the change in electrical properties of the studied concrete structures measured by SmartCem composites can monitor various parameters such as stress, strain, and the progression of cement hydration.

VI.   What is the most influential parameter for the sensitivity of the SmartCem composite? (Paper II, III, IV, V, VI)

- The sensitivity of SmartCem composites, particularly in terms of its ability to accurately detect and respond to changes in various parameters (such as stress, strain, temperature, and humidity), can be influenced by many factors. Among these factors, the type and arrangement of conductive materials play a significant role in determining the sensitivity. The most influential parameter is the concentration or volume fraction of the conductive materials within the cementitious matrix. At lower concentrations, the conductive network might not be well-established, leading to a lower or lack of sensitivity. As the concentration increases, the network becomes more interconnected, resulting in greater changes and in stronger response to variations in parameters being sensed.

6.3   Future research

To gain a comprehensive understanding of SmartCem's properties, future studies should investigate the effects of different synthesis process parameters such as growth time, temperature, and precursor concentration. Investigate the impact of different precursor materials on nanofiber growth and how variations in precursor properties influence the electrical conductivity of the resulting nanomodified cement. Moreover, delve into the relationship between changes in nanofiber properties

(length, diameter, and alignment) resulting from different synthesis parameters and their effects on the formation of the conductive network and overall sensing capabilities.

Future research could focus on advanced analysis techniques to understand the piezoresistive behavior of SmartCem composites in more detail. This could involve exploring the relationship between stress, strain, and electrical resistance under other loading conditions for example cyclic loading and tensile loading.

Extend the scope of SmartCem's sensing capabilities to include other parameters, such as freeze-thaw sensing and chemical exposure sensing. Investigate how these additional parameters interact within the composite and refine the composite's design to enable multi-parameter sensing. This expansion could open doors to new applications and a more comprehensive understanding of SmartCem's versatility.

Assessing SmartCem's long-term performance and durability of real structures over extended periods. Consider extending the testing duration to observe the material's behavior, self-sensing capabilities, and overall integrity over time. This would involve continuous monitoring, data collection, and validation of their effectiveness in diverse and challenging environments, contributing to their practical application.

Application in Real Structures: Exploring more case studies involving the application of SmartCem composites in real-world concrete structures, such as buildings, road could demonstrate their effectiveness in structural health monitoring.

Conduct a cost-effectiveness analysis. Compare the potential benefits of early detection, prevention, and data-driven decision-making with the costs of implementation. This analysis could guide stakeholders in making informed choices regarding the adoption of SmartCem in various construction projects.

References

Al-Dahawi, A., Öztürk, O., Emami, F., Yildirim, G., & Şahmaran, M. (2016). Effect of mixing methods on the electrical properties of cementitious composites incorporating different carbon-based materials. *Construction and Building Materials*, *104*, 160–168. https://doi.org/10.1016/j.conbuildmat.2015.12.072

Al-Dahawi, A., Sarwary, M. H., Öztürk, O., Yildirim, G., Akin, A., Şahmaran, M., & Lachemi, M. (2016a). Electrical percolation threshold of cementitious composites possessing self-sensing functionality incorporating different carbon-based materials. *Smart Materials and Structures*, *25*(10). https://doi.org/10.1088/0964-1726/25/10/105005

Al-Dahawi, A., Sarwary, M. H., Öztürk, O., Yildirim, G., Akin, A., Şahmaran, M., & Lachemi, M. (2016b). Electrical percolation threshold of cementitious composites possessing self-sensing functionality incorporating different carbon-based materials. *Smart Materials and Structures*, *25*(10). https://doi.org/10.1088/0964-1726/25/10/105005

Azhari, F., & Banthia, N. (2012). Cement-based sensors with carbon fibers and carbon nanotubes for piezoresistive sensing. *Cement and Concrete Composites*, *34*(7), 866–873. https://doi.org/10.1016/j.cemconcomp.2012.04.007

Azhari, F., & Banthia, N. (2017). Carbon Fiber-Reinforced Cementitious Composites for Tensile Strain Sensing. *Aci Materials Journal*, *114*, 129–136. https://doi.org/10.14359/51689486

Baeza, F. J., Galao, O., Zornoza, E., & Garcés, P. (2013). Multifunctional cement composites strain and damage sensors applied on reinforced concrete (RC) structural elements. *Materials*, *6*(3), 841–855. https://doi.org/10.3390/ma6030841

Bajwa, N., Li, X., Ajayan, P. M., & Vajtai, R. (2008). Mechanisms for catalytic CVD growth of multiwalled carbon nanotubes. *Journal of Nanoscience and Nanotechnology*, *8*(11), 6054–6064. https://doi.org/10.1166/jnn.2008.SW02

Banthia, N., Djeridane, S., & Pigeon, M. (1992). ELECTRICAL RESISTIVITY OF CARBON AND STEEL MICRO-FIBER REINFORCED CEMENTS. In *CEMENT and CONCRETE RESEARCH* (Vol. 22).

Basheer, P. A. M., Chidiact, S. E., & Long, A. E. (1996). Predictive models for deterioration of concrete structures. In *Construction and Building Materials* (Vol. 10, Issue I).

Benmokrane, B., Ehab El-Salakawy, ;, Sherif El-Gamal, ;, & Goulet, S. (2007). Construction and Testing of an Innovative Concrete Bridge Deck Totally

Reinforced with Glass FRP Bars: Val-Alain Bridge on Highway 20 East. *Journal of Bridge Engineering*, *12*(5), 632–645. https://doi.org/10.1061/ASCE1084-0702200712:5632

Berrocal, C. G., Hornbostel, K., Geiker, M. R., Löfgren, I., Lundgren, K., & Bekas, D. G. (2018). Electrical resistivity measurements in steel fibre reinforced cementitious materials. *Cement and Concrete Composites*, *89*, 216–229. https://doi.org/10.1016/j.cemconcomp.2018.03.015

Bhatia, R., Prasad, V., & Menon, R. (2010). Characterization, electrical percolation and magnetization studies of polystyrene/multiwall carbon nanotube composite films. *Materials Science and Engineering B: Solid-State Materials for Advanced Technology*, *175*(3), 189–194. https://doi.org/10.1016/j.mseb.2010.07.025

Bing, C., Keru, W. U., & Wu, Y. (2006). Characteristics of Resistivity-temperature for Carbon Fiber Reinforced Concrete. In *Journal of Wuhan University of Technology-Mater. Sci. Ed* (Vol. 21, Issue 1).

Boyd, A. J., & Skalny, J. (2007). Environmental deterioration of concrete. In *Environmental Deterioration of Materials* (Vol. 21, pp. 143–184). WIT press. https://doi.org/10.2495/978-1-84564-032-3/05

Buasiri, T., Habermehl-Cwirzen, K., & Cwirzen, A. (2019). State of the Art on Sensing Capability of Poorly or Nonconductive Matrixes with a Special Focus on Portland Cement–Based Materials. *Journal of Materials in Civil Engineering*, *31*(11). https://doi.org/10.1061/(ASCE)MT.1943-5533.0002901

Buasiri, T., Habermehl-Cwirzen, K., Krzeminski, L., & Cwirzen, A. (2019). Piezoresistive load sensing and percolation phenomena in portland cement composite modified with in-situ synthesized carbon nanofibers. *Nanomaterials*, *9*(4). https://doi.org/10.3390/nano9040594

Buasiri, T., Habermehl-Cwirzen, K., Krzeminski, L., & Cwirzen, A. (2020). Role of Carbon Nanofiber on the Electrical Resistivity of Mortar under Compressive Load. *Transportation Research Record: Journal of the Transportation Research Board*, 1–6. https://doi.org/10.1177/0361198120947417

Buasiri, T., Habermehl-Cwirzen, K., Krzeminski, L., & Cwirzen, A. (2021). Novel humidity sensors based on nanomodified Portland cement. *Scientific Reports*, *11*(1). https://doi.org/10.1038/s41598-021-87563-7

Buasiri, T., Habermehl-Cwirzen, K., Krzeminski, L., & Cwirzen, A. (2023). Sensing mechanisms of nanomodified Portland cement composites. *Submitted*.

Buasiri, T., Kothari, A., Habermehl-Cwirzen, K., Krzeminski, L., & Cwirzen, A. (2023). Monitoring temperature and hydration by mortar sensors made of nanomodified Portland cement. *Submitted*.

Cabrera, J. G. (1996). Deterioration of concrete due to reinforcement steel corrosion. *Cement and Concrete Composites*, *18*(1), 47–59. https://doi.org/10.1016/0958-9465(95)00043-7

Chen, B., & Liu, J. (2008). Damage in carbon fiber-reinforced concrete, monitored by both electrical resistance measurement and acoustic emission analysis. *Construction and Building Materials*, *22*(11), 2196–2201. https://doi.org/10.1016/j.conbuildmat.2007.08.004

Chen, P.-W., & Chung, D. D. L. (1993). Carbon fiber reinforced concrete for smart structures capable of non-destructive flaw detection. In *Smart Mater. Struct* (Vol. 2).

Cheng, X., Wang, S., Lu, L., & Huang, S. (2011). Influence of preparation process on piezo-conductance effect of carbon fiber sulfoaluminate cement composite. *Journal of Composite Materials*, *45*(20), 2033–2037. https://doi.org/10.1177/0021998311407990

Chi, J. M., Huang, R., & Yang, C. C. (2002). Effects of carbonation on mechanical properties and durability of concrete using accelerated testing method. *Journal of Marine Science and Technology*, *10*(1), 14–20.

Chuang, W., Geng-sheng, J., Bing-liang, L., Lei, P., Ying, F., Ni, G., & Ke-zhi, L. (2017). Dispersion of carbon fibers and conductivity of carbon fiber-reinforced cement-based composites. *Ceramics International*, *43*(17), 15122–15132. https://doi.org/10.1016/j.ceramint.2017.08.041

Chung, D. D. L. (2001). Comparison of submicron-diameter carbon filaments and conventional carbon fibers as fillers in composite materials. In *Carbon* (Vol. 39).

Chung, D. D. L. (2002a). Piezoresistive Cement-Based Materials for Strain Sensing. *Journal of Intelligent Material Systems and Structures*, *13*(9), 599–609. https://doi.org/10.1106/104538902031861

Chung, D. D. L. (2002b). Piezoresistive cement-based materials for strain sensing. *Journal of Intelligent Material Systems and Structures*, *13*(9), 599–609. https://doi.org/10.1106/104538902031861

Cwirzen, A. (2021). 6 - Effects of carbon nanotubes and carbon nanofibers on concrete properties. In A. Cwirzen (Ed.), *Carbon Nanotubes and Carbon Nanofibers in Concrete-Advantages and Potential Risks* (pp. 171–245). Elsevier. https://doi.org/https://doi.org/10.1016/B978-0-323-85856-4.00009-1

References

Cwirzen, A., Habermehl-Cwirzen, K., & Penttala, V. (2008). Surface decoration of carbon nanotubes and mechanical properties of cement/carbon nanotube composites. *Advances in Cement Research*, *20*(2), 65–73. https://doi.org/10.1680/adcr.2008.20.2.65

Cwirzen, A., Habermehl-Cwirzen, K., Shandakov, D., Nasibulina, L. I., Nasibulin, A. G., Mudimela, P. R., Kauppinen, E. I., & Penttala, V. (2009). Properties of high yield synthesised carbon nano fibres/Portland cement composite. *Advances in Cement Research*, *21*(4), 141–146. https://doi.org/10.1680/adcr.8.00021

Dalla, P. T., Dassios, K. G., Tragazikis, I. K., Exarchos, D. A., & Matikas, T. E. (2016). Carbon nanotubes and nanofibers as strain and damage sensors for smart cement. *Materials Today Communications*, *8*, 196–204. https://doi.org/10.1016/j.mtcomm.2016.07.004

Danoglidis, P. A., Konsta-Gdoutos, M. S., Gdoutos, E. E., & Shah, S. P. (2016). Strength, energy absorption capability and self-sensing properties of multifunctional carbon nanotube reinforced mortars. *Construction and Building Materials*, *120*, 265–274. https://doi.org/10.1016/j.conbuildmat.2016.05.049

Darwin, D., Browning, J. A., Gong, L., & Hughes, S. R. (2008). Effects of deicers on concrete deterioration. *ACI Materials Journal*, *105*(6), 622–627. https://doi.org/SL Report 07-3

De la Torre, Á. G., Cabeza, A., Calvente, A., Bruque, S., & Aranda, M. A. G. (2001). Full phase analysis of portland clinker by penetrating synchrotron powder diffraction. *Analytical Chemistry*, *73*(2), 151–156. https://doi.org/10.1021/ac0006674

Dehghanpour, H., Yilmaz, K., Afshari, F., & Ipek, M. (2020). Electrically conductive concrete: A laboratory-based investigation and numerical analysis approach. *Construction and Building Materials*, *260*. https://doi.org/10.1016/j.conbuildmat.2020.119948

Ding, S., Dong, S., Ashour, A., & Han, B. (2019). Development of sensing concrete: Principles, properties and its applications. *Journal of Applied Physics*, *126*(24). https://doi.org/10.1063/1.5128242

Ding, Y., Chen, Z., Han, Z., Zhang, Y., & Pacheco-Torgal, F. (2013). Nano-carbon black and carbon fiber as conductive materials for the diagnosing of the damage of concrete beam. *Construction and Building Materials*, *43*, 233–241. https://doi.org/10.1016/j.conbuildmat.2013.02.010

Dong, W., Huang, Y., Lehane, B., Aslani, F., & Ma, G. (2021). Mechanical and electrical properties of concrete incorporating an iron-particle contained nano-

graphite by-product. *Construction and Building Materials*, *270*. https://doi.org/10.1016/j.conbuildmat.2020.121377

Dullien, F. (1979). *Porous media; fluid Transport and Pore Structure*. Academic Press.

Dunens, O. M., Mackenzie, K. J., & Harris, A. T. (2009). Synthesis of multiwalled carbon nanotubes on fly ash derived catalysts. *Environmental Science and Technology*, *43*(20), 7889–7894. https://doi.org/10.1021/es901779c

El-Dieb, A. S., El-Ghareeb, M. A., Abdel-Rahman, M. A. H., & Nasr, E. S. A. (2018). Multifunctional electrically conductive concrete using different fillers. *Journal of Building Engineering*, *15*, 61–69. https://doi.org/10.1016/j.jobe.2017.10.012

EN, B. (2019). British Standards Institution (2019) BS EN 12390-3: 2019. Testing Hardened Concrete. Compressive Strength of Test Specimens. British Standards Institution, London. *No. August*.

Fiala, L., Toman, J., Vodička, J., & Ráček, V. (2016). Experimental Study on Electrical Properties of Steel-fibre Reinforced Concrete. *Procedia Engineering*, *151*, 241–248. https://doi.org/10.1016/j.proeng.2016.07.362

Gao, D., Sturm, M., & Mo, Y. L. (2009). Electrical resistance of carbon-nanofiber concrete. *Smart Materials and Structures*, *18*(9), 095039. https://doi.org/10.1088/0964-1726/20/4/049501

Gao, D., Sturm, M., & Mo, Y. L. (2011). Erratum: Electrical resistance of carbon-nanofiber concrete (Smart Mater. Struct. (2010) 18 (095039). In *Smart Materials and Structures* (Vol. 20, Issue 4). https://doi.org/10.1088/0964-1726/20/4/049501

Georgakilas, V., Perman, J. A., Tucek, J., & Zboril, R. (2015). Broad Family of Carbon Nanoallotropes: Classification, Chemistry, and Applications of Fullerenes, Carbon Dots, Nanotubes, Graphene, Nanodiamonds, and Combined Superstructures. In *Chemical Reviews* (Vol. 115, Issue 11, pp. 4744–4822). American Chemical Society. https://doi.org/10.1021/cr500304f

Ghaharpour, F., Bahari, A., Abbasi, M., & Ashkaran, A. A. (2016). Parametric investigation of CNT deposition on cement by CVD process. *Construction and Building Materials*, *113*, 523–535. https://doi.org/10.1016/j.conbuildmat.2016.03.080

Guadagno, L., De Vivo, B., Di Bartolomeo, A., Lamberti, P., Sorrentino, A., Tucci, V., Vertuccio, L., & Vittoria, V. (2011). Effect of functionalization on the thermo-mechanical and electrical behavior of multi-wall carbon nanotube/epoxy composites. *Carbon*, *49*(6), 1919–1930. https://doi.org/10.1016/j.carbon.2011.01.017

Guadagno, L., Raimondo, M., Vittoria, V., Vertuccio, L., Lafdi, K., De Vivo, B., Lamberti, P., Spinelli, G., & Tucci, V. (2013). The role of carbon nanofiber defects on the electrical and mechanical properties of CNF-based resins. *Nanotechnology*, *24*(30), 305704. https://doi.org/10.1088/0957-4484/24/30/305704

Guthy, C., Du, F., Brand, S., Winey, K. I., & Fischer, J. E. (2007). Thermal Conductivity of Single-Walled Carbon Nanotube/PMMA Nanocomposites. *Journal of Heat Transfer*, *129*(8), 1096–1099. https://doi.org/10.1115/1.2737484

Han, B., Ding, S., & Yu, X. (2015). Intrinsic self-sensing concrete and structures: A review. In *Measurement: Journal of the International Measurement Confederation* (Vol. 59, pp. 110–128). Elsevier B.V. https://doi.org/10.1016/j.measurement.2014.09.048

Han, B., Guan, X., & Ou, J. (2007). Electrode design, measuring method and data acquisition system of carbon fiber cement paste piezoresistive sensors. *Sensors and Actuators, A: Physical*, *135*(2), 360–369. https://doi.org/10.1016/j.sna.2006.08.003

Han, B., & Ou, J. (2007). Embedded piezoresistive cement-based stress/strain sensor. *Sensors and Actuators, A: Physical*, *138*(2), 294–298. https://doi.org/10.1016/j.sna.2007.05.011

Han, B., Sun, S., Ding, S., Zhang, L., Yu, X., & Ou, J. (2015). Review of nanocarbon-engineered multifunctional cementitious composites. *Composites Part A: Applied Science and Manufacturing*, *70*, 69–81. https://doi.org/10.1016/j.compositesa.2014.12.002

Han, B., Yu, X., & Kwon, E. (2009). A self-sensing carbon nanotube/cement composite for traffic monitoring. *Nanotechnology*, *20*(44). https://doi.org/10.1088/0957-4484/20/44/445501

Han, B., Yu, X., & Ou, J. (2014a). Applications of Self-Sensing Concrete. In *Self-Sensing Concrete in Smart Structures* (pp. 189–230). Elsevier. https://doi.org/10.1016/b978-0-12-800517-0.00007-1

Han, B., Yu, X., & Ou, J. (2014b). Compositions of Self-Sensing Concrete. In *Self-Sensing Concrete in Smart Structures* (pp. 13–43). Elsevier. https://doi.org/10.1016/b978-0-12-800517-0.00002-2

Han, B., Yu, X., & Ou, J. (2014c). Measurement of Sensing Signal of Self-Sensing Concrete. In *Self-Sensing Concrete in Smart Structures* (pp. 67–93). Elsevier. https://doi.org/10.1016/b978-0-12-800517-0.00004-6

Han, B., Zhang, K., Burnham, T., Kwon, E., & Yu, X. (2013). Integration and road tests of a self-sensing CNT concrete pavement system for traffic detection. *Smart Materials and Structures*, *22*(1). https://doi.org/10.1088/0964-1726/22/1/015020

Han, B., Zhang, L., & Ou, J. (2017). *Smart and Multifunctional Concrete Toward Sustainable Infrastructures*. Springer Nature Singapore Pte Ltd. https://doi.org/10.1007/978-981-10-4349-9

Hilding, J., Grulke, E. A., Zhang, Z. G., & Lockwood, F. (2003). Dispersion of carbon nanotubes in liquids. *Journal of Dispersion Science and Technology*, *24*(1), 1–41. https://doi.org/10.1081/DIS-120017941

Hill, R. (1969). Electrical conduction in ultra thin metal films I. Theoretical. *Proceedings of the Royal Society of London. A. Mathematical and Physical Sciences*, *309*(1498), 377–395. https://doi.org/10.1098/rspa.1969.0048

Hobbs, D. W. (2001). Concrete deterioration: Causes, diagnosis, and minimising risk. In *International Materials Reviews* (Vol. 46, Issue 3, pp. 117–144). https://doi.org/10.1179/095066001101528420

Hou, T.-C., & Lynch, J. P. (2005). Conductivity-based strain monitoring and damage characterization of fiber reinforced cementitious structural components. *Smart Structures and Materials 2005: Sensors and Smart Structures Technologies for Civil, Mechanical, and Aerospace Systems*, *5765*, 419. https://doi.org/10.1117/12.599955

Huang, X. (2009). Fabrication and properties of carbon fibers. In *Materials* (Vol. 2, Issue 4, pp. 2369–2403). https://doi.org/10.3390/ma2042369

Iijima, S. (1991). Helical microtubes of graphitic carbon. *Nature*, *354*(6348), 56–58. https://doi.org/10.1038/354056a0

Kim, H. K., Nam, I. W., & Lee, H. K. (2014). Enhanced effect of carbon nanotube on mechanical and electrical properties of cement composites by incorporation of silica fume. *Composite Structures*, *107*, 60–69. https://doi.org/10.1016/j.compstruct.2013.07.042

Konsta-Gdoutos, M. S., & Aza, C. A. (2014). Self sensing carbon nanotube (CNT) and nanofiber (CNF) cementitious composites for real time damage assessment in smart structures. *Cement and Concrete Composites*, *53*, 162–169. https://doi.org/10.1016/j.cemconcomp.2014.07.003

Lee, S. J., You, I., Zi, G., & Yoo, D. Y. (2017). Experimental Investigation of the Piezoresistive Properties of Cement Composites with Hybrid Carbon Fibers and Nanotubes. *Sensors*, *17*(11), 2516. https://doi.org/10.3390/s17112516

Li, H., Xiao, H., & Ou, J. (2006). Effect of compressive strain on electrical resistivity of carbon black-filled cement-based composites. *Cement and Concrete Composites*, *28*(9), 824–828. https://doi.org/10.1016/j.cemconcomp.2006.05.004

Li, H., Xiao, H., & Ou, J. (2008). Electrical property of cement-based composites filled with carbon black under long-term wet and loading condition. *Composites Science and Technology*, *68*(9), 2114–2119. https://doi.org/10.1016/j.compscitech.2008.03.007

Li, X., Wang, L., Liu, Y., Li, W., Dong, B., & Duan, W. H. (2018). Dispersion of graphene oxide agglomerates in cement paste and its effects on electrical resistivity and flexural strength. *Cement and Concrete Composites*, *92*, 145–154. https://doi.org/10.1016/j.cemconcomp.2018.06.008

Liang, S., Du, H., Zou, N. Y., Chen, Y., & Liu, Y. (2022). Measurement and simulation of electrical resistivity of cement-based materials by using embedded four-probe method. *Construction and Building Materials*, *357*. https://doi.org/10.1016/j.conbuildmat.2022.129344

Liu, Q., Xu, Q., Yu, Q., Gao, R., & Tong, T. (2016). Experimental investigation on mechanical and piezoresistive properties of cementitious materials containing graphene and graphene oxide nanoplatelets. *Construction and Building Materials*, *127*, 565–576. https://doi.org/10.1016/j.conbuildmat.2016.10.024

Liu, X., & Wu, S. (2011). Study on the graphite and carbon fiber modified asphalt concrete. *Construction and Building Materials*, *25*(4), 1807–1811. https://doi.org/10.1016/j.conbuildmat.2010.11.082

Liu, Y., Wang, M., & Wang, W. (2018). Ohmic heating curing of electrically conductive carbon nanofiber/cement-based composites to avoid frost damage under severely low temperature. *Composites Part A: Applied Science and Manufacturing*, *115*, 236–246. https://doi.org/10.1016/j.compositesa.2018.10.008

Liu, Z., Zhang, Y., & Jiang, Q. (2014). Continuous tracking of the relationship between resistivity and pore structure of cement pastes. *Construction and Building Materials*, *53*, 26–31. https://doi.org/10.1016/j.conbuildmat.2013.11.067

Liu, Z., Zhang, Y., Liu, L., & Jiang, Q. (2013). An analytical model for determining the relative electrical resistivity of cement paste and C-S-H gel. *Construction and Building Materials*, *48*, 647–655. https://doi.org/10.1016/j.conbuildmat.2013.07.020

Luo, J., Duan, Z., Zhao, T., & Li, Q. (2011). Hybrid effect of carbon fiber on piezoresistivity of carbon nanotube cement-based composite. *Advanced*

Materials Research, *143–144*, 639–643. https://doi.org/10.4028/www.scientific.net/AMR.143-144.639

MacKenzie, K. J., Dunens, O. M., & Harris, A. T. (2010). An updated review of synthesis parameters and growth mechanisms for carbon nanotubes in fluidized beds. *Industrial and Engineering Chemistry Research*, *49*(11), 5323–5338. https://doi.org/10.1021/ie9019787

Mendoza Reales, O. A., & Dias Toledo Filho, R. (2017). A review on the chemical, mechanical and microstructural characterization of carbon nanotubes-cement based composites. In *Construction and Building Materials* (Vol. 154, pp. 697–710). Elsevier Ltd. https://doi.org/10.1016/j.conbuildmat.2017.07.232

Mo, Y. L., & Roberts, R. H. (2013). Carbon Nanofiber Concrete for Damage Detection of Infrastructure. In *Advances in Nanofibers* (pp. 125–143). INTECH. https://doi.org/10.5772/57096

Monteiro, A. O., Cachim, P. B., Costa, P. M. F. J., & Oeser, M. (2017). Sensitive Smart Concrete Loaded with Carbon Black Nanoparticles for Traffic Monitoring Sensitive Smart Concrete Loaded with Carbon Black. *The Fourth International Conference on Smart Monitoring, Assessment and Rehabilitation of Civil Structures, 13 – 15 September 2017*.

Muralidharan, S., Saraswathy, V., Thangavel, K., & Palaniswamy, N. (2008). Electrochemical studies on the performance characteristics of alkaline solid embeddable sensor for concrete environments. *Sensors and Actuators, B: Chemical*, *130*(2), 864–870. https://doi.org/10.1016/j.snb.2007.10.059

Naeem, F., Lee, H. K., Kim, H. K., & Nam, I. W. (2017). Flexural stress and crack sensing capabilities of MWNT/cement composites. *Composite Structures*, *175*, 86–100. https://doi.org/10.1016/j.compstruct.2017.04.078

Nam, I. W., Souri, H., & Lee, H. K. (2016). Percolation threshold and piezoresistive response of multi-wall carbon nanotube/cement composites. *Smart Structures and Systems*, *18*(2), 217–231. https://doi.org/10.12989/sss.2016.18.2.217

Nasibulin, A. G., Shandakov, S. D., Nasibulina, L. I., Cwirzen, A., Mudimela, P. R., Habermehl-Cwirzen, K., Grishin, D. A., Gavrilov, Y. V., Malm, J. E. M., Tapper, U., Tian, Y., Penttala, V., Karppinen, M. J., & Kauppinen, E. I. (2009). A novel cement-based hybrid material. *New Journal of Physics*, *11*. https://doi.org/10.1088/1367-2630/11/2/023013

Nasibulina, L. I., Anoshkin, I. V., Shandakov, S. D., Nasibulin, A. G., Cwirzen, A., Mudimela, P. R., Habermehl-Cwirzen, K., Malm, J. E. M., Koltsova, T. S., Tian, Y., Vasilieva, E. S., Penttala, V., Tolochko, O. V., Maarit, J. K., & Esko, I. K.

(2010). Direct synthesis of carbon nanofibers on cement particles. *Transportation Research Record*, *2142*, 96–101. https://doi.org/10.3141/2142-14

Ou, J., & Han, B. (2009). Piezoresistive cement-based strain sensors and self-sensing concrete components. *Journal of Intelligent Material Systems and Structures*, *20*(3), 329–336. https://doi.org/10.1177/1045389X08094190

Payakaniti, P., Pinitsoontorn, S., Thongbai, P., Amornkitbamrung, V., & Chindaprasirt, P. (2017). Electrical conductivity and compressive strength of carbon fiber reinforced fly ash geopolymeric composites. *Construction and Building Materials*, *135*, 164–176. https://doi.org/10.1016/j.conbuildmat.2016.12.198

Qi, X., Qin, C., Zhong, W., Au, C., Ye, X., & Du, Y. (2010). Large-scale synthesis of carbon nanomaterials by catalytic chemical vapor deposition: A review of the effects of synthesis parameters and magnetic properties. *Materials*, *3*(8), 4142–4174. https://doi.org/10.3390/ma3084142

Rajabipour, F., & Weiss, J. (2007a). Electrical conductivity of drying cement paste. *Materials and Structures/Materiaux et Constructions*, *40*(10), 1143–1160. https://doi.org/10.1617/s11527-006-9211-z

Rajabipour, F., & Weiss, J. (2007b). Electrical conductivity of drying cement paste. *Materials and Structures/Materiaux et Constructions*, *40*(10), 1143–1160. https://doi.org/10.1617/s11527-006-9211-z

Rana, S., P, S., Fangueiro, R., & Gomes Correia, A. (2016). A review on smart self-sensing composite materials for civil engineering applications. *AIMS Materials Science*, *3*(2), 357–379. https://doi.org/10.3934/matersci.2016.2.357

Ribeiro, F. J., Tangney, P., Louie, S. G., & Cohen, M. L. (2005). Structural and electronic properties of carbon in hybrid diamond-graphite structures. *Physical Review B - Condensed Matter and Materials Physics*, *72*(21). https://doi.org/10.1103/PhysRevB.72.214109

Rovnaník, P., Míková, M., & Kusá, K. (2017). Electrical properties of alkali-Activated slag composite with combined graphite/CNT filler. *IOP Conference Series: Materials Science and Engineering*, *251*(1). https://doi.org/10.1088/1757-899X/251/1/012082

Saafi, M., Andrew, K., Tang, P. L., McGhon, D., Taylor, S., Rahman, M., Yang, S., & Zhou, X. (2013). Multifunctional properties of carbon nanotube/fly ash geopolymeric nanocomposites. *Construction and Building Materials*, *49*, 46–55. https://doi.org/10.1016/j.conbuildmat.2013.08.007

Sasmal, S., Ravivarman, N., Sindu, B. S., & Vignesh, K. (2017). Electrical conductivity and piezo-resistive characteristics of CNT and CNF incorporated cementitious nanocomposites under static and dynamic loading. *Composites Part A: Applied Science and Manufacturing*, *100*, 227–243. https://doi.org/10.1016/j.compositesa.2017.05.018

See, C. H., & Harris, A. T. (2007). A review of carbon nanotube synthesis via fluidized-bed chemical vapor deposition. In *Industrial and Engineering Chemistry Research* (Vol. 46, Issue 4, pp. 997–1012). https://doi.org/10.1021/ie060955b

Shi, Z.-Q., & Chung, D. D. L. (1999). Carbon fiber-reinforced concrete for traffic monitoring and weighing in motion. In *Cement and Concrete Research* (Vol. 29).

Simmons, J. G. (1963). Generalized Formula for the Electric Tunnel Effect between Similar Electrodes Separated by a Thin Insulating Film. *Journal of Applied Physics*, *34*(6), 1793–1803. https://doi.org/10.1063/1.1702682

Simmons, J. G., & Unterkofler, G. J. (1963). Potential Barrier Shape Determination in Tunnel Junctions. In *Journal of Applied Physics* (Vol. 34, Issue 6, pp. 1828–1830). https://doi.org/10.1063/1.1702693

Song, G., Mo, Y. L., Otero, K., & Gu, H. (2006). Health monitoring and rehabilitation of a concrete structure using intelligent materials. *Smart Materials and Structures*, *15*(2), 309–314. https://doi.org/10.1088/0964-1726/15/2/010

Sun, J., Lin, S., Zhang, G., Sun, Y., Zhang, J., Chen, C., Morsy, A. M., & Wang, X. (2021). The effect of graphite and slag on electrical and mechanical properties of electrically conductive cementitious composites. *Construction and Building Materials*, *281*. https://doi.org/10.1016/j.conbuildmat.2021.122606

Sun, M., Li, Z., & Liu, Q. (2002). The electromechanical effect of carbon fiber reinforced cement. *Carbon*, 2273–2275.

Sun, S., Han, B., Jiang, S., Yu, X., Wang, Y., Li, H., & Ou, J. (2017). Nano graphite platelets-enabled piezoresistive cementitious composites for structural health monitoring. *Construction and Building Materials*, *136*, 314–328. https://doi.org/10.1016/j.conbuildmat.2017.01.006

Tang, Q. Y., Chan, Y. C., & Zhang, K. (2011). Fast response resistive humidity sensitivity of polyimide/multiwall carbon nanotube composite films. *Sensors and Actuators, B: Chemical*, *152*(1), 99–106. https://doi.org/10.1016/j.snb.2010.09.016

Teomete, E., & Kocyigit, O. I. (2013). Tensile strain sensitivity of steel fiber reinforced cement matrix composites tested by split tensile test. *Construction and Building Materials*, *47*, 962–968. https://doi.org/10.1016/j.conbuildmat.2013.05.095

Thomoglou, A. K., Falara, M. G., Gkountakou, F. I., Elenas, A., & Chalioris, C. E. (2023). Smart Cementitious Sensors with Nano-, Micro-, and Hybrid-Modified Reinforcement: Mechanical and Electrical Properties. *Sensors*, *23*(5). https://doi.org/10.3390/s23052405

Thostenson, E. T., Ren, Z., & Chou, T.-W. (2001). Advances in the science and technology of carbon nanotubes and their composites: a review. *Composites Science and Technology*, *61*(13), 1899–1912. https://doi.org/10.1016/S0266-3538(01)00094-X

Thostenson, E. T., Ziaee, S., & Chou, T. W. (2009). Processing and electrical properties of carbon nanotube/vinyl ester nanocomposites. *Composites Science and Technology*, *69*(6), 801–804. https://doi.org/10.1016/j.compscitech.2008.06.023

Tian, X., & Hu, H. (2012). Test and Study on Electrical Property of Conductive Concrete. *Procedia Earth and Planetary Science*, *5*, 83–87. https://doi.org/10.1016/j.proeps.2012.01.014

Tu, Y., Liu, D., Yuan, L., & Wang, T. (2021). Early hydration process and kinetics of concrete based on resistivity measurement. *Journal of Advanced Concrete Technology*, *19*(3), 196–206. https://doi.org/10.3151/jact.19.196

Wang, H., Xiang, P., & Jiang, L. (2019). Strain transfer theory of industrialized optical fiber-based sensors in civil engineering: A review on measurement accuracy, design and calibration. In *Sensors and Actuators, A: Physical* (Vol. 285, pp. 414–426). Elsevier B.V. https://doi.org/10.1016/j.sna.2018.11.019

Wang, L., & Aslani, F. (2019). A review on material design, performance, and practical application of electrically conductive cementitious composites. In *Construction and Building Materials* (Vol. 229). Elsevier Ltd. https://doi.org/10.1016/j.conbuildmat.2019.116892

Wang, W., Wu, S., & Dai, H. (2006). Fatigue behavior and life prediction of carbon fiber reinforced concrete under cyclic flexural loading. *Materials Science and Engineering: A*, *434*(1–2), 347–351. https://doi.org/10.1016/j.msea.2006.07.080

Wang, X., Wang, Y., & Jin, Z. (2002). Electrical conductivity characterization and variation of carbon fiber reinforced cement composite. *Journal of Materials Science*, *37*, 223–227.

Warakulwit, C., Yadnum, S., Paluka, V., Phuakkong, O., Niamlaem, M., Pongpaisanseree, K., Sinthupinyo, S., & Limtrakul, J. (2015). Controlled

production of carbon nanofibers over cement clinker via oxidative dehydrogenation of acetylene by intrinsic carbon dioxide. *Chemical Engineering Journal*, *278*, 150–158. https://doi.org/10.1016/j.cej.2014.11.028

Wen, S., & Chung, D. D. L. (1999). Piezoresistivity in continuous carbon fiber cement-matrix composite. *Cement and Concrete Research*, *29*(3), 445–449. https://doi.org/10.1016/S0008-8846(98)00211-7

Wen, S., & Chung, D. D. L. (2001). Carbon fiber-reinforced cement as a strain-sensing coating. *Cement and Concrete Research*, *31*, 665–667.

Wen, S., & Chung, D. D. L. (2003). A comparative study of steel- and carbon-fibre cement as piezoresistive strain sensors. *Advances in Cement Research*, *15*(3), 119–128. https://doi.org/10.1680/adcr.15.3.119.36621

Wen, S., & Chung, D. D. L. (2007). Partial replacement of carbon fiber by carbon black in multifunctional cement-matrix composites. *Carbon*, *45*(3), 505–513. https://doi.org/10.1016/j.carbon.2006.10.024

Wu, J., Liu, J., & Yang, F. (2015). Three-phase composite conductive concrete for pavement deicing. *Construction and Building Materials*, *75*, 129–135. https://doi.org/10.1016/j.conbuildmat.2014.11.004

Wu, S., Dai, H., & Wang, W. (2007). Effect of CFRC layers on the electrical properties and failure mode of RC beams strengthened with CFRC composites. *Smart Materials and Structures*, *16*(6), 2056–2062. https://doi.org/10.1088/0964-1726/16/6/008

Wu, S., Mo, L., Shui, Z., & Chen, Z. (2005). Investigation of the conductivity of asphalt concrete containing conductive fillers. *Carbon*, *43*(7), 1358–1363. https://doi.org/10.1016/j.carbon.2004.12.033

Xiao, H., Li, H., & Ou, J. (2011). Strain sensing properties of cement-based sensors embedded at various stress zones in a bending concrete beam. *Sensors and Actuators, A: Physical*, *167*(2), 581–587. https://doi.org/10.1016/j.sna.2011.03.012

Xie, P., Gu, P., & Beaudoin, J. J. (1996). Electrical percolation phenomena in cement composites containing conductive fibres. In *JOURNAL OF MATERIALS SC1ENCE* (Vol. 31).

Yang, Y., Gupta, M. C., Zalameda, J. N., & Winfree, W. P. (2008). Dispersion behaviour, thermal and electrical conductivities of carbon nanotube-polystyrene nanocomposites. *Micro & Nano Letters*, *3*(2), 35–40. https://doi.org/10.1049/mnl:20070073

Yazdanbakhsh, A., Grasley, Z., Tyson, B., & Al-Rub, R. K. A. (2010). Distribution of Carbon Nanofibers and Nanotubes in Cementitious Composites. *Transportation Research Record*, *2142*(1), 89–95. https://doi.org/10.3141/2142-13

Yazdani, N., & Mohanam, V. (2014). Carbon Nano-Tube and Nano-Fiber in Cement Mortar: Effect of Dosage Rate and Water-Cement Ratio. *International Journal of Material Sciences*, *4*(2), 45. https://doi.org/10.14355/ijmsci.2014.0402.01

Yildirim, G., Aras, G. H., Banyhussan, Q. S., Şahmaran, M., & Lachemi, M. (2015). Estimating the self-healing capability of cementitious composites through non-destructive electrical-based monitoring. *NDT and E International*, *76*, 26–37. https://doi.org/10.1016/j.ndteint.2015.08.005

Yoo, D. Y., You, I., & Lee, S. J. (2017). Electrical properties of cement-based composites with carbon nanotubes, graphene, and graphite nanofibers. *Sensors (Switzerland)*, *17*(5). https://doi.org/10.3390/s17051064

You, I., Yoo, D. Y., Kim, S., Kim, M. J., & Zi, G. (2017). Electrical and self-sensing properties of ultra-high-performance fiber-reinforced concrete with carbon nanotubes. *Sensors (Switzerland)*, *17*(11). https://doi.org/10.3390/s17112481

Young, J. F. (1967). HUMIDITY CONTROL IN THE LABORATORY USING SALT SOLUTIONS-A REVIEW. In *J. appl. Chem* (Vol. 17).

Yu, X., & Kwon, E. (2009). A carbon nanotube/cement composite with piezoresistive properties. *Smart Materials and Structures*, *18*(5). https://doi.org/10.1088/0964-1726/18/5/055010

Zhang, H., Hou, S., & Ou, J. (2016). Smart aggregate-based seismic stress monitoring system using a specially designed charge amplifier. *Journal of Intelligent Material Systems and Structures*, *27*(3), 418–426. https://doi.org/10.1177/1045389X15610909

Zhang, L., Ding, S., Dong, S., Li, Z., Ouyang, J., Yu, X., & Han, B. (2017). Piezoresistivity, mechanisms and model of cement-based materials with CNT/NCB composite fillers. *Materials Research Express*, *4*(12). https://doi.org/10.1088/2053-1591/aa9d1d

Zhang, L., Han, B., Ouyang, J., Yu, X., Sun, S., & Ou, J. (2017). Multifunctionality of cement based composite with electrostatic self-assembled CNT/NCB composite filler. *Archives of Civil and Mechanical Engineering*, *17*(2), 354–364. https://doi.org/10.1016/j.acme.2016.11.001

Zhang, W., Ouyang, J., Ruan, Y., Zheng, Q., Wang, J., Yu, X., & Han, B. (2018). Effect of mix proportion and processing method on the mechanical and electrical

properties of cementitious composites with nano/fiber fillers. *Materials Research Express*, *5*(1). https://doi.org/10.1088/2053-1591/aaa60a

Paper I

State of the art on sensing capability of poorly or nonconductive matrixes with a special focus on Portland cement–based materials

Buasiri, T., Habermehl-Cwirzen, K., Krzeminski, L., & Cwirzen, A.

State-of-the-Art Review

State of the Art on Sensing Capability of Poorly or Nonconductive Matrixes with a Special Focus on Portland Cement–Based Materials

Thanyarat Buasiri[1]; Karin Habermehl-Cwirzen[2]; and Andrzej Cwirzen[3]

Abstract: Concrete, a well-established and well-characterized building material, is also the most used building material in the world. However, many old and new-build structures suffer from premature failures due to extensive deterioration and decreased load-bearing capacity. Consequently, structural monitoring systems are essential to ensure safe usage of concrete structures within and beyond their designed life. Traditional monitoring systems are based on metallic sensors installed in crucial locations throughout the structure. Unfortunately, most of them have relatively low reliability and a very short life span when exposed to often very harsh environments. The ideal solution is therefore to develop a smart concrete having self-sensing capability. A number of studies have shown that conductive cementitious matrixes will undergo changes in their electrical resistivity with variations of stresses and strains or development of microcracking. This behavior can be used as a reliable tool to measure changes. This review provides a comprehensive overview of several nonconductive matrixes, with a special focus on portland cement–based materials, showing self-sensing capabilities by description of detection mechanisms, sensing capabilities, limitations, and potential applications. **DOI:** [10.1061/(ASCE)MT.1943-5533.0002901](https://doi.org/10.1061/(ASCE)MT.1943-5533.0002901). *© 2019 American Society of Civil Engineers.*

Author keywords: Sensing capability; Nonconductive matrixes; Portland cement–based materials; Conductive fibers; Electrical conductivity; Materials sensing.

Introduction

Deterioration of concrete can originate from the corrosion of reinforcement (Cabrera 1996), carbonation (Chi et al. 2002), frost and frost deicing salt attack, seawater attack, and alkali silica reaction, among others (Boyd and Skalny 2007; Darwin et al. 2008). The presence of a monitoring system enables evaluation and assessment of the extent of damage, and estimation (Yazdani and Mohanam 2014) of the remaining load-bearing capacity (Housner et al. 1997). Early detection of developing damages and successive application of a proper repair mechanism enhances the durability and prevents reduction of or even elongates the life span of affected concrete structures (Rana et al. 2016). Structural health monitoring (SHM) is a method aiming to detect the damage of civil structures (Aggelis et al. 2014; Chang et al. 2003; Han et al. 2015a; Sun et al. 2010; Ye et al. 2014) especially bridges, dams, roads, and high-rise buildings. SHM uses embedded sensors designed to discover and measure various crucial parameters like stress, strain, crack formation, humidity, and chloride content. Unfortunately,

most have serious constraints related to poor durability, high cost, and short lifespan (Monteiro et al. 2017).

A new generation of monitoring systems being widely studied at present is based on a self-sensing portland cement–based matrix. The binder matrix itself acts as a sensor using changes in electrical properties when subjected to stress or strain. Theoretically, the self-sensing capability should be able to produce systems that are significantly more reliable, accurate, and sensitive but at lower cost and ensuring a longer service life. This paper reviews sensing mechanisms and effects of various types of conductive materials on the monitoring capabilities of modified nonconductive matrixes, with a special focus on portland cement–based matrixes.

Sensing Mechanism in Nonconductive Matrixes

Nonconductive or poorly conductive composites (i.e., cementitious polymers and ceramics) are widely used in electronics, packaging, as adhesive, interconnections, and electromagnetic shields as well as in automotive, aerospace, and space industries (Awaja et al. 2016; Chen and Chung 1995). Cement-based materials are classified as quasi-brittle materials (Bajare et al. 2012). A hardened cement matrix shows limited electrical conductivity only in the wet state. The addition of electrically conducting material, including, for example, carbon fiber, carbon black, or steel fiber, can induce some conductivity, which could be in some cases utilized in limited structural health monitoring (Wang and Chung 2000). The sensitivity of such a system depends on the type, quantity, and distribution of the incorporated conductive material. A uniform distribution combined with a sufficient amount of conductive material can create a conductive path throughout the binder matrix. The conductivity of such a system will change with the applied load or development of internal damage such as microcracks. The relation

[1]Ph.D. Student, Building Materials, Dept. of Civil, Environmental, and Natural Resources Engineering, Luleå Univ. of Technology, Luleå 97187, Sweden (corresponding author). ORCID: https://orcid.org/0000-0003-0459-7433. Email: thanyarat.buasiri@ltu.se

[2]Senior Lecturer, Building Materials, Dept. of Civil, Environmental, and Natural Resources Engineering, Luleå Univ. of Technology, Luleå 97187, Sweden. Email: karin.habermehl-cwirzen@ltu.se

[3]Professor, Building Materials, Dept. of Civil, Environmental, and Natural Resources Engineering, Luleå Univ. of Technology, Luleå 97187, Sweden. ORCID: https://orcid.org/0000-0001-6287-2240. Email: andrzej.cwirzen@ltu.se

© ASCE 03119003-1 J. Mater. Civ. Eng.

J. Mater. Civ. Eng., 2019, 31(11): 03119003
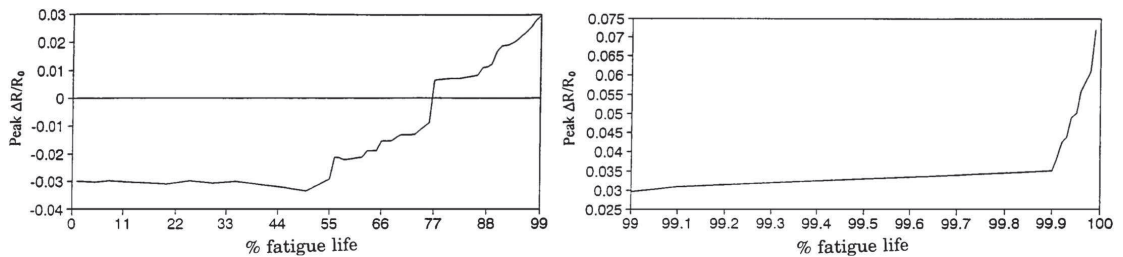
Fig. 1. Variation of the peak $\Delta R/R_0$ with the percentage of fatigue life. (Adapted with permission from Springer Nature: Springer, *Journal of Material Science*, "Sensing damage in carbon fiber and its polymer-matrix and carbon-matrix composites by electrical resistance measurement," X. Wang, S. Wang, and D. D. L. Chung, © 1999.)

between the electrical conductivity and amount of the conductive phase shows a maximum threshold value, which marks the maximum sensitivity of the matrix. Below and above the threshold value, the sensitivity decreases (Baeza et al. 2010). The value is commonly named as the electrical percolation threshold (EPT) (Zeng et al. 2011).

Strain Sensing

Strain sensing refers to the ability of certain materials to sense strain or stress through a change of the electrical resistance when exposed to various forces, i.e., so-called piezoresistive behavior. For a polymer matrix composite, the strain sensitivity is defined as the ratio between the reversible change of the fractional resistance ($\Delta R/R_0$) and the strain amplitude (Chung 2002a). Damage sensitivity is related to the irresistible increase in resistance. The measurement of the electrical response during loading is recorded and used to estimate the strain value (Kuronuma et al. 2012). Resistivity increases due to progressive breakage of the conduction paths under tensile loading, whereas resistivity will decrease in compression due to the fiber push-in, thus increasing the chance of fibers in the adjacent laminae touching one another along the direction of fiber orientation (Chung 1998, 2002a). As a result, electrical resistance rises along the perpendicular direction and declines along the longitudinal direction (Chung 2002a). The measurement of irreversible strain allows structural health monitoring, and the sensing of reversible strain permits dynamic-load monitoring.

The strain sensitivity of composites is measured by calculating the so-called gauge factor (GF). The GF is defined as the ratio of fractional change of the electrical resistance to the fractional change of the strain ($\Delta R/R_0/\varepsilon$). A higher GF indicates better strain sensitivity. Continuous carbon fiber in a polymer matrix creates a sensitive strain sensor having a GF of up to 38. A cement-based matrix with embedded short carbon fibers can reach a very high strain-sensing capability with GF up to 700 (Chung 1998). Higher contents of nanoconducting materials are required if materials are exposed to larger strain/stress levels to prevent premature breakage of the fibers. Nanocomposites have shown sufficiently high strain sensitivity when the filler content is close to the percolation threshold (Georgousis et al. 2015).

Fatigue Sensing

Fatigue is a common cause of damage of structures subjected to repeatable dynamic loading. The measurement of the electrical resistivity proved to be an efficient method to determine fatigue in cyclic loading. Wang et al. (1999) showed that with carbon-fiber

polymer-matrix composites, fatigue sensing can be achieved. It can be clearly seen that the peak of $\Delta R/R_0$ has increased significantly from approximately 50% fatigue life onward, as shown in Fig. 1. At 218,277 cycles in Fig. 2 (55% of fatigue life), $\Delta R/R_0$ showed a continuous increase from cycle to cycle and reached 396,854 cycles when fatigue failure took place. This behavior shows that fiber breakage increased resistivity in the composites. The degree of the damage depended on how the resistivity of cycles changes. Minor fatigue damage was reported when the resistivity increased discontinuously in spurts. A gradual increase in resistivity was attributed to severe fatigue damage with more extensive fiber breakage.

Wang et al. (2008) studied the sensitivity of a reinforced concrete beam incorporating a layer of short carbon fiber–reinforced concrete (CFRC) with diameter and length of carbon fibers of 6 μm and 5 mm, respectively. The aim was to determine its sensing capability under applied repeated fatigue flexural loading at a stress amplitude equal to 0.8 of the ultimate stress. The results showed that $\Delta R/R_0$ increased with applied loading and decreased during unloading in each cycle. Within the first five cycles, the fractional resistance increased slightly from 2.8% to 3.6% due to occurrence of small damage. The failure of the beam occurred after 38 loading cycles, with irreversible fractional resistance increasing up to 179% of its initial value. Limited damage caused only a small reversible change in electrical resistivity due to rearrangement of the fiber distribution. An irreversible increase of the electrical resistance was caused by major damage to and breakdown of the conductive network and fibers. Similar effects were also reported by Wang et al. (2006).

Temperature Sensing

High-temperature sensing is essential in modern power plants, especially in turbine engines, coal gasification systems, materials processing systems, and energy systems (Chung 2002a; Leal-Junior et al. 2018; Moraleda et al. 2013; Zhao et al. 2014). Several different methods are well-studied and used for monitoring in those harsh environments (Zhao et al. 2014). Thermistors, thermocouples resistance, and temperature detectors are traditional sensors using changes in electrical resistivity with temperature variations (Leal-Junior et al. 2018; Tapetado et al. 2015). In conductive polymer composites, the electrons overcome the potential barrier, leading to the so-called tunneling effect. If the distance between adjacent conductive materials is small enough, an effective conductive path is formed. When the path is long enough, it contributes to the conductivity of the composite. A composite with a cellular structure is sensed in a negative temperature coefficient unit

© ASCE   03119003-2   J. Mater. Civ. Eng.

J. Mater. Civ. Eng., 2019, 31(11): 03119003
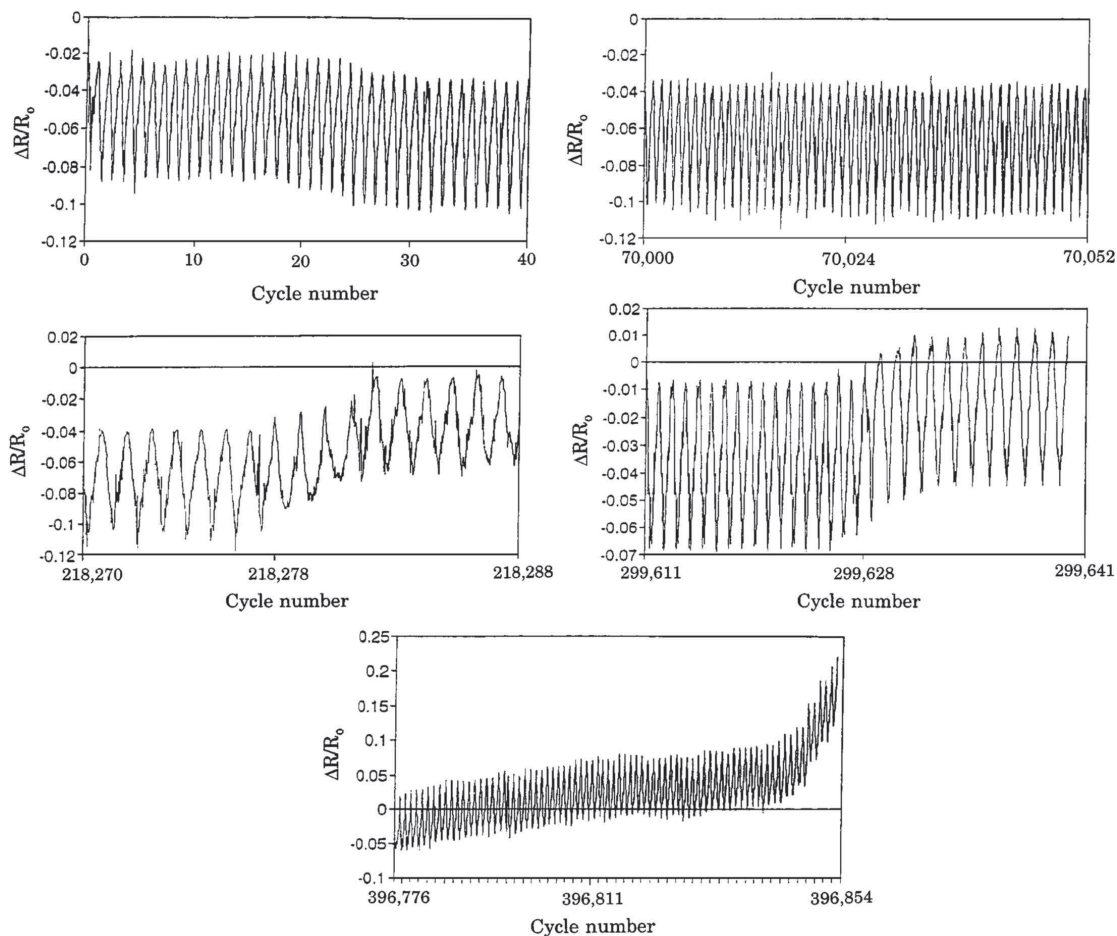
Fig. 2. Variation of $\Delta R/R_0$ with number of cycles in fatigue test in polymer matrix composite with carbon fiber. (Adapted with permission from Springer Nature: Springer, *Journal of Material Science*, "Sensing damage in carbon fiber and its polymer-matrix and carbon-matrix composites by electrical resistance measurement," X. Wang, S. Wang, and D. D. L. Chung, © 1999.)

(NTCU) [Fig. 3(a)]. The resistivity of the composite decreases with increasing temperature.

In contrast, a composite without a cellular structure is used as a sensitive material in the positive temperature coefficient unit (PTCU) [Fig. 3(b)]. In this case, the resistivity of the composite increases with increasing temperature (Wang 2015). An increase in temperature leads to an expansion of the matrix, which increases the distances between the conductive materials. As a result, the resistivity of the composite in the PTCU increases. On the other hand, in the NTCU, the resistivity of the composite decreases when the temperature increases due to expansion of the gas-filled voids. Due to this expansion, the distances between the conductive fillers are reduced, and more conductive networks are formed.

Fig. 4(a) shows the effects of the temperature on the resistivity of polymeric matrixes with conductive filler in NTCU and Fig. 4(b) shows the effects in PTCU systems. PTCU based on a carbon black–filled silicone rubber composite and NTCU based on a carbon-nanotube–filled polyurethane foam composite are good examples

where the effective temperature range for the measurement is between 25°C and 75°C, respectively (Wang 2015). Due to changes in electrical resistivity with increasing temperature, epoxy-based matrixes with continuous carbon fibers used for temperature sensing
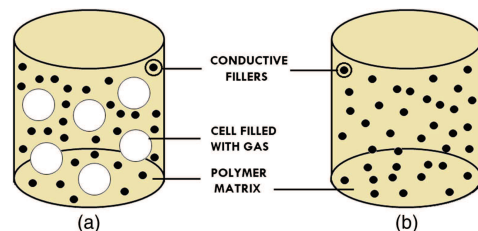
Fig. 3. Conductive polymer composite: (a) with cellular structure; and (b) without cellular structure.

© ASCE   03119003-3   J. Mater. Civ. Eng.

J. Mater. Civ. Eng., 2019, 31(11): 03119003
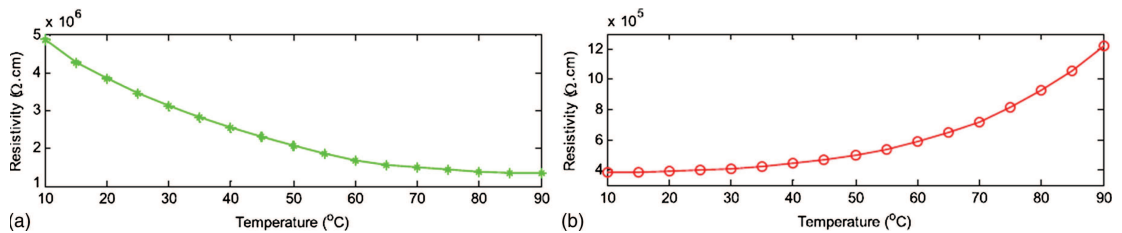
Fig. 4. Variation of resistivity with temperature in (a) carbon nanotube–filled polyurethane foam composite; and (b) carbon black–filled silicone rubber composite. [© 2015 IEEE. Reprinted, with permission, from L. Wang, "Differential structure for temperature sensing based on conductive polymer composites," *IEEE Transactions on Electron Devices* 62 (9): 3025-3028.]

acted as a thermistor (Chung 2002a; Wang and Chung 1998b, 1999) and thermocouple (Chung 2002a; Wang and Chung 1998a).

Crack and Microcrack Sensing

Microcracking, which is one of the major causes of premature failure of composite materials (Awaja et al. 2016; Nairn 2000; Pang and Bond 2005), is difficult to detect due to the limited resolution of visual methods. An alternative method is to use conductive fillers embedded in the matrix to detect the propagation of cracks and microcracks through determination of fibers acting as bridges across cracks (bridging effect) (Awaja et al. 2016). Shindo et al. (2012) investigated the relation between crack formation and the electrical resistance of polymer composites incorporating multi-walled carbon nanotubes (MWCNTs) in tensile loading. The specimen was notched with an initial crack length a_0 equal to 9.3 mm (Fig. 5). During fracture testing, the load was applied at an angle between 0° and 30°. The formed crack propagated straight at the load angle of 0° and inclined at the load angle of 30°. The electrical resistivity increased according to the projected crack length increase, as shown in Fig. 6 (Takeda et al. 2013). MWCNT-based polymer composites were used successfully as a damage sensor by Li et al. (2008a).

Currently Used Systems for Monitoring of Concrete Structures

Nondestructive testing (NDT) is commonly applied to assess the quality of concrete structures. Examples are ultrasonic inspection and Foucault current technique (eddy current technique) used for crack detection. A so-called half-cell potential test is used to assess corrosion of the reinforcement. NDT techniques are often limited to a single-point measurement (Helal et al. 2015). At present, the SHM system has become a well-known method aiming to diagnose the condition of a structure and formulate a prognosis related to various possible environmental conditions. The SHM system consists of various measurement techniques, and each technique has its own application area, advantages and limitations.

A concrete structure can be monitored at any point of its service life. The collected data are crucial for forecasting and risk management with respect to the SHM. The SHM integrates NDT techniques using remote sensing and smart materials to create smart self-monitoring structures. The SHM system consists of sensors and data collection and evaluation systems (Aggelis et al. 2014; Sun et al. 2010). Sensors are chosen based on planned measurements and monitoring strategy. Each type of sensor has different
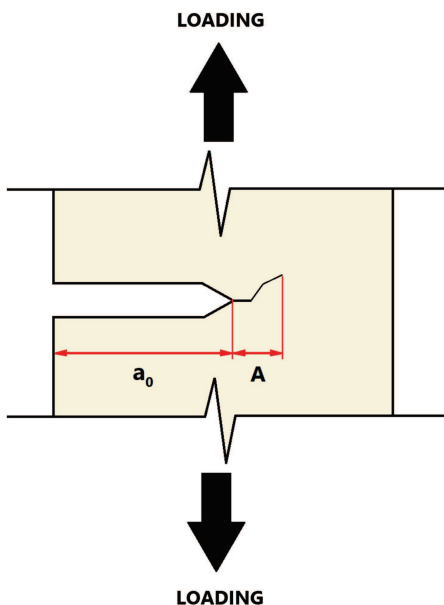
Fig. 5. Fracture mode I test.
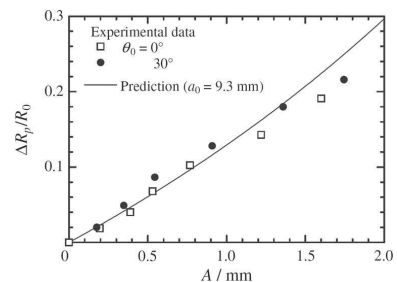
Fig. 6. Variation of resistance change due to crack propagation with projected crack length. (Reprinted from Takeda et al. 2013, with permission from The Japan Institute of Metals and Materials.)

© ASCE   03119003-4   J. Mater. Civ. Eng.

J. Mater. Civ. Eng., 2019, 31(11): 03119003
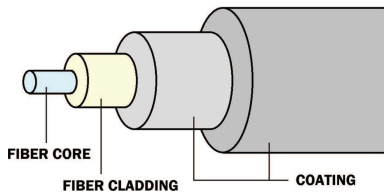
Fig. 7. Schematic diagram of an optical fiber.

sensing capabilities in different applications. Thus the quality of the result obtained from SHM depends on proper design of the system (Lim et al. 2006; Ou and Zhou 2008; Sun et al. 2008; Wan and Leung 2007). The following sections will describe the most commonly used sensors.

Fiber-Optic Sensors

A fiber-optic sensor (FOS) is a fiber-based device that uses fiber optics to transmit light from a superluminescent source. The reflected light shows changes of amplitude, phase, frequency, and polarization state, which are then used to determine changes in temperature and strain (López-Higuera et al. 2011). The fiber optic consists of three parts as shown in Fig. 7. The core and cladding

layer are made of a dielectric material. The index of refraction of the cladding material is less than that of the core to reduce the loss of light transmitted in the core. The coating layer protects the fiber optic against physical damage. FOS can be classified based on the light transmitted in the sensing segment, operating principle, and the application (Fidanboylu and Efendioglu 2009). Some examples include Frabry-Perot FOS, Fiber Braff grating (FBG), and Brillouin-scattering-based FOS. FOS can be used in concrete to monitor strain, displacement, vibration, cracking, corrosion, and chloride concentration. In old structures, FOS are mounted on the surface, whereas in new structures, sensors are usually embedded inside the material. Examples of applications are shown in Fig. 8 (Leung et al. 2008). Fig. 9 gives a schematic overview of available types of FOS (Fidanboylu and Efendioglu 2009).

Piezoelectric Sensors

The conversion of mechanical energy into electrical energy and vice versa is the principle utilized in the piezoelectric effect (Fig. 10). When mechanical stress is applied to a piezoelectric material, an electrical current or voltage is produced. Conversely, when an electric current is applied to a piezoelectric material, it will be polarized, causing it to shrink or expand. This phenomenon enables the detection of impacts and deformations (Tzou et al. 2004). Piezoelectric materials include, for example, ceramics, polymers, and composites. Lead zirconate titanate (PZT) is a commonly used piezoelectric material due to its low cost, light weight, high energy
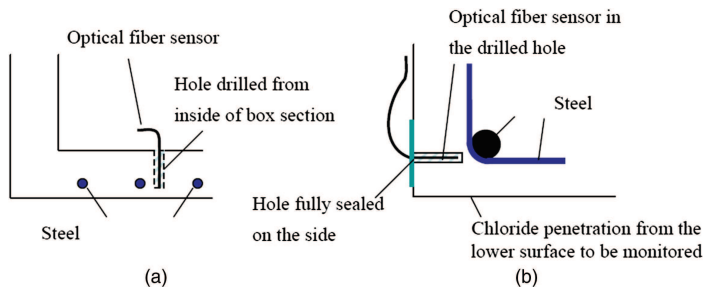
Fig. 8. Possible ways for retrofitting the sensor on an existing structure. [Reprinted from Leung et al. 2008, © MDPI under CC-BY 4.0 (https://creativecommons.org/licenses/by/4.0/).]
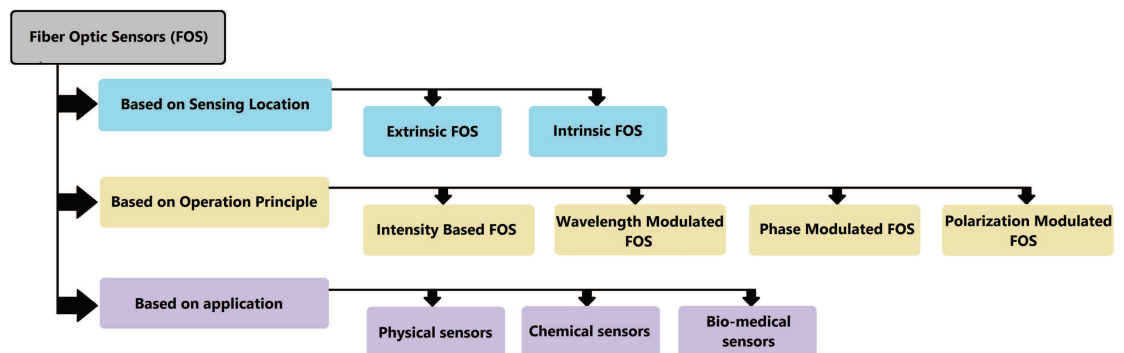
Fig. 9. Fiber optic sensor types.
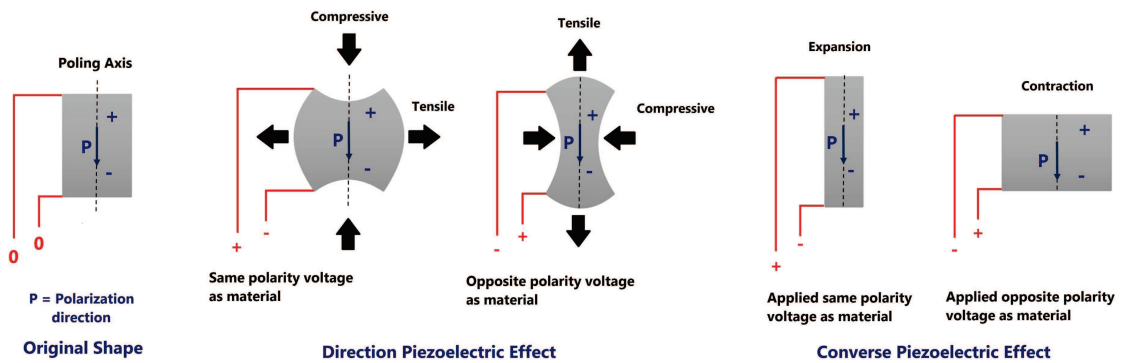
Fig. 10. Piezoelectric effect.

density, and easy implementation. Application of piezoelectric sensors (PS) as actuators and transducers in the SHM is gradually increasing (Chalioris et al. 2016). Embedded PS can also be used as aggregates or fillers (Zhang et al. 2017) to harvest energy from vehicles' movement and for dynamic monitoring of traffic. Such a system is, for example, able to detect and classify passing vehicles (Rana et al. 2016).

Magnetostrictive Sensors

The phenomenon of magnetostriction occurs when ferromagnetic materials, particularly nickel, iron, and cobalt, are able to change their shape or dimensions when placed in a magnetic field. Magnetostrictive materials convert magnetic energy to mechanical energy and vice versa. They are mainly used as transducers for emitting and receiving elastic waves to detect defects, estimate the concrete thickness, and determine the position and distribution of cracks, as well as to monitor acoustic emissions (Ausanio et al. 2005; Calkins et al. 2007; Dong et al. 2011; Hison et al. 2005; Hristoforou and Ktena 2007).

An example usage of magnetostriction is the so-called electromagnetic hammer (EMH). The EMH uses a small magnetostrictive oscillator and receiver consisting of polycrystallized magnetostrictive material (Hattori et al. 2001). The oscillator generates an elastic wave with wide bandwidth at low frequency, which is enhanced by applied additional compressive stress. The oscillator is placed adjacent to the receiver and uses impulse and frequency sweep drive control modes to characterize and evaluate the propagation of cracks in concrete. The system records acoustic reflections at a distance L. Together with the acoustic velocity, v, the delay in propagation, $\Delta t = 2L/v$, and peak frequency, $f = 1/\Delta t$ can be obtained. The presence of defects can be calculated by using $L = v/2 \cdot \Delta t$. The experimental results showed high effectiveness of the system.

Portland Cement–Based Materials Sensing Incorporating Conductive Fibers

Steel Fiber

Steel fibers (SF) are commonly used to reinforce concrete structures. They improve the mechanical properties, particularly flexural and tensile strengths, and limit drying shrinkage cracking.

The primary function of SF in the cementitious matrix is to bridge forming cracks.

In addition, electrical conductivity can be enhanced by addition of SF (Shi et al. 2017). A cement paste incorporating 0.36% by volume of steel fibers and showing sensing capabilities was produced by Wen and Chung (2003). SFs having a diameter of 8 μm and length of 6 mm were used and tested in a cement matrix in repeated tensile and compressive stresses. Teomete and Kocyigit (2013) used between 0.20% and 1.50% by volume of 6-mm-long fibers. The results showed an increased electrical resistivity while under tension, which was related to the formation and propagation of microcracks. The change of electrical resistance was possible above the percolation threshold, which was around 1% by volume of steel fibers. The highest recorded GF of the cement-based matrix incorporating the steel fibers was 5,195, which is much higher than the factors achieved with a metal strain gauge (Wen and Chung 2003).

Carbon Black

Yet another alternative to produce matrixes with sensing capabilities is to add conductive powders, such as, for example, carbon black (CB). CB has a high electrical conductivity, nanosize particles with a high specific surface area to volume ratio, and low cost (Wen and Chung 2007). The amorphous CB is highly compressible, which supports the creation of conductive paths throughout the matrix during loading (Leong et al. 2006; Leong and Chung 2004; Wen and Chung 2007). Li et al. (2006, 2008b) fabricated a strain-sensing cement paste incorporating CB and determined that that percolation threshold oscillated at around 12%–20% by weight of the cement. The resistivity decreased linearly with increasing compressive strain until failure occurred (Fig. 11) (Li et al. 2006). Crack formation was visualized by a bump on the otherwise nearly linear correlation. The strain sensitivity of the GF was 55.28 with 15% by weight of carbon black content.

Results obtained by Lin et al. (2011) showed also that cement matrixes incorporating CB are sensitive to strain. The increase of the tensile strain caused an increase of the matrix's electrical resistivity. Interestingly, in the elastic part of the strain-stress curve, the resistivity remained constant. The formation of microcracks, which appeared on the resistivity-strain curve as significant positive or negative variations of the recorded values, were also detectable, as shown in Fig. 12.
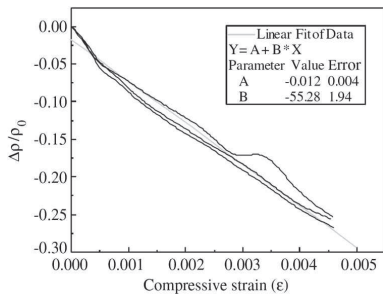
Fig. 11. Variation of fractional resistivity with 15% CB with compressive strain. (Reprinted from *Cement and Concrete Composites*, Vol. 28, H. Li, H.-G. Xiao, and J.-P. Ou, "Effect of compressive strain on electrical resistivity of carbon black-filled cement-based composites," pp. 824–828, © 2006, with permission from Elsevier.)
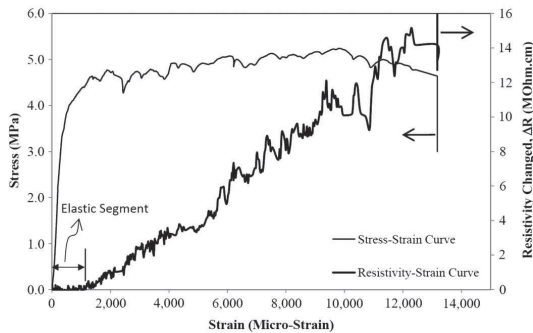
Fig. 12. Variation of resistivity with strain response of elastic and inelastic regime. (Reprinted with permission from V. W. J. Lin, M. Li, J. P. Lyncha, and V. C. Li, "Mechanical and electrical characterization of self-sensing carbon black ECC," *Proc. of SPIE*, Vol. 7983, 2011, © SPIE.)

Carbon Fibers

Carbon fibers (CFs) are formed mostly of carbon atoms and have a diameter in the micrometer range. Studies showed that the addition of CF to portland cement–based mortar enhanced the flexural strength by 85%, flexural toughness by 205%, and compressive strength by 22%. It was also possible to monitor the fatigue damage in cement mortar incorporating 0.5% by weight of CFs (Chen and Chung 1993; Chung and Fu 1996).

The percolation threshold of the CF used in concrete subjected to 2- and 10-MPa loads was about 1% by weight (Shifeng et al. 2007). The electrical resistivity of CFRC was also found to be temperature sensitive with increasing temperature. First, the resistivity decreased due to the increase of the tunneling effect. The electrons move quickly and have more energy to absorb heat energy. After a certain temperature is reached, the unreacted water is fully evaporated, leading to disconnection of some of the conduction paths, which results in an increase of electrical resistivity. The results showed that the CFRC has both negative and positive temperature coefficients (NTC and PTC) (Fig. 13). Materials with a more defined (narrower) peak marking the minimum resistivity, as in the case of composites, can be better used as temperature-sensitive materials.

CFRC showed piezoresistive properties under cyclic loading (Chung 2002b; Wen and Chung 1999, 2003). In the elastic regime, the fractional change in resistance decreased at loading and increased when unloaded. It was found that the irreversible piezoresistivity occurred when the strain was larger than 0.2%. Consequently, the CFRC was not suited for stress-strain sensing under heavy load.

Carbon Nanotubes

Carbon nanotubes (CNTs) have a cylindrical structure consisting of hexagonal graphite sheets rolled in tubes. It is one of the strongest materials in the world (Wong et al. 1997; Yu et al. 2000a, b). One of the first to observe the CNTs was Iijima (1991). CNTs can be classified depending on the applied synthesis conditions, which are single-walled carbon nanotubes (SWCNTs) [Fig. 14(a)] and multiwalled carbon nanotubes (MWCNTs) [Fig. 14(b)]. CNTs are characterized by remarkable physical, mechanical, and electrical properties. They are nanosized, have high strength and Young's modulus, large deformation response, high ductility, high aspect
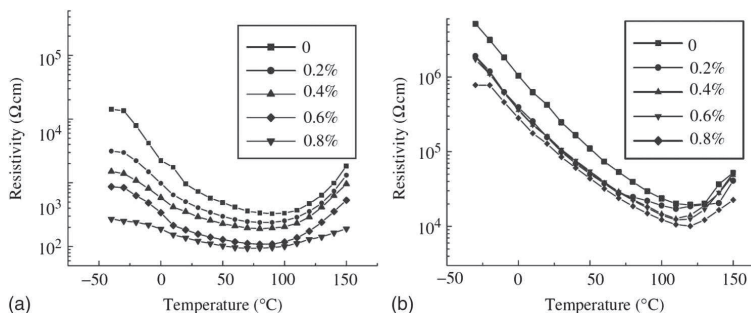
Fig. 13. Variation of resistivity with temperature of CFRC under a load of (a) 2 MPa; and (b) 10 MPa. [H. Shifeng, X. Dongyu, C. Jun, X. Ronghua, L. Lingchao, and C. Xin, "Smart properties of carbon fiber reinforced cement-based composites," *Journal of Composite Materials* 41 (1): 125–131, copyright © 2007 by SAGE, reprinted by permission of SAGE Publications, Ltd.]

© ASCE   03119003-7   J. Mater. Civ. Eng.

J. Mater. Civ. Eng., 2019, 31(11): 03119003
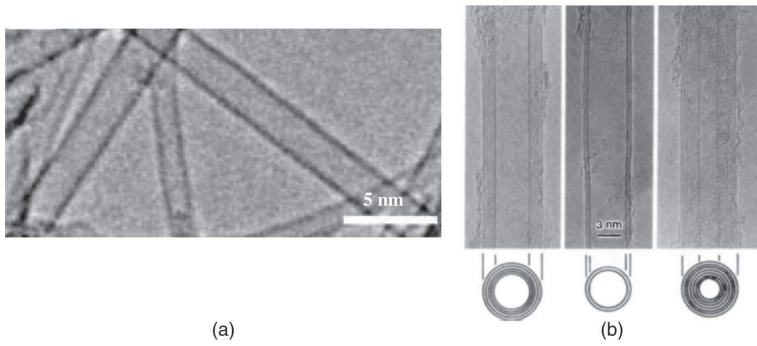
Fig. 14. Transmission electron microscope (TEM) images of (a) SWCNTs [from K. Hata, D. N. Futaba, K. Mizuno, T. Namai, M. Yumura, S. Iijima, "Water-assisted highly efficient synthesis of impurity-free single-walled carbon nanotubes," *Science* 605 (5700): 1362–1364, © 2004, adapted with permission from AAAS]; and (b) MWCNTs with 5, 2, and 7 layers, respectively (adapted with permission from Springer Nature: Springer, *Nature*, "Helical microtubes of graphitic carbon," S. Iijima, © 1991).

ratio, and excellent electrical (Bhatia et al. 2010; Guadagno et al. 2011; Thostenson et al. 2009) and thermal (Guthy et al. 2007; Thostenson et al. 2009; Yang et al. 2008) conductivity (Thostenson et al. 2001). Cementitious binders with incorporated CNTs showed enhanced mechanical properties, including compressive and flexural strength, in a number of studies, e.g., those by Cwirzen et al. (2008) and Konsta-Gdoutos et al. (2010). CNTs were also used to prepare advanced cement-based sensors for SHM (Materazzi et al. 2013).

Due to CNTs' hydrophobic nature and tendency to agglomerate as bundles or ropes, the biggest challenge (Hata et al. 2004) is to ensure their uniform dispersion in the cement matrix. A typical procedure to disperse CNTs in cementitious matrixes is to use a surfactant and intensive sonication to produce a homogeneous water dispersion. The dispersion is then added as a mixing water to the mix.

The sensing properties of the CNT/cement composites are based on changes in electrical resistance. During the last few decades, the possibility of using CNT/cement composites as sensors was studied by a number of researchers. For example, a self-sensing MWCNT/ cement composite used to monitor traffic showed a remarkable responsiveness to loads originating from passing vehicles (Han et al. 2009). Nam et al. (2016) showed that the percolation threshold of

the MWCNT cement–based matrix was 0.25% by weight. With this amount, the highest electrical resistance change was measured. A vehicle-loading test verified that a sensor based on 0.2% by weight of MWCNT was clearly able to detect the change of load.

Carbon Nanofibers

Carbon nanofibers (CNFs) are built of cylindrical graphene layers arranged in stacks of cones, plates, or cups (Guadagno et al. 2013; Mo and Roberts 2013; Rana et al. 2016) to create a cylindrical nanostructure (Fig. 15). Because of their stacked structure, the CNFs have a larger surface area, and the edges of the fiber can be used to help anchor the fiber in the matrix, meaning better bond characteristics (Mo and Roberts 2013). CNFs have diameters up to 200 nm, and a length between 50 and 200 μm (Yazdani and Mohanam 2014). The addition of CNF to a cement-based matrix not only enhanced the electrical properties, but also the advantages gained in the concrete's performance, included increased tensile and flexural strengths, tensile ductility, and flexural toughness, and decreased drying shrinkage (Han et al. 2015b).

CNF-reinforced concrete having a sensing capability was reported by Geo et al. (2009). The electrical resistance decreased when the concentration of CNFs increased due to the tunnel
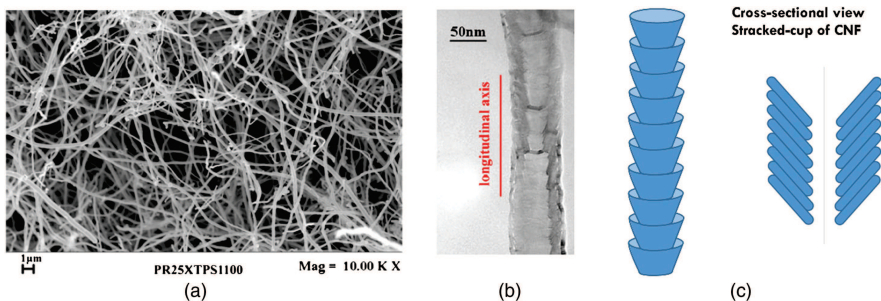
Fig. 15. (a) Scanning electron microscope (SEM) image of CNFs; (b) TEM image of CNFs; and (c) structure of CNFs. [Adapted (a) and (b) from Guadagno et al. 2013, © IOP Publishing Ltd. under CC BY 3.0 (https://creativecommons.org/licenses/by/3.0/).]

© ASCE   03119003-8   J. Mater. Civ. Eng.

J. Mater. Civ. Eng., 2019, 31(11): 03119003

Table 1. Summarized advantages and limitations of cement-based matrix incorporating various types of conductive materials

Conductive material	Size	Percolation threshold	Advantages	Limitations
Steel fiber	Diameter = 8 μm • Length = 6 mm	• 0.27%–0.36% by volume (Wen and Chung 2003)	• SF cement–based matrix is more effective with tensile strain sensing because it has high fiber-fiber contact between each steel fiber under tensile loading (high fractional change in electrical resistivity to fractional strain when applied tensile loading).	• Threshold value will change depending on size, degree of dispersion, and orientation direction of SF. • Less strain and damage sensitivity due to poor fiber-fiber contact when compared with the same amount of other conductive materials.
Carbon black	Average particle = 20–100 nm	• 7.22%–11.39% by volume (Li et al. 2006) • 2.00% by weight of binder (Al-Dahawi et al. 2016)	• Higher specific surface area and aspect ratio of CB enhanced piezoresistive behavior of cement-based matrix at low strain level. • Good dispersion of CB in cementitious matrixes have bridging cracks and pores in nanostructures and microstructures, which leads to high sensing ability.	• Excess CB influence to reduce the rheology of the matrix and cause the mechanical and electrical properties to be decreased. • Performance of sensing capability due to size of CB. • Quality of CB has an effect on level sensing ability of damages (conductive value of fiber itself).
Carbon fibers	Diameter = 8 μm • Length = 3 mm • Length = 6 mm Diameter = 7.5 μm • Length: =6 mm • Length = 12 mm	• 0.20% by volume (Chiarello and Zinno 2005) • 0.15% by volume (Chiarello and Zinno 2005) • 2.00% by volume (Al-Dahawi et al. 2016) • 1.00% by volume (Al-Dahawi et al. 2016)	• Small size of CFs attributed to interfiber continuity and give better damage sensing. • CFs have strain-sensing ability at low strain level and sensed temperature effects at both positive and negative temperatures.	• Longer fibers reduce the threshold value. • Less stress-strain sensing under heavy load. • An amount of CFs below the percolation threshold provides better sensitivity of the piezoresistive response.
Carbon nanofibers	Average diameter = 150 nm	• 1.00% by volume of binder (Gao et al. 2009)	• Nanosized carbon materials enhanced the mechanical properties by the filler effect and have sensing ability for nanoscale and microscale damages. • Good dispersion of CNTs in cementitious matrixes can bridge cracks and pores in nanostuctures and microstructures, which leads to high sensing ability.	• More effective stress-strain sensing for CNF below percolation threshold than above. • High agglomeration and requires uniform distribution of CNFs in matrix for more sensing capability. • Excess amount of CNFs lead to poor dispersion and has a negative effect for damage sensing.
Carbon nanotubes	Diameter = 5–15 nm • Length =< 10 μm Diameter = 20–30 nm • Length = 10–30 μm	• 0.25% by weight of binder (Nam et al. 2016) • 0.15% by weight of binder (Naeem et al. 2017) • 0.55% by weight of binder (Al-Dahawi et al. 2016)	• Higher specific surface area than other carbon nanomaterials. • Higher level of damage sensing. • Good dispersion of CNTs in cementitious matrixes can bridge cracks and pores in nanostructures and microstructures, which leads to high sensing ability. • CNT particles with a diameter close to the diameter of C-S-H gel are wrapped by C-S-H gel and improve dramatically the sensing capability by measuring electrical resistivity.	• Threshold value depends on size, dispersion level, and tunneling level. • High agglomeration and requires uniform distribution of CNTs in matrix for more sensing capability.

Note: C-S-H = calcium-silicate-hydrate.

conductivity effect. Otherwise, excess CNFs did not affect the change in resistivity with increased strain. The stress-strain sensing of a CNF cement–based matrix has been shown for CNFs concentrations below the percolation threshold. Piezoresistive behavior of a cementitious matrix with CNF was studied under cyclic compression load in the elastic regime (Konsta-Gdoutos and Aza 2014). The resistivity tended to decrease during loading, when cracks were closing, and to increase during unloading, when cracks were opening. The average change of resistivity for the sample containing 0.1% by weight of CNF was 5.0% and therefore higher than for the sample containing 0.3% by weight of CNF, showing a change in resistivity of 1.5%. The produced mixes showed a strong piezoresistive behavior sufficient for application in strain sensors.

The main problem with matrixes incorporating CNF is to achieve uniform dispersion of the nanofibers. So far, the best dispersion was obtained when using an intensive ultrasonication and surfactants (Yazdanbakhsh et al. 2010). During measurement of the electrical conductivity in moist conditions, polarization takes place due to the electrolytic effect. Chemical reactions occurring at electrodes liberate hydrogen and oxygen, which deposit around the electrodes in the form of a thin film, which eventually results in a polarization effect. To eliminate the polarization effect, specimens should be dry, and a high-frequency alternating current should be used (Banthia et al. 1992).

Hybrid Fibers

Hybrid fiber systems consisting of two or more types of fibers showed promising results. The approach aims to combine the best performances of each fiber type. In the case of a cement-based matrix, the main effort was to use a mix of microscale and nanoscale fibers, leading to enhanced mechanical properties and better electrical conductivity. Numerous studies focused on hybrid fillers to improve the self-sensing capacity and sensing reliability and sensitivity. For example, Ou and Han (2009) showed reproducible piezoresistive cement–based strain sensors in samples exposed to compressive strain by adding a combination of 0.18% by volume of CFs and 15% by volume of CB. It was possible to detect the compressive strain in concrete beams and columns under field conditions.

Several years later, Luo et al. (2010) investigated the sensitivity of a hybrid consisting of 0.5% by weight of short CFs and 0.1% by weight of MWCNTs. Results showed nearly no improvement of stress-strain sensitivity when compared with the piezoresistive effect obtained from a mix containing 0.1% by weight of MWCNTs. The fractional resistivity change was linear and more effective to improve the self-sensing repeatability and variation stability. Hybrids of dissimilar nanomaterials containing 0.1% by weight of both nano-CB and MWCNTs showed more strain sensitivity under cyclic loading in comparison with material containing only MWCNTs.

Another study showed that a mix of 15% by weight of CFs and 1% by weight of MWCNTs significantly increased the electrical conductivity of the cement matrix, enabling it to be used as a sensor (Azhari and Banthia 2012). Under both monotonically and cyclically applied strain, the material provided better signal quality, improved reliability, and increased sensitivity in comparison with composites incorporating only CF. Composites had the greatest strain-sensing property with incorporation of 0.1% by volume of CFs and 0.5% by volume of MWCNTs. The GF reached 160.3; however, the sensing performance was almost the same with cement composites having 1% by volume of MWCNTs (Lee et al. 2017).

Conclusion

The present paper has reviewed the sensing capability of nonconductive matrixes incorporating various types of conductive materials with a focus on portland cement–based matrixes. In most cases, addition of conductive materials decreased the resistivity and enhanced the mechanical properties of the produced composites. One of the major issues related to nanomaterials is their uniform dispersion in a cementitious binder matrix. A summary of observed advantages and limitations for matrixes incorporating various types of conductive materials together with percolation threshold amounts of fibers in some studies, is given in Table 1.

Acknowledgments

References

Aggelis, D. G., N. Alver, and H. K. Chai. 2014. "Health monitoring of civil infrastructure and materials." *Sci. World J.* 2014: 1–2. https://doi.org/10.1155/2014/435238.

Al-Dahawi, A., M. H. Sarwary, O. Öztürk, G. Yildirim, A. Akin, M. Şahmaran, and M. Lachemi. 2016. "Electrical percolation threshold of cementitious composites possessing self-sensing functionality incorporating different carbon-based materials." *Smart Mater. Struct.* 25 (10): 105005. https://doi.org/10.1088/0964-1726/25/10/105005.

Ausanio, G., A. C. Barone, C. Hison, V. Iannotti, G. Mannara, and L. Lanotte. 2005. "Magnetoelastic sensor application in civil buildings monitoring." *Sens. Actuators, A* 123–124 (Sep): 290–295. https://doi.org/10.1016/j.sna.2005.03.027.

Awaja, F., S. Zhang, M. Tripathi, A. Nikiforov, and N. Pugno. 2016. "Cracks, microcracks and fracture in polymer structures: Formation, detection, autonomic repair." *Prog. Mater. Sci.* 83 (Oct): 536–573. https://doi.org/10.1016/j.pmatsci.2016.07.007.

Azhari, F., and N. Banthia. 2012. "Cement-based sensors with carbon fibers and carbon nanotubes for piezoresistive sensing." *Cem. Concr. Compos.* 34 (7): 866–873. https://doi.org/10.1016/j.cemconcomp.2012.04.007.

Baeza, F. J., D. D. L. Chung, E. Zornoza, L. G. Andión, and P. Garcés. 2010. "Triple percolation in concrete reinforced with carbon fiber." *ACI Mater. J.* 107 (4): 396–402. https://www.doi.org/10.14359/51663866.

Bajare, D., G. Bumanis, G. Sahmenko, and J. Justs. 2012. "High performance and conventional concrete properties affected by ashes obtained from different type of grasses." In *Proc., 12th Int. Conf. on Recent Advances in Concrete Technology and Sustainability Issues.* New York: Curran Associates.

Banthia, N., S. Djeridane, and M. Pigeon. 1992. "Electrical resistivity of carbon and steel micro-fiber reinforced cements." *Cem. Concr. Res.* 22 (5): 804–814. https://doi.org/10.1016/0008-8846(92)90104-4.

Bhatia, R., V. Prasad, and R. Menon. 2010. "Characterization, electrical percolation and magnetization studies of polystyrene/multiwall carbon nanotube composite films." *Mater. Sci. Eng. B: Solid-State Mater. Adv. Technol.* 175 (3): 189–194. https://doi.org/10.1016/j.mseb.2010.07.025.

Boyd, A. J., and J. Skalny. 2007. "Environmental deterioration of concrete." In *Environmental deterioration of materials*, 143–184. Southampton, UK: WIT Press.

Cabrera, J. G. 1996. "Deterioration of concrete due to reinforcement steel corrosion." *Cem. Concr. Compos.* 18 (1): 47–59. https://doi.org/10.1016/0958-9465(95)00043-7.

Calkins, F. T., A. B. Flatau, and M. J. Dapino. 2007. "Overview of magnetostrictive sensor technology." *J. Intell. Mater. Syst. Struct.* 18 (10): 1057–1066. https://doi.org/10.1177/1045389X06072358.

© ASCE   03119003-10   J. Mater. Civ. Eng.

J. Mater. Civ. Eng., 2019, 31(11): 03119003

Chalioris, C. E., C. G. Karayannis, G. M. Angeli, N. A. Papadopoulos, M. J. Favvata, and C. P. Providakis. 2016. "Applications of smart piezoelectric materials in a wireless admittance monitoring system (WiAMS) to structures-tests in RC elements." *Case Stud. Constr. Mater.* 5 (Dec): 1–18. https://doi.org/10.1016/j.cscm.2016.03.003.

Chang, P. C., A. Flatau, and S. C. Liu. 2003. "Review paper: Health monitoring of civil infrastructure." *Struct. Health Monit.: Int. J.* 2 (3): 257–267. https://doi.org/10.1177/1475921703036169.

Chen, P. W., and D. D. L. Chung. 1993. "Concrete reinforced with up to 0.2 vol% of short carbon fibres." *Composites* 24 (1): 33–52. https://doi.org/10.1016/0010-4361(93)90261-6.

Chen, P. W., and D. D. L. Chung. 1995. "Improving the electrical conductivity of composites comprised of short conducting fibers in a nonconducting matrix: The addition of a nonconducting particulate filler." *J. Electron. Mater.* 24 (1): 47–51. https://doi.org/10.1007/BF02659726.

Chi, J. M., R. Huang, and C. C. Yang. 2002. "Effects of carbonation on mechanical properties and durability of concrete using accelerated testing method." *J. Mar. Sci. Technol.* 10 (1): 14–20.

Chiarello, M., and R. Zinno. 2005. "Electrical conductivity of self-monitoring CFRC." *Cem. Concr. Compos.* 27 (4): 463–469. https://doi.org/10.1016/j.cemconcomp.2004.09.001.

Chung, D. D. L. 1998. "Self-monitoring structural materials." *Mater. Sci. Eng. R: Rep.* 22 (2): 57–78. https://doi.org/10.1016/S0927-796X(97)00021-1.

Chung, D. D. L. 2002a. "Composites get smart." *Mater. Today* 5 (1): 30–35. https://doi.org/10.1016/S1369-7021(02)05140-4.

Chung, D. D. L. 2002b. "Piezoresistive cement-based materials for strain sensing." *J. Intell. Mater. Syst. Struct.* 13 (9): 599–609. https://doi.org/10.1106/104538902031861.

Chung, D. D. L., and X. Fu. 1996. "Self monitoring of fatigue damage in carbon fiber reinforced cement." *Cem. Concr. Res.* 26 (1): 15–20. https://doi.org/10.1016/0008-8846(95)00184-0.

Cwirzen, A., K. Habermehl-Cwirzen, and V. Penttala. 2008. "Surface decoration of carbon nanotubes and mechanical properties of cement/carbon nanotube composites." *Adv. Cem. Res.* 20 (2): 65–73. https://doi.org/10.1680/adcr.2008.20.2.65.

Darwin, D., J. A. Browning, L. Gong, and S. R. Hughes. 2008. "Effects of deicers on concrete deterioration." *ACI Mater. J.* 105 (6): 622–627.

Dong, X., J. Ou, and X. Guan. 2011. "Applications of magnetostrictive materials in civil structures: A review." In *Proc., 6th Int. Workshop on Advanced Smart Materials and Smart Structures Technology.* Champaign, IL: Univ. of Illinois at Urbana–Champaign.

Fidanboylu, K., and H. S. Efendioglu. 2009. "Fiber optic sensors and their applications." In *Proc., 5th Int. Advanced Technologies Symp.*, 1–6. Karabük, Turkey: Karabük Univ.

Gao, D., M. Sturm, and Y. L. Mo. 2009. "Electrical resistance of carbon-nanofiber concrete." *Smart Mater. Struct.* 18 (9): 095039. https://doi.org/10.1088/0964-1726/18/9/095039.

Georgousis, G., et al. 2015. "Strain sensing in polymer/carbon nanotube composites by electrical resistance measurement." *Composites Part B* 68 (Jan): 162–169. https://doi.org/10.1016/j.compositesb.2014.08.027.

Guadagno, L., B. De Vivo, A. Di Bartolomeo, P. Lamberti, A. Sorrentino, V. Tucci, L. Vertuccio, and V. Vittoria. 2011. "Effect of functionalization on the thermo-mechanical and electrical behavior of multi-wall carbon nanotube/epoxy composites." *Carbon* 49 (6): 1919–1930. https://doi.org/10.1016/j.carbon.2011.01.017.

Guadagno, L., M. Raimondo, V. Vittoria, L. Vertuccio, K. Lafdi, B. De Vivo, P. Lamberti, G. Spinelli, and V. Tucci. 2013. "The role of carbon nanofiber defects on the electrical and mechanical properties of CNF-based resins." *Nanotechnology* 24 (30): 305704. https://doi.org/10.1088/0957-4484/24/30/305704.

Guthy, C., F. Du, S. Brand, K. I. Winey, and J. E. Fischer. 2007. "Thermal conductivity of single-walled carbon nanotube/PMMA nanocomposites." *J. Heat Transfer* 129 (8): 1096–1099. https://doi.org/10.1115/1.2737484.

Han, B., S. Ding, and X. Yu. 2015a. "Intrinsic self-sensing concrete and structures: A review." *Measurement* 59 (Jan): 110–128. https://doi.org/10.1016/j.measurement.2014.09.048.

Han, B., S. Sun, S. Ding, L. Zhang, X. Yu, and J. Ou. 2015b. "Review of nanocarbon-engineered multifunctional cementitious composites." *Composites Part A* 70 (Mar): 69–81. https://doi.org/10.1016/j.compositesa.2014.12.002.

Han, B., X. Yu, and E. Kwon. 2009. "A self-sensing carbon nanotube/cement composite for traffic monitoring." *Nanotechnology* 20 (44): 445501. https://doi.org/10.1088/0957-4484/20/44/445501.

Hata, K., D. N. Futaba, K. Mizuno, T. Namai, M. Yumura, and S. Iijima. 2004. "Water-assisted highly efficient synthesis of impurity-free single-walled carbon nanotubes." *Science* 306 (5700): 1362–1364. https://doi.org/10.1126/science.1104962.

Hattori, S., T. Shimada, and K. Matsuhashib. 2001. "Highly accurate low frequency elastic wave measurement using magnetostrictive devices." *NDT E Int.* 34 (6): 373–379. https://doi.org/10.1016/S0963-8695(01)00003-2.

Helal, J., M. Sofi, and P. Mendis. 2015. "Non-destructive testing of concrete: A review of methods." *Electron. J. Struct. Eng.* 14 (1): 97–105.

Hison, C., G. Ausanio, A. C. Barone, V. Iannotti, E. Pepe, and L. Lanotte. 2005. "Magnetoelastic sensor for real-time monitoring of elastic deformation and fracture alarm." *Sens. Actuators, A* 125 (1): 10–14. https://doi.org/10.1016/j.sna.2005.05.019.

Housner, G. W., L. A. Bergman, T. K. Caughey, A. G. Chassiakos, R. O. Claus, S. F. Masri, R. E. Skelton, T. T. Soong, B. F. Spencer, and J. T. P. Yao. 1997. "Structural control: Past, present, and future." *J. Eng. Mech.* 123 (9): 897–971. https://doi.org/10.1061/(ASCE)0733-9399(1997)123:9(897).

Hristoforou, E., and A. Ktena. 2007. "Magnetostriction and magnetostrictive materials for sensing applications." *J. Magn. Magn. Mater.* 316 (2): 372–378. https://doi.org/10.1016/j.jmmm.2007.03.025.

Iijima, S. 1991. "Helical microtubes of graphitic carbon." *Nature* 354 (6348): 56–58. https://doi.org/10.1038/354056a0.

Konsta-Gdoutos, M. S., and C. A. Aza. 2014. "Self sensing carbon nanotube (CNT) and nanofiber (CNF) cementitious composites for real time damage assessment in smart structures." *Cem. Concr. Compos.* 53 (Oct): 162–169. https://doi.org/10.1016/j.cemconcomp.2014.07.003.

Konsta-Gdoutos, M. S., Z. S. Metaxa, and S. P. Shah. 2010. "Highly dispersed carbon nanotube reinforced cement based materials." *Cem. Concr. Res.* 40 (7): 1052–1059. https://doi.org/10.1016/j.cemconres.2010.02.015.

Kuronuma, Y., T. Takeda, Y. Shindo, F. Narita, and Z. Wei. 2012. "Electrical resistance-based strain sensing in carbon nanotube/polymer composites under tension: Analytical modeling and experiments." *Compos. Sci. Technol.* 72 (14): 1678–1682. https://doi.org/10.1016/j.compscitech.2012.07.001.

Leal-Junior, A., A. Frizera-Neto, C. Marques, and M. Pontes. 2018. "A polymer optical fiber temperature sensor based on material features." *Sensors* 18 (2): 301. https://doi.org/10.3390/s18010301.

Lee, S. J., I. You, G. Zi, and D. Y. Yoo. 2017. "Experimental investigation of the piezoresistive properties of cement composites with hybrid carbon fibers and nanotubes." *Sensors* 17 (11): 2516. https://doi.org/10.3390/s17112516.

Leong, C. K., Y. Aoyagi, and D. D. L. Chung. 2006. "Carbon black pastes as coatings for improving thermal gap-filling materials." *Carbon* 44 (3): 435–440. https://doi.org/10.1016/j.carbon.2005.09.002.

Leong, C. K., and D. D. L. Chung. 2004. "Carbon black dispersions and carbon-silver combinations as thermal pastes that surpass commercial silver and ceramic pastes in providing high thermal contact conductance." *Carbon* 42 (11): 2323–2327. https://doi.org/10.1016/j.carbon.2004.05.013.

Leung, C. K. Y., K. T. Wan, and L. Chen. 2008. "A novel optical fiber sensor for steel corrosion in concrete structures." *Sensors* 8 (3): 1960–1976. https://doi.org/10.3390/s8031960.

Li, C., E. T. Thostenson, and T. W. Chou. 2008a. "Sensors and actuators based on carbon nanotubes and their composites: A review." *Compos. Sci. Technol.* 68 (6): 1227–1249. https://doi.org/10.1016/j.compscitech.2008.01.006.

Li, H., H. Xiao, and J. Ou. 2006. "Effect of compressive strain on electrical resistivity of carbon black-filled cement-based composites." *Cem. Concr. Compos.* 28 (9): 824–828. https://doi.org/10.1016/j.cemconcomp.2006.05.004.

Li, H., H. Xiao, and J. Ou. 2008b. "Electrical property of cement-based composites filled with carbon black under long-term wet and loading

© ASCE 03119003-11 J. Mater. Civ. Eng.

J. Mater. Civ. Eng., 2019, 31(11): 03119003

condition." *Compos. Sci. Technol.* 68 (9): 2114–2119. https://doi.org/10.1016/j.compscitech.2008.03.007.

Lim, Y. Y., S. Bhalla, and C. K. Soh. 2006. "Structural identification and damage diagnosis using self-sensing piezo-impedance transducers." *Smart Mater. Struct.* 15 (4): 987–995. https://doi.org/10.1088/0964-1726/15/4/012.

Lin, V. W. J., M. Li, J. P. Lynch, and V. C. Li. 2011. "Mechanical and electrical characterization of self-sensing carbon black ECC." In *Proc., Nondestructive Characterization for Composite Materials, Aerospace Engineering, Civil Infrastructure, and Homeland Security*, 798316. Washington, DC: SPIE.

López-Higuera, J. M., L. R. Cobo, A. Q. Incera, and A. Cobo. 2011. "Fiber optic sensors in structural health monitoring." *J. Lightwave Technol.* 29 (4): 587–608. https://doi.org/10.1109/JLT.2011.2106479.

Luo, J. L., Z. D. Duan, T. J. Zhao, and Q. Y. Li. 2010. "Hybrid effect of carbon fiber on piezoresistivity of carbon nanotube cement-based composite." *Adv. Mater. Res.* 143–144: 639–643. https://doi.org/10.4028/www.scientific.net/AMR.143-144.639.

Materazzi, A. L., F. Ubertini, and A. D'Alessandro. 2013. "Carbon nanotube cement-based sensors for dynamic monitoring of concrete structures." In *Proc., FIB Symp.*, 22–24. Lausanne, Switzerland: Fédération Internationale du Béton International Federation for Structural Concrete.

Mo, Y. L., and R. H. Roberts. 2013. "Carbon nanofiber concrete for damage detection of infrastructure." In *Advances in nanofibers*, 125–143. Rijeka, Croatia: INTECH.

Monteiro, A. O., P. B. Cachim, P. M. F. J. Costa, and M. Oeser. 2017. "Sensitive smart concrete loaded with carbon black nanoparticles for traffic monitoring sensitive smart concrete loaded with carbon black." In *Proc., 4th Int. Conf. on Smart Monitoring, Assessment and Rehabilitation of Civil Structures*. Zurich, Switzerland: RWTH Publications.

Moraleda, A., C. García, J. Zaballa, and J. Arrue. 2013. "A temperature sensor based on a polymer optical fiber macro-bend." *Sensors* 13 (10): 13076–13089. https://doi.org/10.3390/s131013076.

Naeem, F., H. K. Lee, H. K. Kim, and I. W. Nam. 2017. "Flexural stress and crack sensing capabilities of MWNT/cement composites." *Compos. Struct.* 175 (Sep): 86–100. https://doi.org/10.1016/j.compstruct.2017.04.078.

Nairn, J. A. 2000. "Matrix microcracking in composites." *Polym. Matrix Compos.* 2: 403–432. https://doi.org/10.1016/B0-08-042993-9/00069-3.

Nam, I. W., H. Souri, and H. K. Lee. 2016. "Percolation threshold and piezoresistive response of multi-wall carbon nanotube/cement composites." *Smart Struct. Syst.* 18 (2): 217–231. https://doi.org/10.12989/sss.2016.18.2.217.

Ou, J., and B. Han. 2008. "Piezoresistive cement-based strain sensors and self-sensing concrete components." *J. Intell. Mater. Syst. Struct.* 20 (3): 329–336. https://doi.org/10.1177/1045389X08094190.

Ou, J., and Z. Zhou. 2008. "Applications of optical fiber sensors of SHM in infrastructures." In *Proc., Smart Sensor Phenomena, Technology, Networks, and Systems*, 693311. Washington, DC: SPIE.

Pang, J. W. C., and I. P. Bond. 2005. "A hollow fibre reinforced polymer composite encompassing self-healing and enhanced damage visibility." *Compos. Sci. Technol.* 65 (11–12): 1791–1799. https://doi.org/10.1016/j.compscitech.2005.03.008.

Rana, S., P. Subramani, R. Fangueiro, and A. G. Correia. 2016. "A review on smart self-sensing composite materials for civil engineering applications." *AIMS Mater. Sci.* 3 (2): 357–379. https://doi.org/10.3934/matersci.2016.2.357.

Shi, L., Y. Lu, and Y. Bai. 2017. "Mechanical and electrical characterisation of steel fiber and carbon black engineered cementitious composites." *Procedia Eng.* 188: 325–332. https://doi.org/10.1016/j.proeng.2017.04.491.

Shifeng, H., X. Dongyu, C. Jun, X. Ronghua, L. Lingchao, and C. Xin. 2007. "Smart properties of carbon fiber reinforced cement-based composites." *J. Compos. Mater.* 41 (1): 125–131. https://doi.org/10.1177/0021998306063378.

Shindo, Y., Y. Kuronuma, T. Takeda, F. Narita, and S. Y. Fu. 2012. "Electrical resistance change and crack behavior in carbon nanotube/polymer composites under tensile loading." *Composites Part B* 43 (1): 39–43. https://doi.org/10.1016/j.compositesb.2011.04.028.

Sun, M., W. J. Staszewski, and R. N. Swamy. 2010. "Smart sensing technologies for structural health monitoring of civil engineering structures." *Adv. Civ. Eng.* 2010: 13. https://doi.org/10.1155/2010/724962.

Sun, M., W. J. Staszewski, R. N. Swamy, and Z. Li. 2008. "Application of low-profile piezoceramic transducers for health monitoring of concrete structures." *NDT E Int.* 41 (8): 589–595. https://doi.org/10.1016/j.ndteint.2008.06.007.

Takeda, T., Y. Shindo, F. Naraoka, Y. Kuronuma, and F. Narita. 2013. "Crack and electrical resistance behaviors of carbon nanotube-based polymer composites under mixed-mode I/II loading." *Mater. Trans.* 54 (7): 1105–1109. https://doi.org/10.2320/matertrans.M2013080.

Tapetado, A., P. J. Pinzón, J. Zubia, and C. Vázquez. 2015. "Polymer optical fiber temperature sensor with dual-wavelength compensation of power fluctuations." *J. Lightwave Technol.* 33 (13): 2716–2723. https://doi.org/10.1109/JLT.2015.2408368.

Teomete, E., and O. I. Kocyigit. 2013. "Tensile strain sensitivity of steel fiber reinforced cement matrix composites tested by split tensile test." *Constr. Build. Mater.* 47 (Oct): 962–968. https://doi.org/10.1016/j.conbuildmat.2013.05.095.

Thostenson, E. T., Z. Ren, and T.-W. Chou. 2001. "Advances in the science and technology of carbon nanotubes and their composites: A review." *Compos. Sci. Technol.* 61 (13): 1899–1912. https://doi.org/10.1016/S0266-3538(01)00094-X.

Thostenson, E. T., S. Ziaee, and T. W. Chou. 2009. "Processing and electrical properties of carbon nanotube/vinyl ester nanocomposites." *Compos. Sci. Technol.* 69 (6): 801–804. https://doi.org/10.1016/j.compscitech.2008.06.023.

Tzou, H. S., H. J. Lee, and S. M. Arnold. 2004. "Smart materials, precision sensors/actuators, smart structures, and structronic systems." *Mech. Adv. Mater. Struct.* 11 (4–5): 367–393. https://doi.org/10.1080/15376490490451552.

Wan, K. T., and C. K. Y. Leung. 2007. "Applications of a distributed fiber optic crack sensor for concrete structures." *Sens. Actuators, A* 135 (2): 458–464. https://doi.org/10.1016/j.sna.2006.09.004.

Wang, L. 2015. "Differential structure for temperature sensing based on conductive polymer composites." *IEEE Trans. Electron Dev.* 62 (9): 3025–3028. https://doi.org/10.1109/TED.2015.2438075.

Wang, S., and D. D. L. Chung. 1998a. "Carbon fiber polymer-matrix composite interfaces as thermocouple junctions." *Compos. Interfaces* 6 (6): 519–529. https://doi.org/10.1163/156855499X00198.

Wang, S., and D. D. L. Chung. 1998b. "Interlaminar interface in carbon fiber polymer-matrix composites, studied by contact electrical resistivity measurement." *Compos. Interfaces* 6 (6): 497–505. https://doi.org/10.1163/156855499X00170.

Wang, S., and D. D. L. Chung. 1999. "Temperature/light sensing using carbon fiber polymer-matrix composite." *Composites Part B* 30 (6): 591–601. https://doi.org/10.1016/S1359-8368(99)00020-7.

Wang, S., and D. D. L. Chung. 2000. "Electrical behavior of carbon fiber polymer-matrix composites in the through-thickness direction." *J. Mater. Sci.* 35 (1): 91–100. https://doi.org/10.1023/A:1004744600284.

Wang, W., H. Dai, and S. Wu. 2008. "Mechanical behavior and electrical property of CFRC-strengthened RC beams under fatigue and monotonic loading." *Mater. Sci. Eng. A* 479 (1–2): 191–196. https://doi.org/10.1016/j.msea.2007.06.046.

Wang, W., S. Wu, and H. Dai. 2006. "Fatigue behavior and life prediction of carbon fiber reinforced concrete under cyclic flexural loading." *Mater. Sci. Eng. A* 434 (1–2): 347–351. https://doi.org/10.1016/j.msea.2006.07.080.

Wang, X., S. Wang, and D. D. L. Chung. 1999. "Sensing damage in carbon fiber and its polymer-matrix and carbon-matrix composites by electrical resistance measurement." *J. Mater. Sci.* 34 (11): 2703–2713. https://doi.org/10.1023/A:1004629505992.

Wen, S., and D. D. L. Chung. 1999. "Piezoresistivity in continuous carbon fiber cement-matrix composite." *Cem. Concr. Res.* 29 (3): 445–449. https://doi.org/10.1016/S0008-8846(98)00211-7.

Wen, S., and D. D. L. Chung. 2003. "A comparative study of steel- and carbon-fibre cement as piezoresistive strain sensors." *Adv. Cem. Res.* 15 (3): 119–128. https://doi.org/10.1680/adcr.2003.15.3.119.

© ASCE 03119003-12 J. Mater. Civ. Eng.

J. Mater. Civ. Eng., 2019, 31(11): 03119003

Wen, S., and D. D. L. Chung. 2007. "Partial replacement of carbon fiber by carbon black in multifunctional cement-matrix composites." *Carbon* 45 (3): 505–513. https://doi.org/10.1016/j.carbon.2006.10.024.

Wong, E. W., P. E. Sheehan, and C. M. Lieber. 1997. "Nanobeam mechanics: Elasticity, strength, and toughness of nanorods and nanotubes." *Science* 277 (5334): 1971–1975. https://doi.org/10.1126/science.277.5334.1971.

Yang, Y., M. C. Gupta, J. N. Zalameda, and W. P. Winfree. 2008. "Dispersion behaviour, thermal and electrical conductivities of carbon nanotube-polystyrene nanocomposites." *Micro Nano Lett.* 3 (2): 35–40. https://doi.org/10.1049/mnl:20070073.

Yazdanbakhsh, A., Z. Grasley, B. Tyson, and R. K. A. Al-Rub. 2010. "Distribution of carbon nanofibers and nanotubes in cementitious composites." *Transp. Res. Rec.* 2142 (1): 89–95. https://doi.org/10.3141/2142-13.

Yazdani, N., and V. Mohanam. 2014. "Carbon nano-tube and nano-fiber in cement mortar: Effect of dosage rate and water-cement ratio." *Int. J. Mater. Sci.* 4 (2): 45. https://doi.org/10.14355/ijmsci.2014.0402.01.

Ye, X. W., Y. H. Su, and J. P. Han. 2014. "Structural health monitoring of civil infrastructure using optical fiber sensing technology: A comprehensive review." *Sci. World J.* 2014: 11. https://doi.org/10.1155/2014/652329.

Yu, M. F., B. S. Files, S. Arepalli, and R. S. Ruoff. 2000a. "Tensile loading of ropes of single wall carbon nanotubes and their mechanical properties." *Phys. Rev. Lett.* 84 (24): 5552–5555. https://doi.org/10.1103/PhysRevLett.84.5552.

Yu, M.-F., O. Lourie, M. J. Dyer, K. Moloni, T. F. Kelly, and R. S. Rouff. 2000b. "Strength and breaking mechanism of multiwalled carbon nanotubes under tensile load." *Science* 287 (5453): 637–640. https://doi.org/10.1126/science.287.5453.637.

Zeng, X., X. Xu, P. M. Shenai, E. Kovalev, C. Baudot, N. Mathews, and Y. Zhao. 2011. "Characteristics of the electrical percolation in carbon nanotubes/polymer nanocomposites." *J. Phys. Chem. C* 115 (44): 21685–21690. https://doi.org/10.1021/jp207388n.

Zhang, X., S. Song, and M. J. Yao. 2017. "Fabrication of embedded piezo-electric sensors and its application in traffic engineering." In *Proc., 2nd IEEE Int. Conf. on Intelligent Transportation Engineering*, 259–265. New York: IEEE.

Zhao, R., G. Shao, Y. Cao, L. An, and C. Xu. 2014. "Temperature sensor made of polymer-derived ceramics for high-temperature applications." *Sens. Actuators, A* 219 (Nov): 58–64. https://doi.org/10.1016/j.sna.2014.08.012.

© ASCE 03119003-13 J. Mater. Civ. Eng.

J. Mater. Civ. Eng., 2019, 31(11): 03119003

Paper II

Piezoresistive load sensing and percolation phenomena in Portland cement composite modified with in-situ synthesized carbon nanofibers

Buasiri, T., Habermehl-Cwirzen, K., Krzeminski, L., & Cwirzen, A.

Piezoresistive Load Sensing and Percolation Phenomena in Portland Cement Composite Modified with In-Situ Synthesized Carbon Nanofibers

Thanyarat Buasiri [1,*], Karin Habermehl-Cwirzen [1], Lukasz Krzeminski [2] and Andrzej Cwirzen [1]

[1] Building Materials, Department of Civil, Environmental and Natural Resources Engineering, Luleå University of Technology, 97187 Luleå, Sweden; karin.habermehl-cwirzen@ltu.se (K.H.-C.); andrzej.cwirzen@ltu.se (A.C.)

[2] The Institute of Engineering Materials and Biomaterials, Silesian University of Technology, 44-100 Gliwice, Poland; lukasz.krzeminski@polsl.pl

* Correspondence: thanyarat.buasiri@ltu.se; Tel.: +46-(0)-92-049-1907

Abstract: Carbon nanofibers (CNFs) were directly synthesized on Portland cement particles by chemical vapor deposition. The so-produced cements contained between 2.51–2.71 wt% of CNFs; depending on the production batch. Several mortar mixes containing between 0 and 10 wt% of the modified cement were produced and the electrical properties at various ages and the load sensing capabilities determined. The percolation threshold related to the electrical conductivity was detected and corresponded to the amount of the present CNFs, 0.271, 0.189, 0.135 and 0.108 wt%. The observed threshold depended on the degree of hydration of the Portland cement. The studied mortars showed a strong piezoresistive response to the applied compressive load reaching a 17% change of the electrical resistivity at an applied load of 3.5 MPa and 90% at 26 MPa. This initial study showed that the studied material is potentially suitable for future development of novel fully integrated monitoring systems for concrete structures.

Keywords: Carbon nanofibers; CVD; percolation; piezoresistive response; compressive load

1. Introduction

Carbon-based materials, especially carbon nanotubes (CNTs) and carbon nanofibers (CNFs), incorporated into Portland cement based matrixes have been studied over the last couple of years. The solidified composite materials showed considerable tensile strength, an increased modulus of elasticity as well as improved thermal and electrical conductivity [1–4]. The nanofibers were shown to bridge cracks and hindered their propagation [5–7]. Furthermore, the hydration processes were enhanced by the formation of additional nucleation sites. The amount of formed calcium silicate hydrate (C-S-H) was reported to be increased while the total porosity decreased [4,8]. The excellent electrical properties of these composites enabled the production of matrixes having load, stress, strain, and crack formation sensing capabilities through piezoresistive response [9]. However, to function properly these composites require the presence of a sufficient amount of the conductive material, evenly dispersed throughout the isolative matrix to create a continuous electrical path. In tension, the electrical resistivity increases due to the progressive breakage of the conduction paths by the formation of cracks. In compression, the resistivity decreases due to fiber push-in which increases the probability that adjacent fibers will gain contact though the tunneling effect [10,11]. Konsta-Gdoutos and Aza [12] produced cementitious matrixes incorporating CNFs showing piezoresistive response under cyclic compression load in the elastic regime. Also other cement-based composites

with conductive additions, e.g. carbon black/cement composites showed sensitivity to compressive and tensile strain [13–15].

Composite systems comprising of isolative and conductive phases may conduct an electrical current due to two mechanisms: Percolation in a continuous conductive network and/or tunneling [16–19]. The tunneling phenomena occurs when the inter-particle distance of the adjacent conductive particles is small enough to enable an electron to tunnel the gap and to form a conductive path [20]. Adding a small amount of conductive material to an insulating matrix only changes the electrical conductivity of the composite slightly as the isolated conductive particles do not form conductive networks. The critical volume fraction of a conductive phase at which a composite transforms from an insulator to a conductor is called the "percolation threshold". The percolation theory assumes that conductive materials including fillers and fiber can create a conductive network within an isolative matrix if their amount is sufficiently high to provide contact points between them. The conductivity σ can be estimated by using a simple power law based on the statistical percolation Equation (1):

$$\sigma \; \alpha \; \left(p - p_c \right)^t \tag{1}$$

where: p is the probability of occupation of a site in a resistor network by a conducting element, p_c is the critical probability for bond percolation and t is the critical exponent. The equation is valid only for $p - p_c \ll 1$ when the fluctuations extend over distances which are much larger than the size of the constituents [21]. Based on Equation (1) the conductivity σ can be calculated according to Equation (2):

$$\sigma = \sigma_0 \left(\Phi - \Phi_c \right)^t \tag{2}$$

where: Φ_c is the concentration of conductive fibers or fillers corresponding to the percolation threshold, σ_0 is the conductivity of the conductive material and t is the critical index of conductivity with a theoretical value between 1.5–1.75 [22].

Within the traditional percolation theory, Equation (2) is based on the assumption that the electrical conductivity is only depended on the conductivity of the filler, in this case of the CNF. However, the maximum conductivity depends also on several other factors related to CNFs but also to the embedding matrix. Studies on polymer-based matrixes showed that increasing the aspect ratio between length and diameter (L/D) of the CNTs produced higher ultimate conductivity values [23]. The electrical conductivity σ_{com} proposed by Hu et al [23] can be calculated according to Equation (3):

$$\sigma_{com} = \sigma_{CNT} \cdot 10^{0.85\{\log(L/D)-1\}} \cdot \left\{ \Phi - \Phi_c \right\}^t \tag{3}$$

where: σ_{CNT} is the electrical conductivity of the CNTs, L is the length of CNTs, D is the diameter of CNTs, Φ is the volume fraction of the CNTs, Φ_c is the percolation threshold and t is a critical exponent determined experimentally.

More curly CNTs incorporated into polymer matrixes resulted in a higher percolation threshold and a lower maximum electrical conductivity [23,24]. The biggest challenge while incorporating CNTs/CNFs into cementitious matrixes is to obtain their uniform dispersion [6,25–27]. Their hydrophobic nature results in a strong tendency to agglomerate. One of the developed solutions was a direct synthesis of CNTs/CNFs on untreated Portland cement particles. The used method is based on the application of a chemical vapor deposition (CVD) process [28–31]. Iron (III) oxide (Fe_2O_3), a main component in Portland cement acted as the main natural catalytic substrate while the other components silica oxide (SiO_2), magnesium oxide (MgO) and aluminium oxide (Al_2O_3) supported the growth of carbon nanomaterials [32–34]. Acetylene was used as carbon source and the synthesis temperatures ranged between 400–700 °C. The amount and the morphology of the synthesized nanofibers strongly depended on the duration of the process. After the hydration process the solidified matrixes showed twice the compressive strength and 40 times higher electrical conductivity

than the reference samples. High electrical conductivity could indicate also a significant piezoresistive response to e.g., stress and strain variations [28,29]. The initial study presented in this publication aimed to determine that response. Solidified matrixes containing various amounts of the nanomodified Portland cement with synthesized in-situ CNFs were subjected to various compression loads and tested for the corresponding piezoresistive response. The long-term goal of this research is to develop a novel monitoring system, which would be fully integrated, or part of a concrete structure.

2. Experimental Details

2.1. Synthesis and Characterization of SmartCem

The nanomodified cement (SmartCem) was produced using a CVD reactor (produced by the CVD Equipment Corporation) located in the laboratory of the Silesian University of Technology in Poland. Two types of SmartCem were produced using different process parameters (Table 1).

Table 1. Synthesis parameters.

Named	Argon (sccm)	Ethylene (sccm)	Hydrogen (sccm)	Synthesis Temperature (°C)	Duration (min)
SmartCem I	600	100	400	750	120
SmartCem II	600	100	500	750	120

Ethylene (99.999%) was used as the precursor, hydrogen (99.99999%) as the reducer and argon as the transporting media. A total of 10 g of an ordinary Portland cement (CEM I 42.5) was used as a substrate for the synthesis of the carbon phase. The cement powder was placed in four parallel-arranged holders made of quartz having a length of 30 mm and a diameter of 8 mm. The holders were arranged according to the gas flow direction to enhance the reaction efficiency and to remove impurities (Figure 1).
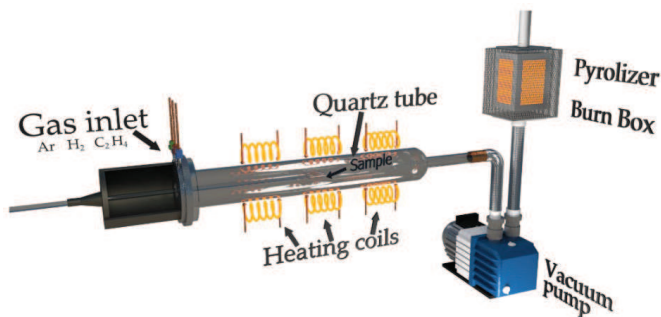
Figure 1. Schematic diagram of a Chemical Vapor Deposition (CVD) process for carbon nanofiber and SmartCem synthesis.

The samples were placed in the quartz tube of CVD reactor having a diameter of 70 mm and a length of 50 cm. The samples were degassed by keeping them at a low pressure (0.001 mbar) at 90 °C for 60 min. In the following step, the temperature was raised to 110 °C and was kept at that level for 20 min to remove gaseous pollutants and moisture. In the next stage, the samples were heated to 740 °C at rate of 5 °C/min. This happened in argon atmosphere at a pressure of 1010 mbar. After stabilizing the temperature, the samples were subjected for 15 min to the reduction reaction in an atmosphere of a mixture of hydrogen and argon with flow rate of 500 sccm and 200 sccm, respectively. After the reduction of the catalyst surface, the reactor temperature was stabilized to 750 °C under 1 SLM argon flow, followed by releasing a mixture of reactive gases for the synthesis: 100 sccm ethylene, 400 sccm or 500 sccm of hydrogen (SmartCem I and SmartCem II respectively) and 600 sccm argon for 120 min. Later all samples were purified from amorphous carbon using a mixture

of hydrogen and argon with a flow rate of 100 sccm and 1000 sccm, respectively. After the cleaning process, the samples were cooled down to 200 °C at a rate of 12 °C/min under an inert atmosphere, degassed under vacuum and cooled down to 20 °C in an argon atmosphere.

2.2. Materials

An ordinary Portland cement (CEM I 42.5) provided by Cementa-Sweden was used for the synthesis of nanomaterials as well as for the production of all mortar samples. Sieved and cleaned quartz sand having a maximum particle size of 150 μm was used as fine aggregate. The workability of the fresh mixes was controlled by the super plasticizing admixture (sp) type Glenium produced by Grace Chemicals. All mortar mixes had a water-cement ratio (w/c) of 0.35 and a sand-cement ratio (s/c) of 1. Mixes contained: 0 wt% (Ref), 2 wt% (S2), 4 wt% (S4), 6 wt% (S6), 8 wt% (S8), and 10 wt% (S10) of nanomodified cement replacing the untreated cement. The mix proportions are shown in Table 2.

Table 2. Mix proportions used for test mortars.

Mix	w/c	s/c	sp (wt% of Cement)	Cement (kg/m³)	SmartCem (wt% of Cement)
Ref	0.35	1.0	0.8	1157	0
S2	0.35	1.0	0.8	1134	2
S4	0.35	1.0	0.8	1111	4
S6	0.35	1.0	0.8	1088	6
S8	0.35	1.0	0.8	1065	8
S10	0.35	1.0	0.8	1042	10

The mortars were mixed using a Bredent vacuum mixer, which minimized the entrapment of air. All samples were cast into Teflon molds without application of any demolding oil and cured in laboratory conditions at 20 ± 2 °C and a relative humidity of 65 ± 5%.

All samples had dimensions of 12 × 12 × 60 mm³. Four copper electrodes were made of 0.25 mm thick plates having a width of 5 mm and a height of 15 mm. The copper plates were immersed vertically 7.5 mm deep into the mortar specimen. The distance between the electrodes was 30 mm and between two sets of electrodes 50 mm (Figure 2).
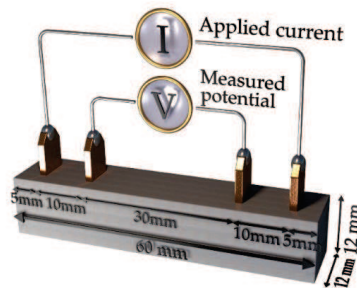
Figure 2. Arrangement of copper electrodes in the mortar sample.

2.3. Methods

The nanomodified cement was characterized using a scanning electron microscope (SEM) type Jeol JSM-IT100. All images were obtained with a secondary electron detector (SE). Thermogravimetric (TG) analysis was performed using a thermal analyzer type NETZSCH STA 449 F3 Jupiter® with a temperature increase rate of 10 °C/min and the maximum applied temperature of 1000 °C.

The electrical resistance was measured using the four-probe method with a digital multimeter type Keysight 34465A. Direct current (DC) was applied between the two outer electrodes and the potential was measured between the two inner electrodes (Figure 2). This configuration showed to

have the lowest variation coefficient and a small scatter of the recorded values [35]. The electrical conductivity σ was calculated using the Equation (4):

$$\sigma = 1/\rho = L/R \cdot A \tag{4}$$

where: ρ is electrical resistivity, L is the internal electrode distance, A is the electrode area, R =V/I is the measured resistance determined by measuring the voltage drop across the specimen, V is the applied current, I.

A compression load with a rate of 0.05 cm/min was applied to the vertically placed beam specimens (Figure 3).
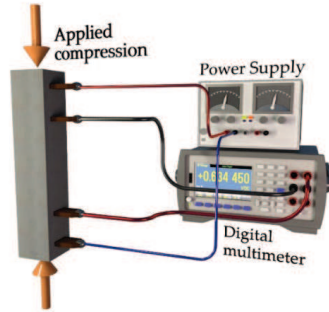
Figure 3. The experimental setup used to measure changes of the electrical resistivity in mortar samples subjected to compression load.

The presence of moisture in any solidified cementitious matrix causes changes to the electrical conductivity when measured over a longer period of time due to polarization caused by the electrolytic effect. The chemical reactions liberate hydrogen and oxygen, which deposit around the measuring electrodes as a thin film, eventually leading to the polarization effect [36]. Earlier studies confirmed that the measured electrical properties of CNT/cement composites were affected by electrode polarization while using DC [37]. Consequently, to limit that negative effect additional calibration measurements were done to determine the time required to obtain more stable readings before the actual measurement of the electrical resistivity was performed. In the used procedure, the electrical resistivity was measured continuously for 2400 s on mortar samples being 1, 3 and 7 days old. The recorded values are shown in Figure 4. The one-day-old mortars showed a constant value during the entire measuring period which is directly related to a very high moisture content due to a low hydration degree of the Portland cement. The measured electrical resistivity of the 3- and 7-day-old test specimens showed slight variations during the first 600–700 s followed by more stable readings. Based on the repeated measurements it was decided that the values for the determination of the electrical resistance will be recorded with a 900 s delay.
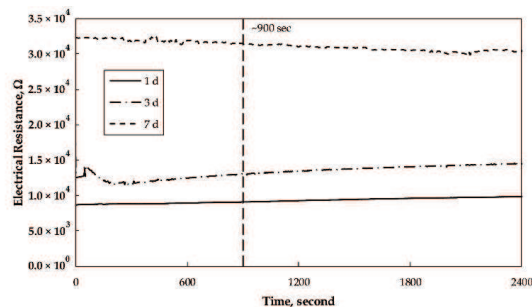
Figure 4. Changes in the electrical resistance with time recorded for mortars containing 8 wt% of the SmartCem I binder 1, 3 and 7 days after casting the specimens.

3. Results and Discussion

The SEM images of the nanomodified cements (SmartCem I and SmartCem II) are shown in Figures 5 and 6. All synthesized CNFs were very curly, had diameters between 10–50 nm and lengths between ~3 μm–~20 μm.
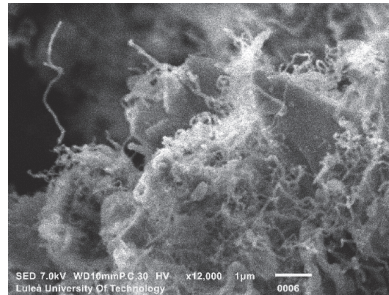
Figure 5. SEM image of SmartCem I.
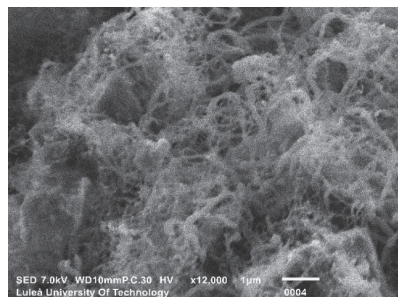
Figure 6. SEM image of SmartCem II.

The nanomodified cements analyzed by TG had two peaks at around 500 °C and 750 °C related to the decomposition of CNFs. The estimated quantities were approximately 2.71 wt% and 2.51 wt% for the SmartCem I and SmartCem II, respectively (Figure 7). The SmartCem I was chosen for further tests due to a lower amount of the hydrogen gas used in the synthesis process and a slightly higher amount of the formed CNFs.
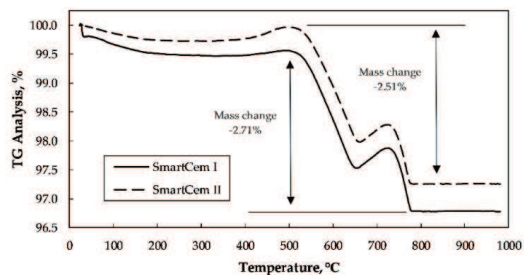
Figure 7. TG Analysis of SmartCem I and SmartCem II.

The electrical conductivity was determined for the reference mortar and for the composite samples containing SmartCem I binder as replacement of Portland cement between 2–10 wt% of cement (Figure 8).
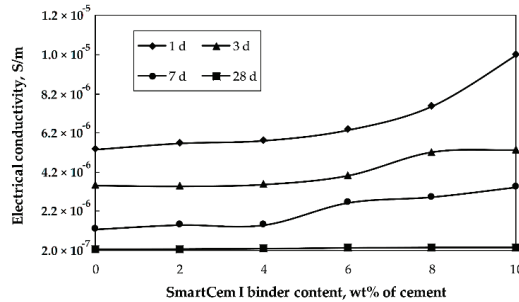
Figure 8. Effects of age and amount of SmartCem I content on the measured electrical conductivity.

The electrical conductivity decreased with age for all samples due to the ongoing hydration process consuming the pore water. The pore water provides limited conductivity for the otherwise electrically non-conductive hardened binder matrix. At later ages most of the capillary pore water was consumed thus decreasing significantly the measured electrical conductivity. The most significant change was observed between 7–28 days, which could be related to the densification of the binder matrix with non-conductive phases, including especially calcium silicate hydrate and calcium hydroxide [38]. Replacement of the Portland cement with SmartCem I altered the measured electrical conductivity depending on the age of the sample. At one day the overall conductivity was significantly higher compared to the aged samples; with a maximum value of 5.4×10^{-6} S/m. Replacement of 2 and 6 wt% of the untreated cement with SmartCem I slightly increased the conductivity followed by a sharp jump up to 1.0×10^{-5} S/m. At higher replacement level, the conductivity of the 7-day-old samples decreased to 1.3×10^{-6} S/m and 3.4×10^{-6} S/m, respectively. The conductivity of the 28-days-old samples was 2.3×10^{-7} S/m for the reference samples and 3.3×10^{-7} S/m for samples containing 8 and 10 wt% of the SmartCem I.

The observed percolation threshold values varied depending on the sample age. In the case of the one-day-old specimen, the maximum conductivity value was reached at the 10 wt% replacement level. In this case, a higher amount of moisture present in the binder matrix created a conducting medium enhancing the measured electrical conductivity. During the following three weeks, the progressing hydration consumed the water and lowered the amount of the conductive medium, which decreased the percolation threshold stepwise from 10, 7 and 5 down to approximately 4 wt% of the SmartCem I. These values corresponded to 0.271, 0.189, 0.135 and 0.108 wt% of CNFs as estimated based on the TG test results. The lowest, 2 wt% of the SmartCem I (corresponding to 0.054 wt% of CNFs), has a minimal effect on the electrical conductivity (Figure 9). The percolation threshold values estimated earlier for Portland cement-based matrixes incorporating multiwall carbon nanotubes oscillated at around 0.20 wt% [39,40]. Whereas values measured in the present research were significantly lower at 0.108 wt% of CNFs. Several factors could contribute to this difference; including CNFs morphology, their distribution within the binder matrix, distance between fibers as well as the microstructure and composition of the isolative binder matrix.
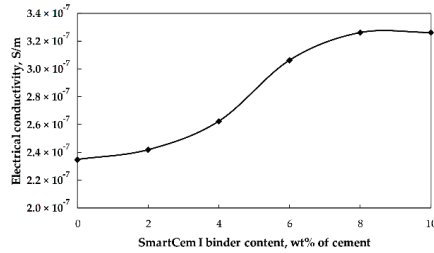
Figure 9. Effects of the SmartCem I content on electrical resistivity of 28 days old samples.

The morphology of the CNFs was shown to affect the percolation threshold and the maximum conductivity. For example, curly shaped CNFs incorporated into polymer-based matrixes increased the percolation threshold concentration from 0.05 to 0.4 vol% [41].

Furthermore, not all CNFs take part in the conduction despite being evenly distributed within the binder matrix due to being too far apart from each other due to their shape or too low amount. The distance providing conductivity is estimated to be just a few nanometers [42]. The overall electrical conductivity depends also on the number of formed percolated networks. The nanofibers do not touch directly each other due to the Van der Wall forces and the conduction occurs through the tunneling effect [43] (Figure 10).
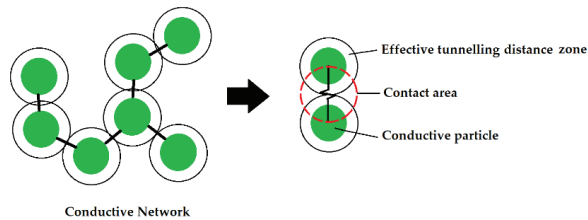
Figure 10. The tunneling effect between conductive particles dispersed in an electrically non-conductive composite.

The tunneling effect is affected by the interfacial transition zone (ITZ) forming between the binder matrix and the CNFs surface. Properties of that zone; its thickness; porosity as well as the chemical composition will strengthen or weaken the effect. The ITZ formed in Portland cement-based matrixes around sand particles and aggregates may range from a few μm to a few hundreds of μm [44,45]. Presumably, in the case of nanosized CNFs the actual ITZ will be only a few nanometers wide. The interfacial transition zones were also observed in polymer-based matrixes incorporating CNTs [46]. Consequently, the observed in the present data decrease of the percolation threshold with age can be related to the general densification of the bulk binder matrix and of the interfacial transition zones.

After 28 days the ultimate measured conductivity of 3.3×10^{-7} S/m was constant for the 8 and 10 wt% replacement levels. The CNFs incorporated into a cement matrix are less homogenously dispersed in comparison with polymer matrixes due to the presence of sand particles and anhydrous cement particles. Attaching CNF directly to the cement particles ensures a very high initial dispersion homogeneity and acts as a carrier during the mixing process. It prevents the formation of agglomerates, but at the same time it creates large non-conductive volumes of unhydrated cement particles [45,47] (Figure 11).
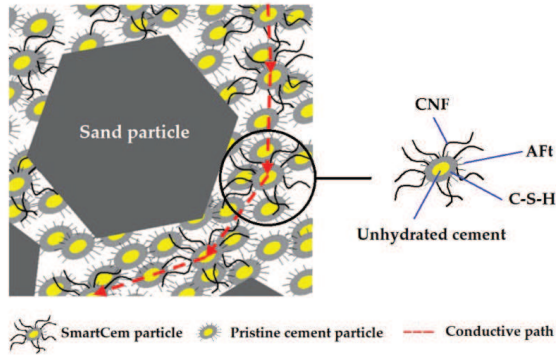
Figure 11. SmartCem with attached carbon nanofibers in hydrated cement matrix.

The piezoresistive response to the applied load was determined on samples produced from three mixes: reference, S8-containing 8 wt% of SmartCem I and S10-containing 10 wt% of the SmartCem I. The recorded dependence between the applied compressive stress and the corresponding measured electrical resistance is shown in Figure 12.
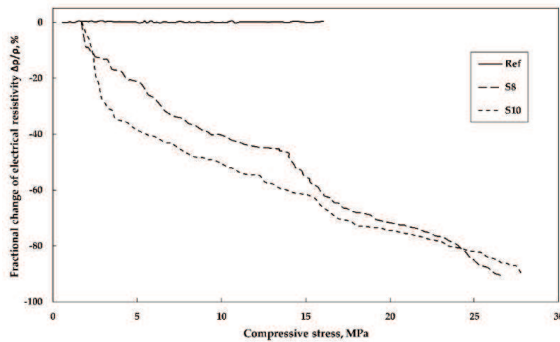
Figure 12. Relationship between fractional change in electrical resistivity and compressive stress.

Both samples, S8 and S10 showed a strong piezoresistive response within the two stages of nearly linear relationships. In the first stage while loading up to 3.5 MPa load, the fractional change of the electrical resistivity reached around 17% and 32% for S8 and S10 respectively. In the second loading stage between 3.5 and 26 MPa the change reached 90%. Portland cement-based mortar incorporating SmartCem I showed also a significant response to strain. The resistivity decreased with increasing compressive strain until the failure occurred (Figure 13). The maximum strain sensitivity of the gauge factor (GF) in this study was calculated based on the fractional resistance change to the change of strain, and equaled to 18.7.
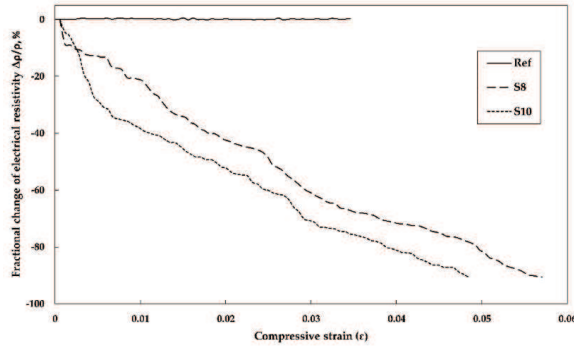
Figure 13. Relationship between fractional change in electrical resistivity and compressive strain.

Earlier studies showed a considerably lower sensitivity. For example, Zhang et al. [48] or Yu and Kwon [49] measured between 6 and 9% change in the electrical resistivity for applied loads of 4 MPa and 5.2 MPa. In both cases, the samples were produced by dispersing 0.06; 0.1 wt% and 2.14 vol% of MWCNTs in water (Table 3).

Table 3. Load sensitivity of cement/CNT composites measured by others and compared with recalculated results obtained for mix S8.

Publication	Amount of Carbon-Based Materials	(Load MPa) Resistance Change, %	(Load, MPa) Resistance Change, %
Yu & Kwon [49]	0	(5.2) 0.0	(8.6) 0.0
Yu & Kwon [49]	0.06 wt% MWCNT	(5.2) 8.8	(8.6) 10.3
Yu & Kwon [49]	0.10 wt% MWCNT	(5.2) 8.4	(8.6) 11.4
Zhang et al. [48]	2.14 vol% MWCNT	(4) 6.8	-
Present result S8	0.20 wt% CNF	(3.5) ~17	(26) ~90

The observed differences can be related, as in the case of the electrical conductivity described earlier, to a number of factors. These include dispersion and morphology of the CNFs/CNTs, their dimensions, curliness but also the microstructure of the binder matrix and the presence of non-conductive inclusions like unhydrated cement particles or sand. In the present case, presumably the strongest effect on the enhanced sensitivity was achieved by the better dispersion of the CNFs. The enhanced dispersion, compared to especially at high pH unstable water dispersions, was obtained by growing CNFs directly on the cement particles.

The piezoresistive response can be related to the intrinsic piezoresistive property of the CNFs themselves, which was observed in earlier studies on films made of single-wall carbon nanotubes. These results showed a nearly linear relation between the applied strain and the measured voltage and were successfully used for strain sensing [50]. The second phenomenon associated with the piezoresistive response is related to changes of the electrical resistance of the contact points between fibers due to the applied load. In this case, the applied load will presumably compress the binder matrix. CNTs incorporated into a polymer matrix decreased the resistivity at the applied compression load [51–53]. A more intensive change of the electrical resistivity in the first stage of the response could be related to the initially stronger densification effect of the more porous part the binder matrix (Figure 12). This could lead to a significant enhancement of the tunneling effect and to the ultimate increase of the electrical conductivity.

4. Conclusions

Carbon nanofibers were directly synthesized on Portland cement particles using chemical vapor deposition in the presence of a mixture of ethylene and hydrogen. The produced materials contained 2.71 wt% and 2.51 wt% of CNFs. Percolation thresholds corresponding to the increase of the electrical conductivity were observed in all samples. The threshold tended to decrease with the ongoing hydration of the Portland cement. The percolation threshold varied between 0.271, 0.189, 0.135 and 0.108 wt% CNFs which corresponded to 10, 7, 5 and 4 wt% of the SmartCem I respectively. The studied mortars showed an extremely strong piezoresistive response to the applied compressive load reaching 17% change at 3.5 MPa and 90% at 26 MPa. The piezoresistive response was related to the intrinsic piezoresistive property of the CNFs and to changes of the electrical resistance at the contact points between fibers. Based on the obtained test results from this initial study, the developed material appears to be potentially suitable for applications for stress sensors and smart concrete structures. Furthermore, the measured piezoresistive response should also be sufficient to determine other changes, including, for example humidity, temperature or crack formation. The current ongoing research focuses on those aspects.

References

1. Reich, S.; Thomsen, C.; Maultzsch, J. *Carbon Nanotubes: Basic Concepts and Physical Properties*; Wiley-VCH: Weinheim, Germany, 2007; ISBN 9783527618040.
2. Popov, V.N. Carbon nanotubes: Properties and application. *Mater. Sci. Eng. R Rep.* **2004**, *43*, 61–102.
3. Dresselhaus, M.S.; Dresselhaus, G.; Eklund, P.C. *Science of Fullerenes and Carbon Nanotubes: Their Properties and Applications.*; Academic press, Elsevier Science Imprint: San Diego, CA, USA, 1996; ISBN 9780080540771.
4. Raki, L.; Beaudoin, J.; Alizadeh, R.; Makar, J.; Sato, T. Cement and concrete nanoscience and nanotechnology. *Materials.* **2010**, *3*, 918–942.
5. Li, G.Y.; Wang, P.M.; Zhao, X. Mechanical behavior and microstructure of cement composites incorporating surface-treated multi-walled carbon nanotubes. *Carbon* **2005**, *43*, 1239–1245.
6. Cwirzen, A.; Habermehl-Cwirzen, K.; Penttala, V. Surface decoration of carbon nanotubes and mechanical properties of cement/carbon nanotube composites. *Adv. Cem. Res.* **2008**, *20*, 65–73.
7. Han, B.; Yu, X.; Ou, J. Multifunctional and Smart Carbon Nanotube Reinforced Cement-Based Materials. In *Nanotechnology in Civil Infrastructure*; Springer Berlin, Heidelberg: Germany 2011; Vol. 14, pp. 1–47 ISBN 9783642166563.
8. Veedu, V. Multifunctional Cementitious Nanocomposite Material and Methods of Making the Same. U.S. Patent 7,875,211 B1, 25 January 2011.
9. Chung, D.D.L. Piezoresistive cement-based materials for strain sensing. *J. Intell. Mater. Syst. Struct.* **2002**, *13*, 599–609.
10. Wen, S.; Chung, D.D.L. A comparative study of steel- and carbon-fibre cement as piezoresistive strain sensors. *Adv. Cem. Res.* **2003**, *15*, 119–128.
11. Wen, S.; Chung, D.D.L. Uniaxial tension in carbon fiber reinforced cement, sensed by electrical resistivity measurement in longitudinal and transverse directions. *Cem. Concr. Res.* **2000**, *30*, 1289–1294.

12. Konsta-Gdoutos, M.S.; Aza, C.A. Self sensing carbon nanotube (CNT) and nanofiber (CNF) cementitious composites for real time damage assessment in smart structures. *Cem. Concr. Compos.* **2014**, *53*, 162–169.

13. Li, H.; Xiao, H. gang; Ou, J. Effect of compressive strain on electrical resistivity of carbon black-filled cement-based composites. *Cem. Concr. Compos.* **2006**, *28*, 824–828.

14. Li, H.; Xiao, H.; Ou, J. Electrical property of cement-based composites filled with carbon black under long-term wet and loading condition. *Compos. Sci. Technol.* **2008**, *68*, 2114–2119.

15. Lin, V.W.J.; Li, M.; Lynch, J.P.; Li, V.C. Mechanical and electrical characterization of self-sensing carbon black ECC. *Proc. SPIE* **2011**, *7983*, 798316.

16. Abeles, B.; Pinch, H.L.; Gittleman, J.I. Percolation conductivity in W-Al2O3 granular metal films. *Phys. Rev. Lett.* **1975**, *35*, 247–250.

17. Sheng, P.; Abeles, B.; Arie, Y. Hopping conductivity in granular metals. *Phys. Rev. Lett.* **1973**, *31*, 44–47.

18. Vionnet-Menot, S.; Grimaldi, C.; Maeder, T.; Strässler, S.; Ryser, P. Tunneling-percolation origin of nonuniversality: Theory and experiments. *Phys. Rev. B Condens. Matter Mater. Phys.* **2005**, *71*, 064201.

19. Balberg, I. Tunnelling and percolation in lattices and the continuum. *J. Phys. D. Appl. Phys.* **2009**, *42*, 064003.

20. Balberg, I. A comprehensive picture of the electrical phenomena in carbon black-polymer composites. *Carbon* **2002**, *40*, 139–143.

21. Stauffer, D.; Bunde, A. Introduction to Percolation Theory. *Phys. Today* **2008**, *40*, 122–123.

22. Rejón, L.; Rosas-Zavala, A.; Porcayo-Calderon, J.; Castaño, V.M. Percolation phenomena in carbon black-filled polymeric concrete. *Polym. Eng. Sci.* **2000**, *40*, 2101–2104.

23. Hu, N.; Masuda, Z.; Yan, C.; Yamamoto, G.; Fukunaga, H.; Hashida, T. The electrical properties of polymer nanocomposites with carbon nanotube fillers. *Nanotechnology* **2008**, *19*, 215701.

24. Alamusi; Hu, N.; Fukunaga, H.; Atobe, S.; Liu, Y.; Li, J. Piezoresistive strain sensors made from carbon nanotubes based polymer nanocomposites. *Sensors* **2011**, *11*, 10691–10723.

25. Konsta-Gdoutos, M.S.; Metaxa, Z.S.; Shah, S.P. Highly dispersed carbon nanotube reinforced cement based materials. *Cem. Concr. Res.* **2010**, *40*, 1052–1059.

26. Han, B.; Sun, S.; Ding, S.; Zhang, L.; Yu, X.; Ou, J. Review of nanocarbon-engineered multifunctional cementitious composites. *Compos. Part A Appl. Sci. Manuf.* **2015**, *70*, 69–81.

27. Makar, J.M.; Beaudoin, J.J. Carbon Nanotubes and Their Application in the Construction Industry. In Proceedings of the 1st International Symposium on Nanotechnology in Construction, 23–25 June 2003; Paisley, Scotland; pp. 331–341.

28. Nasibulin, A.G.; Shandakov, S.D.; Nasibulina, L.I.; Cwirzen, A.; Mudimela, P.R.; Habermehl-Cwirzen, K.; Grishin, D.A.; Gavrilov, Y.V.; Malm, J.E.M.; Tapper, U.; et al. A novel cement-based hybrid material. *New J. Phys.* **2009**, *11*, 023013.

29. Nasibulina, L.; Anoshkin, I.; Shandakov, S.; Nasibulin, A.; Cwirzen, A.; Mudimela, P.; Habermehl-Cwirzen, K.; Malm, J.; Koltsova, T.; Tian, Y.; et al. Direct Synthesis of Carbon Nanofibers on Cement Particles. *Transp. Res. Rec. J. Transp. Res. Board* **2010**, *2142*, 96–101.

30. Mudimela, P.R.; Nasibulina, L.I.; Nasibulin, A.G.; Cwirzen, A.; Valkeapää, M.; Habermehl-Cwirzen, K.; Malm, J.E.M.; Karppinen, M.J.; Penttala, V.; Koltsova, T.S.; et al. Synthesis of carbon nanotubes and nanofibers on silica and cement matrix materials. *J. Nanomater.* **2009**, *2009*, 526128.

31. Ghaharpour, F.; Bahari, A.; Abbasi, M.; Ashkaran, A.A. Parametric investigation of CNT deposition on cement by CVD process. *Constr. Build. Mater.* **2016**, *113*, 523–535.

32. Chen, P.; Zhang, H.B.; Lin, G.D.; Hong, Q.; Tsai, K.R. Growth of carbon nanotubes by catalytic decomposition of CH4 or CO on a Ni-MgO catalyst. *Carbon* **1997**, *35*, 1495–1501.

33. Pan, Z.W.; Xie, S.S.; Chang, B.H.; Sun, L.F.; Zhou, W.Y.; Wang, G. Direct growth of aligned open carbon nanotubes by chemical vapor deposition. *Chem. Phys. Lett.* **1999**, *299*, 97–102.

34. Bae, E.J.; Choi, W.B.; Jeong, K.S.; Chu, J.U.; Park, G.S.; Song, S.; Yoo, I.K. Selective growth of carbon nanotubes on pre-patterned porous anodic aluminum oxide. *Adv. Mater.* **2002**, *14*, 277–279.

35. Chiarello, M.; Zinno, R. Electrical conductivity of self-monitoring CFRC. *Cem. Concr. Compos.* **2005**, *27*, 463–469.

36. Banthia, N.; Djeridane, S.; Pigeon, M. Electrical resistivity of carbon and steel micro-fiber reinforced cements. *Cem. Concr. Res.* **1992**, *22*, 804–814.

37. Coppola, L.; Buoso, A.; Corazza, F. The influence of AC and DC electrical resistance and piezoresistivity measurements of CNTs/cement composites. In Proceedings of the 3rd Workshop on The New Boundaries of Structural Concrete, 3–4 October 2013; Bergamo, Italy; pp. 155–164.

38.   Taylor, H.F.W. *Cement Chemistry*; Thomas Telford: London, United kingdom, 1997; ISBN 0727725920.
39.   Chen, B.; Wu, K.; Yao, W. Conductivity of carbon fiber reinforced cement-based composites. *Cem. Concr. Compos.* **2004**, *26*, 291–297.
40.   Nam, I.W.; Souri, H.; Lee, H.K. Percolation threshold and piezoresistive response of multi-wall carbon nanotube/cement composites. *Smart Struct. Syst.* **2016**, *18*, 217–231.
41.   Li, C.; Thostenson, E.T.; Chou, T.W. Effect of nanotube waviness on the electrical conductivity of carbon nanotube-based composites. *Compos. Sci. Technol.* **2008**, *68*, 1445–1452.
42.   Li, C.; Thostenson, E.T.; Chou, T.W. Dominant role of tunneling resistance in the electrical conductivity of carbon nanotube-based composites. *Appl. Phys. Lett.* **2007**, *91*, 223114.
43.   Liu, Z.; Peng, W.; Zare, Y.; Hui, D.; Rhee, K.Y. Predicting the electrical conductivity in polymer carbon nanotube nanocomposites based on the volume fractions and resistances of the nanoparticle, interphase, and tunneling regions in conductive networks. *RSC Adv.* **2018**, *8*, 19001–19010.
44.   Cwirzen, A.; Penttala, V. Aggregate-cement paste transition zone properties affecting the salt-frost damage of high-performance concretes. *Cem. Concr. Res.* **2005**, *35*, 671–679.
45.   Cwirzen, A. The effect of the heat-treatment regime on the properties of reactive powder concrete. *Adv. Cem. Res.* **2007**, *19*, 25–33.
46.   Zare, Y.; Rhee, K.Y. Development of Hashin-Shtrikman model to determine the roles and properties of interphases in clay/CaCO3/PP ternary nanocomposite. *Appl. Clay Sci.* **2017**, *137*, 176–182.
47.   Cwirzen, A. Controlling Physical Properties of Cementitious Matrixes by Nanomaterials. *Adv. Mater. Res.* **2010**, *123–125*, 639–642.
48.   Zhang, L.; Ding, S.; Dong, S.; Li, Z.; Ouyang, J.; Yu, X.; Han, B. Piezoresistivity, mechanisms and model of cement-based materials with {CNT}/{NCB} composite fillers. *Mater. Res. Express* **2017**, *4*, 125704.
49.   Yu, X.; Kwon, E. A carbon nanotube/cement composite with piezoresistive properties. *Smart Mater. Struct.* **2009**, *18*, 055010.
50.   Dharap, P.; Li, Z.; Nagarajaiah, S.; Barrera, E.V. Nanotube film based on single-wall carbon nanotubes for strain sensing. *Nanotechnology* **2004**, *15*, 379–382.
51.   Tombler, T.W.; Zhou, C.; Alexseyev, L.; Kong, J.; Dai, H.; Liu, L.; Jayanthi, C.S.; Tang, M.; Wu, S.Y. Reversible electromechanical characteristics of carbon nanotubes under local-probe manipulation. *Nature* **2000**, *405*, 769–772.
52.   Cao, J.; Wang, Q.; Dai, H. Electromechanical Properties of Metallic, Quasimetallic, and Semiconducting Carbon Nanotubes under Stretching. *Phys. Rev. Lett.* **2003**, *90*, 4.
53.   Kim, Y.J.; Shin, T.S.; Choi, H. Do; Kwon, J.H.; Chung, Y.-C.; Yoon, H.G. Electrical conductivity of chemically modified multiwalled carbon nanotube/epoxy composites. *Carbon* **2005**, *43*, 23–30.

Paper III

Role of carbon nanofiber on the electrical resistivity of mortar under compressive load

Buasiri, T., Habermehl-Cwirzen, K., Krzeminski, L., & Cwirzen, A.

TRR
JOURNAL OF THE TRANSPORTATION RESEARCH BOARD

Role of Carbon Nanofiber on the Electrical Resistivity of Mortar under Compressive Load

Thanyarat Buasiri[1], Karin Habermehl-Cwirzen[1], Lukasz Krzeminski[2], and Andrzej Cwirzen[1]

Abstract
A nanomodified cement consisting of particles with in situ synthesized carbon nanofibers was developed to introduce a strong load-sensing capability of the hydrated binder matrix. The material was produced using chemical vapor deposition. The nanomodified cement contained 2.71 wt% of carbon nanofibers (CNFs). The electrical properties of the composite were determined. Several mortar samples were prepared by partially substituting ordinary Portland cement with 2, 4, 6, 8, and 10 wt% of the nanomodified cement. Additionally an ordinary Portland cement mortar was used as reference. The results show that the strongest piezoresistive response and therefore the best load-sensing was obtained for the mortar containing the highest amount of CNFs. This mortar contained 10 wt% of nanomodified cement. The fractional change in electrical resistivity of this mortar was 82% and this mortar had a compressive strength of 28 MPa.

In general, structural health monitoring (SHM) in civil engineering is defined as a process that aims to detect a change in the structural properties as a way of identifying damaged structures (*1*). Many methods that monitor concrete structures in SHM systems commonly use strain gauges mounted on the concrete surface or embedded fiber optic sensors. Most of the systems currently in use are prone to mechanical damage and have poor durability and thus a short lifespan. A novel solution is based on smart Portland cements, which after solidification have a strong sensing capability. The main advantage of cement-based sensors is their full material compatibility with the material used to build the structure being monitored. These sensors are expected to have a long service life, easy installation, and limited maintenance. Self-monitoring Portland cement-based materials are becoming more attractive for civil engineering applications. This self-monitoring or so-called self-sensing is made possible by changes in the electrical resistivity of a material. Electrical resistivity is a fundamental material property that shows how strongly the material opposes the flow of an electric current. The self-sensing phenomena in a material is based on the property of an electrically conductive material to show a change in its electrical resistivity if a deformation load is applied. This phenomenon is called piezo resistivity. To provide a cement-based material with this load-sensing capability various

types of conductive materials need to be incorporated into the cementitious matrix.

Studies showed that the addition of carbon nanofibers (CNFs) and carbon nanotubes (CNTs) improve physical, mechanical, chemical, and electrical properties (*2–5*). For example, Cwirzen et al. found that an addition of 0.045 wt% of multi-walled carbon nanotubes (MWCNTs) to a cement paste increased the compressive strength by nearly 50**%** (*6*). Konsta-Gdotous et al. (*7*) produced pastes containing 0.048 wt% of MWCNTs and achieved 30% to 40% higher flexural strengths values. The presence of long MWCNTs appeared to decrease the autogenous shrinkage. Konsta-Gdoutos and Aza (*8*) studied the piezoresistive behavior of a cementitious matrix with CNFs subjected to cyclic compression load in the elastic regime. The electrical resistivity tended to decrease during the loading and to increase while unloading. Similar results were obtained by Yu and Kwon (*9*) where a change in the electrical resistivity of a CNT/cement composite under different compressive loading was observed.

[1]Department of Civil, Environmental and Natural Resources Engineering, Building Materials, Luleå University of Technology, Luleå, Sweden
[2]The Institute of Engineering Materials and Biomaterials, Silesian University of Technology, Gliwice, Poland

Corresponding Author:
Thanyarat Buasiri, thanyarat.buasiri@ltu.se

Specimens reinforced with functionalized CNTs showed a stronger piezoresistive response. A sufficient amount of conductive materials is required to create a continuous interconnected network. The fibers must be evenly distributed throughout the binder matrix. Unfortunately, because of the hydrophobic nature and the tendency of carbon-based materials to agglomerate, it is crucial to ensure their uniform dispersion into the matrix. The nanomodified cement was developed to address the dispersion problem of carbon-based materials in cementitious matrices. The nanomodified cement was produced by synthesizing CNFs directly on the surface of pristine Portland cement particles in a chemical vapor deposition (CVD) reactor. In the processed synthesis, the Fe_2O_3 present in Portland cement acted as a natural catalytic substrate while the other phases supported the growth of CNFs (10–12). Acetylene (C_2H_2) was used as the main carbon source with synthesis temperatures between 525°C and 600°C. Solidified matrices produced from the modified cement showed a very good dispersion of the CNFs (13). Recently, Buasiri et al. reported pilot studies on the sensing capability of the nanomodified cement which showed an excellent load sensitivity of those materials (14). The studied mortars containing around 0.2 wt% of CNFs showed a high sensitivity, reaching around 90%.

The research described in this article aimed to determine the effects of the replacement of Portland cement with various amounts of nanomodified cement on the mechanical properties and the changes in the electrical resistivity under compression loading.

Methods

Synthesis of the Nanomodified Cement

The nanomodified cement was produced using a Carbon Chemical Vapor Deposition (CCVD) reactor located at the Silesian University of Technology in Poland. For the syntheses, pure ethylene (C_2H_4, 99.999%) was used as a main carbon source, pure hydrogen (H_2, 99.99999%) as the reducer and Argon (Ar) as the transporting media. All of the gases were industrial grade. A schematic diagram of the CVD process and the synthesis procedure of the nanomodified cement are shown in Figure 1.

Materials and Sample Preparation

An ordinary Portland cement CEM I 42.5 provided by Cementa-Sweden was used for the synthesis of the nanomodified cement and for the production of the test mortars. Sand with maximum particle size of 150 μm was used as fine aggregate. The nanomodified cement was synthesized by the CVD method shown in Figure 1. The surface morphology of the pristine and modified cements is shown in Figure 2. The quantitative analysis of the
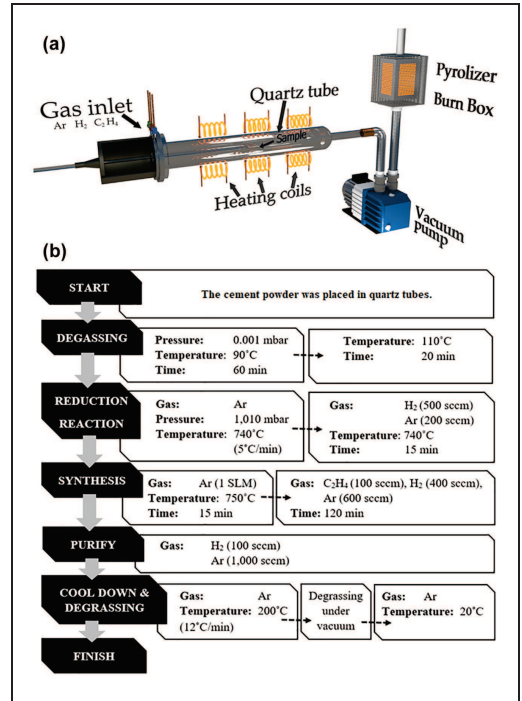
Figure 1. (*a*) A schematic representation of the chemical vapor deposition process for the production of synthesized nanomodified cement (reprinted from [14] © MDPI under CC-BY 4.0 [https://creativecommons.org/licenses/by/4.0/]); and (*b*) the synthesis procedures of the nanomodified cement.

carbon nanomaterials formed in the nanomodified cement was done by thermogravimetry (TG). The total amount of CNFs and other carbon containing phases calculated by percentage of the mass loss was approximately 2.71 wt%. The visually estimated diameters were around 10–50 nm and the lengths between 3 μm and 20 μm with a very curly shape.

All mortar samples had the same water to binder ratio (w/b) of 0.35, sand to binder ratio (s/b) of 1% and 0.8% of the super plasticizer admixture by weight of the binder. The admixture type Glenium produced by Grace Chemical was used to control the workability of fresh mixes. The nanomodified cement replaced 0% (Ref), 2% (S2), 4% (S4), 6% (S6), 8% (S8), and 10% (S10) of the pristine cement by weight of the binder. The proportions of the mortars produced are shown in Table 1. Because of the very limited amount of available nanomodified cement only two samples were produced for each mix.

A small vacuum mixer of the Bredent type was used to produce the mortars. This was done to minimize the
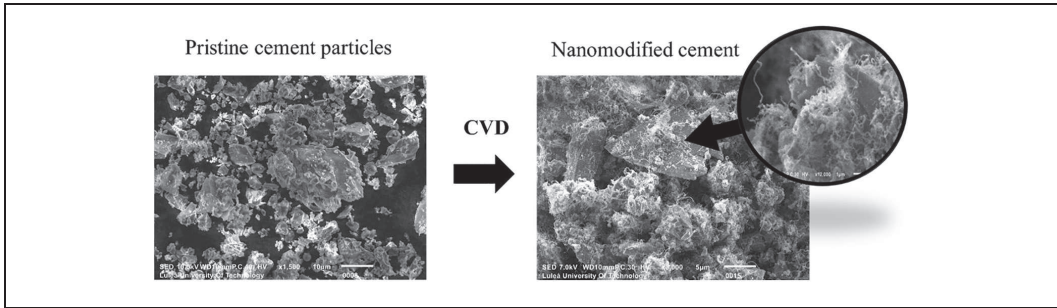
Figure 2. Scanning Electron Microscope images of an ordinary Portland cement and the nanomodified cement consisting with carbon nanofibers.
Note: CVD = chemical vapor deposition.

Table 1. Mix Proportions for Mortar Samples

Mix	w/b	s/b	Superplasticizer (wt% of binder)	Cement (wt% of binder)	Nanomodified cement (wt% of binder)	Calculated quantities of CNFs (wt% of binder)
Ref	0.35	1	0.8	100	0	0.000
S2	0.35	1	0.8	98	2	0.054
S4	0.35	1	0.8	96	4	0.108
S6	0.35	1	0.8	94	6	0.163
S8	0.35	1	0.8	92	8	0.217
S10	0.35	1	0.8	90	10	0.271

Note: w/b = water-to-binder ratio; s/b = sand-to-binder ratio; CNFs = carbon nanofibers.

amount of the trapped air. The mortars were cast into Teflon molds and subsequently cured in water. Before testing, all samples were stored in laboratory conditions at 20°C ± 2°C for 72 h to exclude any possible effects of moisture or temperature variations on the measured electrical properties. The specimens had dimensions of 12 mm × 12 mm × 60 mm with four copper electrodes embedded vertically. The 0.25 mm thick copper electrodes had a width of 5 mm and a height of 15 mm. The electrodes were spaced as shown in Figure 3a.

Load-Sensing Determination

The load-sensing capability in the present research was based on the determination of changes in the electrical resistivity of the samples when subjected to an increasing compression load. Sensing behavior of the cement-based materials under loading can be described by the fractional change in the electrical resistivity (FCR) which can be calculated using Equation 1:

$$FCR = \Delta\rho/\rho_0 \qquad (1)$$

where $\Delta\rho$ is the change in electrical resistivity and ρ_0 is the initial electrical resistivity of the sensing cementitious matrix. The electrical resistivity ρ was calculated following Equation 2:

$$\rho = R \cdot A/L \qquad (2)$$

where
R = V/I is the measured resistance determined by the changed of the voltage V across the specimen when applied the current I,
A is the electrode area, and
L is the internal electrode distance.

The electrical resistance of the produced mortars was measured using the four-probe method during the application of the compressive load. This configuration showed the lowest variation coefficient and smallest scatter of the data (*15*). The 60 cm long electrical wires connected the copper electrodes with a digital multimeter of type Keysight 34465A. The direct current (DC) was applied between the two outer electrodes while the two inner electrodes were used to measure the potential difference. The compressive load with the rate of 0.05 cm/min was applied to the mortar beams. The experimental setup is shown in Figure 3b.

In moist matrices, including cement-based ones, the polarization effect causes chemical reactions liberating hydrogen and oxygen, which deposit around the measuring electrodes as a thin film and cause changes to the electrical response (*16*). To eliminate or minimize this effect, the specimens should be dry, and a high-frequency alternating current should be applied (*17*). In this study,
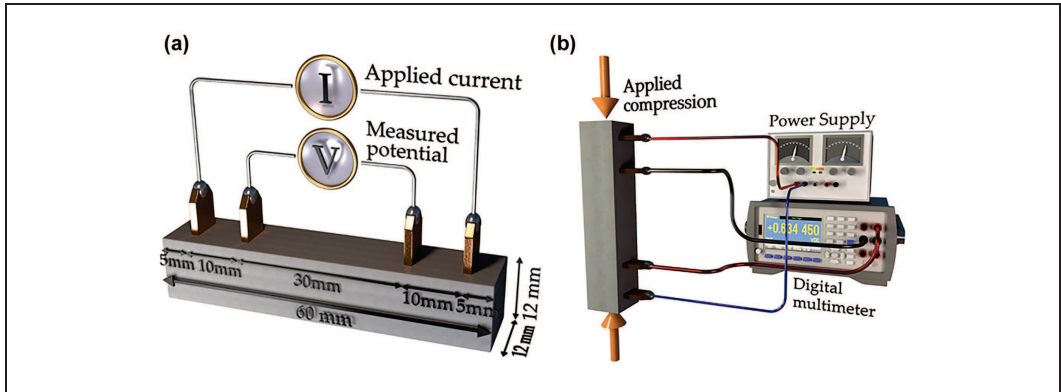
Figure 3. (*a*) Mortar sample with copper electrodes; and (*b*) the test set-up used to measure the electrical response during applied compressive load. (Reprinted from [*14*] © MDPI under CC-BY 4.0 [https://creativecommons.org/licenses/by/4.0/]).

which used DC current, the polarization effects were limited by an additional calibration measurement (*18*) to establish a stable initial reading of the resistance of the solidified matrix before the actual measurement was done.

Results and Discussion

Changes in the electrical resistivity under compressive load were determined on 28-day-old mortar samples containing various amounts of the nanomodified cement; Ref, S2, S4, S6, S8, and S10.

The load-sensing capability is directly related to the piezoresistive response. The conductivity is governed by the concentration of the CNFs and the so-called percolation threshold. The percolation threshold marks an abruptly increasing electrical conductivity when the concentration of the nanomodified cement reaches a certain critical value, the so-called percolation threshold value. The electrical resistivity changes depending on the amount of the conductive filler and creates three consecutive zones; an insulation zone, a percolation zone, and a conduction zone, Figure 4*a* (*19*). Below the percolation zone, the amount of conductive filler is too small to achieve a conductive material. Furthermore, the electrical conductivity will be altered by any mechanical deformation causing changes in the contact area between CNFs, the binder matrix, or both. This leads to a rearrangement of the CNFs and the formation of effective conductive paths thus altering the measurable electrical conductivity, Figure 4*c*.

The observed curves also showed non-linear behavior, which could be related to microcracking of the binder matrix, Figure 5. Other possible factors also include variations of humidity and temperature. However, those factors were assumed insignificant because of the experimental setup used.

The results in Figure 5 showed that the fractional change in electrical resistivity decreased with increasing compressive stress for the samples containing different amounts of the nanomodified cement. This decrease continued until failure occurred. The partial substitution of the pristine cement by the nanomodified cement has affected the piezoresistive response of the mortar samples. There are three groups of piezoresistive response within the sample range, while the reference sample remained unchanged. In the first group, S2 and S4 showed very small piezoresistive effects to the applied load. This could be explained by several factors including the small amount of the nanomodified cement leading to the inter-particle distance of the conductive cement particles being too large. Because of this large inter-particle distance, no electrically conductive path through the sample can be formed. In the following group, the sensitivity of the solidified matrix containing 6 wt% of the nanomodified cement increased moderately to approximately 20%. In the last group, both measured samples S8 and S10 showed a strong piezoresistive response with similar trends. The highest sensitivity was achieved in the samples containing 10 wt% of the nanomodified cement which corresponded to a decrease by 82% of the fractional change of electrical resistivity.

Mortar beams showed a piezoresistive response within two stages of nearly linear relationships. In the first stage, all samples had very high sensitivity to the applied compressive load up to around 6 MPa. In the second loading stage, from 6 MPa until failure, the change was less extensive. The piezoresistive response can be related to the intrinsic piezoresistive property of the CNFs. The applied compressive load leads to a deformation-induced formation of effective conductive paths as well as changes in the tunneling distance and the contact points between CNFs on the nanomodified cement particles.
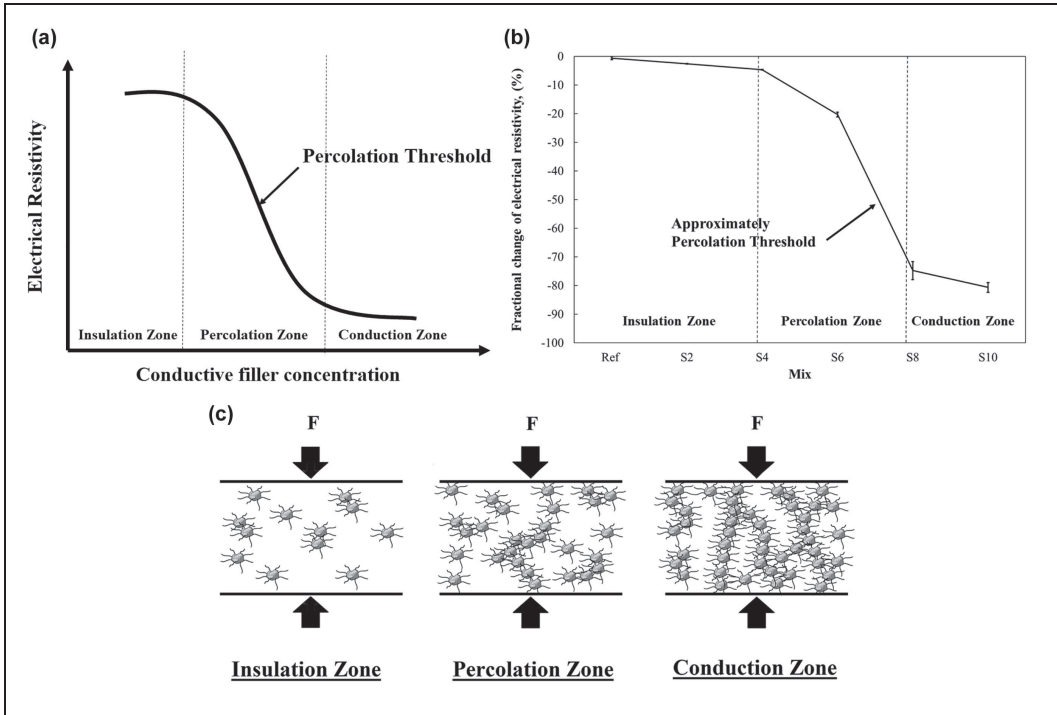
Figure 4. (*a*) General pattern of the percolation process; (*b*) the maximum percentage of fractional change in electrical resistivity with different mixes used in this study; and (*c*) the different load-sensing mechanisms with different formations of the conductive paths in three zones.
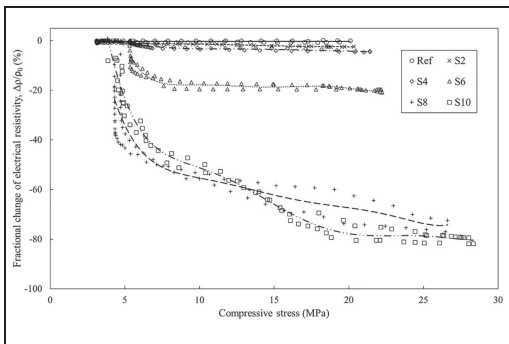
Figure 5. Trends in fractional changes in electrical resistivity and compressive stress for different concentrations of the nanomodified cement. Trend lines are averages of two mortar samples.

The load-sensing capability could be related to the amount of CNFs present in the matrix and thus to the percolation threshold. Based on the results obtained the percolation threshold values of the nanomodified cement were around 7 wt%, Figure 4*b*. The measured values indicate that samples containing 2 wt%, 4 wt%, and 6 wt% of the nanomodified cement are still under the percolation threshold while samples containing 8 wt% and 10 wt% are above it.

Conclusion

The electrical response during compressive loading of a pristine cement sample and samples containing nanomodified cement was recorded to determine the load-sensing capability of the nanomodified cement. A replacement by 10 wt% of the untreated cement by the nanomodified cement showed an extremely strong piezoresistive response to the applied load. The fractional change in the electrical resistivity reached 82% at 28 MPa. The strong piezoresistive response was related to the intrinsic piezoresistive property of the CNFs themselves and to changes of the electrical resistance of the contact points between the nanofibers under the applied load. The results obtained indicate that the nanomodified cement-based material gives a clear piezoresistive response under loading which could be utilized as in-built sensors in structures.

Author Contributions

The authors confirm contribution to the paper as follows: study conception and design: Thanyarat Buasiri, Karin Habermehl-Cwirzen, Lukasz Krzeminski, Andrzej Cwirzen; data collection: Thanyarat Buasiri; analysis and interpretation of results: Thanyarat Buasiri, Karin Habermehl-Cwirzen, Lukasz Krzeminski, Andrzej Cwirzen; draft manuscript preparation: Thanyarat Buasiri, Karin Habermehl-Cwirzen, Lukasz Krzeminski, Andrzej Cwirzen. All authors reviewed the results and approved the final version of the manuscript.

Declaration of Conflicting Interests

The author(s) declared no potential conflicts of interest with respect to the research, authorship, and/or publication of this article.

References

1. Chang, P. C., A. Flatau, and S. C. Liu. Review Paper: Health Monitoring of Civil Infrastructure. *Structural Health Monitoring: An International Journal*, Vol. 2, No. 3, 2003, pp. 257–267. https://doi.org/10.1177/ 1475921703036169.
2. Reich, S., C. Thomsen, and J. Maultzsch. *Carbon Nanotubes: Basic Concepts and Physical Properties*. Wiley-VCH, Weinheim, 2007.
3. Popov, V. Carbon Nanotubes: Properties and Application. *Materials Science and Engineering: R: Reports*, Vol. 43, No. 3, 2004, pp. 61–102. https://doi.org/10.1016/j.mser.2003.10.001.
4. Dresselhaus, M. S., G. Dresselhaus, and P. C. Eklund. *Science of Fullerenes and Carbon Nanotubes: Their Properties and Applications*. Academic Press, Elsevier Science Imprint, San Diego, 1996.
5. Raki, L., J. Beaudoin, R. Alizadeh, J. Makar, and T. Sato. Cement and Concrete Nanoscience and Nanotechnology. *Materials*, Vol. 3, No. 2, 2010, pp. 918–942. https://doi.org/10.3390/ma3020918.
6. Cwirzen, A., K. Habermehl-Cwirzen, and V. Penttala. Surface Decoration of Carbon Nanotubes and Mechanical Properties of Cement/Carbon Nanotube Composites. *Advances in Cement Research*, Vol. 20, No. 2, 2008, pp. 65–73. https://doi.org/10.1680/adcr.2008.20.2.65.
7. Konsta-Gdoutos, M. S., Z. S. Metaxa, and S. P. Shah. Highly Dispersed Carbon Nanotube Reinforced Cement Based Materials. *Cement and Concrete Research*, Vol. 40, No. 7, 2010, pp. 1052–1059. https://doi.org/10.1016/j .cemconres.2010.02.015.

8. Konsta-Gdoutos, M. S., and C. A. Aza. Self Sensing Carbon Nanotube (CNT) and Nanofiber (CNF) Cementitious Composites for Real Time Damage Assessment in Smart Structures. *Cement and Concrete Composites*, Vol. 53, 2014, pp. 162–169. https://doi.org/10.1016/j.cemconcomp .2014.07.003.
9. Yu, X., and E. Kwon. A Carbon Nanotube/Cement Composite with Piezoresistive Properties. *Smart Materials and Structures*, Vol. 18, No. 5, 2009, p. 55010. https://doi.org/ 10.1088/0964-1726/18/5/055010.
10. Chen, P., H. B. Zhang, G. D. Lin, Q. Hong, and K. R. Tsai. Growth of Carbon Nanotubes by Catalytic Decomposition of CH4 or CO on a Ni-MgO Catalyst. *Carbon*, Vol. 35, No. 10–11, 1997, pp. 1495–1501. https://doi.org/ 10.1016/S0008-6223(97)00100-0.
11. Pan, Z. W., S. S. Xie, B. H. Chang, L. F. Sun, W. Y. Zhou, and G. Wang. Direct Growth of Aligned Open Carbon Nanotubes by Chemical Vapor Deposition. *Chemical Physics Letters*, Vol. 299, No. 1, 1999, pp. 97–102. https:// doi.org/10.1016/S0009-2614(98)01240-8.
12. Bae, E. J., W. B. Choi, K. S. Jeong, J. U. Chu, G. S. Park, S. Song, and I. K. Yoo. Selective Growth of Carbon Nanotubes on Pre-Patterned Porous Anodic Aluminum Oxide. *Advanced Materials*, Vol. 14, No. 1, 2002, pp. 277–279. https://doi.org/10.1002/1521-4095(20020219)14:4<277:: AID-ADMA277>3.0.CO;2-A.
13. Nasibulin, A. G., S. D. Shandakov, L. I. Karppinen, A. Nasibulina, P. R. Cwirzen, K. Mudimela, D. A. Habermehl-Cwirzen, Y. V. Grishin, J. E. M. Gavrilov, U. Malm, Y. Tapper, V. Tian, M. J. Penttala, and E. I. Kauppinen. A Novel Cement-Based Hybrid Material. *New Journal of Physics*, Vol. 11, 2009. https://doi.org/10.1088/1367-2630/ 11/2/023013.
14. Buasiri, T., K. Habermehl-Cwirzen, L. Krzeminski, and A. Cwirzen. Piezoresistive Load Sensing and Percolation Phenomena in Portland Cement Composite Modified with In-Situ Synthesized Carbon Nanofibers. *Nanomaterials*, Vol. 9, No. 4, 2019, p. 594. https://doi.org/10.3390/nano9040594.
15. Chiarello, M., and R. Zinno. Electrical Conductivity of Self-Monitoring CFRC. *Cement and Concrete Composites*, Vol. 27, No. 4, 2005, pp. 463–469. https://doi.org/10.1016/ j.cemconcomp.2004.09.001.
16. Banthia, N., S. Djeridane, and M. Pigeon. Electrical Resistivity of Carbon and Steel Micro-Fiber Reinforced Cements. *Cement and Concrete Research*, Vol. 22, No. 5, 1992, pp. 804–814. https://doi.org/10.1016/0008-8846(92)90104-4.
17. Coppola, L., A. Buoso, and F. Corazza. The Influence of AC and DC Electrical Resistance and Piezoresistivity Measurements of CNTs/Cement Composites. 2013. https:// www.semanticscholar.org/paper/The-influence-of-AC-and-DC-electrical-resistance-of-Coppola-Buoso/73d6a9f4130b 8ba92eafa3188dc477aec926a731#references
18. Han, B., S. Ding, and X. Yu. Intrinsic Self-Sensing Concrete and Structures: A Review. *Measurement*, Vol. 59, 2015, pp. 110–128. https://doi.org/10.1016/j.measurement .2014.09.048.
19. Grunlan, J. C. *Carbon Black-Filled Polymer Composites: Property Optimization with Segregated Microstructures*. University of Minnesota, 2001.

Paper IV

Novel humidity sensors based on nanomodified Portland cement

Buasiri, T., Habermehl-Cwirzen, K., Krzeminski, L., & Cwirzen, A.

scientific reports

OPEN

Novel humidity sensors based on nanomodified Portland cement

Thanyarat Buasiri[1]✉, Karin Habermehl-Cwirzen[1], Lukasz Krzeminski[2] & Andrzej Cwirzen[1]

Commonly used humidity sensors are based on metal oxides, polymers or carbon. Their sensing accuracy often deteriorates with time, especially when exposed to higher temperatures or very high humidity. An alternative solution based on the utilization of Portland cement-based mortars containing in-situ grown carbon nanofibers (CNFs) was evaluated in this study. The relationship between the electrical resistivity, CNF content and humidity were determined. The highest sensitivity was observed for samples containing 10 wt.% of the nanomodified cement which corresponded to 0.27 wt.% of CNFs. The highest calculated sensitivity was approximately 0.01024 per 1% change in relative humidity (RH). The measured electrical resistivity is a linear function of the RH in the humidity range between 11 and 97%. The percolation threshold value was estimated to be at around 7 wt.% of the nanomodified cement, corresponding to ~ 0.19 wt.% of CNFs.

Humidity sensing plays an important part in, e.g. production processes or building maintenance. Cement hydration is controlled by moisture content and thus humidity[1]. Uncontrolled or improper moisture diffusion, especially in an early stage of hydration, can result in a number of negative effects. These include increased shrinkage, lower long-term strength and durability problems[2, 3]. An insufficient water content, e.g. related to an excessive evaporation, can hinder the hydration process[4]. Therefore, monitoring the humidity is crucial for concrete technology. The humidity defined as the amount of water vapour present in the gas phase and can be expressed as absolute or relative value. The relative humidity (RH) is the ratio between the measured amount of water vapour and the water vapour required to reach the saturation state at a certain temperature. Measuring the mass of water vapour contained in a unit volume determines to the absolute humidity (AH).

Humidity measurements rely on converting the detected amount of water molecules into a signal that can be measured, analysed, interpreted and quantified. The interaction between water molecules and sensors is controlled by various physical phenomena. The physical phenomenon being measured defines which type of sensor is used. The most conventional types include capacitive, resistive, impedance, quartz crystal microbalance (QCM), optic-fiber, surface acoustic wave (SAW) or resonance sensing[5–7]. The capacitive sensors are the most commonly used with an estimated 75% of the total market share[8]. They are built of two metal plates separated by a thin layer of an non-conductive polymer film[9]. The non-conductive polymer film attracts moisture from the air, which changes the dielectric constant of the hygroscopic layer. Various types of materials have been used for the moisture sensitive layer. The most common include for example polyimide film (DuPont 5878), polymethyl methacrylate (PMMA), porous ceramics, porous silicon, porous silicon carbide, hygroscopic polymers or porous alumina (Al_2O_3)[8, 10, 11]. Capacitive sensors tend to have a variable sensitivity depending on the measured humidity levels. For example sensors using plasma-etched polyimide as the sensing layer showed low sensitivity at a RH up to 70% and very high sensitivity at a RH between 70 and 90% [11]. Similar problems were observed when using porous silicon. In that case, hysteresis was observed at a RH above 60%[9]. The required power demand is rather low but the production technology of this type of sensors is complicated[12]. Resistive sensors overcame some of the problems typical for the capacitive sensors. They also are easier and cheaper to fabricate, have high sensitivity and low power consumption. Metal oxide, polymers, and carbon-based materials are the most frequently used materials for their production. Unfortunately, some of these materials degrade when exposed to high humidity, including for example, metal oxide or polymer sensors[13]. Slow response/recovery time and high operating temperatures remain the main design challenges for these sensors. Sensors based on matrixes containing Portland cement measure also changes of resistivity[14]. In this case, the measured changes were related to alterations of the pore structure leading to either shrinkage or expansion of the matrix, water absorption or desorption hysteresis at the interface. Humidity sensing of such matrixes depends also on the amount of the incorporated conductive material like carbon fibers (CFs). Chen et al.[15] revealed that cementitious matrixes containing less CFs better sense changes of the internal humidity. Different curing conditions are known to affect the sensing

[1]Building Materials, Department of Civil, Environmental and Natural Resources Engineering, Luleå University of Technology, 97187 Luleå, Sweden. [2]The Institute of Engineering Materials and Biomaterials, Silesian University of Technology, 44-100 Gliwice, Poland. ✉email: thanyarat.buasiri@ltu.se
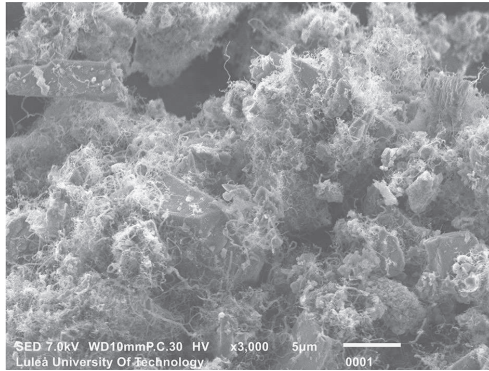
Figure 1. Scanning Electron Microscope image of the nanomodified cement. This figure was taken using InTouchScope software version JSM-IT100 (https://www.jeol.co.jp/en/products/detail/JSM-IT100.html).

capability as well. Sun et al.[16] reported that a cementitious matrix reinforced with CFs cured in air had a more than 2-times lower electrical resistivity compared to the same material being oven cured. Results obtained by Han et al.[17] showed the same trend. Optic fiber humidity sensors can be classified according to their working principles including optical absorption of materials, optical fiber Bragg gratings (FBG), interferometric method, and evanescent wave. The FBG-based sensors have been used to monitor strain and temperature[18–20] as well as humidity in highways[19]. FBG uses a permanent periodic modulation of the reflective index which is formed by an exposure of the core of the optical fiber to an intense optical interference pattern of the light[21]. The humidity sensing is based on an interaction of water molecules with the sensitive core layer. This results in a change of the effective refractive index of the fiber core and in a shift of the Bragg wavelength[22]. Several polymeric materials such as polymide[23, 24], di-ureasil[21] and PMMA[25, 26] have been coated onto an etched FBG to improve the humidity sensitivity. Etching of cladding and coating with graphene oxide[27] or CNTs[22] layer showed sensitivity of ~31 pm/%RH. Furthermore, the modified sensor could detect the relative humidity over a wide range between 20 and 90% at a constant temperature of 25 ˚C[22]. PMMA-based microstructure polymer optical fiber Bragg were studied by Woyessa et al.[28]. The results showed a response having a very low hysteresis and an improved humidity sensitivity (~35 pm/%RH at 90% RH).

Yet, carbon-based materials are widely used to induce the sensing capability into the monitored material. For example, Chung et al.[29–32], Sun et al.[33] and Ou et al.[34] induced piezoresistive properties of cementitious composites by incorporating CFs. Camacho-Ballesta et al.[35] reported that composites containing only 0.05 wt.% of CNTs showed electrical properties sufficient to be used for monitoring. Yu and Kwon[36] revealed CNT/cement composites have high sensitivity of the composite stress response when the CNT doping level is high. Composites based on Portland cement with directly grown CNFs showed even better results in stress/strain monitoring reaching approximately 90% compared with the conventional cementitious material[37]. CNTs and CNFs are commonly added as aqueous dispersions. Unfortunately, their strong hydrophobicity results in a formation of agglomerates. The effect is even stronger in high pH solutions present during the Portland cement hydration. The formation of agglomerates prevents the uniform distribution of the fibers throughout the binder matrix, which is the key condition to create an effective electrically conductive network. Surface functionalization of CNTs and CNFs enhanced the mechanical properties of cement matrixes through a better bond but it also increased the agglomeration[38]. The usage of ultra-sonication in the presence of surfactants produced stable suspensions of well dispersed MWCNTs and functionalized CNTs/CNFs[38, 39]. However, the results showed also that an increasing amount of CNTs/CNFs tends to worsen the fresh mix workability.

The development of an alternative technology enabling to synthesize CNFs directly on cement have limited some of these problems. This method uses a chemical vapour deposition process to grow CNFs directly on cement particles by utilizing naturally embedded Fe and Al as catalysts[37, 40, 41]. Replacing part of Portland cement with this nanomodified cement ensured a uniform distribution of CNFs. It mitigated also the loss of workability and thus significantly increased the maximum amount of CNFs, which could be incorporated into the binder matrix. This method seems to be potentially beneficial to create electrically conductive matrixes sensitive in many aspects including humidity variations. The research described in the present paper focused on investigating potential applicability of nanomodified cement to manufacture sensors for humidity measurements.

Materials and methods

Test sensors were produced as mortar beams composed of a mixture of an ordinary Portland cement (OPC) type CEM I 42.5 provided by Cementa-Sweden and the so-called SmartCem. The SmartCem is a nanomodified Portland cement having CNFs synthesized directly on the surface of pristine cement through Chemical Vapour Deposition (CVD). The total amount of carbon nanofibers (CNFs) grown on the SmartCem was approximately 2.71 wt.%. The used synthesis processes is described in detail elsewhere[37]. The morphology of grown CNFs is shown in Fig. 1.

2

Mix	w/b	s/b	sp (wt.% of binder)	Cement (wt.% of binder)	Nanomodified cement (SmartCem) (wt.% of binder)	Amount of CNFs (wt.% of binder)
Ref	0.35	1.0	0.8	100	0	0.000
S2	0.35	1.0	0.8	98	2	0.054
S4	0.35	1.0	0.8	96	4	0.108
S6	0.35	1.0	0.8	94	6	0.163
S8	0.35	1.0	0.8	92	8	0.217
S10	0.35	1.0	0.8	90	10	0.271

Table 1. Mix proportions.
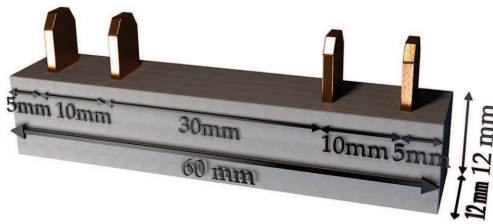
Figure 2. Mortar specimen with four electrodes. This figure was created using Sketchup version 2017 (https://www.sketchup.com), Microsoft PowerPoint version Microsoft 365 (https://www.microsoft.com/en-us/microsoft-365/powerpoint).

Sieved and clean sand with the maximum particle size of 150 μm was used as fine aggregate. The superplasticizer (sp) type Glenium produced by Grace Chemical with a solid content of 30% was used to control the workability of the fresh mix. The water-to-binder ratio and the sand-to-binder ratio (s/b) were constant at 0.35 and 1 respectively. The mix proportions used for the test mortars are shown in Table 1. Three samples were produced for each mix and measured electrical resistivity showed less than 5% variation. Measurements also indicated that 900 s waiting time was required to obtain a stable reading. All measurements were done after that waiting period.

Mortars were mixed using a Bredent vacuum mixer and poured into Teflon moulds. The size of test specimens in this research was selected having dimensions of 12 mm × 12 mm × 60 mm since no standard size setup test for electrical resistance measurement at present. Different specimen geometries can be used; however, the measured resistance should be converted to resistivity by using an appropriate geometry correction factor. Four copper electrodes having dimensions of 5 mm × 15 mm × 0.25 mm were immersed 7.5 mm and 30 mm apart into these samples and connected by electrical wires with the measuring system, Fig. 2.

The effects of the curing conditions on the electrical resistivity were determined a using reference sample (Ref) and the mix containing 4 wt.% of the SmartCem (S4). After casting, the samples were cured at 11%, 43%, 75%, and 97% RH for 28 days, followed by storage in laboratory conditions at $20 \pm 2\,^{\circ}$C. The samples used for the actual humidity measurements were cured for 28 days at $20\,^{\circ}$C and 97 ± 5% RH. The produced humidity sensors contained 0% (Ref), 2% (S2), 4% (S4), 6% (S6), 8% (S8) and 10% (S10) of the SmartCem, calculated as the total binder weight. Before measurements were started, all sensors were kept in humidity chambers at 11%, 43%, 75% or 97% RH for 24 h. The humidity chambers consisted of sealed glass containers containing various types of saturated salt solutions. These included lithium chloride (LiCl), potassium carbonate (K_2CO_3), sodium chloride (NaCl) and potassium sulphate (K_2SO_4) which can maintain relative humidities of 11%, 43%, 75%, and 97%, respectively. A commercial humidity sensor type SHT85 produced by Sensirion was installed in each container as reference. Values measured after 24 h showed less than 5% variation within 24 h.

The electrical resistance was measured using a four-probe method with a digital multimeter type Keysight 34465A. An electrical current was applied to the two outer copper electrodes while the electrical resistivity was measured on the two inner electrodes, Fig. 3. Humidity sensing was determined as a fractional change of the electrical resistivity $FCR_{Humidity}$ and calculated following the Eq. (1):

$$FCR_{Humidity} = \Delta\rho / \rho_0 \tag{1}$$

where: $\Delta\rho$ is the change of electrical resistivity, ρ_0 is the initial electrical resistivity. The electrical resistivity ρ was calculated using Eq. (2):

$$\rho = R \cdot A / L \tag{2}$$

where: R is the measured electrical resistance, L is the internal electrode distance and A is the electrode area. The sensitivity of the sensor to humidity $S_{Humidity}$ was calculated using Eq. (3)[42]:
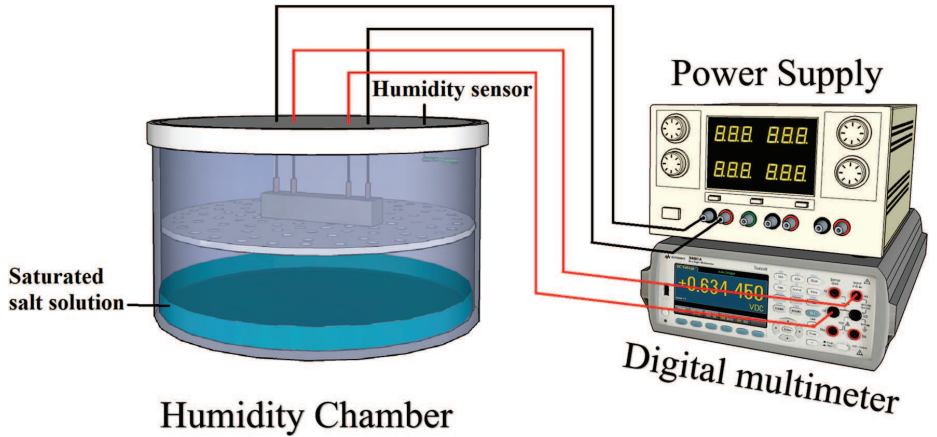
Figure 3. The experimental setup for electrical resistance measurements of mortar samples. This figure was created using Sketchup version 2017 (https://www.sketchup.com), Microsoft PowerPoint version Microsoft 365 (https://www.microsoft.com/en-us/microsoft-365/powerpoint).

Mix	Sample age (days)	Electrical resistivity (Ω cm)			
		Curing condition			
		11%RH	43%RH	75%RH	97%RH
Ref	1	61.24	60.57	16.61	7.06
	3	73.58	68.31	62.92	13.54
	7	254.98	245.23	188.72	22.57
	28	325.05	249.95	220.91	28.50
S4	1	49.05	46.50	13.95	7.06
	3	67.56	54.93	50.62	12.38
	7	139.21	130.41	76.38	14.16
	28	278.41	202.279	116.33	22.19

Table 2. Effects of sample age and curing conditions on electrical resistivity.

$$S_{Humidity} = \frac{\Delta R / R_0}{\Delta(\%RH)} \tag{3}$$

where: ΔR and $\Delta(\%RH)$ refer to the resistance change and the change of relative humidity in percentage, respectively and R_0 is the initial resistance.

Results and discussion

There are many factors influencing electrical resistivity of cementitious matrix. These factors can be divided into two main groups. First group contains factors affecting the intrinsic electrical resistivity, especially including w/c ratio, which determines porosity, aggregate size, aggregate type, curing condition and storage condition. While the second group covers factors affecting the electrical measurement itself. For example, probe spacing, electrode contact and specimen geometry. In this research, all listed factors were kept constant, thus humidity variations can be indicated as the main affecting factor.

The effects of the humidity during curing and the sample age on the electrical resistivity of the material were determined for samples containing 100 wt.% of OPC (Ref) and a combination of 96% of OPC with 4 wt.% of the SmartCem (S4).

In general, the electrical resistivity increased with the curing age due to the consumption of water by the hydrating cement. The electrical resistivity of the S4-samples tended to be lower at all ages and exposures in comparison with the corresponding OPC samples, Table 2. The effect can be related to the creation of an additional conductive network by CNFs being present in the S4-samples. The lowest ultimate resistivity was measured for the sample mix containing 4wt.% of SmartCem (S4) and being cured at 97% RH.

In the next stage, all sensors produced from the reference mix and the S4 mix and cured at different conditions were used to determine their humidity sensing capability. Before the measurement, all produced sensors were
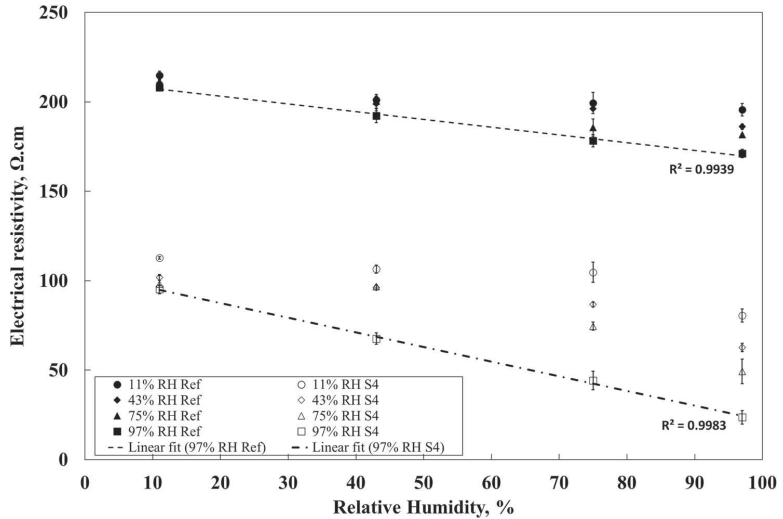
Figure 4. Effects of curing conditions used during production of sensors on the humidity sensing capability. Error bars represent standard errors.

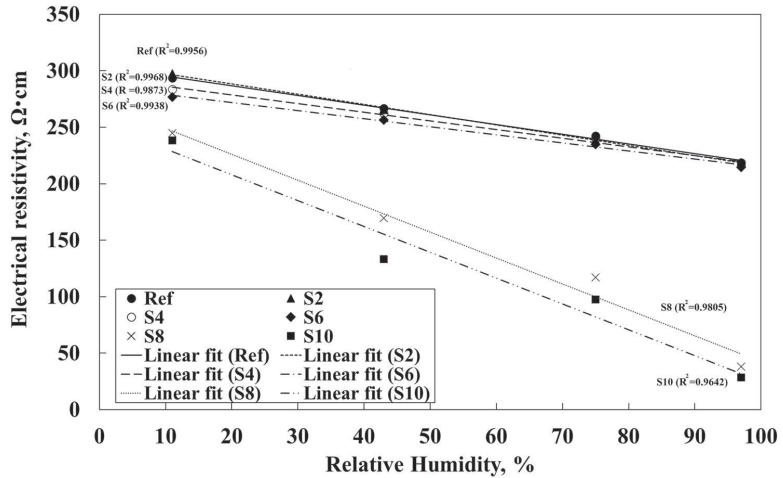| Mix	Sensitivity, $S_{Humidity}$ (/%RH)			
	Curing condition			
	11%RH	43%RH	75%RH	97%RH
Ref	0.00104	0.00134	0.00154	0.00206
S4	0.00126	0.00219	0.00577	0.00874

Table 3. Calculated sensitivity of reference and S4 samples exposed to 11%, 43%, 75% and 97% RH.

stored for 24 h at 60% RH and 20 ± 2 ˚C. The exposure conditions included 11%, 34%, 75% and 97% RH. The resistivity measurements started 24 h later. The obtained results are shown in Fig. 4 and the calculated sensitivity of the composites are shown in Table 3.

Figure 4 shows that in the case of reference samples cured at 11%RH the measured electrical resistivity was around 210 Ω cm when exposed to 11% RH and 200 Ω cm at 97% RH. A slightly higher change in resistivity was measured for samples cured at 97% RH with values of 200 and 170 Ω cm when exposed to 11% and 97% RH, respectively. Additionally, there was nearly no change of the samples containing SmartCem cured at 11% RH in the electrical resistivity until the relative humidity in the test chamber was set to 97%. In that case, the measured electrical resistivity was constant at around 110 Ω cm when exposed to 11%, 43% and 75% RH, while dropping to around 80 Ω cm at 97% RH. Samples cured at 43% and 75% RH showed a better sensitivity but only when exposed to a higher humidity, 75% and 97% RH. Only the sample cured at 97% RH could detect a humidity change in the entire measured range between 11 and 97%RH. Furthermore, for the samples cured at 97% RH the observed relation between electrical resistance and relative humidity was linear. At 11% RH the measured electrical resistivity was around 90 Ω cm while at 97% RH it decreased to 22 Ω cm.

Samples containing only the unmodified Portland cement showed a generally low sensitivity to humidity; independently of the used curing conditions. While samples containing 4 wt.% of the SmartCem showed a significantly higher sensitivity to humidity. In both cases, the lowest sensitivity was measured for samples cured at 11% RH and the highest for cured at 97% RH. The highest calculated sensitivity of 0.00874/%RH was reached for the sensor cured at 97% RH and the sensitivity of the S4 sensor significantly increased when exposing to a humidity greater than 75% RH, Table 3.

Access of moisture during curing of Portland cement affects the hydration process that controls also the developed pore structure. The pore structure and especially connectivity of capillary pores define transport of moisture within the solidified binder matrix. This in turn will ultimately affect the efficiency of a moisture sensor based on Portland cement. It has been shown that hydration of Portland cement stops when the relative humidity drops to around 80%[43]. The hydration degree of tricalcium silicate, measured after 90 days dropped from 36% to only 2% when the RH decreased from 98 to 85%[44]. Furthermore, the hydration is believed to stop when Portlandite, C-S–H and tricalcium silicate are in equilibrium which can occur at a lower RH. Limited hydration

Figure 5. Effects of relative humidity and amount of SmartCem on electrical resistivity of produced sensors. Error bars represent standard errors.

| Mix	CNFs concentration (wt.% of binder)	Sensitivity of sensor, $S_{Humidity}$ (/%RH)	R^2
Ref	0.000	0.00277	0.9956
S2	0.054	0.00278	0.9968
S4	0.108	0.00297	0.9873
S6	0.163	0.00261	0.9938
S8	0.217	0.00982	0.9805
S10	0.271	0.01024	0.9642

Table 4. Calculated sensitivity and R^2 for the produced humidity sensors cured at 97% RH.

leads to a decreased amount of gel pores and coarsening of the pore structure. Tests showed a nearly three times coarser pore structure for samples cured at 80% RH in comparison with water curing[45]. These results can be directly related to the observed research trends that show that the electrical resistivity of the matrix decreased when exposed to high humidity and vice versa. Furthermore, it can be assumed that the presence of CNFs enhances the connectivity between moisture filled pore network and thus increases the electrical sensitivity of the entire system. The tunnelling effect developing between CNFs was strengthened through the presence of water molecules at the fiber–fiber and fiber-matrix interfaces[46, 47].

The described results were used in a second set of sensor production and measurements. These sensors contained different amounts of CNFs to determine what kind of effect the CNF quantity has on the humidity-sensing capability. These sensors contained 0% (Ref), 2 wt.% (S2), 4 wt.% (S4), 6 wt.% (S6), 8 wt.% (S8) and 10 wt.% (S10) of the SmartCem. Based on the best results obtained in the first part of the study, a 97% RH was used for curing. To ensure the stability and exclude any possible effects of moisture or temperature variations on the measured electrical resistivity, the produced sensors were stored in laboratory condition for 72 h before testing.

The test results showed a nearly linear relationship between the measured electrical resistivity and the relative humidity, Fig. 5. The R^2 was over 0.95 in all cases, Table 4. Samples containing 0–6 wt.% of the SmartCem showed a significantly lower sensitivity of around 0.002 /%RH while samples containing 8 wt.% and 10 wt.% of the SmartCem showed a significantly higher sensitivity of 0.00982/%RH and 0.01024/%RH, respectively. The maximum humidity sensitivity of 0.01024/%RH was measured for the sensor containing 10 wt.% of the Smart-Cem. The measured electrical resistivity varied between 280 and 300 Ω cm at 11% RH and 230 Ω cm at 97% RH, Fig. 5. At 11% RH the measured value was around 240 Ω cm for both samples and around 300 Ω cm at 97%RH. Analysis showed that the percolation threshold related to the amount of CNFs humidity sensing was around 7 wt.% which corresponded to around 0.19 wt.% of CNFs, Fig. 6.

Comparison between sensing capability of cementitious matrixes incorporating different types of carbon-based materials is shown in Table 5. Various types of conductive materials showed different humidity sensing capabilities. The observed differences in humidity sensitivity can be related to several factors mentioned earlier. These include the types of the used conductive fibers and their dispersion in the matrix. Matrixes studied in the present research showed significantly higher sensitivity.
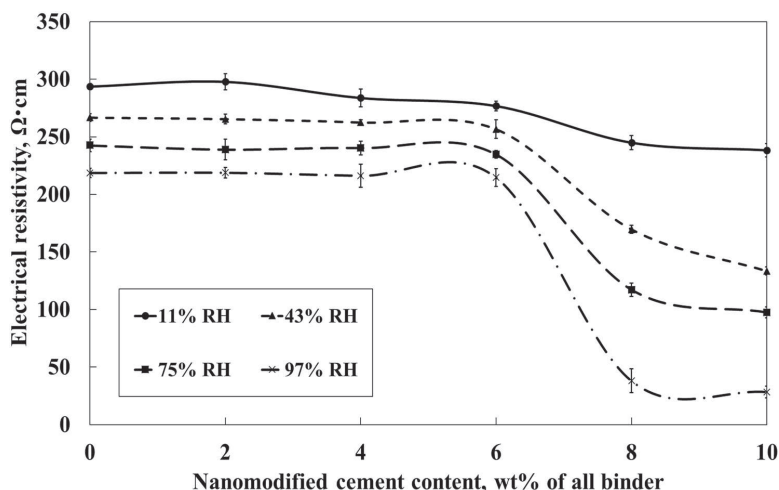
Figure 6. Effects of humidity and amount of nanomodified Smart cement content on the measured electrical resistivity. Error bars represent standard errors.

Reference	Amount of carbon-based materials (wt.% of cement)	Humidity range	Measurement method	Calculated change of the electrical resistivity (%)	Calculated humidity sensitivity (/%RH)
Xiaoming[48]	25% graphite	20–60%	Four-probe	~ 9.09%	~ 0.00227
Carisio et al.[49]	0.20% MWCNT	0–90%	Four-probe	~ 49.33%	~ 0.00548
Carisio et al.[49]	0.35% MWCNT	0–90%	Four-probe	~ 49.64%	~ 0.00551
Present result S10	0.271% CNF 10% SmartCem	11–97%	Four-probe	88.06%	0.01024

Table 5. Sensitivity to humidity of cementitious matrixes incorporating various types of carbon-based materials.

Summarising, the humidity sensing mechanism of the developed SmartCem sensors is related to an alteration of the electrical resistivity. Absorption or desorption of water molecules due to variation of RH in this study change the interconnection between matrix–matrix, fiber–fiber and fiber-matrix resulting in a change in the ultimate electrical resistivity of sensors. For example, water molecules in gaseous state adsorb on the external surface of the sensor and later diffuse into the matrix due to capillary condensation, Fig. 7a. The water vapour condenses into water and gradually fills up the abundant pores. This generates additional "bridges" between existing electrically conductive paths. Consequently, different amounts of water vapour will result in different ultimate electrical resistivity of the sensor, which can be measured, Fig. 7b [50]. A comprehensive micromechanical model was proposed by Jang et al.[51] to predict the effective electrical conductivity of cementitious matrix containing carbon-based filler. This model confirmed that moisture affects the sensing of smart cementitious-based composite.

Conclusion

The study aimed to determine the sensitivity of novel sensors to variations in the humidity. These humidity sensors are based on mortars containing various amounts of the nanomodified Portland cement (SmartCem). It was found that the electrical resistivity of the sensors tended to increase with longer wet curing time due to the alternation of the microstructure and hydration processes. Samples cured at 97% RH showed the highest sensitivity with the sensitivity value reaching 0.01024/%RH. According to the percolation theory, the percolation threshold amount of the nanomodified cement using for humidity monitoring is estimated at 7 wt.% of the SmartCem (~ 0.19 wt.% of CNFs). The humidity sensitivity of the nanomodified cement was related to the intrinsic electrical property, water absorption property, the connectivity as well as the amount of the nanomodified cement to change the contact point between fiber–fiber and fiber-matrix due to the presence of water vapour in the air.
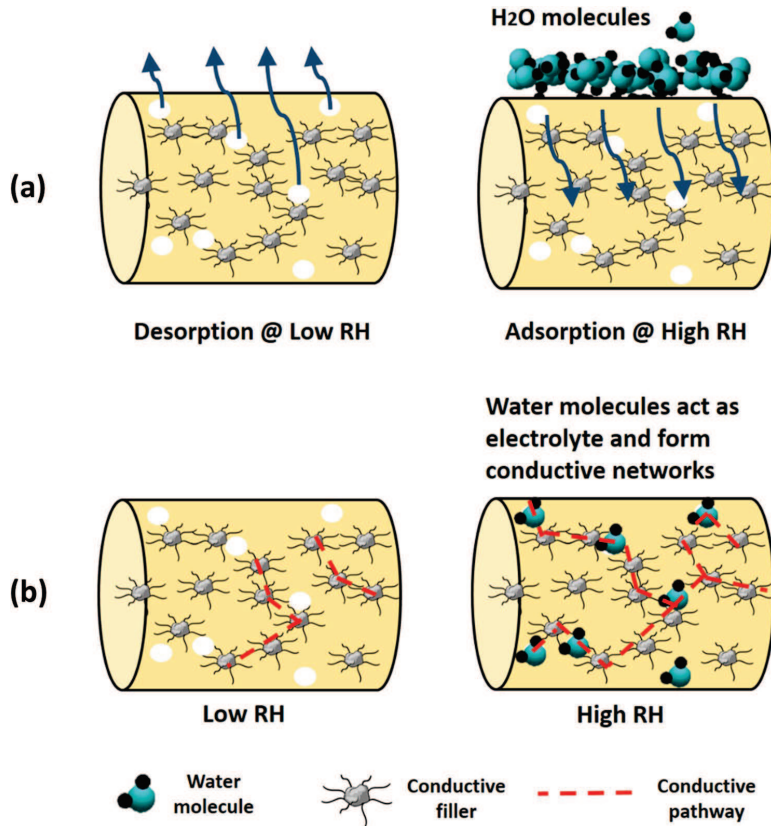
Figure 7. Schematic description of the effect of humidity on (**a**) the microstructure of the matrix (**b**) conductive paths in the matrix. This figure was created using Sketchup version 2017 (https://www.sketchup.com), Microsoft PowerPoint version Microsoft 365 (https://www.microsoft.com/en-us/microsoft-365/powerpoint).

References

1. Delatte, N. J., Williamson, M. S. & Fowler, D. W. Bond strength development with maturity of high-early-strength bonded concrete overlays. *ACI Mater. J.* **97**, 201–207 (2000).
2. Shen, D., Wang, T., Chen, Y., Wang, M. & Jiang, G. Effect of internal curing with super absorbent polymers on the relative humidity of early-age concrete. *Constr. Build. Mater.* **99**, 246–253 (2015).
3. de Medeiros-Junior, R. A., de Lima, M. G. & de Medeiros, M. H. F. Service life of concrete structures considering the effects of temperature and relative humidity on chloride transport. *Environ. Dev. Sustain.* **17**, 1103–1119 (2015).
4. Lothenbach, B., Matschei, T., Möschner, G. & Glasser, F. P. Thermodynamic modelling of the effect of temperature on the hydration and porosity of Portland cement. *Cem. Concr. Res.* **38**, 1–18 (2008).
5. Blank, T. A., Eksperiandova, L. P. & Belikov, K. N. Recent trends of ceramic humidity sensors development: A review. *Sensors Actuators B Chem.* **228**, 416–442 (2016).
6. Lv, C. *et al.* Recent advances in graphene-based humidity sensors. *Nanomaterials* **9** (2019).
7. Yang, S., Jiang, C. & Wei, S. huai. Gas sensing in 2D materials. *Appl. Phys. Rev.* **4** (2017).
8. Zhu, Z. T., Mason, J. T., Dieckmann, R. & Malliaras, G. G. Humidity sensors based on pentacene thin-film transistors. *Appl. Phys. Lett.* **81**, 4643–4645 (2002).
9. Chen, L. & Zhang, J. Capacitive humidity sensors based on the dielectrophoretically manipulated ZnO nanorods. *Sensors Actuators A Phys.* **178**, 88–93 (2012).
10. Story, P. R., Galipeau, D. W. & Mileham, R. D. A study of low-cost sensors for measuring low relative humidity. *Sensors Actuators B. Chem.* **25**, 681–685 (1995).
11. Laville, C., Pellet, C. & Kaoua, G. N. Interdigitated humidity sensors. *1st Annu. Int. IEEE-EMBS Spec. Top. Conf. Microtechnol. Med. Biol. Proc.* 10–15 (2000).
12. Lee, C. Y. & Lee, G. B. Humidity sensors: A review. *Sens. Lett.* **3**, 1–15 (2005).
13. Park, S. Y. *et al.* Room temperature humidity sensors based on rGO/MoS2 hybrid composites synthesized by hydrothermal method. *Sensors Actuators B Chem.* **258**, 775–782 (2018).

14. Schließl, A. *et al.* Assessing the moisture profile of drying concrete using impedance spectroscopy. *Concr. Sci. Eng.* (2000).
15. Chen, B., Wu, K. & Yao, W. Conductivity of carbon fiber reinforced cement-based composites. *Cem. Concr. Compos.* **26**, 291–297 (2004).
16. Sun, M. Q., Liew, R. J. Y., Zhang, M. H. & Li, W. Development of cement-based strain sensor for health monitoring of ultra high strength concrete. *Constr. Build. Mater.* **65**, 630–637 (2014).
17. Han, B. G. & Ou, J. P. The humidity sensing property of cements with added carbon. *Xinxing Tan Cailiao/ New Carbon Mater.* **23**, 382–384 (2008).
18. Alwis, L., Sun, T. & Grattan, K. T. V. Optical fibre-based sensor technology for humidity and moisture measurement: Review of recent progress. *Meas. J. Int. Meas. Confed.* **46**, 4052–4074 (2013).
19. Li, H. N., Li, D. S. & Song, G. B. Recent applications of fiber optic sensors to health monitoring in civil engineering. *Eng. Struct.* **26**, 1647–1657 (2004).
20. Rao, Y. J. Recent progress in applications of in-fibre Bragg grating sensors. *Opt. Lasers Eng.* **31**, 297–324 (1999).
21. Hill, K. O. & Meltz, G. Fiber Bragg grating technology fundamentals and overview. *J. Light. Technol.* **15**, 1263–1275 (1997).
22. Shivananju, B. N. *et al.* Highly sensitive carbon nanotubes coated etched fiber bragg grating sensor for humidity sensing. *IEEE Sens. J.* **14**, 2615–2619 (2014).
23. Lin, Y., Gong, Y., Wu, Y. & Wu, H. Polyimide-coated fiber Bragg grating for relative humidity sensing. *Photon. Sensors* **5**, 60–66 (2015).
24. Berruti, G. *et al.* Radiation hard humidity sensors for high energy physics applications using polyimide-coated fiber Bragg gratings sensors. *Sensors Actuators B Chem.* **177**, 94–102 (2013).
25. Swanson, A. J. *et al.* Development of novel polymer coating for FBG based relative humidity sensing. *Sensors Actuators A Phys.* **249**, 217–224 (2016).
26. David, N. A., Wild, P. M. & Djilali, N. Parametric study of a polymer-coated fibre-optic humidity sensor. *Meas. Sci. Technol.* **23** (2012).
27. Wang, Y. *et al.* Fiber optic relative humidity sensor based on the tilted fiber Bragg grating coated with graphene oxide. *Appl. Phys. Lett.* **109**, 1–6 (2016).
28. Woyessa, G., Nielsen, K., Stefani, A., Markos, C. & Bang, O. Temperature insensitive hysteresis free highly sensitive polymer optical fiber Bragg grating humidity sensor. *Opt. Express* **24**, 1206 (2016).
29. Wen, S. & Chung, D. D. L. Piezoresistivity in continuous carbon fiber cement-matrix composite. *Cem. Concr. Res.* **29**, 445–449 (1999).
30. Wen, S., Wang, S. & Chung, D. D. L. Piezoresistivity in continuous carbon fiber polymer-matrix and cement-matrix composites. *J. Mater. Sci.* **35**, 3669–3675 (2000).
31. Chung, D. D. L. Piezoresistive cement-based materials for strain sensing. *J. Intell. Mater. Syst. Struct.* **13**, 599–609 (2002).
32. Chung, D. D. L. A comparative study of steel- and carbon-fiber cement as piezoresistive strain sensors. *Adv. Cem. Res.* **15**, 119–128 (2003).
33. Sun, M., Liu, Q., Li, Z. & Hu, Y. Study of piezoelectric properties of carbon fiber reinforced concrete and plain cement paste during dynamic loading. *Cem. Concr. Res.* **30**, 1593–1595 (2000).
34. Ou, J. & Han, B. Piezoresistive cement-based strain sensors and self-sensing concrete components. *J. Intell. Mater. Syst. Struct.* **20**, 329–336 (2009).
35. Camacho-Ballesta, C., Zornoza, E. & Garcés, P. Performance of cement-based sensors with CNT for strain sensing. *Adv. Cem. Res.* **28**, 274–284 (2016).
36. Yu, X. & Kwon, E. A carbon nanotube/cement composite with piezoresistive properties. *Smart Mater. Struct.* **18**, 55010 (2009).
37. Buasiri, T., Habermehl-Cwirzen, K., Krzeminski, L. & Cwirzen, A. Piezoresistive load sensing and percolation phenomena in portland cement composite modified with in-situ synthesized carbon nanofibers. *Nanomaterials* **9** (2019).
38. Cwirzen, A., Habermehl-Cwirzen, K. & Penttala, V. Surface decoration of carbon nanotubes and mechanical properties of cement/carbon nanotube composites. *Adv. Cem. Res.* **20**, 65–73 (2008).
39. Konsta-Gdoutos, M. S., Metaxa, Z. S. & Shah, S. P. Highly dispersed carbon nanotube reinforced cement based materials. *Cem. Concr. Res.* **40**, 1052–1059 (2010).
40. Nasibulina, L. I. *et al.* Direct synthesis of carbon nanofibers on cement particles. *Transp. Res. Rec. J. Transp. Res. Board* **2142**, 96–101 (2010).
41. Nasibulin, A. G. *et al.* A novel cement-based hybrid material. *New J. Phys.* https://doi.org/10.1088/1367-2630/11/2/023013 (2009).
42. Tang, Q. Y., Chan, Y. C. & Zhang, K. Fast response resistive humidity sensitivity of polyimide/multiwall carbon nanotube composite films. *Sensors Actuators B Chem.* **152**, 99–106 (2011).
43. Flatt, R. J., Scherer, G. W. & Bullard, J. W. Why alite stops hydrating below 80% relative humidity. *Cem. Concr. Res.* https://doi.org/10.1016/j.cemconres.2011.06.001 (2011).
44. Jensen, O. M., Hansen, P. F., Lachowski, E. E. & Glasser, F. P. Clinker mineral hydration at reduced relative humidities. *Cem. Concr. Res.* https://doi.org/10.1016/S0008-8846(99)00132-5 (1999).
45. Patel, R. G., Killoh, D. C., Parrott, L. J. & Gutteridge, W. A. Influence of curing at different relative humidities upon compound reactions and porosity in Portland cement paste. *Mater. Struct.* https://doi.org/10.1007/BF02473055 (1988).
46. Teomete, E. The effect of temperature and moisture on electrical resistance, strain sensitivity and crack sensitivity of steel fiber reinforced smart cement composite. *Smart Mater. Struct.* **25** (2016).
47. Demircilioğlu, E., Teomete, E., Schlangen, E. & Baeza, F. J. Temperature and moisture effects on electrical resistance and strain sensitivity of smart concrete. *Constr. Build. Mater.* **224**, 420–427 (2019).
48. Xiaoming, F. Effects of environmental temperature and humidity on the electrical properties of carbon fiber graphite cement mortar. *Adv. Mater. Res.* **143–144**, 1022–1026 (2011).
49. Carísio, P. de A. *et al.* Influence of humidity, moisture and temperature on the electric properties of self-sensing cement pastes for post-abandonment well monitoring. In *Offshore Technology Conference Brasil* Vol. 20 (2019).
50. Ding, S., Dong, S., Ashour, A. & Han, B. Development of sensing concrete: Principles, properties and its applications. *J. Appl. Phys.* **126** (2019).
51. Jang, S. H., Hochstein, D. P., Kawashima, S. & Yin, H. Experiments and micromechanical modeling of electrical conductivity of carbon nanotube/cement composites with moisture. *Cem. Concr. Compos.* **77**, 49–59 (2017).

Acknowledgements

Author contributions

T.B. conceived and designed the experiments, L.K., K.H.C. and A.C. were involved in planning and supervised the work, T.B. and A.C. processed the experimental data and performed the analysis, T.B. prepared the original

Competing interests
The authors declare no competing interests.

Additional information
Correspondence and requests for materials should be addressed to T.B.

Reprints and permissions information is available at www.nature.com/reprints.

Publisher's note Springer Nature remains neutral with regard to jurisdictional claims in published maps and institutional affiliations.

Paper V

Monitoring temperature and hydration by mortar sensors made of nanomodified Portland cement

Buasiri, T., Kothari, A., Habermehl-Cwirzen, K., Krzeminski, L., & Cwirzen, A.

Submitted

Monitoring temperature and hydration by mortar sensors made of nanomodified Portland cement

Thanyarat Buasiri [a, *], Ankit Kothari [a], Karin Habermehl-Cwirzen [a], Lukasz Krzeminski [b], and Andrzej Cwirzen [a]

[a] Building Materials, Department of Civil, Environmental and Natural Resources Engineering, Luleå University of Technology, 97187 Luleå, Sweden; thanyarat.buasiri@ltu.se (T.B.); ankit.kothari@ltu.se (A.K.); karin.habermehl-cwirzen@ltu.se (K.H.-C.); andrzej.cwirzen@ltu.se (A.C.)

[b] The Institute of Engineering Materials and Biomaterials, Silesian University of Technology, 44-100 Gliwice, Poland; lukasz.krzeminski@polsl.pl (L.K.)

* Correspondence: thanyarat.buasiri@ltu.se; Tel.: +46-(0)-92-049-1907

Abstract

Mortar beams incorporating carbon nanofibers (CNFs) which were synthesized as in-situ on Portland cement particles were used to produce nanomodified Portland cement sensors (SmartCem sensors). SmartCem sensors exhibited an electrical response comparable to a thermistor with a temperature coefficient of resistivity of -0.0152/°C. The highest temperature-sensing was obtained for the SmartCem sensor containing ~0.271 wt.% of CNFs. The calculated temperature sensitivity was approximately 11.76% higher in comparison with the mortar beam containing only unmodified Portland cement. SmartCem sensors were used to monitor the cement hydration in large-scale self-compacting concrete beams. The measurements were conducted after casting for 7 days. Additionally, commercially available thermocouple and humidity sensors were used as references. The results showed that changes in electrical resistivity measured by the SmartCem sensor were well aligned with the ongoing hydration processes.

Keywords: Nanomodified Portland cement, Carbon nanofibers, CNFs, Temperature sensing, Temperature sensitivity, Temperature sensor, Hydration temperature, Hydration monitoring, Cement-based sensor.

1. Introduction

Cement hydration is an exothermic reaction. This reaction is a complex physical and chemical process that contributes to the development of a rigid load-bearing cementitious matrix. Early microstructural development is essential for predicting the properties of cement-based matrixes. Several methods have been used to monitor and characterize the hydration of cementitious materials and explain their hardening mechanisms [1]. For instance, conduction calorimetry has been utilized to follow the hydration heat. The obtained data can contribute to the explanation of the hydration mechanism, as well as the prediction of setting times, and mechanical properties. Unfortunately, the calorimetric curve does not correspond to practical conditions. In this case, evolution represents a dynamic balance between the heat produced by the hydrating cement paste and the variable environmental conditions. Other widely used methods, such as thermogravimetric and differential thermal analysis (TG-DTA), scanning electronic microscope (SEM), and X-ray diffraction (XRD) have been utilized to identify the hydration products. TG-DTA, SEM, and XRD are unable to provide continuous information about hydration and results can be affected by sample preparation processes, i.e., cutting, polishing, or drying [2]. Alternative non-destructive techniques, including the measurement of electrical properties, have been commonly used in the monitoring of early-age hydration [3]. The method based on measurements of electrical resistivity is especially suitable for monitoring early-age hydration. It also provides continuous data acquisition [4].

Monitoring of concrete temperature is crucial because it provides information that can be directly correlated with the performance of hardened matrixes. Throughout the service life of concrete structures, cement-based materials have frequently been exposed to extreme environmental conditions, e.g., subzero- or extremely high- temperatures, variable humidity, and exposure to carbon dioxide. These could result in changes to the physical, mechanical, chemical, or electrical. During casting and curing processes, the maximum concrete temperature and temperature gradient cannot exceed certain values in order to prevent crack formation and durability issues caused by, for example, delayed ettringite formation. It is commonly accepted that the maximum permissible temperature is set at 160°F (70°C), while the maximum temperature gradient is 35°F (19°C) [5]. The temperature profile can be also used to estimate the maturity index to estimate the early-age compressive strength of concrete [6]. The temperature measurements in fresh and hardened concrete are conventionally done by using either internally embedded or externally attached temperature sensors, i.e., resistance thermometers, thermocouples, or thermistors. These sensors are materials wise incompatible with concrete as being made from metals. They are prone to mechanical damage and often have a short life span. Self-sensing cementitious matrixes and cement-based sensors are expected to eliminate or to limit applications of the currently used sensors. Carbon-based materials, particularly carbon fiber (CF), carbon nanofiber (CNF), and carbon nanotube (CNT), have been used to produce sensing cementitious matrixes with the ability to respond to changes in strain, stress, humidity, or temperature. Monitoring systems based on such sensors have been utilized in various structures [7] to measure temperature development and to follow early-age hydration processes [8].

Chen et al. [9] studied the temperature-resistivity of carbon fiber reinforced concrete (CFRC). The test concrete specimens containing 0.8 vol.% of CFs showed both positive temperature coefficient (PTC) and negative temperature coefficient (NTC) effects during temperature increase. Teomete [10] and Demircilioğlu et al.[11] reported a rapid increase in electrical resistivity at 243 °C for concrete containing 1 vol.% of brass-coated steel fibers and at 150 °C for concrete with 0.8 vol.% of brass fibers. This concrete could be utilized as a pre-alarm fire warning system. McCarter et al. [12] studied temperature sensitivity over the temperature range between 10 and 60 °C. A comparison was made between plain mortar and mortar containing 0.5 vol.% of CFs (3 mm and 6 mm in length). The results

showed the mortar containing CFs was less sensitive to temperature sensitivity and required lower activation energies than conventional mortar. Wen et al. [13] observed that cement paste containing CNFs and silica fume performed well as a negative thermistor. The electrical resistivity decreased as the temperature increased from 1°C to 45°C. Tabatabai and Aljuboori [14] embedded concrete-based sensors without any additives or conductive filers into the concrete deck of the bridge. The surface temperature was varied between -11.5°C and 14°C and the electrical resistance was measured. The electrical resistance changed considerably as the temperature changed from -11.5 to 0 °C but was nearly stable between 0 and 14 °C. The output from the laboratory experiments indicated that the prototype sensors could detect the surface of the ice and frozen concrete. Another example from Mo et al. [15], the cube mortar sensor containing 0.7% CNFs (CNFA) was embedded in the self-compacting concrete cylinder to study the hydration monitoring. The electrical resistance changes were likely followed in the same pattern as cement hydration. These results imply that embedded CNFAs could be used to monitor the early age of concrete.

An alternative novel solution to produce sensitive sensors is the usage of cement covered with synthesized in-situ CNFs (nanomodified Portland cement). Studies [16–18] showed that mortar made with this innovative cement was sensitive to stress, strain, and humidity. The research described in this paper aimed to determine the impact of temperature on the electrical resistivity of such sensors. In addition, the feasibility of using the nanomodified Portland cement sensors (SmartCem sensors) to monitor the hydration processes was examined and compared with regular sensors.

2. Materials and Methods

2.1 Materials and mix proportion

Ordinary Portland cement (CEM I 42.5N) and nanomodified Portland cement (SmartCem) was used as a binder. The SmartCem was produced by synthesizing carbon nanofibers (CNFs) directly on the surface of the cement particles through Chemical Vapor Deposition (CVD) process. The synthesis details are described elsewhere [16,17]. The used SmartCem contained approximately 2.71 wt.% of CNFs. The scanning electron microscope image of the SmartCem is shown in **Figure 1**. Sand having a maximum particle size of 150 µm was used to produce mortars. The polycarboxylate-based superplasticizer (sp) type Glenium produced by Grace Chemical was used. Its amount was constant for all mixes and equaled 0.8 wt.% of the total binder content. All mixes had a water-to-binder (w/b) of 0.35 and a sand-to-binder ratio of 1.0. Mix proportions used for producing the SmartCem sensors are shown in **Table 1**.

The studied sensors were produced as mortar beams with the dimensions of 12 mm x 12 mm x 60 mm, **Figure 2(a)**. The mortar sensors were mixed using a Bredent-type vacuum mixer and cast into house-made Teflon molds. Several mortar beams were produced and contained 0 wt.% (Ref), 2 wt.% (S2), 4 wt.% (S4), 6 wt.% (S6), 8 wt.% (S8), and 10 wt.% (S10) of the SmartCem. Three mortar beams were prepared for each set of tests. Four copper electrodes were made of 0.25 mm thick plates having a width of 5 mm and a height of 15 mm. The copper plates were immersed vertically 7.5 mm deep into the mortar specimen. The distance between the inner electrodes was 30 mm and between the outer electrodes 50 mm. Electrodes were connected by the electrical wires and were covered in the upper part by heat shrink tubes, **Figure 2(b)**. Heat shrink tubing provides electrical insulation, electrical insulation, mechanical protection, environmental sealing, and strain relief which can prevent undesirable resistance cumulative at the electrodes.

Table 1 *Mix proportions for SmartCem sensors*

Mix	w/b	s/b	sp (wt% of binder)	CEM I 42.5N (wt.% of binder)	SmartCem (wt.% of binder)
Ref	0.35	1.0	0.8	100	0
S2	0.35	1.0	0.8	98	2
S4	0.35	1.0	0.8	96	4
S6	0.35	1.0	0.8	94	6
S8	0.35	1.0	0.8	92	8
S10	0.35	1.0	0.8	90	10
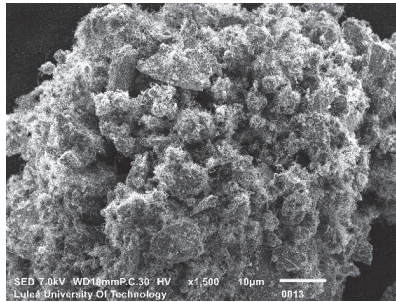
Figure 1. *The morphology of grown CNFs on the nanomodified Portland cement.*

Two types of concrete were prepared to monitor hydration. A normal strength concrete (NC), which contained Portland cement CEM I 42.5N, micro-sand B15 (150 μm), sand size 0-4 mm, coarse aggregate with a maximum size of 8 mm, and a superplasticizer type Glenium. A self-compacting concrete (SCC) was produced and delivered by a local ready-mix concrete producer. The used mix composition contained Portland cement (CEM II/A-V 52.5N) from Cementa-Sweden, Dolomite-KM 200 filler, sand 0-4 mm, and crushed granite aggregates with a maximum particle size of 16 mm. MasterGlenium SKY 823 superplasticizer was added. The detailed mix proportions are shown in **Table 2**.

Table 2. *The concrete mix composition.*

Materials	Self-compacting concrete (SCC)	Normal concrete (NC)
	Proportion (kg/m^3)	Proportion (kg/m^3)
Portland Cement (CEM I 42.5N)	-	400
Portland Cement (CEM II/A-V 52.5N)	340	-
Dolomite filler—KM200	160	-
Fine aggregate (B15)	-	179
Fine aggregate (0–4)	1021	1075
Coarse aggregate (4–8)	-	537
Coarse aggregate (8–16)	802	-
Superplasticizer	-	3.0
MasterGlenium SKY 823	3.4	-
Water	187	180

2.2 Test methods

2.2.1 Temperature monitoring

The electrical properties of the nanomodified Portland cement sensors were measured at various temperatures to study their temperature-resistivity. After casting, the specimens were water-cured for 25 days and desiccated at 20±2˚C for 3 days. Next, all specimens were sealed with a thin plastic sheet as shown in **Figure 2(b)**.

The produced SmartCem sensors were placed in the temperature-controlled chambers, which maintained constant temperatures of -20 ˚C, 20 ˚C, and 40 ˚C for 24 hours. Later the electrical resistance was measured using a four-probe method with a digital multimeter type Keysight 34465A. The direct current was applied to the outer electrodes and the potential difference was measured at the inner electrodes. The used setup is shown in **Figure 2(c)**.
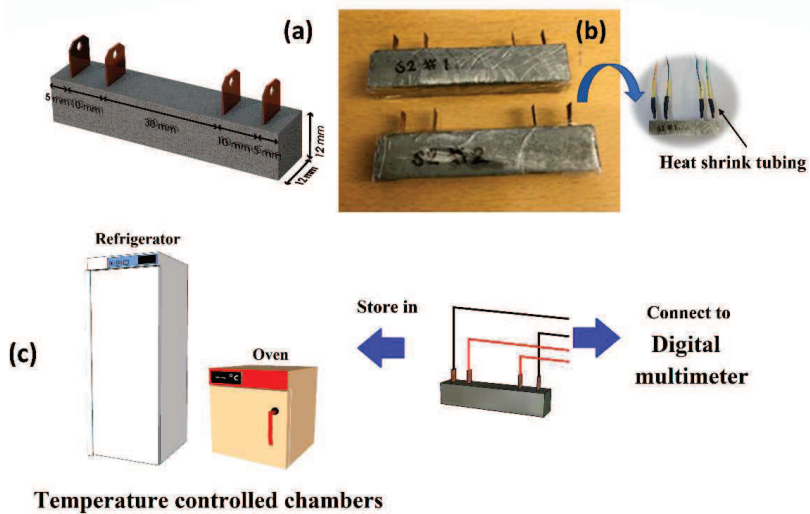
Figure 2. (a) *Mortar sensor* *(b)* *Mortar sensors are wrapped with a thin plastic sheet and covered by heat shrink tubes, and (c)* *A schematic representation of the experimental setup for the temperature-sensitive study of SmartCem sensors.*

The temperature-sensitivity of the SmartCem sensor was described by the temperature coefficient, α, and the activation energy, E_a which was calculated following equations (1), (2), and (3). The electrical resistivity ρ_T of sensing cementitious materials at the desired temperature T was calculated according to **Equation 1** [19–21]:

$$\rho_0 = \frac{\rho_T}{1+\alpha(T-T_0)} \tag{1}$$

where α is a temperature coefficient and ρ_0 is the electrical resistivity at the reference temperature T_0. Another way to describe the temperature-resistivity behavior is to express the electrical resistivity through the motion of free electrons in the pore solution. The activation energy required for the ionic mobility in the liquid phase of a cement-based matrix can be calculated by the application of the Arrhenius law [21–23], **Equation 2** and **Equation 3**:

$$\rho_T = Ae^{-\left(\frac{E_a}{RT}\right)} \tag{2}$$

$$\rho_T = \rho_0 e^{-\left(\frac{E_a}{R}\left(\frac{1}{T}-\frac{1}{T_0}\right)\right)} \tag{3}$$

where A is a pre-exponential constant, E_a is the activation energy for the conduction process (J/mol), and R is the gas constant (8.314 J mol^{-1} K^{-1})
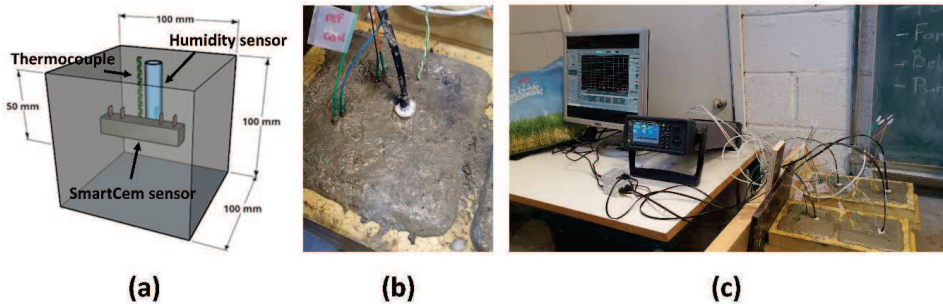
2.2.2 Hydration monitoring

Changes in temperature, humidity, and moisture content were the main factors considered when monitoring the hydration process. The effects of these factors on the measured electrical properties of the SmartCem sensors were studied. The hydration monitoring of the normal strength concrete (NC) was determined using reference sensors (Ref) and nanomodified Portland cement sensors containing 4 wt.% of the SmartCem.

The test sensors were embedded 50 mm below the surface in the 100 mm NC cube immediately after casting. A commercially available humidity sensor type SHT85 produced by Sensirion and a thermocouple were installed as references. The moisture content of the reference samples was measured every 24 hours for 7 days using the oven-drying method and calculated using **Equation 4** [11]:

$$Moisture\ (\ \%\ ) = \frac{\left(W - W_{dry}\right)}{W_{dry}} \times 100 \tag{4}$$

where W is the weight of the concrete sample (g), W_{dry} is the weight of the concrete sample after 24 hours of oven-drying at 110 ˚C ± 5 ˚C (g).

The test setup and the location of the sensors are shown in **Figure 3**. The resistivity of SmartCem sensors and readings from the reference humidity and temperature sensors were recorded for 7 days. All cube samples were kept at 20±2˚C and 60±5 % RH.

(a)   **(b)**   **(c)**

*Figure 3. (a) Sensor placements, (b) arrangement of embedded sensors, and (c) the test setup for hydration monitoring of NC*

SmartCem mortar sensors containing 4 wt.% of the nanomodified cement were embedded into a full-scale reinforced beam. The concrete beam had dimensions of 300 mm × 300 mm × 2500 mm, **Figure 4**. The SmartCem sensor, **Figure 5 (a)**, was embedded 25 mm under the top surface in the mid-span, **Figures 5(b) and Figure 5(c)**. The thermocouple was also immersed nearby the sensor. The monitoring was continued for 7 days.
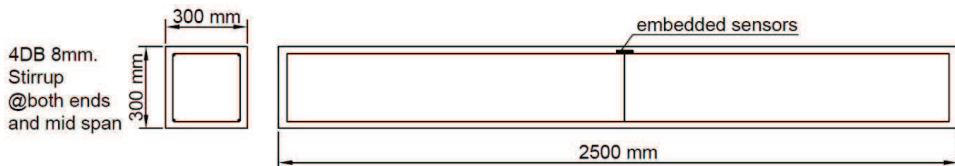
Figure 4. *Full-scale beam used for monitoring of hydration.*
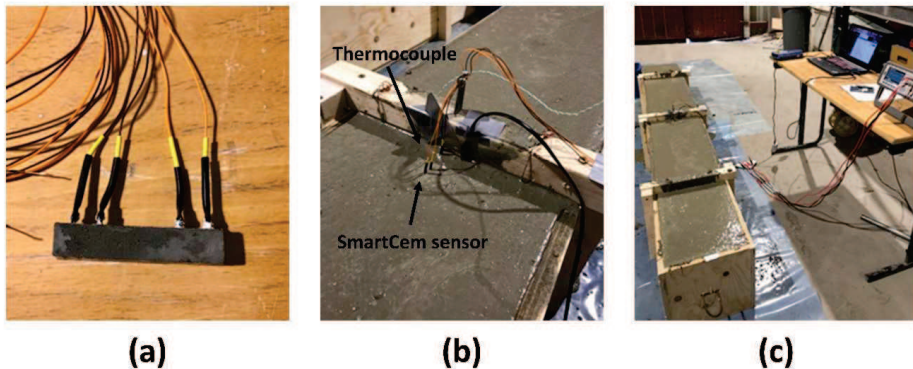
Figure 5. (a) SmartCem sensor (b) Location of the embedded SmartCem sensor and thermocouple (c) SCC beam with hydration monitoring using embedded SmartCem sensor.

3. Result and discussion

3.1 Temperature effects on the electrical resistivity

The temperature versus resistivity relation was determined for SmartCem sensors containing various amounts of the nanomodified Portland cement; Ref (0 wt.%), S2 (2 wt.%), S4 (4 wt.%), S6 (6 wt.%), S8 (8 wt.%), and S10 (10 wt.%). The change of electrical resistivity vs. the temperature determined with the reference thermocouple is presented in **Figure 6**. The results showed a decreasing electrical resistivity with rising temperature for all specimens.
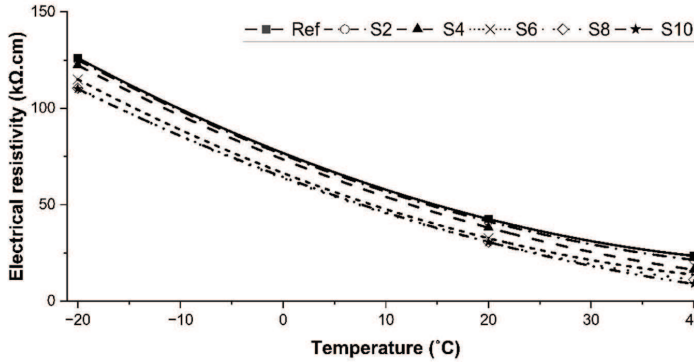
Figure 6. *Effects of temperature on the electrical resistivity of the SmartCem sensors*

The calculated sensitivity of all tested mortar sensors was very similar in the temperature range between -20 ˚C and 40 ˚C, **Table 3**. The sensitivity tended to increase slightly with an increasing amount of the nanomodified cement. This could be related to a higher number of thermally activated charge carriers. A higher amount of CNFs has presumably formed conductive interconnected networks throughout the hardened binder matrix. The highest temperature sensitivity was measured for the sensor containing 10 wt.% of SmartCem. Its sensitivity was approximately 11.76 % higher in comparison with the reference sample and reached -0.0152/˚C.

The activation energy quantifies the amount of thermal energy required for a reaction or transportation process to occur. Thus, it can be interpreted as the amount of thermal energy needed to facilitate the electrons jumping between CNFs distributed in the solidified binder matrix, the so-called electron hopping. The activation energy can be determined by multiplying the slope of the natural logarithm of resistivity and the reciprocal of temperature (**Figure 7**) by the universal gas constant, see **Equation 3**. The calculated activation energy values increased with an increased amount of the nanomodified Portland cement and thus with an increased amount of CNFs, **Table 3**. The presence of CNFs in the studied sensor could slightly increase the activation energy due to the hopping conduction between the cement matrix and CNFs [24]. However, the CNF amount below the percolation threshold leads to the insignificant effect of direct electronic conduction through the CNF network. The percolation threshold value for the studied mortars could be estimated based on **Figure 8**. Independently of the temperature, the percolation threshold was estimated to equal ~5 wt.% of the nanomodified Portland cement, which corresponded to ~0.136 wt.% of CNFs.

Table 3. *Calculated sensitivity of the sensors over the temperature range -20 ˚C to 40 ˚C.*

Mix	Calculated sensitivity, S_{Temp}		
	Temperature coefficient of resistivity, α	Activation energy, E_a	
	(/ ˚C)	(J/mol)	(eV)
Ref	-0.0136	18,649.49	0.193
S2	-0.0138	18,985.30	0.196
S4	-0.0144	19,878.21	0.206
S6	-0.0144	20,305.94	0.210
S8	-0.0148	20,377.94	0.211
S10	-0.0152	20,979.48	0.217
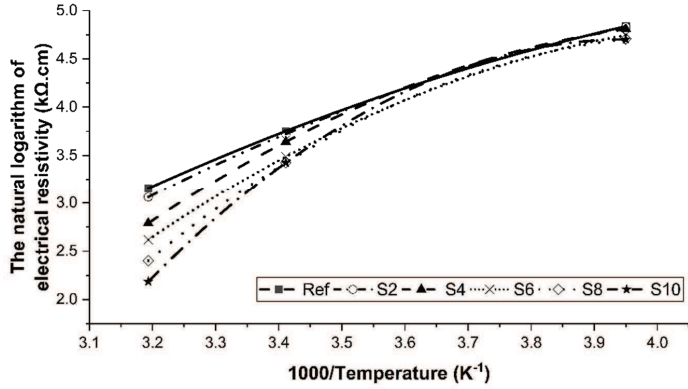
Figure 7. Arrhenius plots for electrical resistivity versus the inverse of temperature for produced sensors.
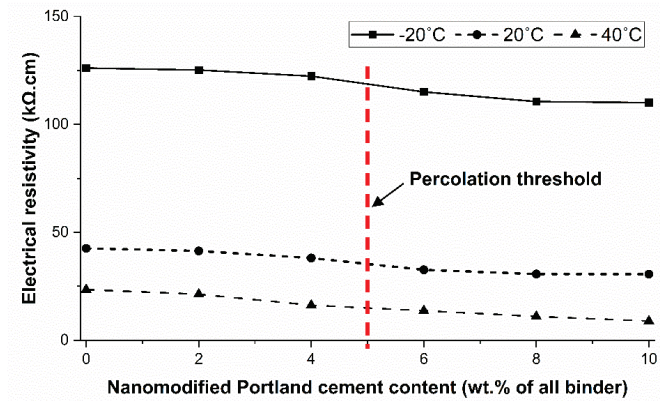
Figure 8. Effects of temperature and amount of nanomodified Portland cement content on the measured electrical resistivity.

3.2 Effects of hydration on electrical resistivity

Monitoring of the early age hydration, for up to 7 days after casting, was done using the NC cube samples, **Figure 3**. One sample contained a SmartCem sensor, thermocouple, and humidity sensor. While the reference sample, in addition to thermocouple and humidity sensors, the reference mortar sensor, which did not contain CNFs. Variations of electrical resistivity recorded during the first 7 days are shown in **Figure 9**. The reference mortar sensor showed a nearly linear increase in resistivity with

time. On the contrary, the mortar sensor containing 4 wt.% of SmartCem showed resistivity change that followed the kinetics of cement hydration.

Figure 9. The change in electrical resistivity of NC was measured by the Ref sensor and the SmartCem sensor for 7 days.

The correlations between the hydration temperature, humidity, and moisture content measured by normal sensors and the electrical resistivity measured by the mortar sensors were weak, **Figures 10, 11, 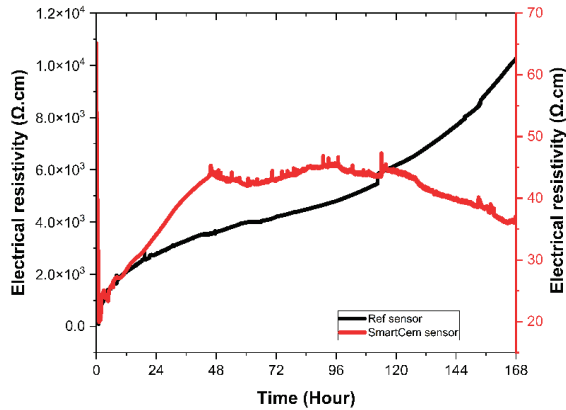and 12.** An inverse dependency between the moisture content of NC and the electrical resistance change was observed in **Figure 12 (a)**. The increasing electrical resistivity of the NC measured by the reference sensor was related only to the decreasing internal moisture content caused by the cement hydration.

The temperature measured in NC cubes varied between 23 ˚C and 25 ˚C, and in this range, the temperature sensitivity of the SmartCem sensor was very low, **Figure 6 and Figure 10**. This result indicated that the electrical resistivity during the early age of the hydration process is independent of the developed temperature. Generally, the electrical resistivity of the Portland cement-based matrixes is affected by the chemical composition of the pore solution, connectivity of pores, fraction of capillary porosity, and the volume fractions of the hydration products [25]. Thus, the observed initial rapid decrease of the resistivity could be related to the increasing concentration of calcium (Ca^{2+}), sodium (Na^+), potassium (K^+), hydroxyl ions (OH^-), and sulfate (SO_4^{2-}) ions due to the ongoing dissolution of Portland cement particles [26]. Later, with progressing hydration processes, the electrical resistivity tended to increase. A continuous increase was observed for the reference mortar sensor during the entire measuring period. In the case of the SmartCem sensors, the maximum measured resistivity reached around 6000 Ω.cm, 48 hours after mixing. At a later age, a nearly constant and slightly decreased resistivity was measured. The reduced number of ions present in the pore solution due to progressing hydration could be indicated as the main cause. Other factors could also include worsened pore connectivity [26–28]. The later gradual decrease of the electrical resistivity, observed after 120 hours, could be related to the densification of the binder matrix microstructure and facilitated electron jumping between CNFs.
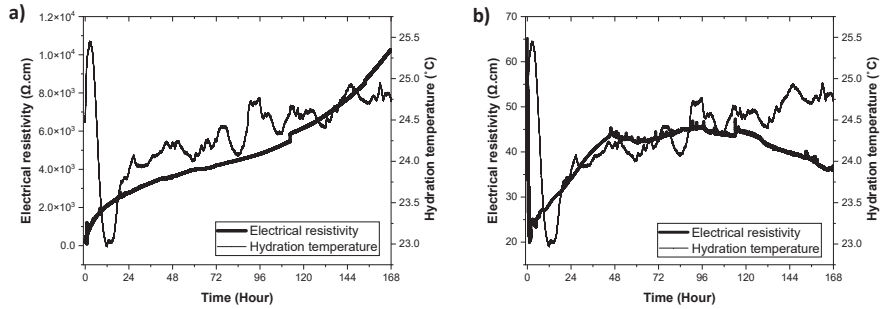
Figure 10. *The change in electrical resistivity of NC was measured by (a) Ref sensor and (b) SmartCem sensor (S4) versus the hydration temperature of NC for 7 days.*
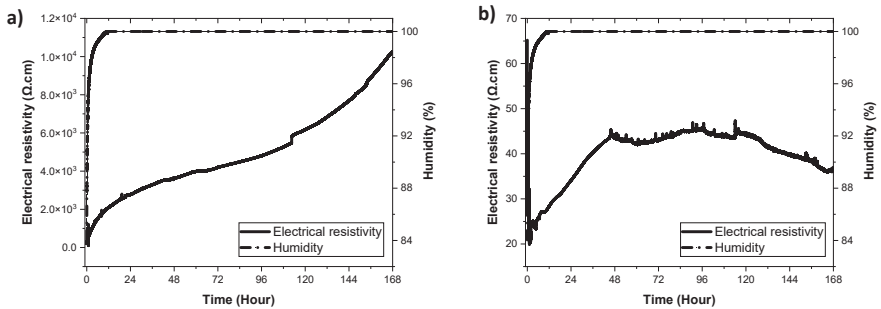
Figure 11. *The change in electrical resistivity of NC was measured by (a) Ref sensor (b) SmartCem sensor (S4) versus internal humidity of NC for 7 days.*
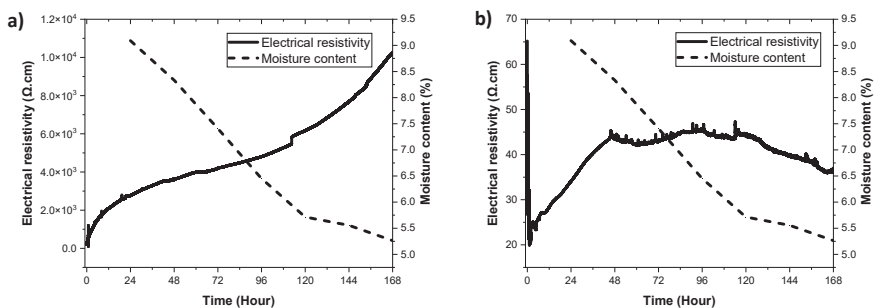
Figure 12. *The change in electrical resistivity of NC was measured by (a) Ref sensor (b) SmartCem sensor (S4) versus moisture content of NC for 7 days.*

The SmartCem sensors (S4), were used to monitor the hydration processes in the large-scale SCC beam, **Figure 4 and Figure 5**. Generally, the electrical resistivity of the SCC beam measured by the embedded SmartCem sensor displays almost the same trend as the thermocouple. The recorded electrical resistivity of SmartCem sensors and temperature measured by thermocouples are shown in **Figure 13**. **In the period I**, (0-5 hours), after embedding the SmartCem sensor into the SCC beam, the electrical resistivity decreased significantly. Rapidly released from Portland cement ions, i.e., K^+, Na^+, $Ca2^+$, OH^-, and SO_4^{2-} dissolved in water and enhanced the electrical conductivity of the pore solution, [1]. During the **IInd period**, the electrical resistivity tended to fluctuate. It could be related to the competitive balance between the ion dissolution and formation of the hydration products, especially including

ettringite and calcium hydroxide. The electrical resistivity increases because the hydration products are formed on the cement particles and cause a delay in the hydration process. While at the same time ions from cement continue to dissolve in the water and form an electrolytic solution, resulting in a decrease in the electrical resistivity of the SCC beam. The end of this period is typically characterized by the initial set. At a later age, during the **IIIrd period** known as acceleration**,** the formation of hydration products is enhanced thus leading to increased electrical resistivity. This could be also related to the significantly decreased number of charged ions present in the pore solution, [26]. The hydration temperature in the SCC beam increased rapidly to reach the maximum mainly due to the hydration of the tricalcium silicate and the tricalcium aluminate. During the **IVth period,** the hydration enters a deceleration controlled by the diffusion of ions, [26]. The hydration slows down thus leading to the observed decrease in electrical resistivity. The hydration products tend to be thicker and larger, and the capillary porosity is significantly reduced leading to decreased electrical resistivity. **In the period V**, the hydration temperature of the SCC beam reached the ambient temperature and remained at that level. The hydration process gradually slowed down and resulted in a slight increase in the measured electrical resistivity.
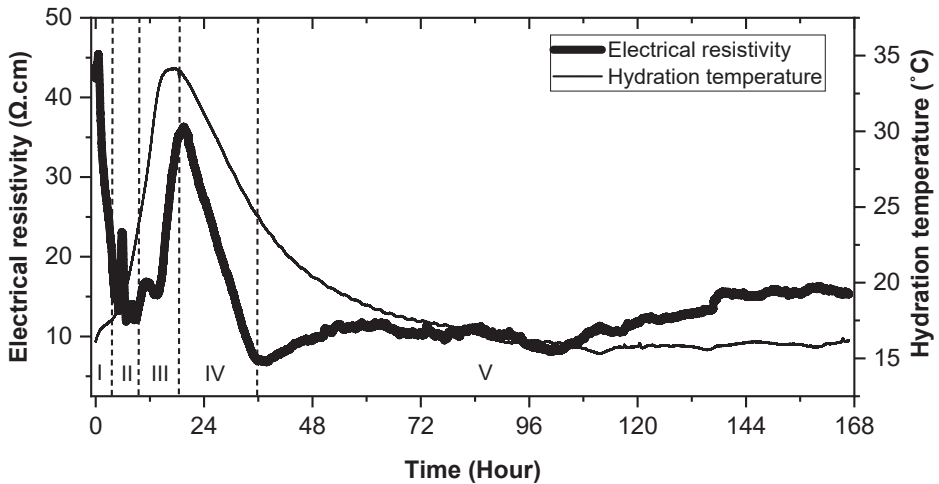
Figure 13. *The measured electrical resistivity of the SCC beam obtained by the SmartCem sensor and the hydration temperature evolution for 7 days.*

Conclusions

The first part of the research focused on the effects of temperature on the electrical resistivity of SmartCem sensors. The second part evaluated the potential to use these sensors to monitor the hydration processes. The main conclusions can be summed up as follows:

- SmartCem sensors are capable of temperature sensing similar to the negative thermistor whose electrical resistivity decreases when the temperature is increased.
- SmartCem sensor containing 10 wt.% of the nanomodified Portland cement (~0.271 wt.% of CNFs) showed the highest sensitivity which was approximately 11.76% higher in comparison with the reference mortar sensor. The temperature coefficient of resistivity was -0.0152/°C.
- The percolation threshold (the amount of the nanomodified Portland cement), for temperature-sensitivity was measured to be 5 wt.% which corresponded to ~0.136 wt.% of CNFs.
- The change in electrical resistivity occurring during hydration in an early period of the studied concrete could be sensed by the embedded SmartCem sensors.
- The variations of electrical resistivity recorded by the SmartCem sensor could reflect physical and chemical changes occurring due to the cement hydration.
- The change in electrical resistivity has been less affected by the hydration temperature.

Acknowledgment

Reference

[1] H.F.W. Taylor, Cement chemistry, 2nd edition, Thomas Telford Publishing, 1997. https://doi.org/10.1680/cc.25929.

[2] J. Zhang, L. Qin, Z. Li, Hydration monitoring of cement-based materials with resistivity and ultrasonic methods, Materials and Structures/Materiaux et Constructions. 42 (2009). https://doi.org/10.1617/s11527-008-9363-0.

[3] X. Wei, L. Xiao, Z. Li, Hyperbolic method to analyze the electrical resistivity curve of Portland cements with superplasticizer, Journal of Wuhan University of Technology-Mater. Sci. Ed. 23 (2008) 245–248. https://doi.org/10.1007/PL00022219.

[4] S.W. Tang, X.H. Cai, Z. He, W. Zhou, H.Y. Shao, Z.J. Li, T. Wu, E. Chen, The review of early hydration of cement-based materials by electrical methods, Constr Build Mater. 146 (2017) 15–29. https://doi.org/10.1016/j.conbuildmat.2017.04.073.

[5] ACI Committee 301, Specifications for Concrete Construction, American Concrete Institute, 2020.

[6] S.M. Trost, M. Fox, Method and system for concrete quality control based on the concrete's maturity, U.S. Patent No. 8,032,244, 2011.

[7]   M.S. Konsta-Gdoutos, C.A. Aza, Self sensing carbon nanotube (CNT) and nanofiber (CNF) cementitious composites for real time damage assessment in smart structures, Cem Concr Compos. (2014). https://doi.org/10.1016/j.cemconcomp.2014.07.003.

[8]   Y.L. Mo, R.N. Howser, A. Gautam, S. Dhonde, G. Song, Temperature Sensing and Hydration Study of Carbon Nanofiber Aggregates, J Aerosp Eng. 33 (2020) 04020002. https://doi.org/10.1061/(asce)as.1943-5525.0001111.

[9]   B. Chen, K. Wu, W. Yao, Characteristics of resistivity-temperature for carbon fiber reinforced concrete, Journal Wuhan University of Technology, Materials Science Edition. 21 (2006) 121–124. https://doi.org/10.1007/BF02861488.

[10]   E. Teomete, The effect of temperature and moisture on electrical resistance, strain sensitivity and crack sensitivity of steel fiber reinforced smart cement composite, Smart Mater Struct. 25 (2016). https://doi.org/10.1088/0964-1726/25/7/075024.

[11]   E. Demircilioğlu, E. Teomete, E. Schlangen, F.J. Baeza, Temperature and moisture effects on electrical resistance and strain sensitivity of smart concrete, Constr Build Mater. 224 (2019) 420–427. https://doi.org/10.1016/j.conbuildmat.2019.07.091.

[12]   W.J. McCarter, G. Starrs, T.M. Chrisp, P.F.G. Banfill, Activation energy and conduction in carbon fibre reinforced cement matrices, J Mater Sci. 42 (2007) 2200–2203. https://doi.org/10.1007/s10853-007-1517-x.

[13]   S. Wen, S. Wang, D.D.L. Chung, Carbon fiber structural composites as thermistors, Sens Actuators A Phys. 78 (1999) 180–188. https://doi.org/10.1016/S0924-4247(99)00240-X.

[14]   H. Tabatabai, M. Aljuboori, A novel concrete-based sensor for detection of ice and water on roads and bridges, Sensors (Switzerland). 17 (2017). https://doi.org/10.3390/s17122912.

[15]   Y.L. Mo, R.N. Howser, A. Gautam, S. Dhonde, G. Song, Temperature Sensing and Hydration Study of Carbon Nanofiber Aggregates, J Aerosp Eng. 33 (2020). https://doi.org/10.1061/(asce)as.1943-5525.0001111.

[16]   T. Buasiri, K. Habermehl-Cwirzen, L. Krzeminski, A. Cwirzen, Piezoresistive load sensing and percolation phenomena in portland cement composite modified with in-situ synthesized carbon nanofibers, Nanomaterials. 9 (2019). https://doi.org/10.3390/nano9040594.

[17]   T. Buasiri, K. Habermehl-Cwirzen, L. Krzeminski, A. Cwirzen, Role of Carbon Nanofiber on the Electrical Resistivity of Mortar under Compressive Load, Transportation Research Record: Journal of the Transportation Research Board. (2020) 1–6. https://doi.org/10.1177/0361198120947417.

[18]   T. Buasiri, K.H. Cwirzen, L. Krzeminski, A. Cwirzen, Novel humidity sensors based on nanomodified Portland cement, Sci Rep. (2021) 1–10. https://doi.org/10.1038/s41598-021-87563-7.

[19]   J.F. Garcı, Influence of temperature and humidity on Portland cement mortar resistivity monitored with inner sensors, (2009) 294–299. https://doi.org/10.1002/maco.200805075.

[20]   W.J. Mccarter, Field monitoring of electrical conductivity of cover-zone concrete, 27 (2005) 809–817. https://doi.org/10.1016/j.cemconcomp.2005.03.008.

[21] T.M. Chrisp, G. Starrs, W.J. McCarter, E. Rouchotas, J. Blewett, Temperature-conductivity relationships for concrete: An activation energy approach, J Mater Sci Lett. 20 (2001) 1085–1087. https://doi.org/10.1023/A:1010926426753.

[22] W.J. Mccarter, Temperature on Conduction and Polarization in Portland Cement Mortar, 15 (1995) 411–415.

[23] X. Wei, Effect of temperature on the electrical resistivity of Portland cement pastes, 24 (2012).

[24] S. Wen, S. Wang, D.D.L. Chung, Carbon fiber structural composites as thermistors, 1999. www.elsevier.nlrlocatersna.

[25] Z. Liu, Y. Zhang, Q. Jiang, Continuous tracking of the relationship between resistivity and pore structure of cement pastes, Constr Build Mater. 53 (2014) 26–31. https://doi.org/10.1016/j.conbuildmat.2013.11.067.

[26] Y. Tu, D. Liu, L. Yuan, T. Wang, Early hydration process and kinetics of concrete based on resistivity measurement, Journal of Advanced Concrete Technology. 19 (2021) 196–206. https://doi.org/10.3151/jact.19.196.

[27] X. Wei, L. Xiao, Electrical resistivity monitoring and characterisation of early age concrete, Magazine of Concrete Research. 65 (2013) 600–607. https://doi.org/10.1680/macr.12.00127.

[28] S.A.A. El-Enein, M.F. Kotkata, G.B. Hanna, M. Saad, M.M.A. el Razek, Electrical conductivity of concrete containing silica fume, Cem Concr Res. 25 (1995) 1615–1620. https://doi.org/10.1016/0008-8846(95)00156-5.

Paper VI

Sensing mechanisms of nanomodified Portland cement composites

Buasiri, T., Habermehl-Cwirzen, K., Krzeminski, L., & Cwirzen, A.

Submitted

Sensing mechanisms of nanomodified Portland cement composites

Thanyarat Buasiri [1, *], Karin Habermehl-Cwirzen [1], Lukasz Krzeminski [2], and Andrzej Cwirzen[1]

[1] Building Materials, Department of Civil, Environmental and Natural Resources Engineering, Luleå University of Technology, 97187 Luleå, Sweden; thanyarat.buasiri@ltu.se (T.B.); karin.habermehl-cwirzen@ltu.se (K.H.-C.); andrzej.cwirzen@ltu.se (A.C.)

[2] The Institute of Engineering Materials and Biomaterials, Silesian University of Technology, 44-100 Gliwice, Poland; lukasz.krzeminski@polsl.pl (L.K.)

* Corresponding author: thanyarat.buasiri@ltu.se

Abstract

Mortar sensors were fabricated as beams incorporating different amounts of carbon nanofibers (CNFs) synthesized in-situ on cement particles. Changes in electrical resistivity were measured and compared to recorded changes in compressive stress, temperature, and humidity. Sensing mechanisms and corresponding models were developed. The findings of the study indicate that the piezoresistive effect is influenced by the critical concentration of CNFs inside the composite matrix and the tunneling effect. In addition, water absorption and desorption, as well as the amount of chemically bound water played an important role in humidity sensing. Thermal fluctuation-induced tunneling conduction was dominant for the temperature sensitivity.

1. Introduction

Self-sensing cement-based composites refer to composites that possess the ability to sense various physical and chemical parameters. These composites are alternatively referred to as self-monitoring, intrinsic self-sensing, or self-diagnosing cement-based composites [1]. The sensed parameters include stress or strain, temperature, humidity, and damage. Their fabrication involves the dispersion of conductive phases into the conventional cement-based matrix to form an electrically conductive network. Typical conductive materials proposed for use in self-sensing cementitious composites include carbon fibers (CFs) [2,3], carbon nanotubes (CNTs) [4–7], carbon black (CB) [8], graphene nanoplatelets (GNPs) [9] , or combinations of conductive fibers [10,11]. Sensing cement-based composites can monitor different factors by measuring changes in electrical properties, i.e., electrical resistivity or electrical conductivity. The subsequent section will discuss the factors that impact the electrical properties of cement-based composites.

The electrical resistivity of the cement-based composites is described by percolation theory. The theory assumes that the change in electrical resistivity depends on the amount of dispersed conductive material. There are three conditions that have been identified: the insulation zone, the percolation zone, and the conduction zone. **Figure 1** shows the electrical resistivity of a cement-based composite versus the concentration of conductive materials, as well as the distribution and interconnection of conductive fibers in the cementitious composite [12]. In general, the electrical resistivity of cementitious composites decreases as the amount of conductive material added to the composites increases. A higher concentration of conductive materials enhances the formation of conductive networks [13]. When the quantity of conductive phases is lower than the percolation threshold, the absence of conductive networks leads to a little change in electrical resistivity. Once the quantity of the added conductive materials reaches the percolation zone, the neighboring conductive materials initiate interaction with one another, resulting in the formation of conductive networks. As a consequence, there is a significant reduction in electrical resistivity [14]. When the quantity of conductive material is above the percolation threshold, the electrical resistivity may not change substantially because the conductive network is already well established. The additional conductive materials may become redundant or simply contribute to the existing network without causing a significant change in resistivity, as shown in point 4 in **Figure 1**.
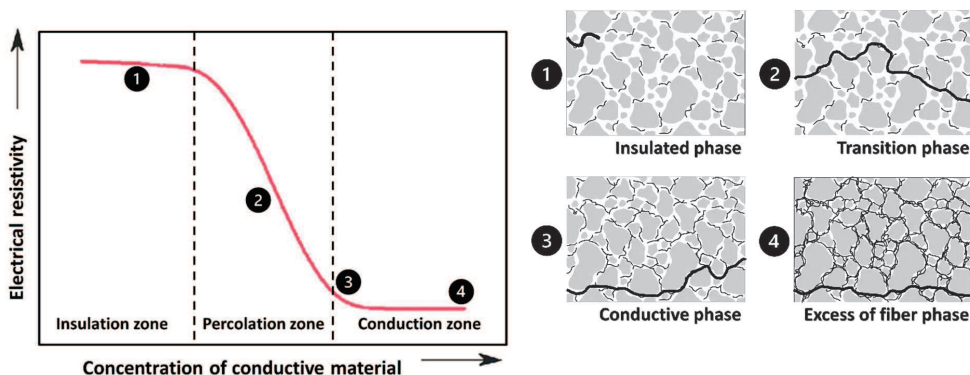

Figure 1. The percolation concept of cementitious composite incorporating conductive materials.

The electrical properties of cementitious composites are affected by the duration of curing due to changes in the microstructure resulting from the filling of internal pores with additional hydration products throughout the continuous hydration process [15]. The electrical resistivity is low at the beginning and increases with age [16–20]. At an early age, the amount of chemically unbound free water is higher, which enables the development of ionic conduction [21]. Over time, there is a decrease in both the total porosity and moisture content, leading to an increase in resistivity [19,22]. Furthermore, it is probable that the hydration products may cover the conductive phases and disconnect the conductive network, leading to a sudden rise in electrical resistivity [20].

An application of external loads results in a change in the electrical resistivity of the sensing cement-based composite. The electrical resistivity increases when subjected to tensile loading, which is attributed to the gradual breakdown of its conductive networks and the subsequent development of microcracks [23,24]. Due to the formation of damage following the achievement of the maximum tensile strain, the electrical resistivity changes more rapidly. This suggests that in addition to being a function of tensile strain, the fracture behavior of the material under tension also affects the sensing response of cementitious composites [25]. Conversely, the reduction of the electrical resistivity occurs due to the compression caused by the shortening of the distance between the conductive phases and the fiber push-in. This leads to the tunneling effect and fibers contacting each other [23,24].

Temperature variations are also detected by the cement-based composites containing conductive fibers. The mechanism is controlled by the transition barrier and the conductivity related to the tunneling effect. As the temperature increases, some electrons will gain additional energy and will act as charge carriers. They will transfer this energy between conductive fibers due to the tunneling phenomena. It will result in decreased electrical resistivity [26]. The temperature variation also induces thermal expansion and contraction. Both effects can change the distance between the conductive phases [27]. Therefore, the resistivity decreases due to the tunneling effect of rising temperatures until a certain threshold is reached. Beyond that threshold, the electrical resistivity increases due to the dominance of thermal expansion [26].

Absorption and desorption of moisture change the electrical resistivity of sensing cementitious composites. When subjected to low ambient relative humidity, these composites undergo evaporation of moisture. While exposure to high ambient relative humidity causes condensation and a gradual filling up of the capillary pores [28], **Figure 2**. This results in the development of supplementary connections that occur among the pre-existing electrically conductive pathways. Consequently, the ultimate electrical resistivity varies and depends on the exposure and its history [29]. At a certain threshold of relative humidity, the primary factor influencing conductivity is the water induced between filler particles and the filler-matrix [30,31].
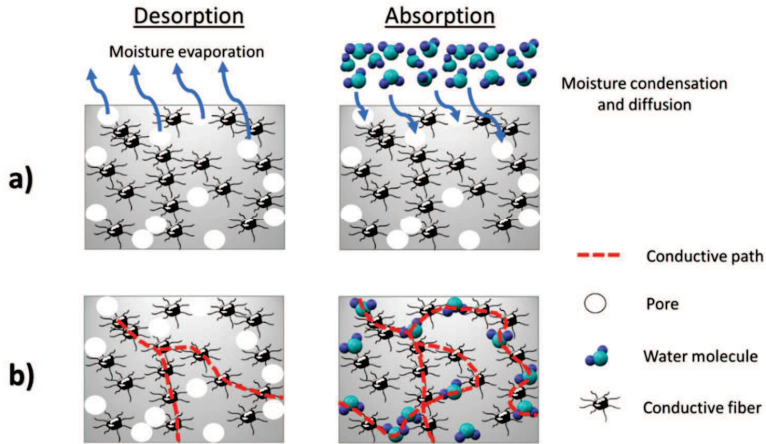
Figure 2. The effects of ambient humidity on a) moisture transport and b) formation of conductive paths

There are several other factors that influence the electrical properties of cement-based composites, such as the specimen's size, creep behavior under long-term loading, exposure to freeze-thaw cycles, and the penetration of chloride ions [32].

A uniform dispersion of conductive materials is crucial to ensuring the proper formation of internal conductive networks. Well-dispersed conductive fibers can induce and enhance sensitivity, as well as the mechanical and electrical properties of the cementitious composites [33]. The dispersion of conductive phases, especially nanomaterials, usually requires the application of additional processes and treatments, e.g., ultrasonication [34] or wrapping with surfactants [35]. Another novel solution is to use carbon nanofibers that were synthesized in situ directly on cement particles. The sensitivity of matrixes made from this material appeared to be very high [36–38].

This study focused on the sensing mechanisms of nanomodified Portland cement composites and their response to variations in compressive stress, temperature, and ambient humidity. The contribution of different factors influencing electrical properties and response was evaluated and modelled.

2. Materials and Experimental program

Ordinary Portland cement (CEM I 42.5N) was used as a binder. Nanomodified Portland cement (SmartCem), which contained approximately 0.271 wt.% of in-situ synthesized carbon nanofibers (CNFs) was used as a conductive material to prepare mortar samples. The synthesis processes as well as the basic properties of the nanomodified Portland cement are described elsewhere [37,39]. Sand has an average particle size of 150 μm was used. The workability of the mixtures was controlled using a polycarboxylate-based superplasticizer (SP) type Glenium manufactured by Grace Chemicals. The water-binder (w/b) ratio and the sand-binder (s/b) ratio for all mortar mixtures were set at 0.35 and 1, respectively. Three specimens were made for each mixture, and the corresponding mix proportions are shown in **Table 1.**

Mix	CEM I 42.5N (wt.%)	SmartCem (wt.%)	SP (wt.%)	w/b	s/b
Ref	100	0	0.8	0.35	1
S2	98	2	0.8	0.35	1
S4	96	4	0.8	0.35	1
S6	94	6	0.8	0.35	1
S8	92	8	0.8	0.35	1
S10	90	10	0.8	0.35	1

Mortars were mixed using a small-volume vacuum mixer type Bredent and cast into Teflon molds having dimensions of 12x12x60 mm^3. Four copper electrodes having a size of 7.5x15 mm were placed into the specimens with a distance between the inner electrodes of 30 mm and the outer electrodes of 50 mm. After de-molding, specimens were cured in water at 20±2˚C in laboratory.

The electrical resistance was determined with the four-probe method, using a Keysight 34465A digital multimeter. The electrical conductivity (σ_n) was calculated using the **equation (1):**

$$\sigma_n = 1/\rho = L/(RA) \tag{1}$$

And the fractional change of electrical resistivity (FCR) can be calculated as shown in **equation (2):**

$$FCR(\%) = \frac{\rho - \rho_0}{\rho_0} \times 100 = \left(\frac{\rho}{\rho_0} - 1\right) \times 100 \tag{2}$$

where: ρ is electrical resistivity, ρ_0 is initial electrical resistivity, L is the distance between internal electrodes, R is electrical resistance, and A is electrode area.

The piezoresistive behavior of nanomodified Portland cement composite was studied under applied compressive stress after 28 days of curing with a loading rate of 0.05 cm/min which was sustained until the sample failure, **Figure 3 a)**. To study the sensitivity to humidity variations, the 28-day-old beams were placed into the humidity chambers. The humidity chambers consisted of sealed glass containers that contained a variety of saturated salt solutions, **Figure 3 b).** The substances used in this study were lithium chloride (LiCl), potassium carbonate (K_2CO_3), sodium chloride (NaCl), and potassium sulphate (K_2SO_4), which can maintain relative humidity of approximately of 11±2%, 43±2%, 75±2%, and 97±2%, respectively [40]. The chambers were equipped with the SHT85 commercial humidity sensor as well. The electrical resistance was measured after 24 hours of exposure. The effect of temperature was investigated by measuring the electrical resistance of the 28-day-old specimens at -20 ˚C, 0 ˚C, 20 ˚C and 40 ˚C. Before the test, all specimens were sealed with a thin plastic sheet. The measurements were done after 24 hours of exposure. The test setup used is shown in **Figure 3 c).** The mathematical analysis and modelling were done using OriginPro 2023 software.
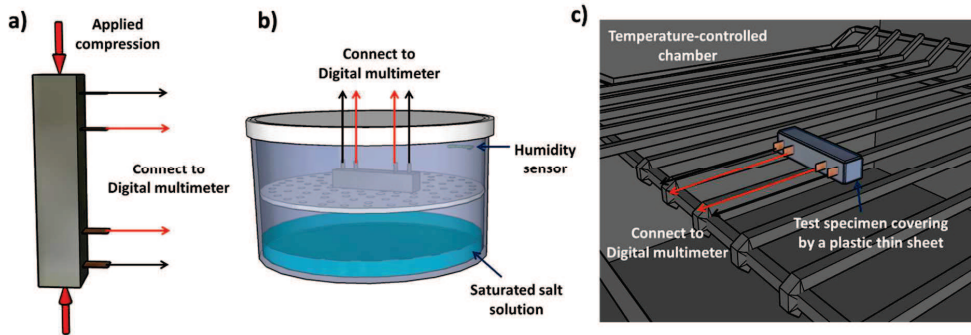
Figure 3. *Schematic diagrams of the test setup of nanomodified Portland cement mortar for a) piezoresistive sensing, b) humidity sensing, and c) temperature sensing*

3. Results and discussion

A piezoresistive effect can be defined as a change in electrical resistivity due to externally applied stress or strain [41]. Mortars containing SmartCem mortar showed this effect. The fractional change in the electrical resistivity (FCR) of samples S2, S4, S6, S8, and S10 decreased with increasing compressive stress, while no change was measured for the reference beam containing unmodified Portland cement, **Figure 4.** The observed results exhibited a non-linear pattern. In the case of samples S2 and S4, the fractional change in electrical resistivity was nearly unchanged with the applied stress. This can be attributed to the limited quantity of CNFs, which was below the percolation threshold. Consequently, the distance between the conductive CNFs was too large, which limited the formation of an electrically conductive paths. A moderate piezoresistive effect was measured for sample S6, which contained 6 wt.% of the SmartCem and was very strong at 8 and 10 wt.% replacement (samples S8 and S10). The strongest effect was reached for S10 sample with FCR of 83% at 27 MPa.
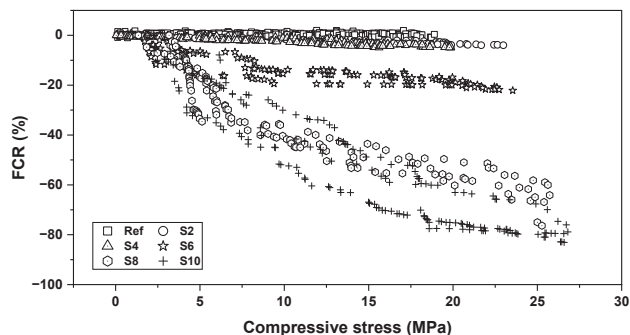
Figure 4. *Fractional change in electrical resistivity of the nanomodified Portland cement mortars under compressive stress.*

Figure 5 illustrates the effect of ambient relative humidity on the measured electrical conductivity. There are two groups of responses. Within the first group, the electrical conductivity of Ref, S2, S4, and

S6 showed a low sensitivity to changes in the ambient humidity. Conversely, the second group, S8 and S10, demonstrated a stronger sensitivity. As mentioned earlier, this could be attributed to the increased amount of CNFs distributed in the binder matrix. The water vapor undergoes condensation and progressively occupies more and more pores and voids. This process facilitates the formation of additional conductive bridges that enhance the already existing electrically conductive pathways present within the composite [42]. The highest sensitivity was observed in S10 samples, with the maximum electrical conductivity around 40 x10^{-3} S m^{-1} at 97 %RH.

Figure 5. The relationship between the electrical conductivity and the ambient humidity of the nanomdified Portland cement mortars.

The electrical conductivity of all nanomodified Portland cement mortars increased with temperature, **Figure 6**. The results indicated that the specimens incorporating SmartCem had a low sensitivity to temperatures between -20°C and 20°C. While, at 40°C, the sensitivity gradually increased with higher SmartCem content. More CNFs had presumably formed more extensive, conductively interconnected networks throughout the hardened binder matrix. At higher temperatures, the thermal energy excites more electrons across the bandgap, leading to increased conductivity. Based on the range of temperature in these studies and the obtained results, the SmartCem matrixes exhibit temperature-sensing characteristics similar to those of a negative thermistor, in which the resistance of the composite decreases as the temperature increases.

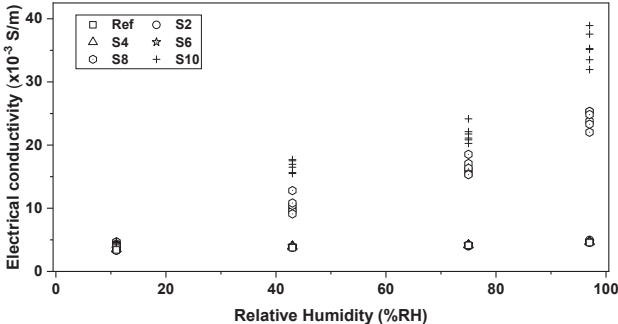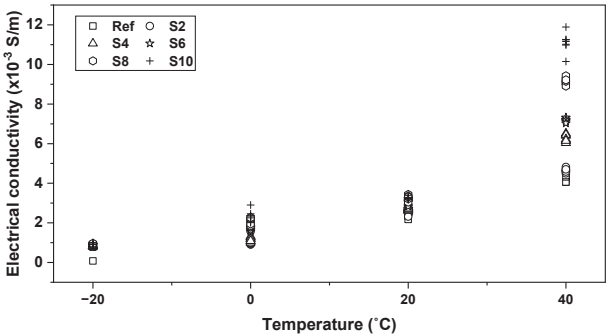*Figure 6. The relationship between the electrical conductivity and the temperature of the nanomdified Portland cement mortars*

When compressive stress is applied to a composite matrix, the distance between the dispersed conductive materials is altered. The matrix deforms as the compression load is increased, which results in the reconstruction of the present electrically conductive paths, **Figure 7 a)**. When the gap between the conductive materials is small enough, the electron can move to the adjacent conductive materials, resulting in the formation of conductive paths, **Figure 7 b)**.
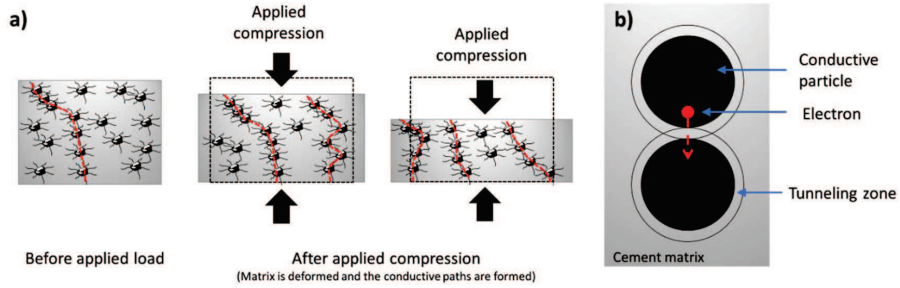
Figure 7. a) *Formations of the conductive paths before and after applied compression and* *b)* *The tunneling effect between conductive particles*

The present work assumes a uniform dispersion of all conductive particles (CNFs) throughout the matrix. The resistance of each conductive path (R_i) is a combination of the resistance of the conductive particle (R_c) and the resistance of the matrix between the adjacent conductive particles (R_m), **equation (3)** [13]. Since the electrical resistivity of the conducting particle is much smaller than that of the cement matrix, the resistance across the conducting particle may be disregarded. The resistance of the effective conductive path can be simplified as **equation (4)**:

$$R_i \approx n_i R_c + (n_i - 1) R_m \tag{3}$$

$$R_i \approx n_i R_m \tag{4}$$

where: n_i is the quantity of conductive particles present inside each individual path.

The electrical resistance of the nanomodified composite (R) can be estimated as the parallel electrical resistance of effective conductive paths inside the composite, as shown in **equation (5)**:

$$R = \cfrac{1}{\cfrac{1}{R_1} + \cfrac{1}{R_2} + \cfrac{1}{R_3} + ... + \cfrac{1}{R_k}} ...... = \cfrac{1}{\cfrac{1}{n_1 R_m} + \cfrac{1}{n_2 R_m} + \cfrac{1}{n_3 R_m} + ... + \cfrac{1}{n_k R_m}} = \cfrac{R_m}{\alpha} \tag{5}$$

$$\alpha = \frac{1}{n_1} + \frac{1}{n_2} + \frac{1}{n_3} + ... + \frac{1}{n_k} \tag{6}$$

The model of tunneling current density (J) proposed by Simmons [43,44] is shown in **equation (7):**

$$J = \frac{3(2m\varphi)^{1/2}}{2s} \left(\frac{e}{\hbar}\right)^2 V \times \exp\left(-\left(\frac{4\pi s}{\hbar}\right)(2m\varphi)^{1/2}\right) \tag{7}$$

Based on **equation (7)**, the resistance (R_m) can be derived as **equation (8)**:

$$R_m = \frac{8\pi \hbar s}{3e^2 \gamma a^2} \exp(\gamma s) \tag{8}$$

$$\gamma = \frac{4\pi (2m\varphi)^{1/2}}{\hbar} \tag{9}$$

where: $\hbar$ is the Planck's constant, m is the electron mass, e is the electron charge, s is the tunneling distance between adjacent conductive particles, φ is the height of the potential barrier between adjacent particles, V is the voltage drop cross tunnel, and a^2 is the effective cross-section area.

Then, the electrical resistance of the nanomodified Portland cement composite R can be calculated as **equation (10)**:

$$R = \left(\frac{1}{\alpha}\right)\left(\frac{8\pi \hbar s}{3e^2 \gamma a^2}\right)\exp(\gamma s) \tag{10}$$

Therefore, the electrical resistivity of the nanomodified Portland cement composite (ρ) can be expressed using **equation (11)**:

$$\rho = \frac{RA}{L} = \frac{A}{L}\left(\frac{1}{\alpha}\right)\left(\frac{8\pi \hbar s}{3e^2 \gamma a^2}\right)\exp(\gamma s) \tag{11}$$

Under compressive stress, the electrical resistivity of the nanomodified Portland cement composite changes from the initial resistivity without the applied stress (ρ_0) to the resistivity due to the applied compressive stress (ρ). The relationship between ρ_0 and ρ is expressed by the **equation (12)**:

$$\frac{\rho}{\rho_0} = \frac{s}{s_0}\exp(\gamma(s - s_0)) \tag{12}$$

From the stress-strain relationship under compression, as shown in **equation (13)**:

$$\sigma = E\varepsilon = E\left(\frac{s - s_0}{s_0}\right) \tag{13}$$

$$s - s_0 = \frac{s_0 \sigma}{E} \tag{14}$$

Substituting **equation (14)** into **equation (12)** yields

$$\frac{\rho}{\rho_0} = \left(1 + \frac{\sigma}{E}\right)\exp\left(\frac{\gamma s_0 \sigma}{E}\right) \tag{15}$$

Then, making a Taylor expansion of the exponential function of the **equation (15)**, it becomes the **equation (16)**:

$$\frac{\rho}{\rho_0} = \left(1 + \frac{\sigma}{E}\right)\left(1 + \frac{\gamma s_0}{E}\sigma + \frac{1}{2!}\left(\frac{\gamma s_0}{E}\right)^2 \sigma^2 + \frac{1}{3!}\left(\frac{\gamma s_0}{E}\right)^3 \sigma^3 + \ldots\right) = 1 + A\sigma + B\sigma^2 + C\sigma^3 + \ldots$$

(16)

where: A, B, C are the coefficients of the polynomial equation.

The fractional change in the electrical resistivity of nanomodified Portland cement composites (FCR) can be calculated using the **equation (17)**:

$$FCR(\%) = \frac{\rho - \rho_0}{\rho_0} \times 100 = \left(\frac{\rho}{\rho_0} - 1\right) \times 100$$

(17)

Substituting **equation (16)** into **equation (17)**, yields

$$FCR(\%) = \left(A\sigma + B\sigma^2 + C\sigma^3 + \ldots\right) \times 100$$

(18)

From the proposed model in **equation (18)**, the quadratic polynomial was used to fit the FCR curve of the experimental data from the current work and the data found in the literature [37,38], as shown in **Figure 8**. **Table 2** shows the coefficients of fitted experimental data based on the model **equation (18)** derived from the tunneling behavior under compressive stress. The calculated coefficients of determination (R^2) indicate a relatively high accuracy of the developed model. It can be concluded that the piezoresistive behavior of the examined composites can be effectively described by the combination of efficient conductive paths and the principles of tunneling theory.

Table 2. Parameter obtained from fitting curves in Figure 8

Mix	A	B	Model equation	R^2
S2	-0.20290	0.00202	FCR (%) = -0.2029σ + 0.00202σ²	0.96631
S4	-0.25448	0.00129	FCR (%) = -0.25448σ + 0.00129σ²	0.94201
S6	-2.03052	0.05924	FCR (%) = -2.03052σ + 0.05924σ²	0.9661
S8	-5.03367	0.08409	FCR (%) = -5.03367σ + 0.08409σ²	0.96725
S10	-5.30494	0.08396	FCR (%) = -5.30494σ + 0.08396σ²	0.98119
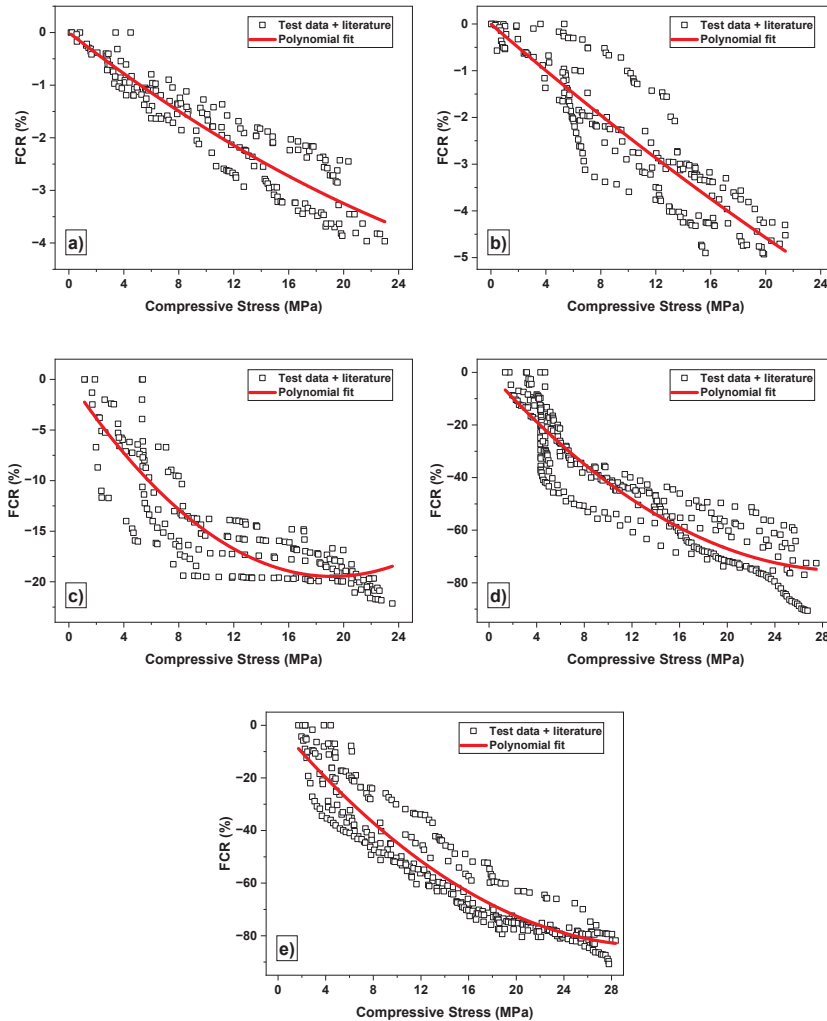
Figure 8. Fitted curve with the experimental data from current studies and literature on the FCR of nanomodified Portland cement mortars under compressive stress of a) S2, b) S4, c) S6, d) S8, and e) S10.

There are three types of water present in cement-based composites: free water held in capillaries, physically bound surface-absorbed water, and chemically bound water present in hydration products [45–47]. The chemically bound water does not readily absorb or release moisture in response to changes in ambient humidity, but it can evaporate at temperatures > 500 °C [29]. It is firmly incorporated into the solid structure of the cement-based composites and does not exhibit the same moisture exchange properties as free or physically bound water. Furthermore, in this study, the measurements were done using 28-day-old samples in which hydration was largely finalized which enabled to neglect these effects. Consequently, the effect of moisture content (or internal humidity) caused by the variation in ambient humidity could be attributed only to the movement of the free water.

Absorption and desorption of water molecules affect the electrical connectivity of the conductive phases due to capillary condensation. At a certain level of humidity, the water molecules provide transportation paths for ions and increase the electrical conductivity of the matrix. **Figure 9** shows the moisture being absorbed and desorbed in pores due to variations in the relative humidity. Through exposure to low-level relative humidity, moisture evaporates from the exposed surface, **Figure 9a)**. When the ambient relative humidity is sufficiently low, all the capillary moisture is removed, **Figure 9b)**. At higher ambient relative humidity, moisture starts to condense first in smaller pores and eventually reaches a saturated state, filling the entire pore system, **Figure 9c) and Figure 9d)** [28].
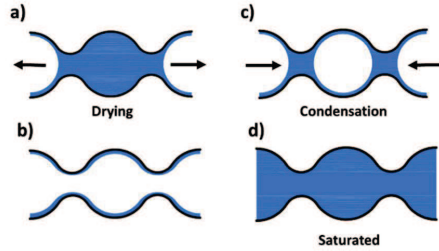
Figure 9. *The effect of ambient humidity on the moisture movement inside the pore.*

A modified parallel law can be used to describe the effective electrical conductivity of cementitious composites (σ_e), as a composite system made of n phases [48].

$$\sigma_e = \sum_{i=1}^{n} \left(\sigma_i \phi_i \beta_i \right) \tag{19}$$

where: σ_i, ϕ_i and β_i are the electrical conductivity, volume fraction, and connectivity factor of each constitutive component i.

Assuming that the conductive CNFs and liquid phase are responsible for the electrical conductivity of nanomodified Portland cement composites for sensing changes in humidity (σ_h), the **equation (19)** can be simplified as **equation (20):**

$$\sigma_{e,h} = \sigma_c \phi_c \beta_c + \sigma_l \phi_l \beta_l \tag{20}$$

where: σ_c, ϕ_c and β_c are the electrical conductivity, volume fraction, and connectivity of the conductive filler (CNFs), σ_l, ϕ_l and β_l are the electrical conductivity, volume fraction of liquid filled in the pores, and pore connectivity of the liquid phase.

The volume fraction of the pore fluid (ϕ_l) is approximately the total volume of saturated pores located inside the composite due to the capillary condensation (V_{sat}) divided by the total volume of all constituents of the composite (V_t). The present work assumes all the pores inside the composite have an ellipsoidal shape. The determination of a maximum pore radius (r_{max}) that keeps saturated is contingent upon the surrounding humidity levels and can be described by Kelvin's equation for porous materials [49] as follows **equation (21):**

$$r_{\max} = \frac{-2\gamma V_m}{R_g T \left[\ln\left(RH\right)\right]} = \frac{-2\gamma V_m}{R_g T \left[\ln\left(\%RH/100\right)\right]} \tag{21}$$

where: γ and V_m are the surface tension and the molar volume of the pore fluid, R_g is the universal gas constant, T is an absolute temperature in Kelvin, and RH is the ambient relative humidity.

The total volume of saturated pores V_{sat} in this work assumes a combination of several single saturated pores. Their size and number are linked to ambient humidity levels. The maximum saturated pore radius follows the **equation (21)** and all pores with smaller sizes are assumed to be saturated. While pores having a radius greater than $r_{\max}$ are empty. Therefore, the electrical conductivity of the nanomodified Portland cement composite $\sigma_{e,h}$ can be simplified as shown in **equation (22):**

$$\sigma_{e,h} = \sigma_c \phi_c \beta_c + \sum \left(\sigma_l \frac{V_{sat}}{V_t} \beta_l\right)_{r \le r_{\max}} \tag{22}$$

Based on the assumption of pore shape and the maximum size of a saturated pore in **equation (21)**, the electrical conductivity from **equation (22)** can be derived as shown in **equation (23):**

$$\sigma_{e,h} = \sigma_c \phi_c \beta_c + \sum \left(\sigma_l \frac{n_i \frac{4}{3}\pi r_1 r_2 r_3}{V_t} \beta_l\right)_{r=\max} + \sum \left(\sigma_l \frac{n_j V_{psat}}{V_t} \beta_l\right)_{r<r_{\max}} \tag{23}$$

where: r_1, r_2 and r_3 are the radii of pores in different three-dimensional directions, with the radius in one direction equal to $r_{\max}$, n_i and n_j is the total number of saturated pores, and V_{psat} is the volume of a single saturated pore. Replacing r_1 with r_{max} from **equation (21)** enabled to derive the **equation (24):**

$$\sigma_{e,h} = \sigma_c \phi_c \beta_c + \sum \left(\sigma_l \frac{n_i \frac{4}{3}\pi \left(\frac{-2\gamma V_m}{R_g T \left[\ln\left(\%RH/100\right)\right]}\right) r_2 r_3}{V_t} \beta_l\right)_{r=\max} + \sum \left(\sigma_l \frac{n_j V_{psat}}{V_t} \beta_l\right)_{r<r_{\max}} \tag{24}$$

The electrical conductivity of the nanomodified Portland cement composite describing the humidity-dependent behavior can be simplified as:

$$\sigma_{e,h} = A + \frac{B}{\left[\ln\left(\%RH/100\right)\right]} \tag{25}$$

where: A and B are the coefficients of the nonlinear equation.

From **Figure 10,** nonlinear equation according to the proposed **equation (25)** was used to fit both the experimental data and data from the literature [36]. **Table 3** shows the calculated A, B coefficients and the obtained R^2 values for the proposed equations.

Table 3. Parameter obtained from fitting curves in Figure 10

Mix	A	B	Model equation	R^2
S2	3.70585	-0.03029	$\sigma_{e,h} = 3.70585 - 0.03029 / \left[\ln \left(\%RH/100 \right) \right]$	0.72864
S4	3.83140	-0.02675	$\sigma_{e,h} = 3.83140 - 0.02675 / \left[\ln \left(\%RH/100 \right) \right]$	0.74896
S6	3.89876	-0.02582	$\sigma_{e,h} = 3.8955 - 0.02582 / \left[\ln \left(\%RH/100 \right) \right]$	0.72793
S8	9.46367	-0.46153	$\sigma_{e,h} = 9.4637 - 0.46153 / \left[\ln \left(\%RH/100 \right) \right]$	0.71535
S10	12.87000	-0.70635	$\sigma_{e,h} = 12.87000 - 0.70635 / \left[\ln \left(\%RH/100 \right) \right]$	0.73391

The proposed models, **equation (25),** showed R^2 value just above 0.71 for all mixes, which indicates a relatively low statistical significance. The model demonstrated that the conductivity of the conductive phases and liquid phases is important to describe the humidity-sensitive property of the nanomodified Portland cement composite. The findings confirmed that the electrical conductivity of the nanomodified Portland cement matrix is attributed to the moving free water held in capillaries as well as absorbed water held by the surface forces. The model's low accuracy can be explained by neglecting the conductivity of the binder matrix. Its electrical conductivity depends on the type of conductive filler used, its dispersion, and its connectivity. These effects were partially included in the statistically determined A and B coefficients, but definitely more detailed studies should be performed.
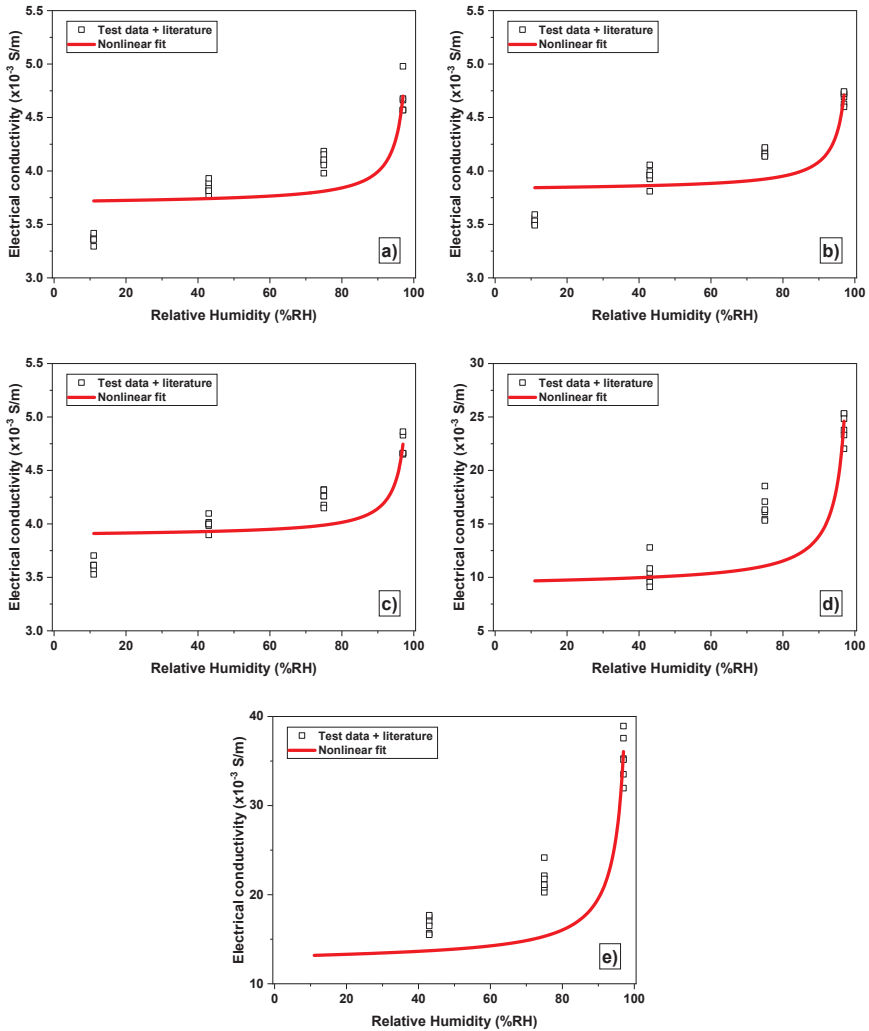
Figure 10. Fitted curve with experimental data from current studies and literature on the electrical conductivity of nanomodified Portland cement mortars on the ambient humidity variation of a) S2, b) S4, c) S6, d) S8, and e) S10.

Temperature influences the conductivity of the cement-based composites. It could be explained by 1) thermal deformation of the composite matrix; 2) movement of the thermally activated charge carriers and thermal fluctuation-induced tunneling conduction [29].

The thermal expansion or contraction of nanomodified Portland cement composite occurs as a response to temperature alterations. Composites demonstrate thermal expansion when heated and thermal contraction when cooled. The thermal expansion of nanomodified Portland cement composite may result in a potential separation or loosening of contacts between the conductive fibers due to larger distances or the creation of gaps. This has the potential to result in a decrease in the electrical conductivity of the composite. Conversely, during the thermal contraction occurring at lower temperatures, the shrinking of the composite matrix may result in compression or tighter contact

between conductive fibers. This improved contact can enhance the formation of the conductive paths and potentially enhance the conductivity.

The impact of thermal fluctuation-induced tunneling is related to higher temperatures, which provide additional kinetic energy to charge carriers. This enables them to overcome energy barriers and move more freely through the matrix, leading to higher electrical conductivity. The phenomenon of thermal activation of charge carriers is often linked to the concept of activation energy, which represents the minimum amount of energy needed for charge carriers to shift from localized states to ones with higher mobility.

A model of tunneling current density J as a function of temperature was proposed in 1936 by Hill [50]

$$J = \frac{8\pi me}{\hbar^3 B^2} \sinh\left(\frac{eV}{R_g T}\right) \frac{\pi B R_g T}{\sin \pi B R_g T} \exp(A\varphi^{1/2}) \exp\left(-\frac{E_a}{R_g T}\right) \tag{26}$$

where: $A = 4\pi s (2m)^{1/2}/\hbar$; $B = A/2\varphi^{1/2}$, $\hbar$ is the Planck's constant, m is the electron mass, e is the electron charge, s is the tunneling distance between adjacent conductive particles, φ is the height of the potential barrier between adjacent particles, V is the voltage drop cross tunnel, T is an absolute temperature in Kelvin, R_g is the universal gas constant, and E_a is the activated energy.

Generally, $eV \ll kT$, the term of $\sinh(eV/kT)$ is approximately equal to eV/kT. Therefore, the tunneling current is given by:

$$J = \frac{\varphi e^2 BV}{s^2 \hbar \sin \pi B R_g T} \exp\left(\frac{4\pi(2m\varphi)^{1/2} s}{\hbar} - \frac{E_a}{R_g T}\right) \tag{27}$$

Therefore, the tunneling gap s could be related to the thermal expansion or contraction of cement-based composites. The coefficient of linear thermal expansion in cementitious composited α_c can be calculated using the following equation:

$$\alpha_c = \left(\frac{\Delta s}{s_0}\right)\left(\frac{1}{\Delta T}\right) = \left(\frac{s}{s_0} - 1\right)\left(\frac{1}{T - T_0}\right) \tag{28}$$

Therefore,

$$s = s_0\left[1 + \alpha_c(T - T_0)\right] \tag{29}$$

where: s_0 is initial tunneling distance and T_0 is an initial temperature.

Substituting **equation (29)** into **equation (27)**, obtained

$$J = \frac{\varphi e^2 BV}{\left(s_0\left[1 + \alpha_c(T - T_0)\right]\right)^2 \hbar \sin \pi B R_g T} \exp\left(\frac{4\pi(2m\varphi)^{1/2}\left(s_0\left[1 + \alpha_c(T - T_0)\right]\right)}{\hbar} - \frac{E_a}{R_g T}\right) \tag{30}$$

Normally $\alpha_c(T-T_0) \ll 1$, the term of $\left(s_0\left[1+\alpha_c(T-T_0)\right]\right)^2 \approx s_0^2$. Then,

$$J \approx \frac{k_1 V}{s_0^2} \exp\left(k_2 s_0\left[1+\alpha_c(T-T_0)\right] \quad \frac{E_a}{R_g T}\right) \qquad (31)$$

where: $k_1 = \varphi e^2 B / \hbar \sin \pi B R_g T$, $k_2 = 4\pi(2m\varphi)^{1/2}/\hbar$

Based on the **equation (31)**, the electrical resistance of the nanomodified Portland cement composites due to the tunneling effect and thermal deformation can be calculated as follows:

$$R_t = \frac{s_0^2}{k_1 a^2} \exp\left(-k_2 s_0\left[1+\alpha_c(T-T_0)\right] + \frac{E_a}{R_g T}\right) \qquad (32)$$

where: a^2 is the effective cross-section area.

The form of electrical conductivity as follows:

$$\sigma_{e,t} = \frac{L}{R_t A_e} = \frac{L k_1 a^2}{A_e s_0^2} \exp\left(k_2 s_0\left[1+\alpha_c(T-T_0)\right] \quad \frac{E_a}{R_g T}\right) \qquad (33)$$

However, in the present work, the thermal deformation of the nanomodified Portland cement composite has been disregarded because the impact of thermal expansion within the temperature range employed in this study is negligible. The predominant influence stems from thermal fluctuation-induced tunneling conduction. The electrical conductivity of the nanomodified Portland cement composite describing the temperature-dependent behavior can be explained by the following equation:

$$\sigma_{e,t} = \frac{L k_1 a^2}{A_e s_0^2} \exp\left(-\frac{E_a}{R_g T}\right) \qquad (34)$$

Based on equation (34) can be simplified as follows:

$$\sigma_{e,t} = C \exp\left(-\frac{D}{T}\right) = C \exp\left(-\frac{D}{T_c + 273.15}\right) \qquad (35)$$

where: C, D are constant and T_c is the temperature in Celsius.

The proposed nonlinear **equation (35)** was used to fit both the experimental data and data from the literature. **Table 4** shows the coefficient of fitted experimental data based on the proposed model.

Table 4. *Parameter obtained from fitting curves in Figure 11*

Mix	C	D	Model equation	R²
S2	43.536	2865.747	$\sigma_{e,t} = 43.536 \exp\left(-2865.747/T_c + 273.15\right)$	0.97890
S4	445.447	3500.952	$\sigma_{e,t} = 445.447 \exp\left(-3500.952/T_c + 273.15\right)$	0.98770
S6	304.125	3340.836	$\sigma_{e,t} = 304.125 \exp\left(-3340.836/T_c + 273.15\right)$	0.98604
S8	1678.733	3800.974	$\sigma_{e,t} = 1678.733 \exp\left(-3800.974/T_c + 273.15\right)$	0.97461
S10	16732.194	4460.158	$\sigma_{e,t} = 16732.194 \exp\left(-4460.158/T_c + 273.15\right)$	0.96225

The analysis of the coefficient of determination (R^2) of the proposed models in **equation (35)** indicates that the model closely matches the experimental data, with R^2 values greater than 0.95 for all mixes. It is demonstrated that thermal fluctuation-induced tunneling conduction can describe the temperature-sensitive behavior of the nanomodified Portland cement composite. The findings confirmed that the tunneling effect by thermal induction is important in the sensing behavior of nanomodified Portland cement composites within the studied temperature range.
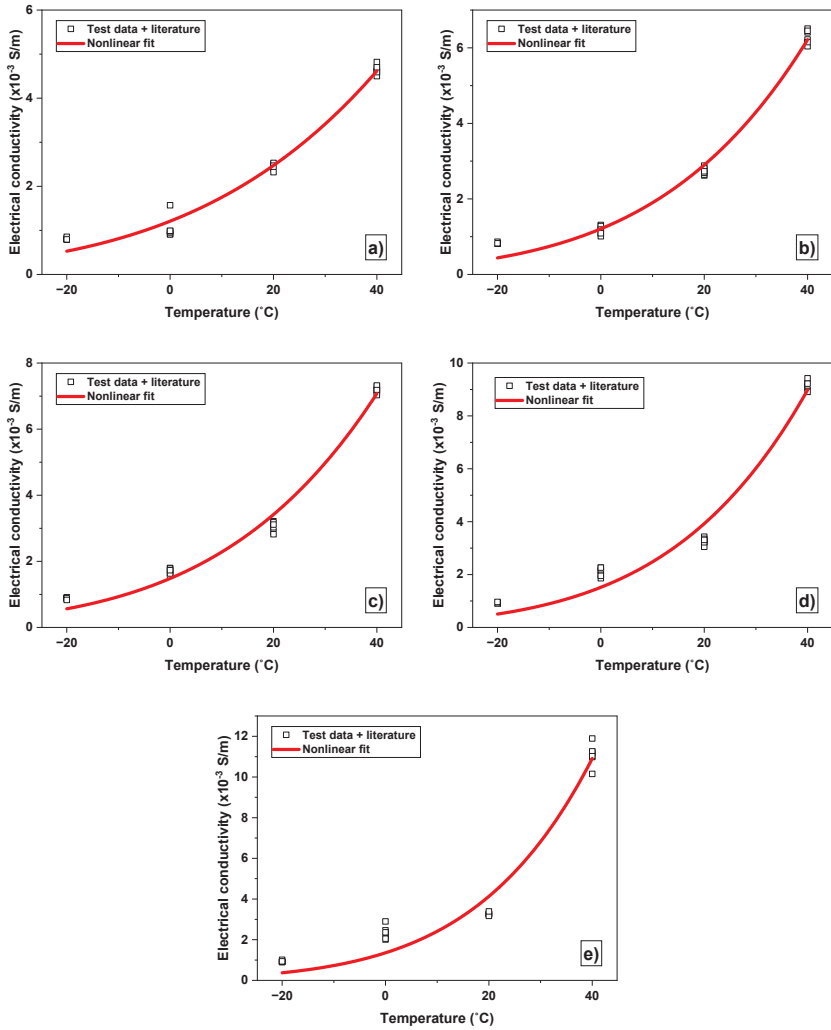
Figure 11. Fitted curve with experimental data from current studies and literature on the electrical conductivity of nanomodified Portland cement mortars on the temperature variation of a) S2, b) S4, c) S6, d) S8, and e) S10.

4. Conclusion

Sensing behaviors, mechanisms, and models of the response of nanomodified Portland cement mortars to variations in compressive stress, humidity, and temperature were investigated. The primary outcomes of this study can be succinctly summarized as follows:

- The nanomodified Portland cement composites showed sensing capability to detect variations of compressive stress, humidity, and temperature by measuring the change in electrical resistivity.
- The maximum sensitivity was observed in S10 specimen, containing 10 wt.% of the nanomodified Portland cement for compressive stress, humidity, and temperature sensing.
- The developed models can predict the electrical response of nanomodified Portland cement mortars when subjected to changes in stress, humidity, and temperature.
- The proposed models confirmed that the piezoresistive effect is related to the threshold amount of CNFs present in the composite matrix and due to the tunneling effect. In addition, water absorption and desorption, as well as the amount of chemically bound water, played an important role in humidity sensing. Thermal fluctuation-induced tunneling conduction was dominant for the temperature sensitivity.
- The model addressing humidity showed the lowest accuracy due to neglecting the effect of the conducting binder matrix.

Acknowledgment

Reference

[1]   B. Han, L. Zhang, J. Ou, Smart and Multifunctional Concrete Toward Sustainable Infrastructures, Springer Nature Singapore Pte Ltd., 2017. https://doi.org/10.1007/978-981-10-4349-9.

[2]   D.G. Meehan, Shoukai Wang, D.D.L. Chung, Electrical-resistance-based sensing of impact damage in carbon fiber reinforced cement-based materials, J Intell Mater Syst Struct. 21 (2010) 83–105. https://doi.org/10.1177/1045389X09354786.

[3]   P.-W. Chen, D.D.L. Chung, Carbon fiber reinforced concrete for smart structures capable of non-destructive flaw detection, 1993. http://iopscience.iop.org/0964-1726/2/1/004.

[4]   F. Azhari, N. Banthia, Cement-based sensors with carbon fibers and carbon nanotubes for piezoresistive sensing, Cem Concr Compos. 34 (2012) 866–873. https://doi.org/10.1016/j.cemconcomp.2012.04.007.

[5]   G.Y. Li, P.M. Wang, X. Zhao, Pressure-sensitive properties and microstructure of carbon nanotube reinforced cement composites, Cem Concr Compos. 29 (2007) 377–382. https://doi.org/10.1016/j.cemconcomp.2006.12.011.

[6]   C. Camacho-Ballesta, E. Zornoza, P. Garcés, Performance of cement-based sensors with CNT for strain sensing, Advances in Cement Research. 28 (2016) 274–284. https://doi.org/10.1680/adcr.14.00120.

[7]   X. Yu, E. Kwon, A carbon nanotube/cement composite with piezoresistive properties, Smart Mater Struct. 18 (2009). https://doi.org/10.1088/0964-1726/18/5/055010.

[8]   H. Li, J. Ou, Smart concrete, sensors and self-sensing concrete structures, Key Eng Mater. 400–402 (2009) 69–80. https://doi.org/10.4028/www.scientific.net/kem.400-402.69.

[9]   J.L. Le, H. Du, S.D. Pang, Use of 2-D Graphene Nanoplatelets (GNP) in cement composites for structural health evaluation, Compos B Eng. 67 (2014) 555–563. https://doi.org/10.1016/j.compositesb.2014.08.005.

[10]   S. Wen, D.D.L. Chung, Partial replacement of carbon fiber by carbon black in multifunctional cement-matrix composites, Carbon N Y. 45 (2007) 505–513. https://doi.org/10.1016/j.carbon.2006.10.024.

[11]   J. Luo, Z. Duan, T. Zhao, Q. Li, Hybrid effect of carbon fiber on piezoresistivity of carbon nanotube cement-based composite, in: Adv Mat Res, 2011: pp. 639–643. https://doi.org/10.4028/www.scientific.net/AMR.143-144.639.

[12]   B. Chen, K. Wu, W. Yao, Conductivity of carbon fiber reinforced cement-based composites, Cem Concr Compos. 26 (2004) 291–297. https://doi.org/10.1016/S0958-9465(02)00138-5.

[13]   L. Zhang, S. Ding, S. Dong, Z. Li, J. Ouyang, X. Yu, B. Han, Piezoresistivity, mechanisms and model of cement-based materials with CNT/NCB composite fillers, Mater Res Express. 4 (2017). https://doi.org/10.1088/2053-1591/aa9d1d.

[14]   D.D.L. Chung, Piezoresistive cement-based materials for strain sensing, J Intell Mater Syst Struct. 13 (2002) 599–609. https://doi.org/10.1106/104538902031861.

[15]   Z. Liu, Y. Zhang, L. Liu, Q. Jiang, An analytical model for determining the relative electrical resistivity of cement paste and C-S-H gel, Constr Build Mater. 48 (2013) 647–655. https://doi.org/10.1016/j.conbuildmat.2013.07.020.

[16]   F. Xuli., C. D.D.L., Effect of curing age on the self-monitoring behavior of carbon fiber reinforced mortar, Cem Concr Res. 27 (1997) 1313–1318.

[17]   G. Yildirim, G.H. Aras, Q.S. Banyhussan, M. Şahmaran, M. Lachemi, Estimating the self-healing capability of cementitious composites through non-destructive electrical-based monitoring, NDT and E International. 76 (2015) 26–37. https://doi.org/10.1016/j.ndteint.2015.08.005.

[18]   O. Galao, F.J. Baeza, E. Zornoza, P. Garcés, Strain and damage sensing properties on multifunctional cement composites with CNF admixture, Cem Concr Compos. 46 (2014) 90–98. https://doi.org/10.1016/j.cemconcomp.2013.11.009.

[19]   G. Yildirim, G.H. Aras, Q.S. Banyhussan, M. Şahmaran, M. Lachemi, Estimating the self-healing capability of cementitious composites through non-destructive electrical-based monitoring, NDT and E International. 76 (2015) 26–37. https://doi.org/10.1016/j.ndteint.2015.08.005.

[20]   A. Al-Dahawi, M.H. Sarwary, O. Öztürk, G. Yildirim, A. Akin, M. Şahmaran, M. Lachemi, Electrical percolation threshold of cementitious composites possessing self-sensing functionality incorporating different carbon-based materials, Smart Mater Struct. 25 (2016). https://doi.org/10.1088/0964-1726/25/10/105005.

[21]   M. Sun, Z. Li, Q. Liu, The electromechanical effect of carbon fiber reinforced cement, Carbon N Y. (2002) 2273–2275.

[22]   A. Al-Dahawi, O. Öztürk, F. Emami, G. Yildirim, M. Şahmaran, Effect of mixing methods on the electrical properties of cementitious composites incorporating different carbon-based materials, Constr Build Mater. 104 (2016) 160–168. https://doi.org/10.1016/j.conbuildmat.2015.12.072.

[23]   D.D.L. Chung, Composites get smart, Materials Today. 5 (2002) 30–35. https://doi.org/10.1016/S1369-7021(02)05140-4.

[24]   D.D.L. Chung, Self-monitoring structural materials, n.d.

[25]   V.W.J. Lin, M. Li, J.P. Lynch, V.C. Li, Mechanical and electrical characterization of self-sensing carbon black ECC, in: Nondestructive Characterization for Composite Materials, Aerospace Engineering, Civil Infrastructure, and Homeland Security 2011, SPIE, 2011: p. 798316. https://doi.org/10.1117/12.880178.

[26]   C. Bing, W.U. Keru, Y. Wu, Characteristics of Resistivity-temperature for Carbon Fiber Reinforced Concrete, 2006.

[27]   Z. Bekzhanova, S.A. Memon, J.R. Kim, Self-sensing cementitious composites: Review and perspective, Nanomaterials. 11 (2021). https://doi.org/10.3390/nano11092355.

[28]   F. Rajabipour, J. Weiss, Electrical conductivity of drying cement paste, Materials and Structures/Materiaux et Constructions. 40 (2007) 1143–1160. https://doi.org/10.1617/s11527-006-9211-z.

[29]   S. Ding, S. Dong, A. Ashour, B. Han, Development of sensing concrete: Principles, properties and its applications, J Appl Phys. 126 (2019). https://doi.org/10.1063/1.5128242.

[30]   E. Teomete, The effect of temperature and moisture on electrical resistance, strain sensitivity and crack sensitivity of steel fiber reinforced smart cement composite, Smart Mater Struct. 25 (2016). https://doi.org/10.1088/0964-1726/25/7/075024.

[31]   E. Demircilioğlu, E. Teomete, E. Schlangen, F.J. Baeza, Temperature and moisture effects on electrical resistance and strain sensitivity of smart concrete, Constr Build Mater. 224 (2019) 420–427. https://doi.org/10.1016/j.conbuildmat.2019.07.091.

[32]   W. Elkey, E.J. Sellevold, Electrical resistivity of concrete, Norwegian Public Roads Administration, Oslo, 1995.

[33]   T. Buasiri, K. Habermehl-Cwirzen, A. Cwirzen, State of the Art on Sensing Capability of Poorly or Nonconductive Matrixes with a Special Focus on Portland Cement–Based Materials, Journal of Materials in Civil Engineering. 31 (2019). https://doi.org/10.1061/(ASCE)MT.1943-5533.0002901.

[34]   J. Hilding, E.A. Grulke, Z.G. Zhang, F. Lockwood, Dispersion of carbon nanotubes in liquids, J Dispers Sci Technol. 24 (2003) 1–41. https://doi.org/10.1081/DIS-120017941.

[35]   A. Cwirzen, K. Habermehl-Cwirzen, V. Penttala, Surface decoration of carbon nanotubes and mechanical properties of cement/carbon nanotube composites, Advances in Cement Research. 20 (2008) 65–73. https://doi.org/10.1680/adcr.2008.20.2.65.

[36]   T. Buasiri, K.H. Cwirzen, L. Krzeminski, A. Cwirzen, Novel humidity sensors based on nanomodified Portland cement, Sci Rep. (2021) 1–10. https://doi.org/10.1038/s41598-021-87563-7.

[37]   T. Buasiri, K. Habermehl-Cwirzen, L. Krzeminski, A. Cwirzen, Role of Carbon Nanofiber on the Electrical Resistivity of Mortar under Compressive Load, Transportation Research Record: Journal of the Transportation Research Board. (2020) 1–6. https://doi.org/10.1177/0361198120947417.

[38]   T. Buasiri, K. Habermehl-Cwirzen, L. Krzeminski, A. Cwirzen, Piezoresistive load sensing and percolation phenomena in portland cement composite modified with in-situ synthesized carbon nanofibers, Nanomaterials. 9 (2019). https://doi.org/10.3390/nano9040594.

[39]   T. Buasiri, K. Habermehl-Cwirzen, L. Krzeminski, A. Cwirzen, Piezoresistive Load Sensing and Percolation Phenomena in Portland Cement Composite Modified with In-Situ Synthesized Carbon Nanofibers, Nanomaterials. (2019). https://doi.org/10.3390/nano9040594.

[40]   J.F. Young, HUMIDITY CONTROL IN THE LABORATORY USING SALT SOLUTIONS-A REVIEW, 1967.

[41]   A.S. Fiorillo, C.D. Critello, A.S. Pullano, Theory, technology and applications of piezoresistive sensors: A review, Sens Actuators A Phys. 281 (2018) 156–175. https://doi.org/10.1016/j.sna.2018.07.006.

[42]   S. Ding, S. Dong, A. Ashour, B. Han, Development of sensing concrete: Principles, properties and its applications, J Appl Phys. 126 (2019). https://doi.org/10.1063/1.5128242.

[43]   J.G. Simmons, G.J. Unterkofler, Potential Barrier Shape Determination in Tunnel Junctions, J Appl Phys. 34 (1963) 1828–1830. https://doi.org/10.1063/1.1702693.

[44]   J.G. Simmons, Generalized Formula for the Electric Tunnel Effect between Similar Electrodes Separated by a Thin Insulating Film, J Appl Phys. 34 (1963) 1793–1803. https://doi.org/10.1063/1.1702682.

[45]   B. Chen, K. Wu, W. Yao, Conductivity of carbon fiber reinforced cement-based composites, Cem Concr Compos. 26 (2004) 291–297. https://doi.org/10.1016/S0958-9465(02)00138-5.

[46]   S. Dong, B. Han, J. Ou, Z. Li, L. Han, X. Yu, Electrically conductive behaviors and mechanisms of short-cut super-fine stainless wire reinforced reactive powder concrete, Cem Concr Compos. 72 (2016) 48–65. https://doi.org/10.1016/j.cemconcomp.2016.05.022.

[47]   A. Schießl, W. Weiss, J. Shane, N.S. Berke, T.O. Mason, S. Shah, Assessing the moisture profile of drying concrete using impedance spectroscopy, Concrete Science and Engineering. 2 (2000) 106–116.

[48]   F. Rajabipour, J. Weiss, Electrical conductivity of drying cement paste, Materials and Structures/Materiaux et Constructions. 40 (2007) 1143–1160. https://doi.org/10.1617/s11527-006-9211-z.

[49]   F. Dullien, Porous media; fluid Transport and Pore Structure, Academic Press, New York, 1979.

[50]   R. Hill, Electrical conduction in ultra thin metal films I. Theoretical, Proceedings of the Royal Society of London. A. Mathematical and Physical Sciences. 309 (1969) 377–395. https://doi.org/10.1098/rspa.1969.0048.

LULEÅ
UNIVERSITY
OF TECHNOLOGY